Modeling, Simulation, and Control of a Polypyrrole-Based Conducting Polymer Actuator

by

Thomas A. Bowers

B.S. Mechanical Engineering (2002)

Arizona State University

Submitted to the Department of Mechanical Engineering
in Partial Fulfillment of the Requirements for the Degree of
Master of Science in Mechanical Engineering

at the

Massachusetts Institute of Technology

February 2004

Signature of Author _____
Department of Mechanical Engineering
January 16, 2004

Certified by _____
Neville Hogan
Professor of Mechanical Engineering
Thesis Supervisor

Accepted by _____
Ain A. Sonin
Chairman, Department Committee on Graduate Students

Modeling, Simulation, and Control of a Polypyrrole-Based Conducting Polymer Actuator

by

Thomas A. Bowers

Submitted to the Department of Mechanical Engineering
on January 16, 2004 in Partial Fulfillment of the
Requirements for the Degree of Master of Science in
Mechanical Engineering

Abstract

A detailed model was developed for an ionic electro-active polymer (EAP) actuator. The electrical and chemical domains of the system were modeled using a simple electrical circuit. Ionic charge storage within the polymer was described using a linear reticulated model. This model improves upon the continuum diffusive model introduced in prior work by providing a low order model of diffusion that can be analyzed in the context of modern and classical control methods. Additionally, the reticulated diffusion model describes the dynamics of ionic charge distribution within the polymer, which enables a more precise calculation of electromechanical coupling.

An interesting observation of ionic electro-active polymers is that they exhibit enormous asymmetry in coupling from electrical to mechanical domains. While electrical potentials produce large linear displacements (5% strain or greater), uniaxially-applied mechanical loads result in a negligible electrical back effect. This is surprising, suggesting that there are huge entropic losses when applying mechanical loads. After examining the mechanics of the system it was theorized that the apparent lack of coupling is actually the result of the Poisson Effect, which causes changes in the volume of an object when uniaxial loads are applied. A derivation of the stored electrical energy and strain energy led directly to a set of constitutive equations that are able to account for the asymmetric coupling observed in EAP. The solution to the uniaxial loading boundary condition was developed fully and compared to prior work.

Experimental results from an EAP actuator composed of polypyrrole, a widely-used conducting polymer, validate the electro-mechanical coupling model. MATLAB was used to simulate the response of the actuator and the results compared to the experimental data. Results verify that the model accurately describes the electrical, mechanical, and coupled behavior of the system. The correlation between the model and experimental data is very good for electrically-induced strains up to 3% and applied potentials up to 1 Volt above the potential of zero charge (PZC); these are within the typical operating range of polypyrrole. The model is sufficiently simple to allow real-time control while also exceeding prior models in its ability to predict polymer behavior in normal operating ranges.

Thesis Supervisor: Neville Hogan
Title: Professor of Mechanical Engineering

Acknowledgments

This thesis could not have been completed without the support of numerous individuals. Professor Neville Hogan has been a patient and resourceful advisor. He stimulated my passion for modeling of dynamic systems, which made this thesis both enjoyable and addicting to work on. It was his keen understanding of physical systems that led me to analyze the constitutive relationship between energy domains in electro-active polymers. The resulting polymer constitutive model is the backbone of my research and represents the major contribution from this work. I consider myself very privileged to have had the opportunity to learn from Professor Hogan and hope that I may one day possess at least a fraction of his engineering facility.

Professor Ian Hunter recognized the potential of conducting polymer actuators and led a major research effort to understand the capabilities of these materials. John Madden was one of the first students to work on conducting polymers with Professor Hunter. His contributions to conducting polymer actuators provided the foundation that enabled this work to occur. I was lucky enough to interact with Patrick Anquetil and Peter Madden who were very familiar with John's work and helped me to get a better handle on it. They also provided very useful insight from their own research on conducting polymers. Patrick has been an enthusiastic observer of my research and has given me invaluable feedback. In addition, he has offered significant assistance with experimentation, helping me to make sense of experimental data. I cannot begin to estimate how much time he saved me by fully automating the electrical and mechanical inputs to the dynamic testing equipment. I must also acknowledge Derek Rinderknecht, who created the device that was used for all experimentation.

My understanding of polymers has grown tremendously through the cooperative efforts of "The Polymer Group," a multi-disciplinary team of graduate students who share a passion for electro-active polymer materials and devices. Rachel Zimet eased my transition into experimental electrochemistry and provided considerable information about the material science of electro-active polymers. Nate Vandesteeg also offered his materials science and electrochemistry expertise. Bryan Schmid never complained when I invaded his work space and flattered me as the first person to utilize my polymer constitutive equations. Nic Sabourin helped to synthesize one of the polymer samples that was used in experimentation and validation of my polymer model. Laura Proctor has been an enthusiastic member of The Polymer Group and always lightens the mood in the lab. Naomi Davidson kept me sane during long hours of testing and helped me to realize when to stop running experiments.

I am very grateful for the feedback, assistance and moral support I received from the members of Professor Hogan's research group. In particular, I would like to thank Steve Buerger, whose assistance with system analysis and control was greatly appreciated. Jerry Palazzolo helped me considerably when I was first learning modeling and simulation in MATLAB. James Celestino stands out best for his role as captain of the Newman Lab intramural softball and hockey teams, but his contributions to all aspects of lab culture were priceless. I would like to thank Jason Wheeler for trading center field for first base, and also for consulting on non-linear control design. Doug Eastman and Chan Rhyou were excellent collaborators when we first began researching electro-rheological fluids, magneto-rheological fluids, and electro-active polymers. While I did not work directly with the other members of the group on a regular basis, they all added something memorable to my experience at MIT: Mike Roberts always seemed to be in the lab later than me, which made me feel a little better about occasional all-nighters; Laura DiPietro offered assistance with LabView, which allowed me to complete my 2.141 term project; Sue Fasoli was the lab supplier of Girl Scout cookies and a caring member of the group; Miranda Newberry attempted to converse with me in Spanish, although I usually could not understand much more than, "¡Hola!". The newest member of the group, Sarah Mendelowitz, shows great promise for the future of the lab. I cannot thank Julie Bentley enough for

keeping the lab running smoothly and for frequently helping me find rooms for group meetings at the last minute. Dr. Igo Krebs offered many good ideas for improvement of my research.

There are many people who helped in getting me to MIT and in easing my transition to the East Coast. Dr. Avinash Singhal from Arizona State University has always had faith in my abilities and has been a mentor and friend. Dr. Thomas Sugar from ASU gave me the opportunity to work on electromechanical systems, which peeked my interest in controls. I do not think that I could have made it to or survived at MIT without Dan Burns, who was my mover, ballast, spotter, and keeper. Dan was an excellent sounding board for all things related to my research and offered his input whenever he could. Leslie Regan did everything in her power to ensure that my time at MIT went smoothly from beginning to end.

My family has been a constant source of encouragement and I cannot thank them enough for their limitless emotional support. My mother, Beverly, has always found the time and energy to let me know that I am loved, and uses every occasion as an excuse to send me goodies. My father, James, has supported every decision I have made and helped to open doors for me along the way. I will always look up to my brother, David, who has done more for me than he will ever know.

I am indebted to Anna Marie Wallace, who has given more of herself than I ever could have hoped. She has been a beacon of light throughout the long, cold winters (and springs, and falls) that define New England.

The Institute for Soldier Nanotechnologies at MIT has provided a wealth of resources enabling this research to take place. I would like to thank all the faculty, staff and students of the ISN for their colossal efforts in establishing a first-rate research environment. This research was supported by the U.S. Army through the Institute for Soldier Nanotechnologies, under Contract DAAD-19-02-D-0002 with the U.S. Army Research Office. The content does not necessarily reflect the position of the Government, and no official endorsement should be inferred.

Contents

List of Figures

List of Tables

List of Abbreviations

CNT – carbon nanotube(s)

CP – conducting polymer(s)

EAP – electro-active polymer(s)

FOM – figure of merit

IPMC – ionic polymer metal composite(s)

$TEAPF_6$ – tetraethylammonium hexafluorophoshate

OCP – open circuit potential

PANI – polyanilene

PC – propylene carbonate

PD – proportional-plus-derivative control

PI – proportional-plus-integral control

PID – proportional-plus-integral-plus-derivative control

PPy – polypyrrole

PRBS – pseudo-random binary sequence

PZC – potential of zero charge

SLM – Standard Linear Model

List of Symbols Used

a = polymer thickness, m
a_0 = initial polymer thickness, m
α = strain to charge ratio, C^{-1}
A = cross-sectional area, m^2
b = damping coefficient, kg/s
γ = adaptation gain
Γ = diffusive transmission line delay parameter
c_V = specific volumetric capacitance, F/m^3
C_E = counter electrode double-layer capacitance, F
C_P = polymer double-layer capacitance, F
C_V = total volumetric capacitance, F
δ = double-layer thickness, m
D = diffusion coefficient, m^2/s
e = feedback error
e_V = electrical potential, V
ε_0 = permittivity of free space, 8.85e-12 F/m
$\varepsilon_{xx,yy,zz}$ = axial strains in x, y, or z direction
ε_V = volumetric strain
E = Young's modulus, N/m^2
E_e = stored electrical energy, J
E_ε = stored mechanical (strain) energy, J
$F_{x,y,z}$ = axial forces in x, y, or z direction, N
h = adaptation filter input gain
$\boldsymbol{\theta}$ = vector of feedback gains for adaptive control
θ_0 = proportional feedback gain of output for adaptive control
$\boldsymbol{\theta_1}$ = proportional feedback gain of filtered output for adaptive control
$\boldsymbol{\theta_2}$ = proportional feedback gain of filtered input for adaptive control
i_P = double layer ion current, A
i_V = polymer volume ion current, A
k = high frequency gain
K_d = derivative feedback gain
K_i = integral feedback gain
K_p = proportional feedback gain
κ = dielectric of electrolyte solvent
l = polymer length, m

l_0 = initial polymer length, m
Λ = filter gain matrix for adaptive control
M = transmission matrix
n = number of reticulated elements in diffusion model
ν = Poisson's ratio
q_p = ionic charge stored in polymer double-layer, C
$\boldsymbol{q_V}$ = vector of ionic charge states in polymer volume, C
q_V, Q_V = total ionic charge stored in polymer volume, C
r = reference signal
R_c = polymer-electrode contact resistance, Ω
R_E = electrolyte electrical resistance, Ω
R_P = polymer resistance, Ω
R_V = diffusion resistance, Ω
R_Σ = sum of circuit resistances, Ω
s = Laplace frequency domain variable
$\sigma_{P,I,D,PI,PD,PID}$ = closed-loop poles of various P, I, D controller structures
$\sigma_{x,y,z}$ = axial stress in x, y, or z direction, N/m^2
t = time, s
u = input signal
V = polymer volume, m^3
V_0 = initial polymer volume, m^3
w = polymer width, m
w_0 = initial polymer width, m
W_m = model of desired plant for adaptive control
W_p = model of actual plant for adaptive control
x = direction aligned with polymer length
ξ = damping coefficient
y = direction aligned with polymer width; response of actual plant for adaptive control
y_m = response of desired plant for adaptive control
Y = polymer admittance, Siemens
z = direction aligned with polymer thickness
Z = polymer impedance, Ω
$\boldsymbol{\omega}$ = vector of feedback variables for adaptive control
$\boldsymbol{\omega_1}$ = filtered feedback of control input for adaptive control
$\boldsymbol{\omega_2}$ = filtered feedback of plant output for adaptive control

Chapter 1

Introduction

Electro-active polymers (EAP) are in a relatively new class of materials that includes conducting polymers (CP), ionic polymer metal composites (IPMC), and gel polymers, among others. These polymeric materials exhibit a variety of interesting behaviors under the influence of electrical or chemical loading. Responses can include variations in stiffness, conductivity, or even coloration. One behavior that is of particular interest to mechanical engineers is the ability of some EAP to change dimension when loaded electrically or chemically. Because of their ability to change shape, these materials can be used as actuators in mechanical systems [1,2]. There are numerous EAP materials that demonstrate this shape-changing ability, and several provide stresses and strains that make them suitable replacements for more traditional actuator technologies. The current capabilities of these materials make them especially attractive for use as artificial muscle in systems that interact with humans. This is due to both the range of active performance and the passive properties of the materials. In addition, while actuators such as motors, solenoids, hydraulics, and combustion engines lose performance at small scales, EAP are able to perform equally well or better at micro- and even nano-scale. This makes EAP materials ideal for small scale actuation tasks.

Comparing EAP to other actuation technologies gives some indication of the types of mechanical systems that are particularly suited to EAP. The active mechanical properties of EAP are very similar to mammalian skeletal muscle. Depending on the type of polymer used, the materials can actively strain anywhere from 2 to 300 percent [3]. By comparison, *in vitro* mammalian muscle typically has a physiological maximum of ±10 percent active strain [4]. The tensile strengths of EAP are generally superior to muscle with maximum active stresses as high as 450 MPa [1]. *In vitro* mammalian muscle is estimated to have maximum exertion of only about 350 kPa [5,6]. Output power densities of EAP are currently less than muscle with reported values ranging from 5.8 W/kg [7] up to 150 W/kg [8] with other reported values falling in this range [9,10]. However, expectations are that the power densities of EAP will reach as high as 4 kW/kg [11]. By comparison, human muscle has a peak output power density of about 50 to 200 W/kg [4]. This puts EAP materials in about the same region of the

actuator design space as muscle, but with better force production and strain capabilities, and potentially better work density.

In addition to their active properties, EAP have remarkable similarity to muscle in their passive behavior. The elasticity of EAP materials ranges from 100 kPa up to 2 GPa and is usually adjustable to some degree during the polymerization process. Muscle has been found to exhibit passive elasticity ranging from about 7 to 127 kPa [12] depending on the frequency of perturbation and activation level. It has been found that some EAP also exhibit variable elasticity [13]. Variable impedance of this nature is a key characteristic of skeletal muscle, which allows humans to successfully perform a variety of tasks of significantly different exertion levels without losing stability [14-16]. While muscle can actively change stiffness by more than an order of magnitude, reported changes in EAP stiffness are only a factor of 5. EAP also provide viscoelastic damping, which improves the stability characteristics of EAP-based systems just as muscles and surrounding tissues reduce instabilities in the human body through damping [17].Another important characteristic of many EAP is their ability to hold a load statically without requiring additional energy. This makes them much more efficient than many types of actuators, including muscle, which require additional energy to hold a load. The passive characteristics of EAP make them ideal materials for use in biomimetic systems and in systems that must interact with humans [18]. In this regard, EAP offer a unique chance to augment the human body with synthetic materials that can act in a similar manner as biological tissues, but with potential for improved performance.

1.1 Motivation

One of the current limitations in the use of EAP as actuators is the complex nature of their behavior. In order to provide robust, real-time control of these actuators, low order models of their behavior need to be generated. Simple mathematical models that can competently describe the response of these materials to stimuli will allow them to be used as actuators, sensors, energy storage (batteries), wires and even transistors. Eventually it may be possible to build entire electromechanical devices out of EAP materials in the same way that silicon-based devices are currently being employed.

One of the most perplexing elements of EAP function is the interaction between energy domains. While the electrochemical interactions in EAP are understood fairly well, energetic interactions with the mechanical domain have yet to be adequately modeled and added to the description of EAP behavior. In particular, there have been observations of EAP that seem to suggest an asymmetric transduction of energy from electrical to mechanical domains. While electrical inputs result in

significant mechanical strains, EAP subjected to uniaxial loads demonstrate almost no back response in the electrical domain. However, linear transducers must symmetrically convert energy between domains. For instance, power input to a motor in the form of voltage and current is converted to mechanical power in the form of torque and angular velocity. If the system was driven mechanically as an electrical generator, the resulting output in the electrical domain would be an equivalent power in voltage and current. Both of these processes would have some power lost due to friction and electrical resistance; however, for a linear system the amount of power lost is independent of the direction of energy transduction. The observed behavior in EAP suggests that there are huge losses from mechanical inputs to electrical outputs and that the system is highly asymmetric, similar to a diode. However, there is no significant heating to validate entropy production, which indicates that the input mechanical energy may be stored in the system. It is clear that a better description of the transduction of energy between domains is essential to developing a sufficient model of EAP operation.

1.2 Goals

This research is the first step in a project aimed at achieving a simple, model-based feedback controller for ionic EAP with a dynamic response that equals or exceeds that of the well-known biological knee-jerk reflex. Low-order models will be developed with sufficient fidelity to enable an "artificial reflex loop" to control key mechanical variables including position, stiffness and damping.

In analyzing electro-active polymers it is desirable to develop a robust analysis methodology that can be extended to similar systems through the use of a common notation. To achieve this commonality among many similar systems, the bond graph notation is utilized in order to express the transduction of power between physical domains using physically relevant parameters. This powerful analysis method developed by Henry M. Paynter [19] of MIT allows all physical systems to be treated as networks of energy storage or dissipation elements. Utilization of simple, low-order models of system behavior makes it very easy to apply well-developed control methods for single-input-single-output (SISO) or multiple-input-multiple-output (MIMO) systems. The ultimate goal of modeling will be to deduce control-relevant models of electromechanically active materials that can be extended to many similar systems.

1.3 Background

While electro-active polymers have been around for decades, they were not suitable for actuation until developments in materials in the early 1990s led to increases in strength and achievable strain [3]. There are two classes of EAP that can be feasibly used for actuation: electronic EAP and ionic EAP. Electronic EAP include electrostatic actuators, electrostrictive actuators and dielectric elastomers. Electrostatic polymers operate due to the interaction forces of a parallel plate capacitor. Strain results when oppositely charged sides of the actuator are attracted by coulomb forces causing contraction against the compliant polymer material. Electrostrictive actuators and dielectric elastomers operate due to Maxwell stress, which causes materials to contract in the direction parallel to an applied electric field while they expand perpendicular to it. Electronic EAP are able to respond very rapidly to electrical inputs with attainable strains up to 300% [20]. However, due to the small sizes of the actuators—typically a few micrometers—these actuators need to be stacked in order to produce macroscale actuation [21]. Additionally, because electronic EAP are field dependent, large voltages on the order of kilovolts are generally required.

Ionic EAP operate through electrochemical interaction with ions in electrolyte solutions. The reactions associated with ion transport typically require activation potentials less that a volt, making ionic EAP ideal for many mobile systems and in systems that are intended to interact with humans. As ionic EAP are stimulated either electrically or chemically they absorb ions from a surrounding liquid electrolyte in order to maintain charge neutrality. The diffusion of ions into the EAP—during oxidation or reduction—causes the polymers to expand, resulting in useable strain. When electrical loading is reversed or the concentration of electrolyte is decreased the polymers are able to contract reversibly.

Some ionic EAP include gel polymers, ionic polymer metal composites (IPMC), carbon nanotubes (CNT) and conducting polymers (CP). Gel polymers are probably not feasible for use as artificial muscle or in other systems requiring significant loading due to their weak mechanical properties, but much of the analysis of ionic EAP also applies to these materials. While IPMC, CNT and CP have similar mechanical properties, their electrical behaviors set them apart. Like their name implies, ionic polymer metal composites are a combination of an electrically conducting metal with an ionically conducting polymer. The conductivity of the metal allows electrons to flow throughout the composite material when it is loaded electrically. Charge transfer extends to the polymer through a diffusive process known as “electron hopping” [22,23]. This allows electrolyte ions to diffuse into the polymer in order to maintain charge neutrality, which leads to expansion of the material and useable strain.

Because IPMC incorporate electrically insulating polymers, these actuators exhibit both electrical charge and ionic charge transfer dynamics, which increases the time required for actuation.

Conducting polymers and carbon nanotubes, on the other hand, are naturally conductive materials. This inherent conductivity is the result of the conjugated structure of the polymer backbone, which enables charge carriers to move freely along the polymer chain. Conductivity is further increased by doping with ions, similar to doping of semiconductors. Doping adds free electrons or holes to the polymer which can move along the polymer backbone as they are balanced by electrolyte ions. The conductivities of CP are highly variable and depend on the oxidation level of the polymer and on the amount of polymerization. Some CP have been produced with conductivities as high as copper wire (polyacetylene) [24]. This high conductivity allows relatively thick films to be used because of the minimization of electrical charge transfer dynamics. However, the polymers are still rate limited by the diffusion of ionic species, which will be discussed in more detail in Chapter 2. Another limitation of ionic EAP is that they must be in contact with an electrolyte in order to operate, which generally requires an aqueous environment. However, solutions to this problem have been developed using solid or gel electrolyte in encapsulated devices [25,26].

There are many conducting polymer materials used for actuators including polyacetylene, polyaniline, polythiophene, and polypyrrole (PPy). The structures for three of these common conducting polymers are shown in Figure 1-1.

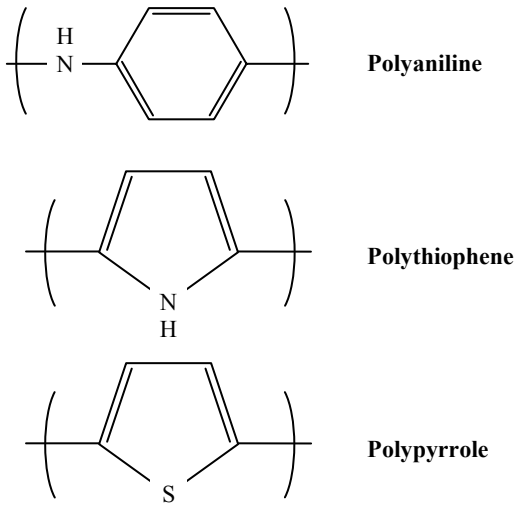

Figure 1-1: Single Units of Polymer Structure in Three Common Conducting Polymer Materials

There is a significant amount of research devoted to conducting polymers due to their potential as actuators [1-3,8-11,18,25-36]. Additional applications include wires, strain gages, transistors, and power storage [3,8,18]. Several researchers are examining the underlying mechanisms involved in CP actuation [9-11,22,27]. There are also considerable efforts to develop dynamic models of these materials [11,22,28,37]. One of the major focuses of EAP research is on improvement of material properties with an attempt to increase the performance capabilities of CP actuators [2,4,11,30-32,38-41]. These efforts have led to conducting polymers that are capable of 12% linear strains [32]. Some devices have already been developed using CP actuators [35,36,42]. However, before conducting polymer actuators can feasibly compete with traditional actuator technologies it is essential to develop low-order models of the materials. These models will allow improvement in EAP actuators through understanding of the factors influencing performance and will also allow real-time feedback control.

1.4 Summary

Electro-active polymers have the potential to replace traditional actuators and are capable of performing as artificial muscle. Conducting polymers are particularly suited to this task since they require potentials of less than 1 Volt and can provide strains of up to 12%. While models of EAP actuators have been developed, these models are unable to describe some of the important dynamics of these materials. Constitutive equations will be developed to deal with the apparent asymmetry in energy transduction between the electrical and mechanical domains. A general analysis methodology will be utilized such that the analysis can be easily adapted to similar systems.

1.5 Chapter References

[1] Baughman, R.H., R.L. Shacklette, and R.L. Elsenbaumer, "Micro electromechanical actuators based on conducting polymers," *Topics in Molecular Organization and Engineering, Vol. 7: Molecular Electronics*, P.I. Lazarev, Ed., Dordrecht: Kluwer Academic Publishers , (1991): 267-289.

[2] Baughman, R.H., "Conducting polymer artificial muscles," *Synthetic Metals*, **78** (1996): 339-353.

[3] Bar-Cohen, Yoseph, "Electro-active polymers: current capabilities and challenges," *Smart Structures and Materials 2002: Electroactive Polymer Actuators and Devices (EAPAD)*, Yoseph Bar-Cohen, Ed., *Proceedings of SPIE*, **4695** (2002): 1-7.

[4] Hunter, Ian W. and S. Lafontaine, "A Comparison of Muscle with Artificial Actuators." *Technical Digest IEEE Solid State Sensors and Actuators Workshop*, IEEE (1992): 178-185.

[5] Lieber, Richard L., "Skeletal Muscle is a Biological Example of a Linear Electro-Active Actuator," *Proceedings of SPIE's 6th Annual International Symposium on Smart Structures and Materials*, SPIE, (1999): 1-7.

[6] Huxley, A.F., *Reflections on Muscle*, Princeton, New Jersey: Princeton University Press, 1980.

[7] Caldwell, D.G., "Pseudomuscular actuator for use in dextrous manipulation," *Medical and Biological Engineering and Computing*, **28** (1980): 595-600.

[8] Madden, John D.W., Peter G.A. Madden, and Ian W. Hunter, "Conducting polymer actuators as engineering materials," *Smart Structures and Materials 2002: Electroactive Polymer Actuators and Devices (EAPAD)*, Yoseph Bar-Cohen, Ed., *Proceedings of SPIE*, **4695** (2002): 176-190.

[9] Madden, John D., Ryan A. Cush, Tanya S. Kanigan, and Ian W. Hunter, "Fast contracting polypyrrole actuators," *Synthetic Metals*, **113** (2000): 185-192.

[10] Della Santa, A., D. De Rossi and A. Mazzoldi, "Performance and work capacity of a polypyrrole conducting polymer linear actuator," *Synthetic Metals*, **90** (1997): 93-100.

[11] Madden, John D. W., *Conducting Polymer Actuators*, Ph.D. Thesis, MIT, Cambridge, MA, 2000.

[12] Levinson, Stephen F., Masahiko Shinagawa, and Takuso Sato, "Sonoelastic Determination of Human Skeletal Muscle Elasticity," *Journal of Biomechanics*, **28**, No. 10, (1995): 1145-1154.

[13] Spinks, Geoffrey M., Dezhi Zhou, Lu Liu and Gordon G. Wallace, "The amounts per cycle of polypyrrole electromechanical actuators," *Smart Materials and Structures*, **12** (2003): 468-472.

[14] Hogan, Neville, "Adaptive control of mechanical impedance by coactivation of antagonist muscles," *IEEE Transactions*, AC-**29** (1984): 681-690.

[15] Hogan, Neville, "The Mechanics of Multi-Joint Posture and Movement Control," *Biological Cybernetics*, **52** (1985): 315-331.

[16] Hogan, Neville, "Stable Execution of Contact Tasks Using Impedance Control," *Proceedings of the IEEE Conference on Robotics and Automation*, (1987): 1047-1054.

[17] Hill, A.V., "Production and Absorption of Work by Muscle," *Science*, New Series, **131**, No. 3404 (1960): 897-903.

[18] Madden, Peter G., John D. Madden, Patrick A. Anquetil, Hsiao-hua Yu, Timothy M. Swager, and Ian W. Hunter, "Conducting Polymers as Building Blocks for Biomimetic Systems," *2001 Bio-Robotics Symposium*, The University of New Hampshire, August 27-29, 2001.

[19] Paynter, Henry M., *Analysis and Design of Engineering Systems*, Cambridge: MIT Press, 1961.

[20] Kornbluh, Roy, and Ron Pelrine, "Application of Dielectric EAP Actuators," Chapter 16 in *Electroactive Polymer (EAP) Actuators as Artificial Muscles – Reality, Potential and Challenges*, Yoseph Bar-Cohen, Ed., SPIE Press, 2001: 457-495.

[21] Pelrine, Ron, Roy Kornbluh, Qibing Pei, and Jose Joseph, "High-Speed Electrically Actuated Elastomers with Over 100% Strain." *Science*, **287** (2000): 836-839.

[22] Lyons, Michael E.G., "Charge Percolation in Electroactive Polymers," Chapter 1 in *Electroactive Polymer Electrochemistry, Part 1: Fundamentals*, Michael E.G. Lyons, Ed., New York: Plenum Press, 1994, 1-235.

[23] Kaufmann, F.B., A.H. Schroeder, E.M. Engler, S.R. Kramer, and J.Q. Chambers, "Ion and Electron Transport in Stable, Electroactive Tetrathiafulvalene Polymer Coated Electrodes," *Journal of the American Chemical Society*, **102** (1980): 483-488.

[24] Kohlman, R.S. and A.J. Epstein, "Insulator-Metal Transition and Inhomogeneous Metallic State in Conducting Polymers," Terje A. Skotheim, Ronald L. Elsenbaumer and John R. Reynolds, Eds., *Handbook of Conducting Polymers 2nd Edition*, New York: Marcel Dekker, 1998, 85-122.

[25] Madden, John D., Ryan A. Cush, Tanya S. Kanigan, Colin J. Brenan, and Ian W. Hunter, "Encapsulated polypyrrole actuators," *Synthetic Metals*, **105** (1999): 61-64.

[26] Baughman, R.H., "Electrochemical mechanical actuators based on conducting polymers," *Workshop on Multifunctional Polymers and Smart Polymer Systems*, Wollongong, 1996.

[27] Gandhi, M.R., P. Murray, G.M. Spinks and G.G. Wallace, "Mechanism of electromechanical actuation in polypyrrole," *Synthetic Metals*, **73** (1995): 247-256.

[28] Mazzoldi, A., A. Della Santa, and D. De Rossi, "Conducting Polymer Actuators: Properties and Modeling," in *Polymer Sensors and Actuators*, Y. Osada, and D. E. De Rossi, Eds., pp. 207-244, Springer Verlag, Heidelberg, 2000.

[29] Kaneko, Masamitsu, Masanori Fukui, Wataru Takashima and Keiichi Kaneto, "Electrolyte and strain dependences of chemomechanical deformation of polyaniline film," *Synthetic Metals*, **84** (1997) 795-796.

[30] Wallace, Gordon G., Jie Ding, Lui Lu, Geoffrey M. Spinks, and Dezhi Zhou, "Factors Influencing Performance of Electrochemical Actuators Based on Inherently Conducting Polymers (ICPs)," *Smart Structures and Materials 2002: Electroactive Polymer Actuators and Devices (EAPAD)*, Yoseph Bar-Cohen, Ed., *Proceedings of SPIE*, **4695** (2002): 8-16.

[31] Ding, Jie, Lu Liu, Geoffrey M. Spinks, Dehzi Zhou, Gordon G. Wallace, and John Gillespie, "High performance conducting polymer actuators utilizing a tubular geometry and helical wire interconnects," *Synthetic Metals*, **138** (2003): 391-398.

[32] Bay, Lasse, Keld West, Peter Sommer-Larsen, Steen Skaarup, and Mohammed Benslimane, "A Conducting Polymer Artificial Muscle with 12% Linear Strain," *Advanced Materials*, **15**, No. 3, (2003): 310-313.

[33] Kaneto, K., M. Kaneko, Y. Min and Alan G. MacDiarmid, "Artificial muscle: Electromechanical actuators using polyaniline films," *Synthetic Metals*, **71** (1995) 2211-2212.

[34] Hutchinson, A.S., T.W. Lewis, S.E. Moulton, G.M. Spinks, and G.G. Wallace, "Development of polypyrrole-based electromechanical actuators," *Synthetic Metals*, **113** (2000): 121-127.

[35] Smela, Elisabeth, "Conjugated Polymer Actuators for Biomedical Applications," *Advanced Materials*, **15**, No. 6 (2003): 481-494.

[36] Smela, Elisabeth, Olle Inganas, and Ingemar Lundstrom, "Controlled Folding of Micrometer-Size Structures," *Science*, New Series, **268**, No. 5218 (1995): 1735-1738.

[37] Fahlman, M., J.L. Bredas and W.R. Salaneck, "Experimental and theoretical studies of the π-electronic structure of conjugated polymers and the low work function metal/conjugated polymer interaction," *Synthetic Metals*, **78** (1996): 237-246.

[38] Mazurkiewicz, J.H., P.C. Innis, G.G. Wallace, D.R. MacFarlane and M. Forsyth, "Conducting Polymer Electrochemistry in Ionic Liquids," *Synthetic Metals*, **135-136** (2003) 31-32.

[39] Madden, John D., Peter G. Madden, Patrick A. Anquetil, and Ian W. Hunter, "Load and Time Dependence of Displacement in a Conducting Polymer Actuator," *Materials Research Society Symposium Proceedings*, **698** (2002), EE4.3: 137-144.

[40] Sayyah, S.M., S.S. Abd El-Rehim and M.M. El-Deeb, "Electropolymerization of Pyrrole and Characterization of the Obtained Polymer Films," *Journal of Applied Polymer Science*, **90** (2003): 1783-1792.

[41] Lewis, Trevor W., Geoffrey M. Spinks, Gordon G. Wallace, Alberto Mazzoldi, and Danilo De Rossi, "Investigation of the applied potential limits for polypyrrole when employed as the active components of a two-electrode device," *Synthetic Metals*, **122** (2001): 379-385.

[42] Lee, Seung-Ki, Sang-Jo Lee, Ho-Jeong An, Seung-Eun Cha, Jun Keun Chang, Byungkyu Kim and James Jungho Pak, "Biomedical Applications of Electroactive Polymers and Shape Memory Alloys," *Smart Structures and Materials 2002: Electroactive Polymer Actuators and Devices (EAPAD)*, Yoseph Bar-Cohen, Ed., *Proceedings of SPIE*, **4695** (2002): 17-31.

Chapter 2

Electrochemistry

This chapter discusses the basics of electrochemistry and how it applies to electro-active polymers, specifically focusing on conducting polymers. The interactions of the electrical and chemical domains are discussed in detail. Mechanisms for transduction of energy to the mechanical domain are introduced. A more rigorous analysis of energy transduction between domains is presented in Chapter 3.

2.1 Ionic EAP Electrochemical Cell

Ionic EAP are interesting in that they are carriers of both electrical and ionic charge. It is this property that allows them to be used as both actuators and power storage devices. For ionic and electrical conduction to occur, EAP are immersed in an electrolytic solution and connected to an electrical power supply. The electrochemical circuit is completed by a conducting counter electrode that is also immersed in the electrolyte. The basic architecture of the electrochemical circuit is shown below in Figure 2-1.

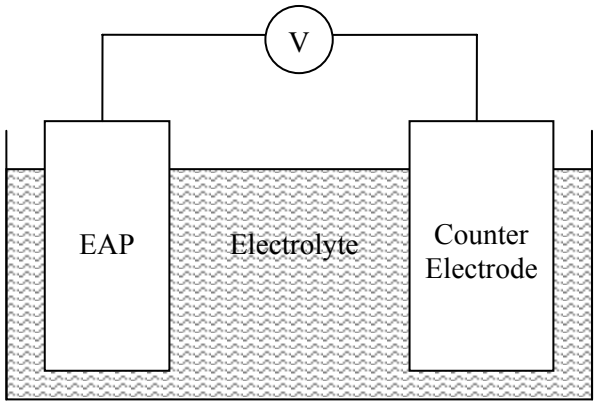

Figure 2-1: Basic EAP Electrochemical Cell Consisting of EAP, Counter Electrode, Electrolyte, and Voltage Supply

Application of an electrical potential to the EAP results in movement of electrical charge carriers in the polymer. The charge carriers in EAP—called polarons, bipolarons, and solitons—are similar to electrons and holes in semiconductors [1]. In the case of conducting polymers charge moves freely along the conjugated backbone structure of the polymer chains making them highly conductive. The displacement of electrical charge in the polymer is balanced by movement of electrolyte ions in solution. The electrolyte ions bond closely with molecules of the liquid in which they are dissolved allowing them to travel freely in solution. The movement of electrolyte ions enables the electrochemical circuit to conduct electricity through ionic charge transfer.

2.2 Electrical Double Layer

As ions move toward the polymer and counter electrode, ion concentrations increase near their surfaces. However, electrons cannot flow through the electrolyte and ions cannot bond with the polymer or counter electrode unless the oxidation or reduction potential of the materials is reached. Therefore, a region is formed at the surface of the electrodes where oppositely charged electrical and ionic charge carriers are separated by only a few nanometers. The region of densely packed electrolyte ions that forms adjacent to a charged surface is known as the electrical double layer, and is electrically equivalent to a parallel plate capacitor. Within the double-layer the concentrations of electrolyte ions vary depending on potential. Additionally, the distance separating the ion layer from the surface of the electrode can vary depending on whether or not the ion is surrounded by solvent molecules. The ion is said to be specifically adsorbed if it is able to shed the solvent molecules surrounding it. The exact geometry of the double layer depends on the potential applied, but a general architecture of the double layer is illustrated in Figure 2-2.

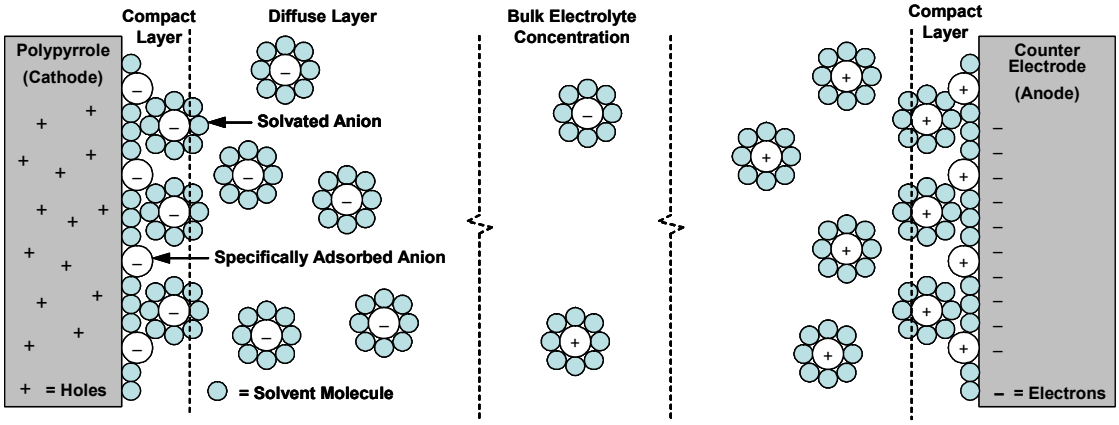

Figure 2-2: Double Layer Architecture Showing Compact and Diffuse Layer, adapted from Bard [2]

Several models of the electrical double layer have been proposed to account for the complex arrangements of solvated and specifically adsorbed ions, as well as to account for the diffuse layer, a less concentrated region of ions outside the compact region of the double layer. The simplest model of the double layer is known as the Helmholz model. It treats the double layer as a single surface of ions that is a fixed distance from the surface of the charged material. With ionic species separated from electrical charge carriers at a certain distance and potential the resulting energy storage is identical to a parallel plate capacitor. While more complicated models of the electrical double layer exist, at potentials exceeding about 100 mV the behavior of the double layer is dominated by the capacitive dynamics predicted by the Helmholz model. A qualitative description of the relationship between applied potential and the double layer width is presented in Figure 2-3. For low potentials a significant portion of the potential drop occurs in the diffuse layer. This is because there is a weak attraction between the electrode surface and electrolyte ions. Clearly as potential is increased the contributions from the diffuse layer diminish and the majority of the applied potential is lost in the compact region of the double layer. The Helmholz model competently describes the electrostatics of the compact layer.

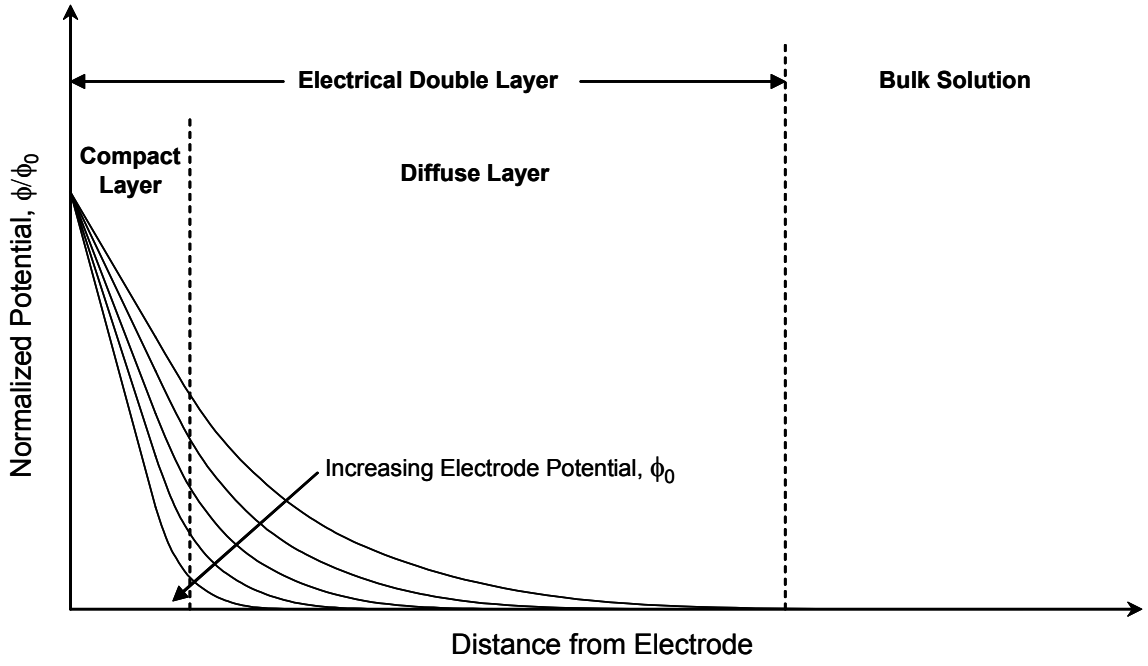

Figure 2-3: Relationship between Applied Potential and Effective Double Layer Width, adapted from Bard [2]

When a potential is applied to a conducting polymer EAP that is immersed in an electrolyte the double layer forms almost instantaneously. The capacitance of the double layer is relatively small so

few ions are needed to establish the applied potential across it. At this point the system is not very interesting; it is merely a tiny electrolytic capacitor. However, the formation of the double layer is essential to the operation of electrically stimulated EAP actuators.

2.3 Ion Diffusion

The most important mechanism in ionic EAP is ion diffusion. This process allows EAP to perform as actuators, capacitors, and even transistors. When an electrical potential is applied to a conducting polymer EAP the conductivity of the material results in an almost uniform potential throughout, with only minor ohmic losses far from electrical contact. Because there is virtually no electrical potential gradient within the polymer, ions at the surface are not drawn into the polymer electrically. However, with the formation of the densely packed electrical double layer an ion concentration gradient is established. This gradient forces the highly concentrated ions at the surface of the polymer to diffuse into it. As the ions enter the polymer they take up volume causing the polymer to expand. There are also interactions between the ions and the polymer chain that result in straightening of the chain as electrical energy is converted to mechanical energy. As more and more ions enter the polymer the amount of charge stored in the system increases. Because the volume of the polymer is typically several orders of magnitude more than the double layer volume, the relative ion storage associated with the EAP volumetric capacitance is huge. For this reason, EAP show significant promise as energy storage devices (batteries) in addition to their potential as actuators.

It is evident that the rate of diffusion, the process that plays the key role in EAP, is extremely important to the performance of EAP devices. There are several factors that contribute to the diffusion rate. One of the most important factors is the size of the electrolyte ions used in the EAP actuator. If the ions are too large they cannot fit within the polymer matrix and no ion storage or actuation occurs. Some EAP electrolytic cells are engineered such that only one species of electrolyte ion is capable of diffusing into the polymer. This simplifies the system by ensuring that a gradient of positive and negative ions are never simultaneously within the polymer. Certainly the dynamics of the system become more complicated if two (or more) species of ions are allowed to interact within the polymer. If two ionic species are able to flow within the polymer it is very difficult to determine the ionic state of the system as neutrality can still be maintained with both ionic species present within the polymer.

While it is clear that large electrolyte ions limit the speed of diffusion, another concern, which is presented in Chapter 3, is whether the incorporated ions are too small. Because the double layer

thickness is directly proportional to ion radius, small radii result in large capacitances. If the actuator capacitance becomes too large the number of ions needed to balance the applied potential may become a limiting factor. More ions mean more current, which can be a potential problem depending on the power source. More current also means that more power is dissipated due to ohmic losses. In addition, the need for more ions may require that more electrolyte be provided to the system, increasing weight. Certainly, there is an ideal ion size that allows for a tolerable diffusion rate while also maximizing strain and reducing losses and weight penalties. There are other factors affecting diffusion that allow for some flexibility in ion size.

Perhaps the most influential and easiest parameter to adjust is the thickness of the polymer. It has been shown by several authors that the diffusion rate has a quadratic dependence on the thickness of the polymer. Of course, while thinner samples have faster dynamics they are limited by the amount of load they can carry. Because of this it may be necessary to use many EAP actuators in parallel in order to provide useable forces for macroscale actuation. The resulting actuators would be remarkably similar to muscle fibers, which also have massively parallel architectures in order to provide sufficient load production. Potential limitations to this approach are the ability to manufacture extremely thin free-standing polymers and the ability to apply electrical contacts to large polymer arrays.

2.4 Polymer Synthesis

There are several techniques used to synthesize conducting polymers and other types of EAP. The most common method uses electrochemical deposition. This process is explained in detail by Reynolds *et al* [3]. The polymerization process begins with a solution containing an electrolyte and monomers of the desired polymer material. A working and counter electrode are immersed in the solution to complete the electrochemical circuit. Application of an electrical load causes oxidation of the monomer at the surface of the working electrode. Oxidation results in the removal of an electron from the monomer unit, yielding an unstable free-radical cation. Pairs of unstable ions group together to form dimers, which can then combine with other radical monomers, dimers, or oligomers. Eventually, insoluble polymer films are created.

The material used for all experimentation in this work was polypyrrole (PPy). Samples were prepared using electrochemical deposition onto a glassy carbon crucible. The solvent used during the polymerization process was propylene carbonate (PC). The electrolyte used was tetraethylammonium hexafluorophosphate ($TEAPF_6$). The solution used for electrochemical deposition consisted of 0.05M

$TEAPF_6$ (Aldrich) and 0.05M pyrrole monomer (Aldrich) in PC, plus 1% distilled water. The solution was prepared in a nitrogenous environment to prevent oxidation of the pyrrole monomer. Deposition took place at -40ºC, which has been found to improve the electrical properties of synthesized polymer. An electrical load of $0.125mA/cm^2$ was applied for 16 hours, yielding polymers with thicknesses ranging from 18 to 24μm. At these thicknesses the polymers are cohesive enough to be removed from the glassy carbon crucible and used as free standing films. The samples had mechanical stiffnesses of about 300 to 400 MPa. Conductivity of samples varied between about 800 and 1000 S/m.

2.5 Summary

Electrochemical processes are essential to the operation of ionic electro-active polymer actuators. The interactions in the electrical and chemical domains involve movement of electrical and ionic charge carriers in order to balance applied potentials. The movement of electrolyte ions becomes useful as these ions diffuse into the somewhat porous polymer material. The diffusion process results in volumetric strains, which can be utilized for mechanical actuation. Synthesis of ionic EAP materials has developed to the point that polymers with varying electrical and mechanical properties can be produced. With repeatable synthesis of materials that have controlled properties comes the ability to produce a high volume of actuators with desired actuation characteristics.

2.6 Chapter References

[1] Lyons, Michael E.G., "Charge Percolation in Electroactive Polymers," Chapter 1 in *Electroactive Polymer Electrochemistry, Part 1: Fundamentals*, Michael E.G. Lyons, Ed., New York: Plenum Press, 1994, 1-235.

[2] Bard, A.J. and L.R. Faulkner, *Electrochemical Methods, Fundamentals and Applications*, New York: Wiley, 1980.

[3] Reynolds, John R., Charles K. Baker, Cynthia A. Jolly, Paul A. Poropatic, and Jose P. Ruiz, "Electrically Conductive Polymers," Chapter 1 in *Conductive Polymers and Plastics*, James M. Margolis, Ed., New York: Chapman and Hall, 1989, 1-40.

Chapter 3

Modeling

The electrochemical and mechanical domains are modeled with low order reticulated structures. Bond graph notation is utilized to represent energy storage and dissipation elements in EAP systems. The coupling between electrical and mechanical domains is developed using a two-port capacitive energy storage element. Analytical results are compared to published analyses. Results apply specifically to a linear, elastic, isotropic actuator with an orthogonal geometry, though the method can be extended to other materials and geometries.

3.1 Simple Electrochemical Model

The entire electrochemical process can be described adequately using an electrical circuit model. Energy storage within the electrolytic cell is the result of interaction between ions and electrical charge carriers. These interactions involve stored potential energy and can therefore be modeled using capacitive circuit elements (possibly nonlinear). Significant energy storage occurs in three places in the EAP electrolytic cell. The first is at the surface of the polymer, where cations and electrons, or alternatively, anions and holes, form an electrochemical double layer with properties similar to a parallel plate capacitor. The second is at the counter electrode surface, where a double layer forms between the ion species and charge carrier not involved at the polymer surface. The third region of energy storage is within the bulk of the polymer, where diffused ions of the same species as those in the polymer double layer balance the electrical charge in the polymer.

There are also energy-dissipating elements in the system, which cause irreversible losses through entropy production. In the electrical domain these losses are the result of finite polymer conductivity and the bonding or contact resistance between the polymer and its electrical input terminals, which both result in ohmic losses. In the chemical domain irreversible losses result from movement of ions through solution (though this is generally a negligible contribution) and from the resistance associated with diffusion of electrolyte ions into the polymer.

The topology of the representative circuit model is determined by considering the electrochemical potentials and ionic currents in the system. The concentration of ions within the polymer volume is equal to the concentration in the polymer double layer such that these two regions are effectively at the same electrochemical potential. This indicates that there is a parallel structure between the polymer volumetric capacitance and polymer double layer capacitance. While the polymer volume and double layer both accept the same ion species, the counter electrode double layer is the only element that involves the remaining ion species. Therefore, the ionic current at the counter electrode double layer must balance the ionic currents in the polymer double layer and polymer volume. This indicates that the counter electrode double layer is in series with the other two capacitive elements. Similarly, resistances to electrical current in the polymer and to ionic current in the electrolyte depend on the total electrical current through the circuit; this also results in a series configuration. Resistance to ion diffusion does not limit ion flow within the electrolyte; therefore, this resistance is in parallel with the double layer capacitance and in series with the volumetric capacitance. The complete structure of the EAP electrochemical circuit is depicted in Figure 3-1.

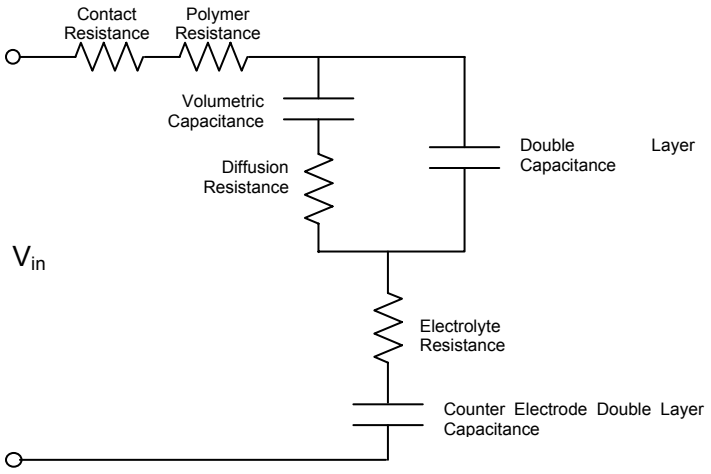

Figure 3-1: Basic Structure of EAP Electrochemical Circuit

The circuit can be represented using the bond graph structure presented in Figure 3-2(a), which demonstrates that the system can be put into full integral causality. This property allows the system to be represented by a set of differential equations. To determine the minimum number of states needed to describe the system it is put into maximum derivative causality, Figure 3-2(b). The number of energy storing elements that can be put into both derivative and integral causality determines the minimum system order required to describe the dynamics of the system. From Figure 3-2(b) it is clear that the counter electrode capacitance, C_E, does not contribute additional information about the

dynamics of the system; it is merely a free integrator. This makes sense intuitively because the amount of charge stored at the electrode double layer should be equal to the sum of the charge stored in the polymer double layer and within the polymer volume.

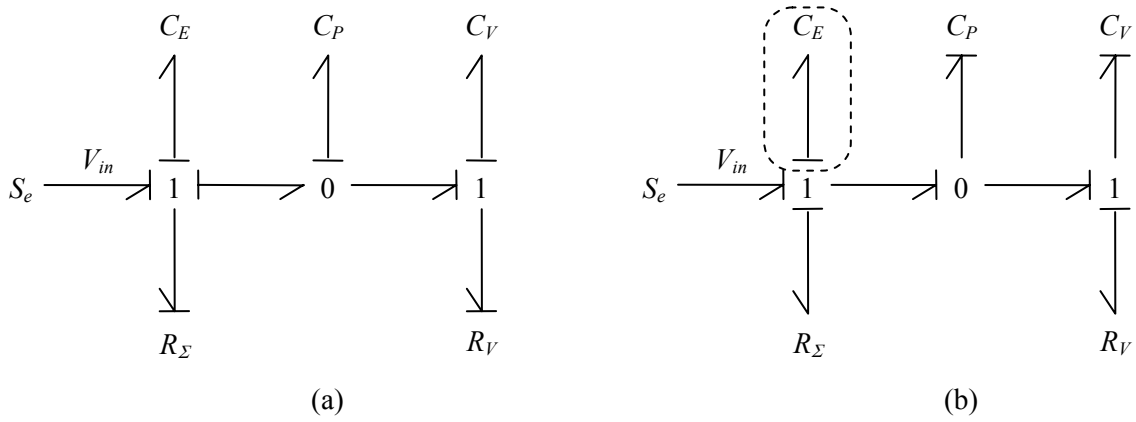

Figure 3-2: (a) Bond Graph Depiction of Simple EAP Electrochemical Circuit with Full Integral Causality. (b) Same Model with Maximum Derivative Causality to Determine Minimum System Order

With the knowledge that the charge stored in the counter electrode double layer is redundant, it is possible to use the two remaining states to express the dynamics of the system. A state-space equation for the simple EAP electrochemical circuit is as follows:

$$\begin{bmatrix} i_P \\ i_V \end{bmatrix} = \begin{bmatrix} -\frac{1}{R_\Sigma C_E} - \frac{1}{R_\Sigma C_P} - \frac{1}{R_V C_P} & -\frac{1}{R_\Sigma C_E} + \frac{1}{R_V C_V} \\ \frac{1}{R_V C_P} & -\frac{1}{R_V C_V} \end{bmatrix} \begin{bmatrix} q_P \\ q_V \end{bmatrix} + \begin{bmatrix} \frac{1}{R_\Sigma} \\ 0 \end{bmatrix} V_{in} \tag{3.1}$$

where R_Σ is the sum of R_E, R_P and R_C, C_E is the counter electrode double layer capacitance, C_P is the polymer double layer capacitance, and C_V and R_V are the total volumetric capacitance and diffusion resistance respectively. The double layer capacitances, C_P and C_E, are determined from the Helmholz model which takes the form of a parallel plate capacitor:

$$C_{P,E} = \frac{\kappa \varepsilon_0 A_{P,E}}{\delta_{P,E}} \tag{3.2}$$

where κ is the dielectric of the electrolyte solvent, which is the same everywhere in the EAP electrolytic cell; ε_0 is the permittivity of free space; A_P and A_E are the surface areas of the double-

layers, which depend on the dimensions of the electrodes; and δ_P and δ_E are the thicknesses of the double layers, which are generally assumed to be directly proportional to the radius of the ion species at the associated double layer. If the polymer is a free-standing film, both of its faces must be included in the polymer double layer surface area to determine the total polymer double layer capacitance. Dividing the capacitance of the double layer by its volume gives an ion concentration in the form of a specific volumetric capacitance with units of F/m^3:

$$c_V = \frac{\kappa\varepsilon_0}{\delta^2} \tag{3.3}$$

Since the concentration of ions within the polymer equilibrates with the concentration of ions in the double layer—as diffusion suggests—the total capacitance of the polymer is given by the product of polymer volume, V, and specific volumetric capacitance, c_V. For a free standing polymer film there are two double layers contributing to the double layer capacitance, so the effective surface area of the polymer is twice the actual area of the polymer face. Therefore, the total volumetric capacitance is given as:

$$C_V = \frac{\kappa\varepsilon_0}{\delta^2} V = C_P \frac{a}{2\delta} \tag{3.4}$$

The right hand side of this expression shows that the amount of ionic charge stored in the polymer volume is proportional to the ratio of the polymer thickness, a, and total double layer thickness (2δ for a free-standing polymer). Depending on the type of material used, polymer films typically need to be at least 1μm thick before they are mechanically cohesive enough to be used as free-standing films. Because the double layer thickness is typically only a few nanometers, the amount of charge stored in the double layer is usually several orders of magnitude less than the charge stored in the polymer volume. For this reason, it may be possible in some instances to further simplify the electrical circuit by removing the polymer double layer from the electrochemical model.

While the preceding circuit model is a sufficient first estimate of the electrochemical behavior of the system, the actual ionic diffusion process is better represented by a continuum model based on the solution of partial differential equations. Madden developed the following continuum-based frequency domain model to describe the admittance of a free-standing polymer film [1]:

$$Y(s) = \frac{s}{R} \frac{\frac{\sqrt{D}}{\delta} \cdot \tanh\left(\frac{a}{2} \cdot \sqrt{\frac{s}{D}}\right) + \sqrt{s}}{\frac{\sqrt{s}}{RC} + s^{3/2} + \frac{\sqrt{D}}{\delta} s \cdot \tanh\left(\frac{a}{2} \cdot \sqrt{\frac{s}{D}}\right)} \tag{3.5}$$

where s is the frequency domain variable, R is the total resistance of the circuit, C is the total volumetric capacitance, D is a coefficient characterizing the speed of diffusion, δ is the width of the double layer gap, and a is the thickness of the polymer. The admittance transfer function results from the solution of the Fick diffusion equation [2] for a free standing film, which has equal boundary conditions due to identical double layer potentials at each polymer face. The correlation between the linear circuit model and the continuum model is demonstrated in Figure 3-3, which shows the frequency response of polypyrrole admittance as predicted by the simple electrochemical circuit model along with the continuum diffusion model of admittance derived by Madden. The parameters used to generate this result are identical to those presented by Madden: R = 31 Ω, $c_V = 1.3\times10^8$ F/m^3, $D = 2.1\times10^{-12}$ m^2/s, $\delta = 2$ nm and $a = 8.5$ μm.

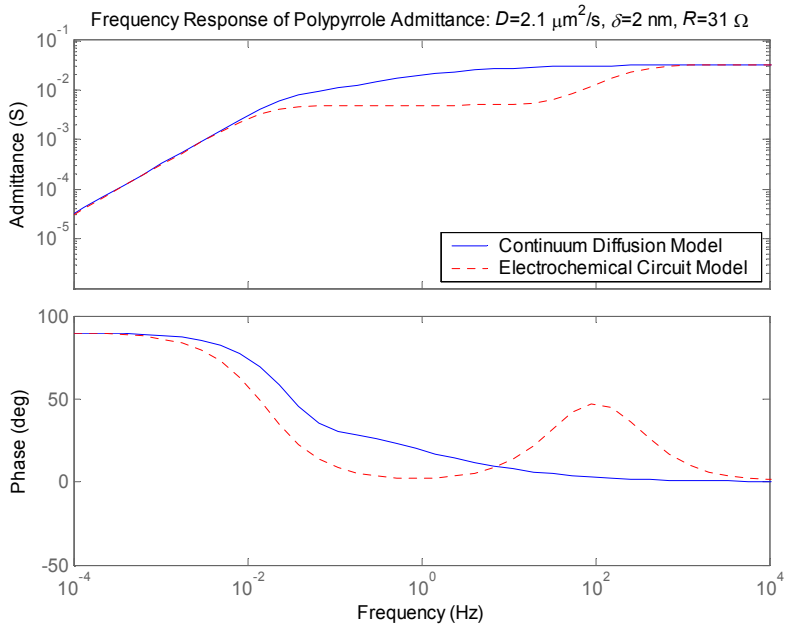

Figure 3-3: Frequency Response of Polypyrrole Admittance from Simple Electrochemical Circuit Model and Continuum Model

It is clear that for this set of parameters the two-state electrochemical circuit model is only able to capture the dynamics of the actuator at low and high frequencies. Although it is possible to use the continuum model of the polymer, it has some limitations in the information it provides. Specifically, the continuum admittance transfer function lumps all of the charge stored in the system into one state, which requires additional analysis to determine ion distribution in the polymer and the mechanical stresses and strains resulting from that ion distribution. It is much simpler from a controls perspective to use a low-order lumped parameter model because it allows for classical system analysis techniques and also allows for delineation of all the observable states. However, it is apparent from Figure 3-3 that a revised model is needed to better represent diffusion dynamics at mid-range frequencies.

3.2 Reticulated Diffusion Model

The simple electrochemical model introduced in Section 3.1 assumes uniform diffusion of ions from the polymer surface into the bulk of the polymer with a single time constant, $R_V C_V$. However, because diffusion does not occur instantaneously throughout the polymer it is best represented as a continuum process. Several authors have noted that diffusion in EAP is analogous to current traveling through a transmission line [1,3]. This can be modeled using a reticulated network of linear circuit elements [4]. The major benefit of using a reticulated network description of diffusion is that it allows for a state space representation of the EAP electrochemical domain rather than the continuum description. This enables the use of linear system analysis techniques and also provides more flexibility when considering how ions within the polymer generate mechanical loading and strains. Figure 3-4 illustrates the reticulation of a thin film polymer across its thickness in order to approximate diffusion into the film. The diffusion transmission line has the electrical circuit structure depicted in Figure 3-5 where voltage is equivalent to ion concentration and current corresponds to ion flow into the polymer. As the number of elements in the reticulated diffusion model increases, the predicted dynamics converge to the continuum model. This result is demonstrated in the following analysis using the "T"-network element depicted below in Figure 3-6a, which can be represented by the bond graph shown in Figure 3-6b.

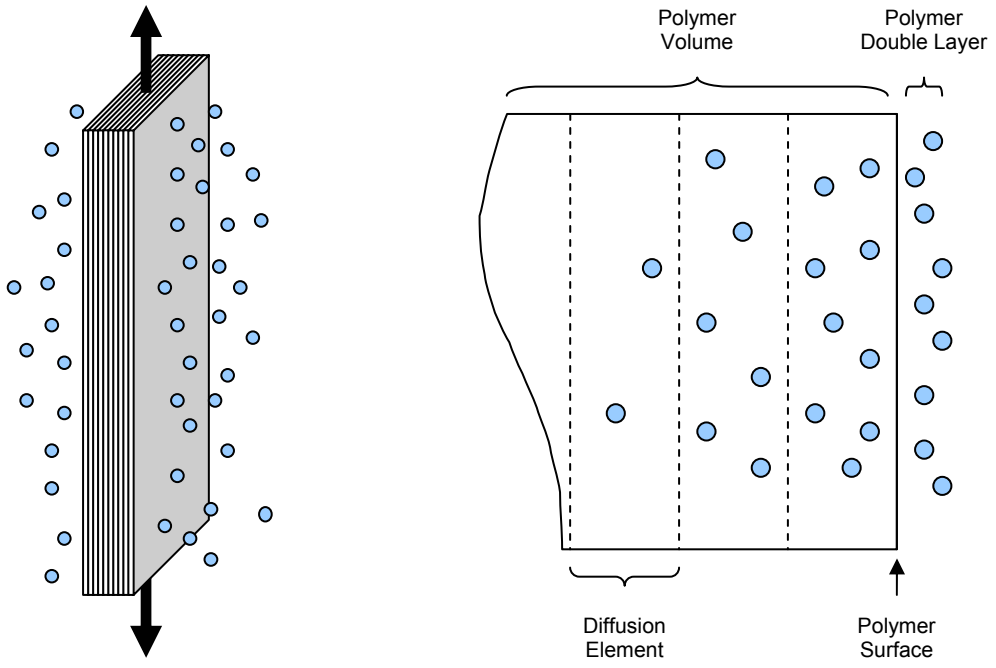

Figure 3-4: Reticulation of Thin-Film Polymer into Diffusion Elements

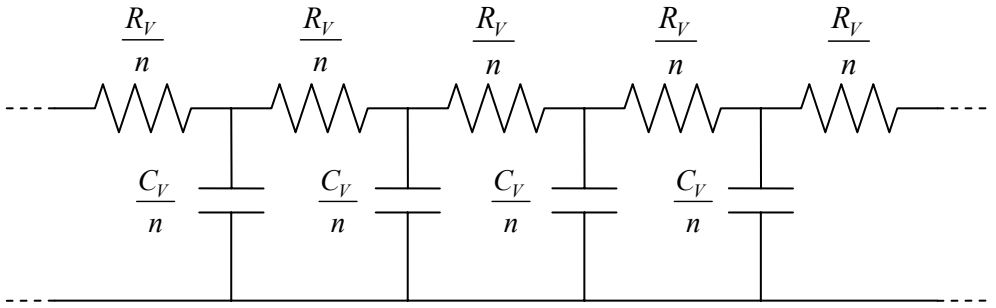

Figure 3-5: Electrical Circuit Model of Diffusion Elements

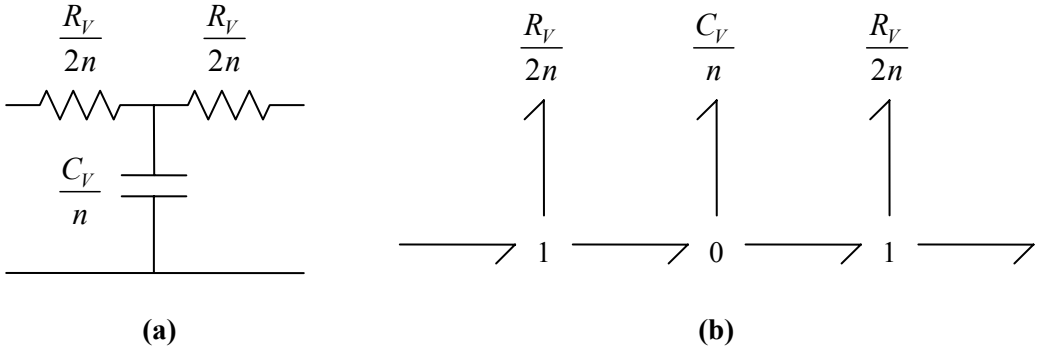

Figure 3-6: T-Network Transmission Line Element

The power equations for the individual circuit elements lead to the following transmission equations:

$\begin{bmatrix} V_{in} \\ i_{in} \end{bmatrix} = \begin{bmatrix} 1 & Z \\ 0 & 1 \end{bmatrix} \begin{bmatrix} V_{out} \\ i_{out} \end{bmatrix}$ where $Z = \frac{R_V}{2n}$ is the series impedance for the resistive elements.

$\begin{bmatrix} V_{in} \\ i_{in} \end{bmatrix} = \begin{bmatrix} 1 & 0 \\ Y & 1 \end{bmatrix} \begin{bmatrix} V_{out} \\ i_{out} \end{bmatrix}$ where $Y = \frac{sC_V}{n}$ is the shunt admittance for the capacitive elements and s is the Laplace variable.

Concatenating these matrices gives the following T-network transmission matrix:

$$\begin{bmatrix} 1 & Z \\ 0 & 1 \end{bmatrix} \begin{bmatrix} 1 & 0 \\ Y & 1 \end{bmatrix} \begin{bmatrix} 1 & Z \\ 0 & 1 \end{bmatrix} = \begin{bmatrix} 1+YZ & 2Z+YZ^2 \\ Y & 1+YZ \end{bmatrix} = \begin{bmatrix} 1+\frac{sR_VC_V}{2n^2} & \frac{R_V}{n}+\frac{R_V^2C_V}{4n^3} \\ \frac{sC_V}{n} & 1+\frac{sR_VC_V}{2n^2} \end{bmatrix} \tag{3.6}$$

This matrix is of the form:

$$M = \begin{bmatrix} \cosh\frac{\Gamma}{n} & Z_0 \sinh\frac{\Gamma}{n} \\ Y_0 \sinh\frac{\Gamma}{n} & \cosh\frac{\Gamma}{n} \end{bmatrix} \text{ where } Z_0 = Y_0^{-1} \tag{3.7}$$

Solving for Γ gives:

$$\Gamma = n \cosh^{-1}\left(1+\frac{sR_VC_V}{2n^2}\right) \tag{3.8}$$

To solve for Z_0, the upper triangular term is divided by the lower triangular term. From the inverse relationship of Z_0 and Y_0 this gives:

$$Z_0 = \sqrt{\frac{R_V}{sC_V}+\frac{R_V^2}{4n^2}} \tag{3.9}$$

As the number of elements in the transmission line network, n, approaches infinity, these values tend toward the actual transmission line delay parameter, Γ, and the impedance, Z_0:

$$\cosh\frac{\Gamma}{n} = 1 + \frac{1}{2}\left(\frac{\Gamma}{n}\right)^2 + \frac{1}{24}\left(\frac{\Gamma}{n}\right)^4 + \frac{1}{720}\left(\frac{\Gamma}{n}\right)^6 + \ldots = 1 + \frac{sR_VC_V}{2n^2}$$

$$1 + \frac{1}{2}\left(\frac{\Gamma}{n}\right)^2 \approx 1 + \frac{sR_VC_V}{2n^2} \tag{3.10}$$

$$\Gamma \to \sqrt{sR_VC_V}$$

$$Z_0 = \sqrt{\frac{R_V}{sC_V} + \frac{R_V^2}{4n^2}} \to \sqrt{\frac{R_V}{sC_V}} \tag{3.11}$$

Substituting these values into the finite length transmission matrix, M^n, leads to the following expression as n approaches infinity:

$$\begin{bmatrix} V_{in} \\ i_{in} \end{bmatrix} = \begin{bmatrix} \cosh\sqrt{sR_VC_V} & \sqrt{\frac{R_V}{sC_V}}\sinh\sqrt{sR_VC_V} \\ \sqrt{\frac{sC_V}{R_V}}\sinh\sqrt{sR_VC_V} & \cosh\sqrt{sR_VC_V} \end{bmatrix} \begin{bmatrix} V_{out} \\ i_{out} \end{bmatrix} \tag{3.12}$$

For the geometry considered in this analysis, both faces of the polymer are at the polymer double layer potential, V_P. Due to this symmetry, the input current, i_{in}, is equal and opposite to the current out, i_{out}, giving the following equality:

$$\begin{bmatrix} V_p \\ i_V \end{bmatrix} = \begin{bmatrix} \cosh\sqrt{sR_VC_V} & \sqrt{\frac{R_V}{sC_V}}\sinh\sqrt{sR_VC_V} \\ \sqrt{\frac{sC_V}{R_V}}\sinh\sqrt{sR_VC_V} & \cosh\sqrt{sR_VC_V} \end{bmatrix} \begin{bmatrix} V_P \\ -i_V \end{bmatrix} \tag{3.13}$$

By considering the reduction in input potential due to the other elements in the EAP circuit, V_P can be expressed in terms of V_{in}. The counter electrode double layer capacitance is not considered in order to give a result that is similar to Madden's analysis. Solving (3.13) for the complete system electrical inputs, V_{in} and i_{in}, leads to the following expression for the admittance transfer function (i_{in}/V_{in}):

$$\begin{bmatrix} V_P \\ \dfrac{i_{in} - sC_P V_P}{2} \end{bmatrix} = \begin{bmatrix} \cosh\sqrt{sR_V C_V} & \sqrt{\dfrac{R_V}{sC_V}}\sinh\sqrt{sR_V C_V} \\ \sqrt{\dfrac{sC_V}{R_V}}\sinh\sqrt{sR_V C_V} & \cosh\sqrt{sR_V C_V} \end{bmatrix} \begin{bmatrix} V_P \\ \dfrac{-i_{in} + sC_P V_P}{2} \end{bmatrix}$$

$$V_P\left(1 - \cosh\sqrt{sR_V C_V} - \frac{sC_P}{2}\sqrt{\frac{R_V}{sC_V}}\sinh\sqrt{sR_V C_V}\right) = -\left(\sqrt{\frac{R_V}{sC_V}}\sinh\sqrt{sR_V C_V}\right)\frac{i_{in}}{2}$$

$$\frac{i_{in}}{V_P} = \frac{-2 + 2\cosh\sqrt{sR_V C_V} + sC_P\sqrt{\dfrac{R_V}{sC_V}}\sinh\sqrt{sR_V C_V}}{\sqrt{\dfrac{R_V}{sC_V}}\sinh\sqrt{sR_V C_V}} = 2\sqrt{\frac{sC_V}{R_V}}\tanh\frac{\sqrt{sR_V C_V}}{2} + sC_P \qquad (3.14)$$

$$V_P = V_{in} - R_\Sigma i_{in}$$

$$\frac{i_{in}}{V_{in}} = \frac{2\sqrt{\dfrac{sC_V}{R_V}}\tanh\dfrac{\sqrt{sR_V C_V}}{2} + sC_P}{1 + 2R_\Sigma\sqrt{\dfrac{sC_V}{R_V}}\tanh\dfrac{\sqrt{sR_V C_V}}{2} + sR_\Sigma C_P} = \frac{s}{R_\Sigma}\cdot\frac{2\sqrt{\dfrac{C_V}{R_V C_P^2}}\tanh\dfrac{\sqrt{sR_V C_V}}{2} + \sqrt{s}}{\dfrac{\sqrt{s}}{R_\Sigma C_P} + 2\sqrt{\dfrac{C_V}{R_V C_P^2}}\cdot s\cdot\tanh\dfrac{\sqrt{sR_V C_V}}{2} + s^{3/2}}$$

This result is analogous to that presented by Madden, (3.5), with the following equivalencies:

$$\begin{aligned} 2\sqrt{\frac{C_V}{R_V C_P^2}} &= \frac{\sqrt{D}}{\delta} \rightarrow C_V = \left(\frac{DC_p^2}{4\delta^2}\right)R_V \\ \frac{\sqrt{R_V C_V}}{2} &= \frac{a}{2}\sqrt{\frac{1}{D}} \rightarrow \left(\frac{DC_p^2}{16\delta^2}\right)R_V^2 = \frac{a^2}{4D} \\ R_V &= \frac{2a\delta}{DC_P} \\ C_V &= C_P\frac{a}{2\delta} \end{aligned} \qquad (3.15)$$

Note that this value of C_V is equivalent to the value predicted in (3.4) for a free standing polymer film. These values of R_V and C_V can be used in the reticulated model of the diffusion process, which gives a low order description of the polymer electrochemical behavior. The bond graph of the polymer using a four element diffusion model is shown in Figure 3-7. This form can be extended to include more elements with symmetry allowing for a reduction in the number of energy storage and dissipation elements in the diffusion chain from *n* to (*n*+1)/2 for an odd number of elements or to *n*/2 for an even number of elements.

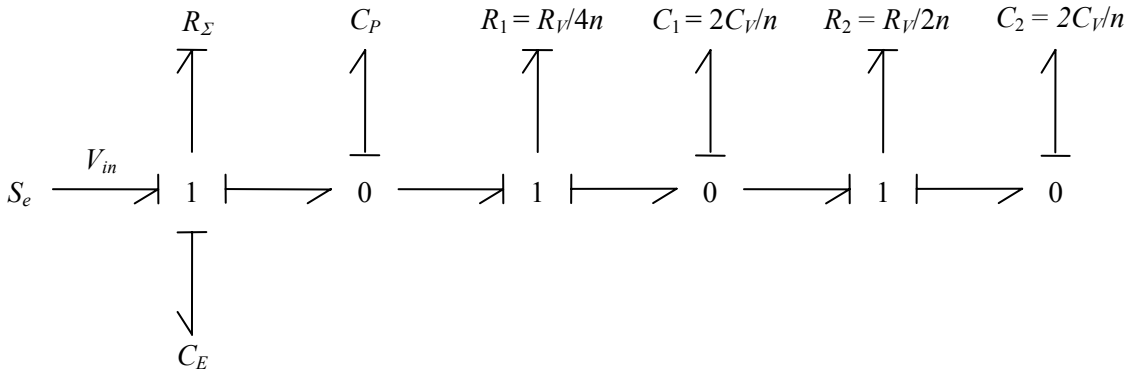

Figure 3-7: Bond Graph Representation of 4-Element Reticulated Electrochemical Diffusion Model

Although full integral causality in the bond graph indicates that there are four system states (corresponding to each of the capacitances), derivative causality demonstrates that one of the states is a free integrator (as shown previously in Figure 3-6b). The charge stored in the counter electrode double layer is equal to the sum of the charge stored in the other capacitors; therefore, a state space representation of the system is given by the following third order equation:

$$\begin{bmatrix} i_P \\ i_1 \\ i_2 \end{bmatrix} = \begin{bmatrix} -\frac{1}{R_\Sigma C_E} - \frac{1}{R_\Sigma C_P} - \frac{1}{R_V C_P} & \frac{1}{R_1 C_1} - \frac{1}{R_\Sigma C_E} & -\frac{1}{R_\Sigma C_E} \\ -\frac{1}{R_1 C_P} & -\frac{1}{R_1 C_1} - \frac{1}{R_2 C_1} & \frac{1}{R_2 C_2} \\ 0 & \frac{1}{R_2 C_1} & -\frac{1}{R_2 C_2} \end{bmatrix} \begin{bmatrix} q_P \\ q_1 \\ q_2 \end{bmatrix} + \begin{bmatrix} \frac{1}{R_\Sigma} \\ 0 \\ 0 \end{bmatrix} V_{in} \qquad (3.16)$$

where R_1, R_2, C_1, and C_2 are the equivalent resistances and capacitances of the first and second elements in the simplified four element diffusion model depicted in Figure 3-7.

Using this approach the linear reticulated model converges to the continuum model as the number of diffusion elements increases. This is clearly shown in Figure 3-8, which shows the frequency response of the basic electrochemical circuit model from (3.1), the continuum model in (3.5), and two variations of the reticulated diffusion model. The parameters used for this simulation are identical to those listed previously for Figure 3-3.

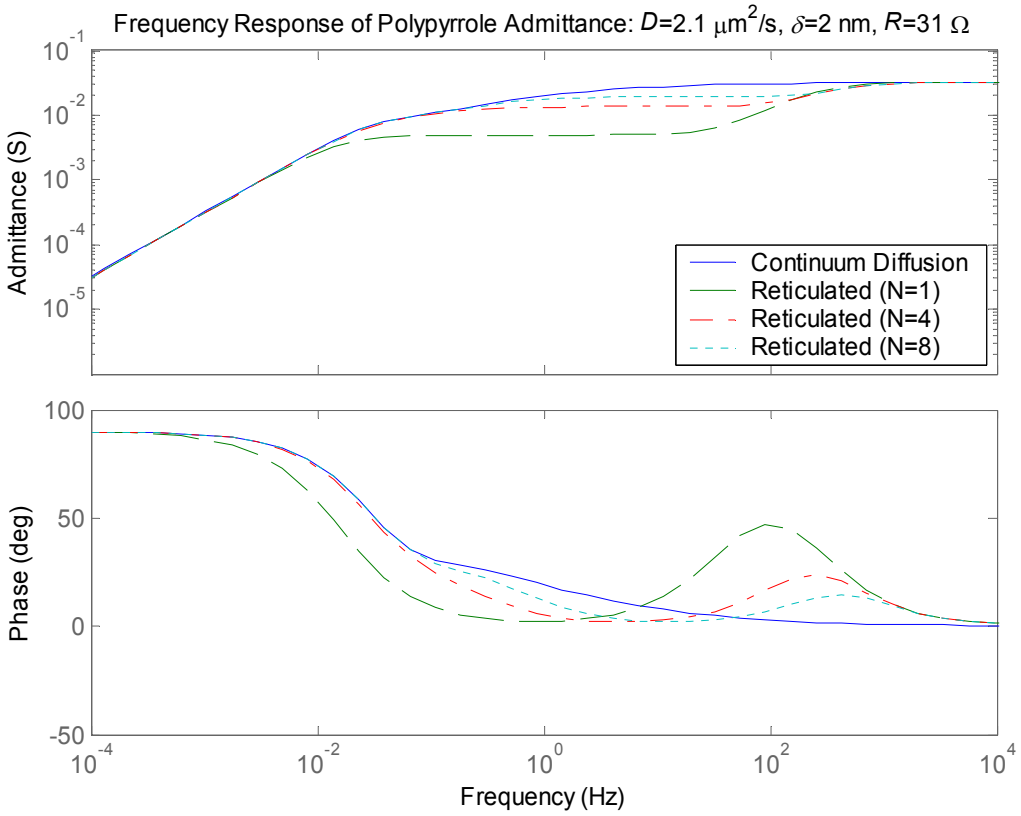

Figure 3-8: Frequency Response of Polypyrrole Admittance for Reticulated and Continuum Models

Use of a low order linear model increases computational processing speed, which is valuable for real-time control of an EAP actuator. More importantly, the reticulated model provides an easily solvable set of ordinary differential equations to describe ion diffusion in the system. This is essential to modeling the response of the polymer to a variety of time domain inputs. In addition, the reticulated model explicitly describes the profile of ion concentration throughout the polymer. It will be demonstrated in Section 3.6 that this critical to determining the electrochemically-induced strain.

3.2.1 Counter Electrode Dynamics

One element included in this model that is absent in Madden's model is the counter electrode double layer. This may have been ignored by Madden because the majority of his work was performed on systems using a potentiostat, which eliminates the dynamics at the double layer by referencing all potentials to the reference electrode. However, when used in a portable device it is likely that potentials will be applied relative to the counter electrode, which will require its inclusion in the system model. Additionally, it is probable that the counter electrode double layer will have a

capacitance on the same order of magnitude as the polymer double layer making this a significant contributor to the time response of the system and to the input potentials required.

Another possibility is that EAP materials will be used for both electrodes [5]. In this configuration, the polymers can alternate as the working and counter electrodes and operate like opposing muscles. Given the preceding model of the polymer it is relatively easy to extend the electrical model to an EAP counter electrode to develop a full model of this configuration. While it may be valuable to use EAP as the working and counter electrodes, special attention must be given to the treatment of positive and negative ions in the system. As discussed in Section 2.3, the diffusion of either type of ion into the polymer results in positive strains. If only one species of ion is small enough to enter the polymer, this problem is simple to deal with. However, for an electrolyte with two viable diffusive ions the system becomes more complicated and difficult to analyze.

3.3 Electro-Mechanical Coupling

The reticulated circuit model presented in Section 3.2 sufficiently describes the electrical response of the polymer; however, as an actuator, the electrical to mechanical coupling is essential to understanding the system. Polymer strains result from both ion diffusion into the bulk of the polymer and forces applied to the polymer. This suggests that a multi-port energy storage element, loosely analogous to a variable-gap capacitor, can describe the interaction between the electrical and mechanical domains. The bond graph shown in Figure 3-9 depicts the EAP actuator as a two-port capacitor with a multi-bond on the mechanical side to allow application of forces in all three dimensions.

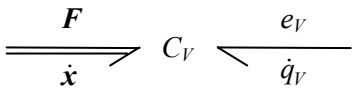

Figure 3-9: Bond Graph Representation of an EAP Actuator as a Two-Port Compliance, with a Multi-bond in the Mechanical Domain to Account for Three-Dimensional Stress-Strain Relations

It has been found that there is an appreciable coupling from the electrical to mechanical domain in EAP. However, it has also been noted that in samples subjected to uniaxially-applied loads there is very little back effect. As an energy storing transducer, the EAP actuator should exhibit equivalent energy transduction between domains. This seems to suggest that there are significant losses at the mechanical port that are not being accounted for. There is no apparent mechanism for loss in the

actuator, and the available data does not show substantial heating due to entropy production. This indicates that for mechanical inputs most of the energy is being stored rather than lost or converted to electrical energy. After considering the mechanics of the system and realizing that electrical energy storage depends on the volume rather than the length of the polymer, it is theorized that the apparent asymmetry in the coupling is actually the result of Poisson's Effect. This geometric coupling effect describes how the dimensions of an object will change under a uniaxial load. A material with Poisson's ratio (ν) of 0.5 will exhibit no change of volume under load, while an object with a ratio near zero will have a volumetric strain equal to the imposed linear strain, as the other dimensions remain constant. Most polymeric materials have large Poisson's ratios such that linear strains result in minimal volume changes. In the case of an EAP this would result in minimal electrical effects for large linear strains. However, electrical inputs would produce strains in all three dimensions, only one of which is utilized in a linear actuator. While this is perceived as an asymmetry in coupling, which would invalidate the claim that EAP are simply energy-storing transducers, it is actually a symmetric coupling that is very sensitive to electrical inputs and insensitive to axially-applied loads. To examine this theory of EAP coupling behavior, constitutive equations were formulated using conservation of energy principles. This requires an examination of the energy stored in the polymer in electrical and mechanical form.

By storing ionic charge the polymer acts as a capacitor with total volumetric capacitance, C_V, determined by the product of its specific volumetric capacitance, c_V (F/m^3), and volume, V. The steady-state charge stored within the polymer is then related to the applied potential according to the following constitutive equation:

$$e_V = \frac{q_V}{c_V V} \tag{3.17}$$

where e_V is the electrochemical potential at the polymer double layer, q_V is the charge stored in the polymer, c_V is the specific volumetric capacitance, and V is the polymer volume. The specific volumetric capacitance is determined by the ion concentration in the polymer double-layer, which depends on the size of the ions and the applied potential. In the potential range that most EAP operate the specific volumetric capacitance can be considered constant, which is the assumption used in this analysis.

It is very important to note that the electrochemical potential, e_V, is measured relative to the potential of zero charge (PZC) of the electrochemical cell. The PZC is the potential at which the concentration

of ions in the polymer double layer, and thus in the polymer, is neutral. This is essentially the ground state of an EAP electrochemical cell. The PZC should not be confused with the open-cell potential (OCP) of the EAP system. The OCP demonstrates the preferred state of the polymer, which may favor an oxidized or reduced state. Determination of the PZC in an EAP electrochemical cell can be difficult, but it can be accomplished by examining the strain of the polymer, which will be demonstrated in Chapter 4.

The electrochemical energy stored in the EAP actuator is readily obtained from (3.17). However, because the volume of the polymer is also a function of the force applied (through stress-strain relations), the charge and voltage also depend on mechanical loading. To evaluate the coupling between the domains, the energy stored in both the electrical and mechanical domains must be determined. The electrical potential energy is found by integrating potential with respect to charge while assuming constant volume:

$$\mathrm{E}_e = \int e_V \mathrm{d}q_V = \frac{q_V^2}{2c_V V} \tag{3.18}$$

In the mechanical domain, potential energy is contributed by the deformation of the polymer, which is assumed to be a linear, elastic, isotropic material in order to simplify the analysis. While this may not be a valid description of the material, it will allow insight that more complicated models do not[*]. A similar analysis can be performed for a material with non uniform properties and it will be shown in Section 3.6 that viscoelastic effects are also easy to add to the dynamic model.

Using a simplified description of EAP mechanical properties gives the familiar strain energy equation:

$$\mathrm{E}_\varepsilon = \int F_x \mathrm{d}x + \int F_y \mathrm{d}y + \int F_z \mathrm{d}z \tag{3.19}$$

which, in terms of stresses and strains, becomes:

---

[*] The mechanism for electrochemically-induced strains in conducting polymers favors the direction of the polymer chain. Several researchers are working towards stretch-aligning the polymers in order to provide maximum uniaxial strain. This produces considerable anisotropy, which should be taken into account when formulating the constitutive equations for these materials.

$$\mathrm{E}_{\varepsilon} = V_0\left(\int \sigma_x \mathrm{d}\varepsilon_{xx} + \int \sigma_y \mathrm{d}\varepsilon_{yy} + \int \sigma_z \mathrm{d}\varepsilon_{zz}\right) \tag{3.20}$$

To solve for the strain energy the stresses and strains are rewritten in terms of volumetric and deviatoric components. The volumetric strain is proportional to the mean stress, while the deviatoric stresses deform the polymer along the principle axes without changing its volume.

$$\mathrm{E}_{\varepsilon} = V_0\left(\int S_x \mathrm{d}\varepsilon'_{xx} + \int S_y \mathrm{d}\varepsilon'_{yy} + \int S_z \mathrm{d}\varepsilon'_{zz} + \int \sigma_m \mathrm{d}\varepsilon_V\right) \tag{3.21}$$

where, assuming small strains:

$$\varepsilon_V = \varepsilon_{xx} + \varepsilon_{yy} + \varepsilon_{zz} \tag{3.22}$$

$$\sigma_m = \frac{\sigma_x + \sigma_y + \sigma_z}{3} \tag{3.23}$$

$$S_{x,y,z} = \sigma_{x,y,z} - \sigma_m \tag{3.24}$$

$$\varepsilon'_{xx,yy,zz} = \varepsilon_{xx,yy,zz} - \frac{\varepsilon_V}{3} \tag{3.25}$$

Hooke's Law for stress-strain relations describes geometric changes resulting from the Poisson Effect. For a triaxially loaded isotropic material the relationship between directional stresses and strains is as follows:

$$\begin{bmatrix} \varepsilon_{xx} \\ \varepsilon_{yy} \\ \varepsilon_{zz} \end{bmatrix} = \frac{1}{E}\begin{bmatrix} 1 & -\nu & -\nu \\ -\nu & 1 & -\nu \\ -\nu & -\nu & 1 \end{bmatrix}\begin{bmatrix} \sigma_x \\ \sigma_y \\ \sigma_z \end{bmatrix} \tag{3.26}$$

Using this equation along with (3.22) and (3.23), the volumetric strain can be expressed solely in terms of the mean stress:

$$\varepsilon_V = \varepsilon_{xx} + \varepsilon_{yy} + \varepsilon_{zz} = \frac{1}{E}\left(\sigma_x + \sigma_y + \sigma_z - 2\nu\left(\sigma_x + \sigma_y + \sigma_z\right)\right) = \frac{3(1-2\nu)}{E}\sigma_m \tag{3.27}$$

Similarly, the deviatoric strains can be expressed in terms of deviatoric stresses. First the actual strain is expressed in terms of deviatoric and mean stress using (3.26) and (3.24):

$$\varepsilon_{xx} = \frac{1}{E}\left(\sigma_x - \nu\left(\sigma_y + \sigma_z\right)\right) = \frac{1}{E}\left((1+\nu)S_x + (1-2\nu)\sigma_m\right) \tag{3.28}$$

Substituting (3.27) and (3.28) back into (3.25) gives:

$$\varepsilon'_{xx} = \frac{1}{E}\left((1+\nu)S_x + (1-2\nu)\sigma_m\right) - \frac{(1-2\nu)}{E}\sigma_m = \frac{(1+\nu)S_x}{E} \tag{3.29}$$

Similar constitutive equations exist for the deviatoric components in the *y* and *z* direction. From these relations the strain energy becomes:

$$\mathrm{E}_\varepsilon = V_0\left(\frac{E}{1+\nu}\frac{\varepsilon'^2_{xx} + \varepsilon'^2_{yy} + \varepsilon'^2_{zz}}{2} + \frac{E}{3(1-2\nu)}\frac{{\varepsilon_V}^2}{2}\right) \tag{3.30}$$

The total potential energy stored in the polymer is the sum of the electrical potential energy and the strain energy:

$$\mathrm{E}_{total} = \frac{q_V^2}{2c_V V} + V_0\left(\frac{E}{1+\nu}\frac{\varepsilon'^2_{xx} + \varepsilon'^2_{yy} + \varepsilon'^2_{zz}}{2} + \frac{E}{3(1-2\nu)}\frac{{\varepsilon_V}^2}{2}\right) \tag{3.31}$$

This can be rewritten in terms of true energy variables (displacements):

$$\begin{aligned}\mathrm{E}_{total} = {} & \frac{q_V^2}{2c_V V_0\left(1 + \frac{\Delta x}{x_0} + \frac{\Delta y}{y_0} + \frac{\Delta z}{z_0}\right)} + \frac{V_0 E}{6(1-2\nu)}\left(\frac{\Delta x}{x_0} + \frac{\Delta y}{y_0} + \frac{\Delta z}{z_0}\right)^2 + \ldots \\ & \frac{V_0 E}{2(1+\nu)}\left[\left(2\frac{\Delta x}{3x_0} - \frac{\Delta y}{3y_0} - \frac{\Delta z}{3z_0}\right)^2 + \left(2\frac{\Delta y}{3y_0} - \frac{\Delta x}{3x_0} - \frac{\Delta z}{3z_0}\right)^2 + \left(2\frac{\Delta z}{3z_0} - \frac{\Delta x}{3x_0} - \frac{\Delta y}{3y_0}\right)^2\right]\end{aligned} \tag{3.32}$$

The effort variables—e_V, F_x, F_y, and F_z—are found by differentiating the total potential energy with respect to their associated displacement variables—q_V, Δx, Δy, and Δz:

$$e_V = \frac{q_V}{c_V xyz} \tag{3.33}$$

$$F_x = -\frac{q_V^2}{2c_V x^2 yz} + \frac{Ey_0 z_0}{(1+\nu)(1-2\nu)}\left[\frac{\Delta x}{x_0}(1-\nu) + \nu\left(\frac{\Delta y}{y_0} + \frac{\Delta z}{z_0}\right)\right] \tag{3.34}$$

$$F_x = -\frac{q_V^2}{2c_V x^2 yz} + \frac{Ey_0 z_0}{(1+\nu)(1-2\nu)}\left[\frac{\Delta y}{y_0}(1-\nu) + \nu\left(\frac{\Delta x}{x_0} + \frac{\Delta z}{z_0}\right)\right] \tag{3.35}$$

$$F_x = -\frac{q_V^2}{2c_V x^2 yz} + \frac{Ey_0 z_0}{(1+\nu)(1-2\nu)}\left[\frac{\Delta z}{z_0}(1-\nu) + \nu\left(\frac{\Delta x}{x_0} + \frac{\Delta z}{z_0}\right)\right] \tag{3.36}$$

In terms of stresses and strains, the effort variables are converted as follows:

$$e_V = \frac{q_V}{c_V V_0 (1+\varepsilon_V)} \tag{3.37}$$

$$\sigma_{x,y,z} = -\frac{q_V^2}{2c_V V_0^2 (1+\varepsilon_V)^2} + \frac{E\left((1-2\nu)\varepsilon_{xx,yy,zz} + \nu\left(\varepsilon_{xx} + \varepsilon_{yy} + \varepsilon_{zz}\right)\right)}{(1+\nu)(1-2\nu)} \tag{3.38}$$

Solving (3.37) for q_V and substituting it into (3.38) leads to a more tractable set of constitutive equations that have a linear dependence on strain:

$$\sigma_{x,y,z} = -\frac{c_V e_V^2}{2} + \frac{E\left((1-2\nu)\varepsilon_{xx,yy,zz} + \nu\left(\varepsilon_{xx} + \varepsilon_{yy} + \varepsilon_{zz}\right)\right)}{(1+\nu)(1-2\nu)} \tag{3.39}$$

These directional stress equations can be solved for any set of boundary conditions.

The uniaxial loading case is of particular interest when using the polymer as a linear actuator. The solution to this condition is found by realizing that the strains in the *y* and *z* directions are equal and that the stresses in these directions are identically zero. Using these input conditions the stress in the *x* direction simplifies to:

$$\sigma_x = \frac{E}{(1+\nu)}\left(\varepsilon_{xx} - \varepsilon_{yy}\right) \tag{3.40}$$

The strain in the *y* or *z* direction can be expressed in terms of the strain in the *x* direction:

$$\varepsilon_{yy,zz} = \frac{(1+\nu)(1-2\nu)c_V e_V^2}{2E} - \nu\varepsilon_{xx} \tag{3.41}$$

Substituting this into (3.40) yields:

$$\sigma_x = -\frac{(1-2\nu)c_V e_V^2}{2} + E\varepsilon_{xx} \tag{3.42}$$

Solving for the strains:

$$\varepsilon_{xx} = \frac{(1-2\nu)c_V e_V^2}{2E} + \frac{\sigma_x}{E} \tag{3.43}$$

$$\varepsilon_{yy,zz} = \frac{(1-2\nu)c_V e_V^2}{2E} - \nu\frac{\sigma_x}{E} \tag{3.44}$$

$$\varepsilon_V = \frac{3(1-2\nu)c_V e_V^2}{2E} + \frac{(1-2\nu)\sigma_x}{E} \tag{3.45}$$

Examining the volumetric strain equation, (3.45), it is apparent that it has the form of a uniaxially-loaded object also subjected to a hydrostatic pressure. The bulk modulus of the polymer is given by

$$K = \frac{E}{3(1-2\nu)} \tag{3.46}$$

Thus the hydrostatic pressure term is:

$$P = \frac{c_V e_V^2}{2} \tag{3.47}$$

Solving (3.45) in terms of the polymer volume yields:

$$V = V_0\left(1 + \frac{(1-2\nu)}{E}\left(\frac{3}{2}c_V e_V^2 + \sigma_x\right)\right) \tag{3.48}$$

From the electrical constitutive equation, (3.37), the electrical charge is proportional to the product of electrical potential and volume. Therefore,

$$q_V = c_V e_V V_0\left(1 + \frac{(1-2\nu)}{E}\left(\frac{3}{2}c_V e_V^2 + \sigma_x\right)\right) \tag{3.49}$$

It is apparent from this expression that the magnitude of coupling from the mechanical to electrical domain is highly dependent on Poisson's ratio. For high values of Poisson's ratio, there is minimal volume change as a result of uniaxial loading and, therefore, negligible change in electrical charge stored.

From this analysis it is evident where the *apparent* asymmetry in coupling arises for a uniaxially-loaded EAP. To demonstrate that the coupling between domains is actually symmetric, the generalized compliance matrix is determined. Equations (3.43) and (3.49) are rewritten in terms of the generalized displacement variables for a uniaxially-loaded EAP (q_V and Δx) and their respective efforts (e_V and F_x):

$$q_V = c_V e_V V_0\left(1 + \frac{(1-2\nu)}{E}\left(\frac{3}{2}c_V e_V^2 + \frac{F_x}{y_0 z_0}\right)\right) \tag{3.50}$$

$$\Delta x = x_0\left(\frac{(1-2\nu)c_V e_V^2}{2E} + \frac{F_x}{y_0 z_0 E}\right) \tag{3.51}$$

The generalized compliance matrix is the Jacobian, found by taking the gradient of these displacement variables with respect to the efforts:

$$\begin{bmatrix} q_V \\ \Delta x \end{bmatrix} = \begin{bmatrix} c_V V_0 + \dfrac{9(1-2\nu)V_0 c_V^2 e_V^2}{2E} + \dfrac{(1-2\nu)x_0 c_V F_x}{E} & \dfrac{(1-2\nu)x_0 c_V e_V}{E} \\ \dfrac{(1-2\nu)x_0 c_V e_V}{E} & \dfrac{x_0}{y_0 z_0 E} \end{bmatrix} \begin{bmatrix} e_V \\ F_x \end{bmatrix} \tag{3.52}$$

This matrix is clearly symmetric, which indicates that the coupling between the electrical and mechanical domains is symmetric. To analyze the nature of the perceived asymmetry in the coupling it is necessary to examine the sensitivity of this matrix to input conditions and parameters. The magnitude of coupling is highly dependent on Poisson's ratio due to the quantity (1-2ν) in the off-diagonal elements of the compliance matrix. In fact, for ν equal to 0.5 there is no coupling between domains as this term goes to zero. Because EAP are polymeric materials with ratios near 0.5, uniaxial loading has only a minimal effect on the charge stored in the polymer.

The generalized compliance represents a linearization about a particular operating point, so the coupling terms are also dependent on initial conditions. For instance, when the polymer is at the PZC, there is no charge stored within the polymer and the coupling terms between electrical and mechanical domains again go to zero. The cross-coupling term in the compliance matrix can be evaluated for a set of operating points given the following EAP parameters:

$$\begin{aligned} x_0 &= 0.012 \quad \text{m} \\ y_0 &= 0.0035 \quad \text{m} \\ z_0 &= 0.000019 \quad \text{m} \\ \nu &= 0.426 \\ c_V &= 1.3\times 10^8 \quad \text{F/m}^3 \\ E &= 0.18 \quad \text{GPa} \end{aligned} \tag{3.53}$$

The coupling term varies linearly with electrical potential and does not vary with force as seen in (3.52). The relationship between the coupling term and applied potential for the preceding set of parameters is as shown in Table 3-1.

Table 3-1: Variation in Coupling Term versus Electrical Input

Potential (V)	Coupling Term
0	0
0.2	0.000257
0.4	0.000514
0.6	0.000770

From this set of coupling terms it is possible to determine the effect that small changes in potential have on displacement. Near zero potential (PZC) a 0.1 Volt increase in potential will result in a negligible amount of linear displacement (none according to Table 3-1). With an initial potential of 0.2 Volts the addition or subtraction of 0.1 Volt results in a positive or negative displacement of about 25.7 μm (±0.2%). At 0.4 Volts the effect of a 0.1 Volt change in potential is a displacement of 51.4 μm (±0.4%). Similarly, at 0.6 Volts the change is 77.0 μm (±0.6%). Plotting this trend gives the relationship between potential and displacement that is seen in Figure 3-10. By considering infinitesimal changes in potential this curve will become the quadratic relationship described by the original nonlinear constitutive equation.

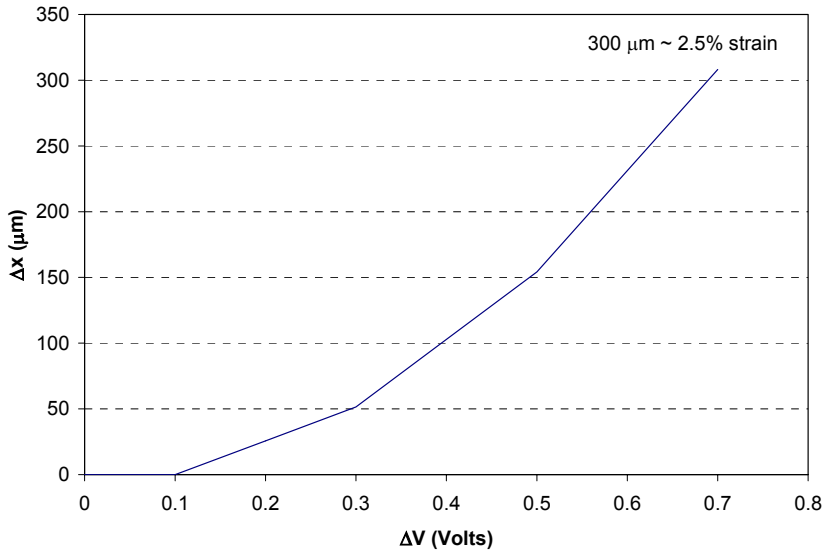

Figure 3-10: Displacement versus Electrical Potential from Generalized Compliance Matrix

At any potential the change in charge versus force is linear. For instance, at a potential of 0.2 Volts the charge varies linearly with force with a slope of 0.000257 C/N. The force needed to produce a strain of 2.5% is only about 0.3 N for the parameters considered; therefore, with a linear strain of

about 2.5% only 0.000077 Coulombs of charge are added to the EAP. If the applied potential is higher, the amount of coupling is also increased. From Figure 3-10, a strain of 2.5% results from a potential of 0.7 Volts with no mechanical force applied. The charge corresponding to this potential is about 0.078 Coulombs. If a 0.3 N force is then applied, in effect doubling the strain, the change in charge is only 0.00027 Coulombs. This is more than two orders of magnitude smaller than the charge needed to produce the same strain! While this appears to be an asymmetry in the coupling between domains it is simply the result of the Poisson Effect, which allows the polymer to stretch under load with very little change in volume. Clearly, the proposed model of EAP is able to describe the interesting "asymmetry" observed in EAP.

3.4 EAP Figure of Merit (FOM)

To compare EAP to other actuators and transducers such as piezoelectric materials their figure of merit can be determined. The figure of merit is a dimensionless number that quantifies the amount of coupling between energy domains. From the generalized compliance matrix, (3.52), the figure of merit is determined by dividing the product of the off-diagonal terms by the product of the diagonal terms. Because the off-diagonal terms in EAP depend on the voltage applied, the figure of merit also varies with voltage.

While the uniaxial loading condition allows for the evaluation of EAP as linear actuators, there are other loading conditions that may prove to be more valuable for other EAP applications. For instance, under hydrostatic loading, EAP deform uniformly in all directions, which diminishes the influence of the Poisson Effect. To evaluate the merit of EAP under hydrostatic loading, the constitutive equations and generalized compliance matrix are found by assuming that the stresses and strains in all directions are uniform. The resulting constitutive equations, with q_V and ΔV as displacement variables, are as follows:

$$\Delta V = V_0\left(1+\frac{3(1-2\nu)}{E}\left(\frac{c_V e_V^2}{2}+\sigma\right)\right) \tag{3.54}$$

$$q_V = c_V e_V V_0\left(1+\frac{3(1-2\nu)}{E}\left(\frac{c_V e_V^2}{2}+\sigma\right)\right) \tag{3.55}$$

The associated generalized compliance matrix is found by taking the gradient of these displacements with respect to e_V and σ, which is the uniform hydrostatic pressure:

$$\begin{bmatrix} q_V \\ \Delta V \end{bmatrix} = \begin{bmatrix} c_V V_0 + \dfrac{9(1-2\nu)V_0 c_V^2 e_V^2}{2E} + \dfrac{3(1-2\nu)c_V\sigma}{E} & \dfrac{3(1-2\nu)V_0 c_V e_V}{E} \\ \dfrac{3(1-2\nu)V_0 c_V e_V}{E} & \dfrac{3(1-2\nu)V_0}{E} \end{bmatrix} \begin{bmatrix} e_V \\ \sigma \end{bmatrix} \tag{3.56}$$

The generalized compliance matrices for the uniaxial loading and hydrostatic loading cases are used to find the figure of merit versus applied potential as seen in Table 3-2. These values are for the parameter set that was listed in (3.53).

Table 3-2: Variation in Figure of Merit versus Electrical Input for a Uniaxially- and Hydrostatically-Loaded Polymer

Potential (V vs. PZC)	Uniaxial FOM	Hydrostatic FOM
0	0	0
0.2	0.00062	0.01258
0.4	0.00235	0.04764
0.6	0.00485	0.09840
0.8	0.00774	0.15692
1.0	0.01068	0.21652
5.0	0.03036	0.61548
10.0	0.03222	0.65309
15.0	0.03259	0.66056
20.0	0.03272	0.66322

Plotting the FOM versus potential, Figure 3-11, demonstrates the asymptotic behavior of the FOM as it approaches a theoretical maximum determined by the form of the generalized compliance matrix. It is clear from Figure 3-11 that EAP are much better transducers when loaded hydrostatically than when loaded uniaxially. The coupling constant for hydrostatic loading is about 20 times greater than the coupling constant associated with a uniaxially-loaded polymer. The limit on the figure of merit for the hydrostatic case approaches 0.66, which is more than double the FOM for most piezoelectric materials.

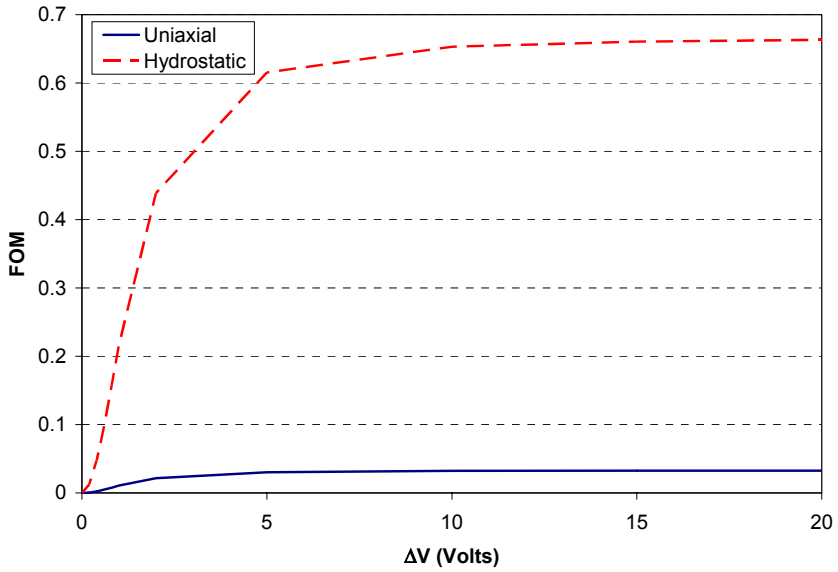

Figure 3-11: Figure of Merit versus Electrical Potential for Uniaxial and Hydrostatic Loading

The hydrostatic FOM is limited by the middle term of the upper diagonal element in the compliance matrix. This term provides a fixed coupling of 0.66 at all potentials:

$$\text{FOM} = \left(\frac{E}{3(1-2\nu)c_V e_V^2} + \frac{3}{2} + \frac{\sigma}{c_V V_0 e_V^2} \right)^{-1} \tag{3.57}$$

At high potentials the middle term dominates due to the inverse quadratic dependence on e_V in the other two terms. Unfortunately, the limit on applied potentials at the double-layer is between 1-2V due to polymer breakdown. Such a low potential does not allow the theoretical maximum cross-coupling to be achieved for the set of parameters used in this analysis. However, improvement can be made by increasing the specific capacitance, c_V, as this term also reduces the effects from the first and last terms in the FOM. To increase the specific capacitance a solvent with higher dielectric constant can be used, or the double-layer thickness can be reduced, which is effectively accomplished by utilizing an electrolyte with smaller ions. It is also clear that the polymer volume, elasticity, Poisson's ratio and applied stress have some impact on the figure of merit.

3.5 Electromechanical Coupling Model Validation

To validate the result of the electromechanical coupling analysis, it is compared to previously published results. The uniaxially loaded polymer has been examined thoroughly by Madden [1] and

Mazzoldi *et al* [6]. These authors describe the coupling from charge to strain using similar linear models:

$$\varepsilon_{xx} = \frac{\alpha q_v}{V} + \frac{\sigma_x}{E} \tag{3.58}$$

where α is an empirically derived constant. This can be compared to (3.43), which in terms of charge is given by the following:

$$\varepsilon_{xx} = \frac{(1-2\nu)q_V^2}{2Ec_V V^2} + \frac{\sigma_x}{E} \tag{3.59}$$

The most obvious difference between the models is the quadratic dependence on charge in the proposed model. While the linear constitutive equations presented by Madden and Mazzoldi are sufficient for examining the strains that result from electrical loads within a certain operating range, the nonlinear equation suggests that they break down when electrical loads exceed that range. By relying on empirical results to derive the proportionality constant, the linear models lack a direct connection to physically meaningful parameters, which limits understanding of the parameters that are critical to the performance of EAP.

Certainly the linear models do predict the mechanical behavior of polypyrrole within a certain operating range. To verify that the quadratic model can recreate the linear coupling constant, the axial strain equation, (3.59), is linearized, resulting in the following equality:

$$\alpha = \frac{(1-2\nu)q_V}{Ec_V V} = \frac{(1-2\nu)e_V}{E}, \text{ with units of } \mathrm{m^3/C} \tag{3.60}$$

Published values of α are 1.2×10^{-10} $\mathrm{m^3/C}$ [1] and 3×10^{-11} $\mathrm{m^3/C}$ [6]; both authors measure elasticity, E, of about 800MPa; and Mazzoldi *et al* reported Poisson's ratio, ν, of 0.426. Using the published values of α, E, and ν, the operating potentials that were used during experimentation can be estimated:

$$e_V = \frac{E}{(1-2\nu)}\alpha = 0.65\text{V for Madden and } 0.16\text{V for Mazzoldi } \textit{et al} \tag{3.61}$$

It must be reiterated that e_V in this model is measured with respect to the potential of zero charge (PZC) for the electrochemical cell. It will be shown in Chapter 4 that the PZC for polypyrrole in 0.1 M $TEAPF_6$ (as examined by Madden) is approximately -0.6 V vs. $Ag/AgClO_4$. Therefore, the estimated operating potential of 0.65V would be about 0.05V vs. $Ag/AgClO_4$, which is right in the middle of the testing range specified by Madden. This validates that the coupling equation derived from energy methods can recreate the empirically-derived α, but using physically-relevant parameters. The estimated operating potential required to reproduce the coefficient obtained by Mazzoldi *et al* gives an applied potential of -0.44 vs. $Ag/AgClO_4$. However, no reference was given to the potentials that were used during testing and the electrolyte may have been different, so this value cannot be corroborated.

Certainly the agreement between the coupling coefficient determined by Madden and the linearized coefficient based on physical parameters validates the nonlinear constitutive equation. If the nonlinear coupling equation is correct, it will be able to accurately predict a much larger range of actuator behavior. To verify that the coupling equation derived here is more effective than the linear model, several experiments were performed using a wide range of typical electrical and mechanical loads. These results are presented in Chapter 4.

3.6 Mechanical Model

As a polymeric material, polypyrrole exhibits viscoelastic behavior, including creep. While this behavior may be negligible when the polymer is subject to light loading, it becomes very important as the loading on the polymer is increased. Because EAP operate under tension, creep can become a critical factor in the implementation of an EAP actuator. Additionally, electrochemical loads may result in large internal stresses. It is essential to include the viscoelastic properties of the polymer in the dynamic model in order to fully characterize the actuator mechanical domain.

The actual viscoelasticity of the polymer is due to continuum interactions in the material. As with the reticulated electrical model used to describe continuum diffusion, a low-order reticulated model can be used to model the mechanical domain. A common model of viscoelasticity, known as the Standard Linear Model (SLM) [7], is depicted in Figure 3-12. This model includes an elastic element in parallel with Maxwell viscoelastic elements, which determine the rate-dependent elasticity of the material. The combination of viscous elements allows stress relaxation during constant displacement, or creep during constant loading. The single elastic element, k_1, is needed to account for the return of the polymer to its original shape when it is unloaded.

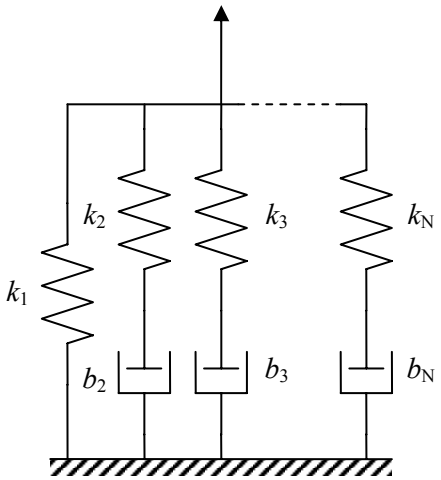

Figure 3-12: Standard Linear Model of Viscoelasticity with Maxwell Elements

The number of elements included in the viscoelastic model depends on the complexity of the mechanical behavior of the material and the time range of anticipated loading. If the duration of loading is expected to be only a few seconds, it may be possible to use a single viscoelastic element to describe the behavior of the system. However, if the material is expected to be loaded for hours or days additional viscoelastic elements may be needed to describe the longer time response associated with creep.

The dynamic equations of the SLM can be quickly determined using the bond graph notation. Figure 3-13 is the bond graph representation of the SLM viscoelastic structure with two viscoelastic elements shown.

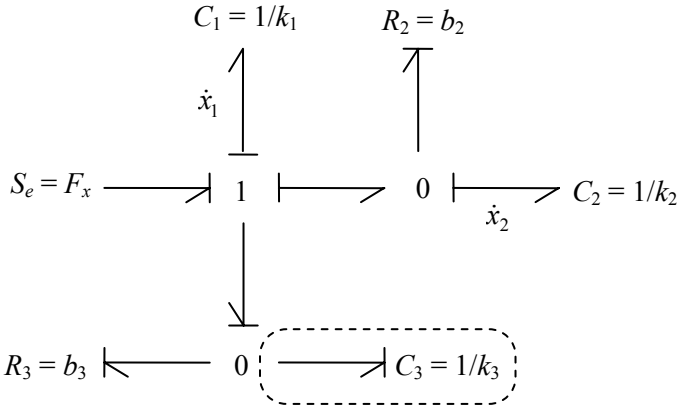

Figure 3-13: Bond Graph of SLM with Two Maxwell Viscoelastic Elements

This model assumes effort as the input to keep the same causality as the electrochemical coupling model. The dashed lines around the third compliance, C_3, highlight that the element must be put into derivative causality. This indicates that the model is over-causal and has only two independent states despite having three energy storing elements. The differential equations for the model can be determined, though they are more complex due to the coupled dynamics of the third element:

$$\begin{aligned}\left(1+\frac{k_1}{k_3}+\frac{k_2}{k_3}\right)\dot{x}_1 &= \frac{1}{b_3}F_x+\frac{1}{k_3}\dot{F}_x-\frac{k_1}{b_3}x_1-\left(\frac{k_2}{b_3}+\frac{k_2^2}{b_2k_3}\right)x_2\\ \left(1+\frac{k_1}{k_3}+\frac{k_2}{k_3}\right)\dot{x}_2 &= \frac{1}{b_3}F_x+\frac{1}{k_3}\dot{F}_x-\frac{k_1}{b_3}x_1-\left(\frac{k_2}{b_3}-\frac{k_2}{b_2}-\frac{k_1k_2}{b_2k_3}\right)x_2\end{aligned} \tag{3.62}$$

Unfortunately, the derivative of the effort source, $\dot{F}_x$, appears in these equations. If the effort source is treated as ideal, such that it can be a discontinuous function like a step input, then the derivative of the input is not defined at the discontinuity. To alleviate this difficulty a virtual damper is added in parallel with the entire system as depicted in Figure 3-14. The damper allows the model to be put into full integral causality as demonstrated by the bond graph depicted in Figure 3-15. An alternative approach would be to use velocity as the input variable; however, this approach makes it difficult to analyze the step responses that were used during isotonic testing.

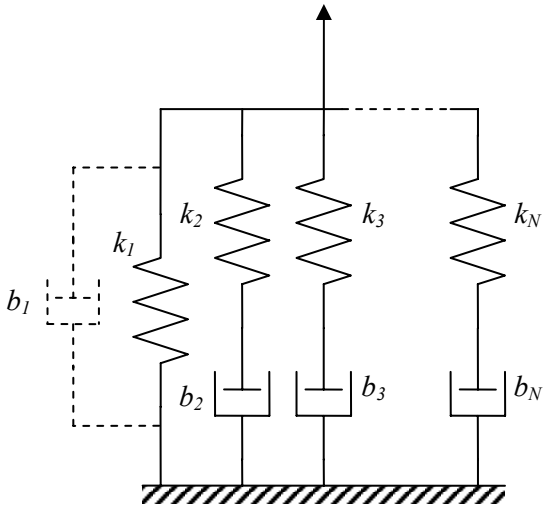

Figure 3-14: Maxwell Viscoelastic Model with Virtual Damper to Achieve Full Integral Causality

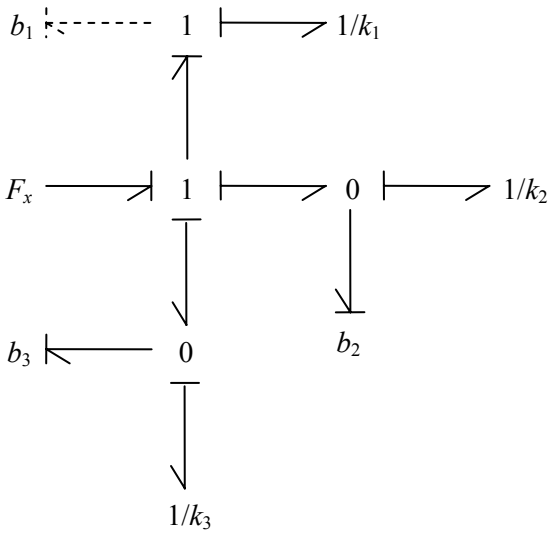

Figure 3-15: Bond Graph of 3-Element Maxwell Model with Virtual Damper for Full Integral Causality

The differential equations corresponding to this model are given in state-space form as:

$$\begin{bmatrix} \dot{x}_1 \\ \dot{x}_2 \\ \dot{x}_3 \end{bmatrix} = \begin{bmatrix} -\frac{k_1}{b_1} & -\frac{k_2}{b_1} & -\frac{k_3}{b_1} \\ -\frac{k_1}{b_1} & -\frac{k_2}{b_1} - \frac{k_2}{b_2} & -\frac{k_3}{b_1} \\ -\frac{k_1}{b_1} & -\frac{k_2}{b_1} & -\frac{k_3}{b_1} - \frac{k_3}{b_3} \end{bmatrix} \begin{bmatrix} x_1 \\ x_2 \\ x_3 \end{bmatrix} + \frac{F_x}{b_1} \tag{3.63}$$

This model can be used to describe the dynamics of the mechanical domain when loaded by any effort function, $F_x(t)$. In the case of EAP, the input force is a combination of mechanical and electrochemical loading. It was shown in Section 3.5 that the total uniaxial stress is determined by the sum of the mechanical stress and electrochemical stress:

$$\sigma = \frac{(1-2\nu)q_V^2}{2c_V V^2} + \sigma_x \tag{3.64}$$

While the constitutive equation assumes uniform charge in the polymer, it was shown in Section 3.2 that the charge distribution across the polymer thickness, a, is determined by the ion diffusion model. Therefore, the constitutive equation must be modified to account for non-uniform charge distribution. This is simple to do as illustrated in Figure 3-16, which depicts N diffusion elements each containing

a single viscoelastic element and an electrochemical stress generator that depends on the concentration of ions at that location, q_k (k = 1, 2, … N).

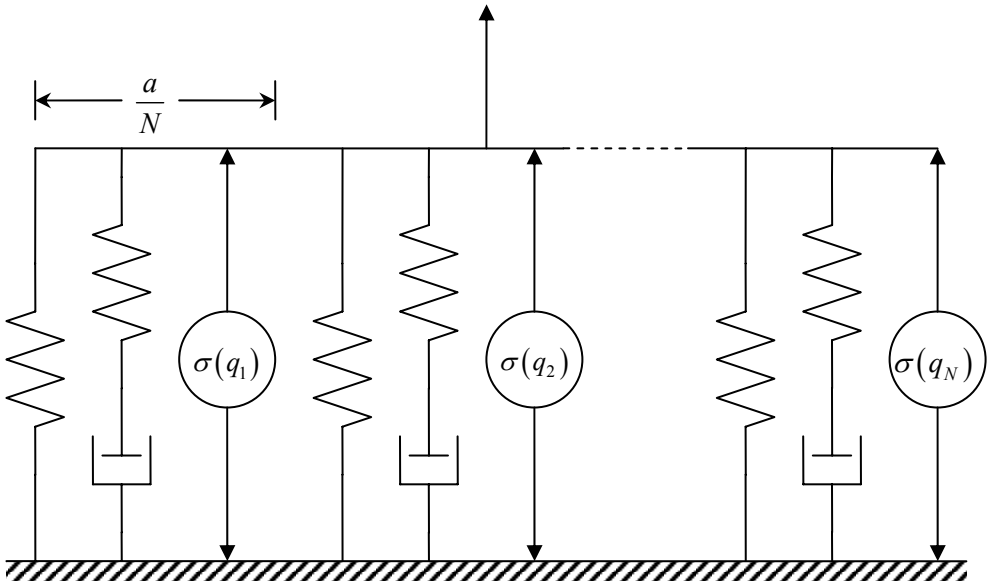

Figure 3-16: *N*-Element Diffusion Model with Viscoelasticity

Each electrochemical stress component has a quadratic dependence on its associated volume, which is the total polymer volume divided by the number of elements used in the diffusion model: V/N. Multiplying each electrical stress by the cross-section over which it acts gives its total force contribution. Summing all forces in the x direction then gives the following:

$$F_x = \frac{(1-2\nu)}{2c_V} \frac{q_1^2 + q_2^2 + \cdots + q_N^2}{\left(\frac{V}{N}\right)^2} \frac{w \cdot a}{N} + \sigma_x \cdot w \cdot a \tag{3.65}$$

So rather than exhibiting a quadratic dependence on the total volumetric charge, q_V, the electrically induced force is proportional to the inner product of the state vector: $N \cdot \boldsymbol{q}_V^T \boldsymbol{q}_V$, where $\boldsymbol{q}_V$ is the state vector of N diffusion elements. As with the diffusion analysis, symmetry of a free-standing polymer allows the number of states to be reduced to $N/2$. With this reduction in the number of states each electrochemical stress element has a volume of $2V/N$ and a cross-sectional area of $2wa/N$. The resultant force in the axial direction then simplifies to:

$$F_x = \left(\frac{(1-2\nu)}{2c_V} \frac{\boldsymbol{q}_V^T \boldsymbol{q}_V}{V^2} \frac{N}{2} + \sigma_x \right) \cdot w \cdot a \tag{3.66}$$

Because (3.66) includes the diffusion dynamics, it provides a much better approximation of the electrically induced force allowing for a better overall model of the polymer dynamics. To demonstrate this, consider a non-uniform charge distribution over three diffusion elements with values of 1/2, 1/3, and 1/6 Coulombs. If the charge distribution is assumed to be uniform, the dependence on charge is given by q_V^2, which results in a value of 1 C^2. If the non-uniform charge distribution is considered the resulting contribution is $N \cdot \boldsymbol{q}_V^T \boldsymbol{q}_V$, which equals 1.167 C^2. The assumption of uniform charge distribution gives an error of 14.3% in this simple case, with potential for much larger error depending on the actual charge distribution in the polymer.

The result given in (3.66) can be incorporated into the mechanical dynamics, (3.63), giving:

$$\begin{bmatrix} \dot{x}_1 \\ \dot{x}_2 \\ \dot{x}_3 \end{bmatrix} = \begin{bmatrix} -\frac{k_1}{b_1} & -\frac{k_2}{b_1} & -\frac{k_3}{b_1} \\ -\frac{k_1}{b_1} & -\frac{k_2}{b_1} - \frac{k_2}{b_2} & -\frac{k_3}{b_1} \\ -\frac{k_1}{b_1} & -\frac{k_2}{b_1} & -\frac{k_3}{b_1} - \frac{k_3}{b_3} \end{bmatrix} \begin{bmatrix} x_1 \\ x_2 \\ x_3 \end{bmatrix} + \left(N \cdot \frac{(1-2\nu)\boldsymbol{q}_V^T \boldsymbol{q}_V}{4c_V V^2} + \sigma_x \right) \cdot \frac{wa}{b_1} \tag{3.67}$$

This equation can be rewritten using elastic modulus variables (N/m^2), rather than the spring stiffness variables (N/m) that depend on the dimensions of the sample:

$$\begin{bmatrix} \dot{x}_1 \\ \dot{x}_2 \\ \dot{x}_3 \end{bmatrix} = \left(\begin{bmatrix} -\frac{E_1}{l_0} & -\frac{E_2}{l_0} & -\frac{E_3}{l_0} \\ -\frac{E_1}{l_0} & -\frac{E_2}{l_0} - \frac{b_1 E_2}{l_0 b_2} & -\frac{E_3}{l_0} \\ -\frac{E_1}{l_0} & -\frac{E_2}{l_0} & -\frac{E_3}{l_0} - \frac{b_1 E_3}{l_0 b_3} \end{bmatrix} \begin{bmatrix} x_1 \\ x_2 \\ x_3 \end{bmatrix} + \left(\frac{N(1-2\nu)\boldsymbol{q}_V^T \boldsymbol{q}_V}{4c_V V^2} + \sigma_x \right) \right) \cdot \frac{wa}{b_1} \tag{3.68}$$

If the material is assumed to be isotropic, the dynamics in the *y* and *z* directions are identical to (3.68) except that the mechanically induced stress is negatively proportional to Poisson's ratio (for the uniaxial loading case) and the corresponding cross-sectional dimensions depend on the direction being considered.

3.7 Summary

This chapter presented low-order models to describe the electrochemical, mechanical, and coupled dynamics of an EAP actuator. The electrical and mechanical domains were independently treated as reticulated networks of energy storage and dissipation elements in order to account for the continuum nature of EAP materials. Energy conservation principles were utilized in order to describe the transduction of energy between the electrical and mechanical domains. The total potential energy of the system was determined using contributions from electrical and mechanical inputs. This allowed for a determination of input efforts from the partial derivative of potential energy with respect to displacement variables. The uniaxially loaded polymer was examined in detail in order to demonstrate that the coupling between domains is highly dependent on Poisson's ratio. The symmetry of the generalized compliance matrix demonstrated that the polymer is solely an energy storing transducer despite exhibiting behavior suggesting that it also contributes significant entropic losses. The nonlinear coupling equation is the first published result that used physically relevant parameters to demonstrate the interactions between the electrochemical and mechanical domains in EAP.

3.8 Chapter References

[1] Madden, John D. W., *Conducting Polymer Actuators*, Ph.D. Thesis, MIT, Cambridge, MA, 2000.

[2] Bard, A.J. and L.R. Faulkner, *Electrochemical Methods, Fundamentals and Applications*, New York: Wiley, 1980.

[3] Albery, John W. and Andrew R. Mount, "Transmission Lines for Conducting Polymers," Chapter 4 in *Electroactive Polymer Electrochemistry, Part 1: Fundamentals*, Michael E.G. Lyons, Ed., New York: Plenum Press, 1994, 443-483.

[4] Peres, Pedro L.D., Ivanil S. Bonatti and Amauri Lopes, "Transmission Line Modeling: A Circuit Theory Approach," *SIAM Review*, Society for Industrial and Applied Mathematics, **40**, No. 2 (1998): 347-352.

[5] Lewis, Trevor W., Geoffrey M. Spinks, Gordon G. Wallace, Alberto Mazzoldi, and Danilo De Rossi, "investigation of the applied potential limits for polypyrrole when employed as the active components of a two-electrode device," *Synthetic Metals*, **122** (2001): 379-385.

[6] Mazzoldi, A., A. Della Santa, and D. De Rossi, "Conducting Polymer Actuators: Properties and Modeling," in *Polymer Sensors and Actuators*, Y. Osada, and D. E. De Rossi, Eds., pp. 207-244, Springer Verlag, Heidelberg, 2000.

[7] Della Santa, A., D. De Rossi and A. Mazzoldi, "Characterization and modeling of a conducting polymer muscle-like linear actuator," *Smart Materials and Structures*, **6** (1997): 23-34.

Chapter 4

Experimentation

To validate and parameterize the model developed in Chapter 3 a wide range of electrical and mechanical tests were performed on a sample EAP material. Polypyrrole was used for all tests because it is a well known and highly developed conducting polymer. The electrolyte used in all tests was 0.1 M tetraethylammonium hexafluorophosphate ($TEAPF_6$) in propylene carbonate (PC).

4.1 Experimental Setup

Dynamic mechanical and electrical tests were performed using the apparatus shown in Figure 4-1, which was developed by Derek Rinderknecht [1] to test electromechanical responses of conducting polymer actuators.

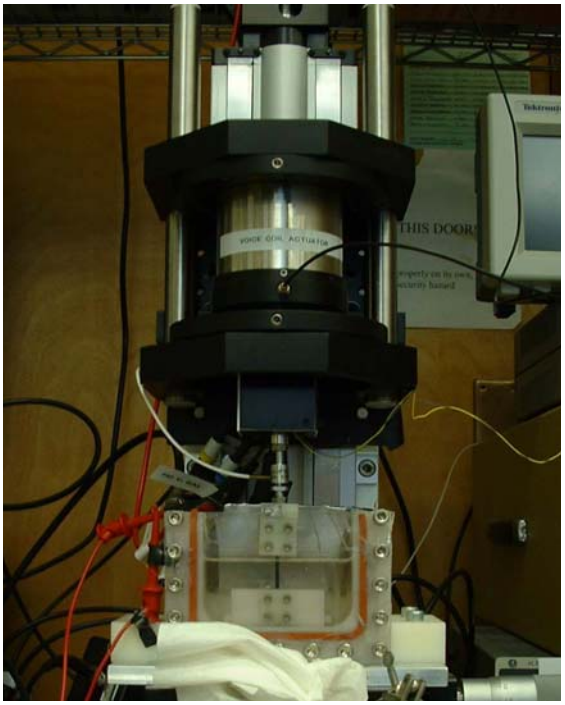

Figure 4-1: Dynamic Mechanical and Electrochemical Testing Equipment

The polymer film is held in the test fixture with clamps at both ends. These clamps also provide electrical contact to an AMEL Instruments General Purpose Potentiostat Model 2051, which is used to apply electrical loads to the electrochemical cell. The potentiostat sets the potential between the polymer (working electrode) and counter electrode based on the potential measured between the working and reference electrodes. The potentiostat also has a galvanostat mode that can be used to apply a constant current to the electrochemical circuit. The reference electrodes used in all experiments were composed of $Ag/AgClO_4$. All experiments used a 0.1 M electrolyte solution of tetraethylammonium hexafluourophosphate ($TEAPF_6$) in propylene carbonate (PC), which provides ionic transport in the cell. Mechanical loading is provided by a voice coil actuator (Bruel & Kjaer Minishaker 4810) that is controlled using feedback from a force transducer to allow for isotonic testing. A position sensing photodiode (Pacific Silicon Sensors PPS-DL100-7PCBA) measures polymer displacements with a resolution of 250nm. Electrical and mechanical waveforms were implemented using Visual Basic software.

The polypyrrole samples used in all experiments were prepared from pyrrole monomer (Aldrich) according to the process described in Section 2.4. After synthesis the samples tested were approximately 20 μm thick. The thickness of each test sample was determined using a micrometer, which only gives an accuracy of about ±2μm due to the elasticity of the polymer. Because diffusion dynamics are highly dependent on thickness, any inaccuracies in measurement may result in prediction errors for diffusion dynamics and volumetric capacitance. A more accurate measurement method may be needed to improve model prediction. Sample widths varied from 2.5 to 7 mm and lengths varied from 11.87 to 18.40 mm. Table 4-1 gives dimensions of samples used in testing.

Table 4-1: Polypyrrole Sample Dimensions

Sample	Synthesis Date	Test Date	Length, mm	Width, mm	Thickness, μm
PPy4	June 5, 2003	June 13, 2003	12.95	7.0	19
PPy6	June 5, 2003	July 6-9, 2003	11.87	3.5	19
PPy7	Sept. 8, 2003	Sept. 8-9, 2003	18.40	2.5	21
PPy8	Sept. 8, 2003	Dec. 17-18, 2003	16.50	2.9	18
PPy9	Sept. 8, 2003	Jan. 4-8, 2004	13.50	3.0	24

The conductivities of samples also varied with a range of 800-1000 S/m. The total resistance of the electrical side of the electrochemical circuit was measured before testing. Because potential is applied

to both ends of the polymer film during testing it is possible to measure the total resistance of the polymer while it is mounted in the test apparatus. This resistance is divided in half to give the equivalent resistance of the electrical circuit, R_{Σ}.

4.2 System Identification

It is possible to understand the dynamics of a linear system by obtaining its response to various input signals. Ideally, the input signal will stimulate all of the important dynamics of the system and allow for a determination of the poles and zeros of the system transfer functions. Based on the analysis in Chapter 3, the electrical and mechanical domains in EAP are essentially linear, with minimal coupling between domains for materials with high Poisson's ratios. This allows linear system identification techniques to be used in examining the uncoupled dynamics of the electrical and mechanical domains.

To fully characterize the frequency response of a system it is necessary to input a signal that has power contributions over all frequencies. While it is not physically possible to do this, it is possible to input signals that have power contributions over a wide range of frequencies. According to Ljung [2] the best waveform to use for frequency domain characterization is a pseudo-random binary sequence (PRBS). The PRBS has uniform power for all of the frequencies that are within the bandwidth of the signal, and negligible power at all other frequencies. If the frequency range of dominant system dynamics is known, it is possible to design a PRBS that will excite only this range of frequencies.

The PRBS is a zero mean, Gaussian waveform consisting of binary inputs. The signal is constructed using an *n*-bit shift register, where the number of bits determines the frequency resolution of the output signal. To create the "random" sequence, selected characters in the register are summed. The result, which is a binary number, is fed to the input of the register as depicted in Figure 4-2.

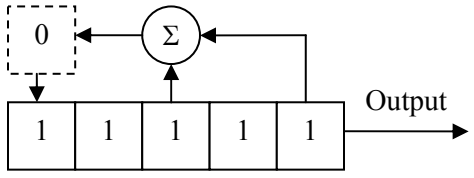

Figure 4-2: Maximum Length 5-bit Pseudo-Random Binary Sequence Shift Register

The last bit in the register is the output signal at that time step. At the next time step the values in the register shift to the right and the process is repeated. For a shift register with *n* bits, the optimum

PRBS signal is 2^n -1 bits long and then continues to repeat itself. The maximum length signal provides constant power at all frequencies contained in the signal spectrum. PRBS signals have been analyzed extensively and the maximum length signals tabulated. The maximum length 5-bit PRBS shift register is depicted in Figure 4-2.

The PRBS has the best possible ratio of peak power content to average power content, which is known as a crest factor. For a maximum length PRBS the crest factor is 1. The difficulty in using a PRBS, however, is that in order to analyze a large frequency range it is necessary to use a PRBS with many bits. Implementation of a large-bit PRBS using software alone is difficult.

An alternative to the PRBS that is easier to implement in software is a swept sinusoid or "chirp" signal. Although this signal does not have constant power at all frequencies, it has a good power spectrum with a crest factor of $\sqrt{2}$. The chirp signal is given by the following sinusoid which can be repeated every T seconds to increase the reliability of the data:

$$u(t) = A\cos\left(\omega_1 t + \left(\frac{\omega_2 - \omega_1}{2T}\right)t^2\right) \tag{4.1}$$

where A is the amplitude of the signal, ω_1 is the lowest frequency content, ω_2 is the highest frequency content, and T is the period of the chirp signal in seconds. To get the desired spectral properties from the chirp signal the period needs to be at least $2\pi/\omega_1$ seconds. To avoid aliasing of the high frequency components of the signal the sampling rate needs to be higher than the Nyquist frequency, which is twice the maximum input signal frequency. It is desirable to use an even higher sampling rate in order to reduce spectral leakage, which can distort the high frequency signal components [3]. For all frequency sweep experiments in this research the sampling rate used is at least ten times the highest frequency of the input signal.

4.3 Mechanical Testing

Characterization of the mechanical domain was done at constant potential. From the analysis in Section 3.3, it is clear that there is no coupling between electrical and mechanical domains when the electrochemical potential is zero. For an electrochemical cell, zero potential corresponds to a neutral concentration of ions at the polymer double layer. This is called the potential of zero charge (PZC). For polypyrrole in 0.1 M $TEAPF_6$ the PZC was found to be approximately -0.6 Volts versus an

$Ag/AgClO_4$ reference electrode. All mechanical tests were performed at the PZC to eliminate electromechanical coupling dynamics.

4.3.1 Isotonic Testing

Isotonic testing allows for an examination of polymer viscoelasticity. By subjecting the polymer samples to uniform loading for long durations it is possible to observe creep. Several isotonic tests were performed at various loads in order to determine how loading affects creep. Figure 4-3 shows the strain of a polymer subjected to the isotonic loading profile depicted in the lower half of the figure. Nominal stresses ranged from 1 to 5 MPa and were applied for an hour. The polymer was then allowed to relax under a 100 kPa nominal load for an hour before the next load was applied. The data shown is for sample PPy9, which was 13.5mm long, 3mm wide, and 24μm thick.

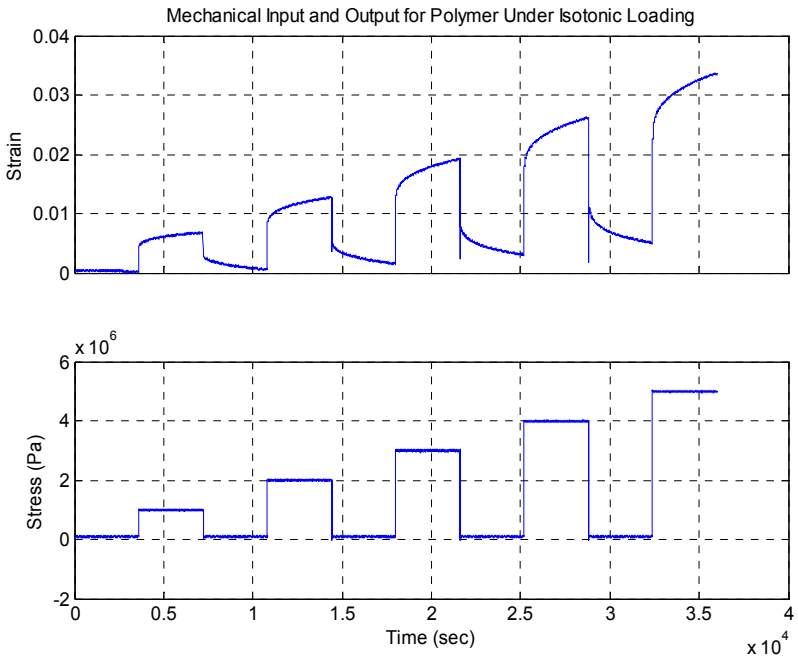

Figure 4-3: Strain and Stress versus Time for Isotonic Mechanical Testing at -0.6 V vs. $Ag/AgClO_4$

The overshoots in the strain profile upon reduction in loading are due to the transients in the force-feedback control. This data appears to exhibit a linear dependence on force as expected. To compare the linearity of the curves, Figure 4-4 shows the strain profiles from Figure 4-3 plotted from the onset of isotonic loading. The initial strain at the onset of loading has been subtracted from each curve as this is a residual viscoelastic effect.

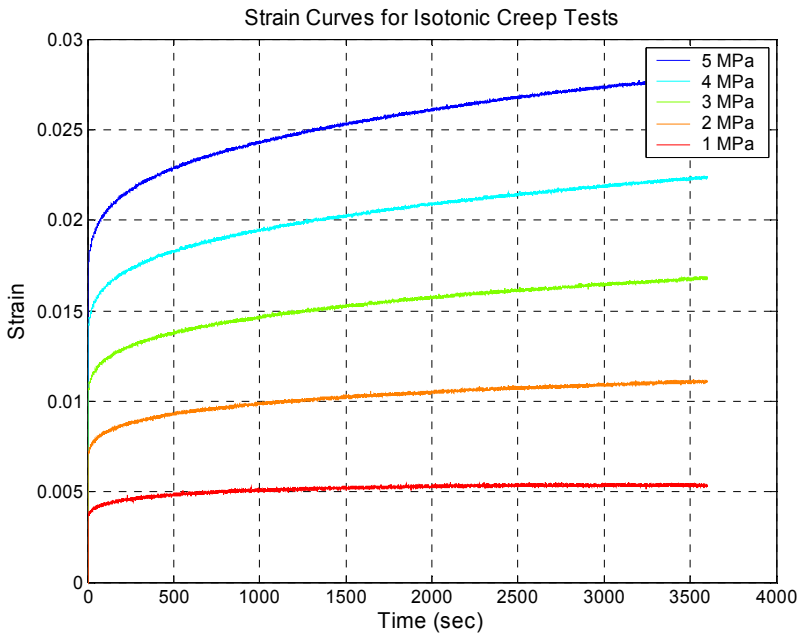

Figure 4-4: Isotonic Tests on 20µm Polypyrrole Sample at -0.6V vs. $Ag/AgClO_4$

When normalized by the nominal axial stress in the polymer the curves converge very well as shown in Figure 4-5. This demonstrates the linearity of polypyrrole viscoelasticity in the range of 1 to 5 MPa and supports the use of a linear model of viscoelasticity.

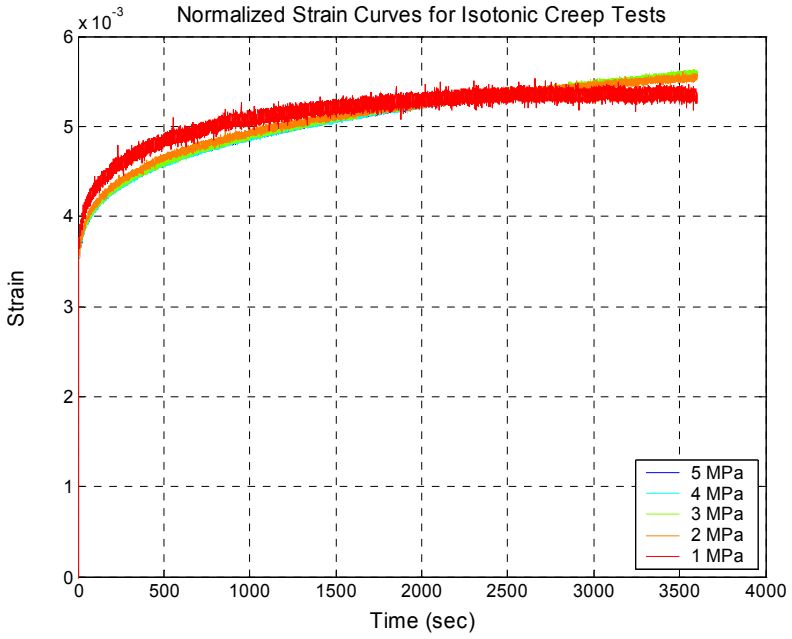

Figure 4-5: Stress-Normalized Viscoelasticity of Polypyrrole

While it appears that the time response of the polymer viscoelasticity is approximately first order with a very long time constant, the actual nature of the viscoelastic response is best observed in a logarithmic plot of strain and time as demonstrated in Figure 4-6.

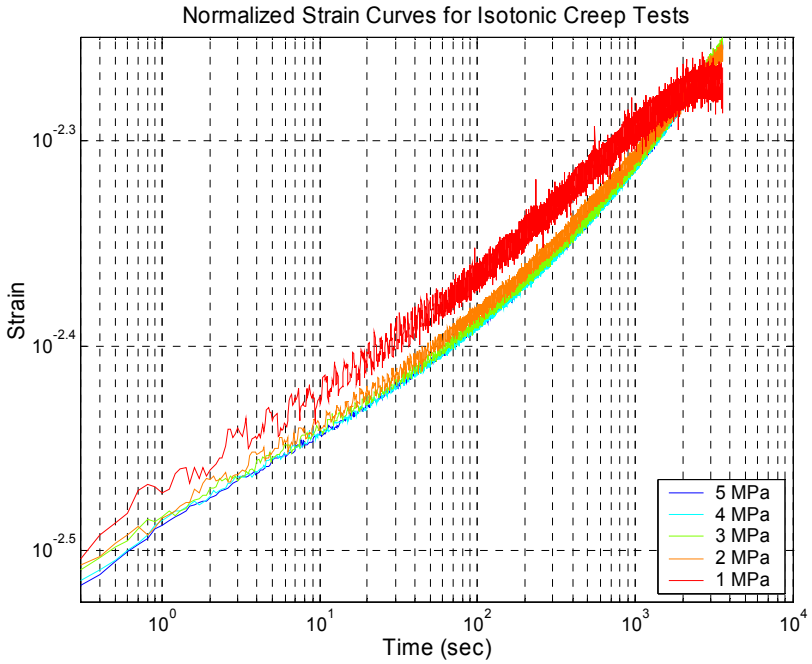

Figure 4-6: Logarithmic Plot of Isotonic Tests 1-5 MPa, Normalized by Load, 24 μm Polypyrrole Sample

When viewed in this scale it is interesting to note that the strain response is approximately linear with the logarithm of time. This suggests that the viscoelastic model must incorporate one element for every decade of loading time as each linear viscoelastic element has an exponential decay that spans approximately one decade.

While the preceding figures demonstrate the linearity of the material, the extent of creep dynamics requires longer duration testing. Figure 4-7 depicts the response of the same polymer sample loaded isotonically by a 3 MPa nominal stress for 4 hours. Data was collected at 10 Hz in order to capture the fast dynamics that occurred when the polymer was initially loaded.

Although the viscoelastic behavior of the polymer again appears to be first order, Figure 4-8, which is a log-log plot of the strain versus time, shows that the step response has contributions throughout the frequency domain.

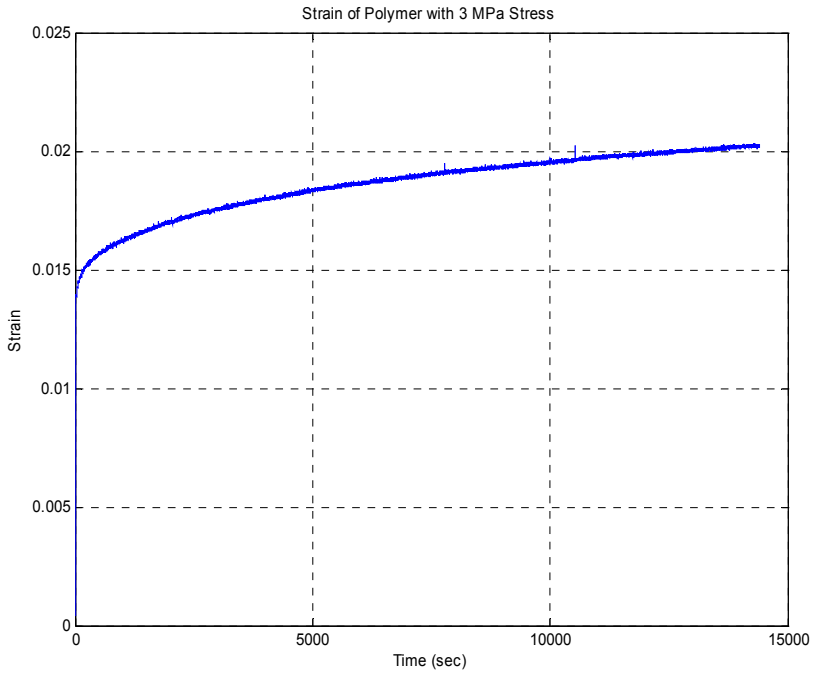

Figure 4-7: Creep of Polypyrrole under Nominal 3MPa Load

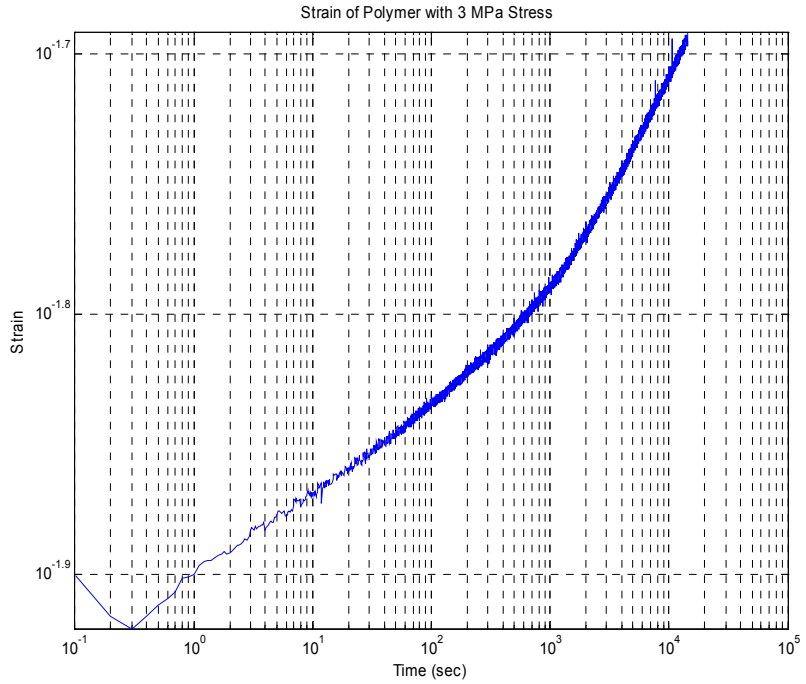

Figure 4-8: Log-Log Plot of Strain versus Time for Isotonically Loaded Polypyrrole Sample

From this relatively linear relationship, the unit step response of the polymer is approximated by:

$$\varepsilon_x = \varepsilon_0 t^c \tag{4.2}$$

where c is the slope of the log-log strain curve and ε_0 is the normalized strain at t = 1 second. The derivative of the step response gives the impulse response:

$$h(t) = c\varepsilon_0 t^{c-1} \tag{4.3}$$

While (4.3) provides a valuable time domain description of creep with only two parameters to determine, it is difficult to include this model with the lumped parameter model of the rest of the system. That would require convolution of the impulse response with the input stress function, or alternatively both must be converted to the frequency domain.

It is evident that the lumped parameter viscoelastic model from Section 3.6 can provide a more tractable set of dynamics described by ordinary differential equations. Because the polypyrrole viscoelasticity spans several decades of the frequency domain, it is necessary to include viscoelastic elements with time constants at every decade to maintain the linear curve. If the duration of anticipated loading is only a few hundred seconds, the viscoelastic model needs only three Maxwell viscoelastic elements in addition to the parallel elastic element. The time constants of the viscoelastic elements should be about 1, 10, and 100 seconds to maintain the linearity of the log-log plot. The curve shown in Figure 4-9 demonstrates the time response of a three element viscoelastic model with time constants at every decade. The roll-off from each of the poles is evident as a slight curvature at each decade.

For longer anticipated loading, the viscoelastic model must include additional elements. The additional elements also allow more freedom in dictating the slope of the frequency response curve. If enough elements are included in the viscoelastic model it is possible to match any observed response. However, it is wise to include only the minimum number of elements needed to competently describe the mechanical response in order to simplify analysis.

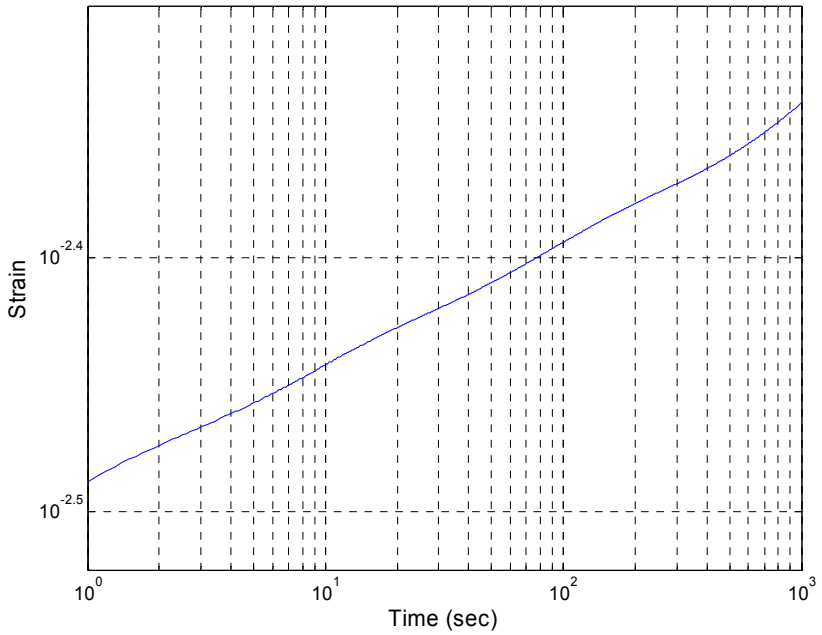

Figure 4-9: Simulation of Three-Element Viscoelastic Model

4.3.2 Mechanical Frequency Sweep

While the step response from the preceding section provided a suitable model of viscoelasticity, a swept sinusoid input can also be used to determine the frequency response of the mechanical domain. While it would be ideal to characterize the mechanical properties of the sample over a large frequency range there are some limitations to the test apparatus that prevent this. Limitations occur primarily at high frequencies due to unmodeled system and feedback dynamics. Because the load on the polymer is applied using force feedback, the closed loop response is determined by feedback gains. In addition, the masses of the moving parts in the system begin to contribute to the response at higher frequencies. Fortunately, the frequency range of the viscoelastic effects is primarily below about 1 Hz, with undamped elasticity and unmodeled inertia dominating at higher frequencies. Testing the polymer at lower frequencies requires much longer tests, as described in Section 4.2, which provides a limitation to the lowest frequencies analyzed simply due to the size of data files.

To get unbiased data for the mechanical frequency sweep, the polymer samples were first loaded to the mean load of the desired input for an hour in order to reach quasi-equilibrium (small strains always result due to creep). The mean load can be chosen arbitrarily within the linear range of the mechanical behavior. The previous experiment demonstrated that the polymer exhibited linear

viscoelasticity up to at least 5 MPa. The mean load for this test was chosen to be 3 MPa. The amplitude of the swept sinusoid was 1 MPa with a frequency range of 100 μHz to 1 Hz. The sampling rate was 10 Hz to avoid aliasing of the high frequency signal and the period of the signal was 20,000 seconds to improve the resolution of the low frequency content of the response. However, spectral leakage may still corrupt the data near the cutoff frequencies. Sample PPy9, which was used for isotonic testing, was also used in this test. The frequency response is shown in Figure 4-10.

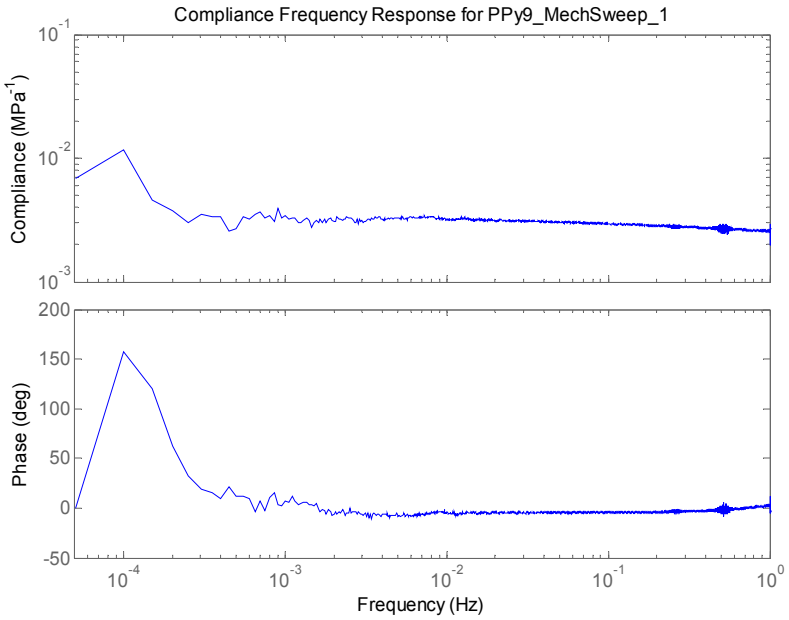

Figure 4-10: Mechanical Frequency Response of 24 μm Polypyrrole Sample

The response exhibits very little complexity except at low frequencies. However, the apparent dynamics at low frequency are most likely due to spectral leakage of DC frequency components. Similarly, the noisy bursts at 0.5 and 0.25Hz are the result of spectral leakage due to truncation of the input signal at 1Hz. Although this frequency response appears suspect, its result can be validated by considering (4.3), which was the linear logarithmic function presented in the previous section to approximate the mechanical impulse response of the polymer. The Laplace Transform of the linearized impulse response gives:

$$H(s) = \frac{c\varepsilon_0 \Gamma(c)}{s^c} \tag{4.4}$$

The value of c is very small (~10^{-8}), which allows this transfer function to be approximated by:

$$H(s) \approx \varepsilon_0 \tag{4.5}$$

This suggests that the compliance of the polymer is almost constant for all frequencies with no phase lag, which is qualitatively similar to Figure 4-10. The result can also be corroborated quantitatively using the polymer compliance from Figure 4-6, which is approximately $10^{-2.495}$ MPa^{-1} at 1 second. This value is almost equivalent to the polymer compliance from Figure 4-10, which is about $10^{-2.485}$ MPa^{-1} at 1Hz. The agreement between these results suggests that both the swept sinusoid and step input provide enough information to reasonably determine the mechanical dynamics of a polymer sample.

4.3.3 Mechanical Failure Testing

To determine the limits on the linear behavior of polymer elasticity a destructive test was performed on a polymer sample. An approximate ramp in displacement was achieved by inputting a current directly to the voice coil actuator using a digital power supply. To eliminate the majority of viscoelastic effects the strain rate was approximately 1%/s. The sample used was PPy6, which is 11.87mm long, 3.5mm wide, and 19μm thick. The stress-strain curve for the polymer is shown in Figure 4-11. The stair-step profile of the curve is due to the quantization of the current input to the voice coil actuator.

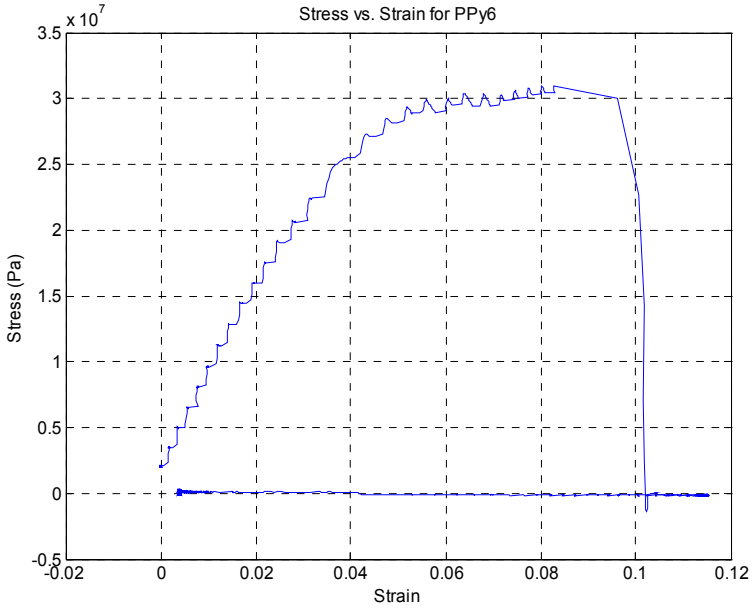

Figure 4-11: Stress-Strain Curve of Polypyrrole Demonstrating Nonlinear Elasticity and Critical Failure

It is evident from this result that the polymer exhibits linear elasticity up to about 25 MPa. Critical failure of the sample occurred at about 31 MPa with a strain of 8.25%. This demonstrates that the assumption of linear elasticity is valid for loading up to about 75% of the polymer ultimate strength. This may also hint at the possibility of using the polymer as an actuator with variable elasticity, similar the skeletal muscle; however, this may be limited by the ability of the polymer to reversibly recover from loading near the stress-strain nonlinearity, as yielding of materials is generally undesirable.

4.4 Electrical Testing

Testing in the electrical domain allows for validation of the electrical model developed in Section 3.2. For this set of tests the mechanical domain was subjected to isotonic loads while various inputs were applied electrically. This allowed for observation of electrical behavior and tracking of polymer displacements while imposing minimal mechanically-induced cross-coupling effects.

4.4.1 Electrical Frequency Sweep

Examining the results obtained by Madden [4], the frequency range of interest for a typical polypyrrole sample is from about 10^{-4} to 10^{2} Hertz. To get data at all frequencies of interest it is then necessary to collect data for at least 10,000 seconds with a sampling rate of at least 1 kHz. Increasing the period of the signal increases the resolution of frequencies in the Fourier transform, which is of more importance in the low frequency range of a logarithmic plot. Most of the frequency response data presented by Madden is for an 8.5 μm sample. For the sample analyzed here, which was 24 μm, it is possible to reduce the high frequency input to 1 Hz, which allows a sampling rate of 10 Hz. The input waveform for the electrical frequency sweep experiments had a period of 25,000 seconds with a minimum frequency of 40 μHz, maximum frequency of 1 Hz, and a sampling rate of 10 Hz. These tests were also performed on sample PPy9, which was used in the viscoelastic testing. The frequency response of the polymer admittance is shown below in Figure 4-12 for three different tests. The center potential for all tests was -0.2 V vs. $Ag/AgClO_4$ and the amplitude of the signal was adjusted from 0.2 to 0.5 Volts. As with the mechanical frequency sweep there appears to be some spectral leakage near the lower cutoff frequency that distorts the frequency response. However, the results from the three tests indicate that the experiment is repeatable and that the electrical domain is linear for the range of potentials used and the frequencies considered.

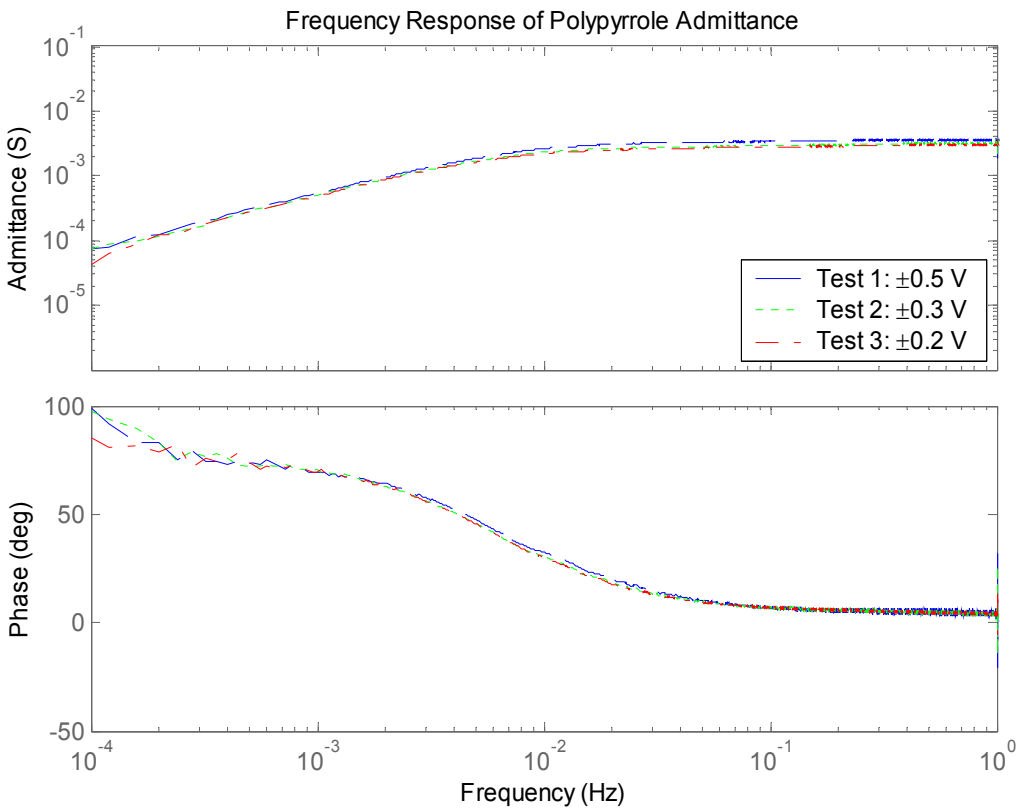

Figure 4-12: Frequency Response of Polypyrrole Admittance with Center Potential of -0.2 V vs. $Ag/AgClO_4$, for 24 μm Sample

Using the continuum model formulated by Madden it is possible to estimate the free parameters of the electrical domain by attempting to fit this curve. The high frequency response, which is almost entirely resistive, gives a total circuit resistance of 270 Ω. Because the polymer dimensions are known, the two remaining free variables are the specific volumetric capacitance, c_V and the diffusion constant, D. The parameters are fit to the data as shown in Figure 4-13, giving D=8μm^2/s and c_V=0.08 F/mm^2.

From the frequency response it is evident that the polymer exhibits fairly typical first order behavior in the range from 10^{-2} to 1 Hz. The diffusion time constant has only a minimal effect on the frequency response, indicating that the time constant of the bulk system—determined by the total resistance and capacitance—is larger than the time constant of diffusion. At lower frequencies the magnitude of the measured frequency response is slightly greater and the phase is slightly less. The continuum model exhibits 90 degrees of phase separation at low frequencies while the data appears to approach 75

degrees. The cause of this trend in the data is unknown though it may be the result of nonstationarity during the experiment due to viscoelastic effects.

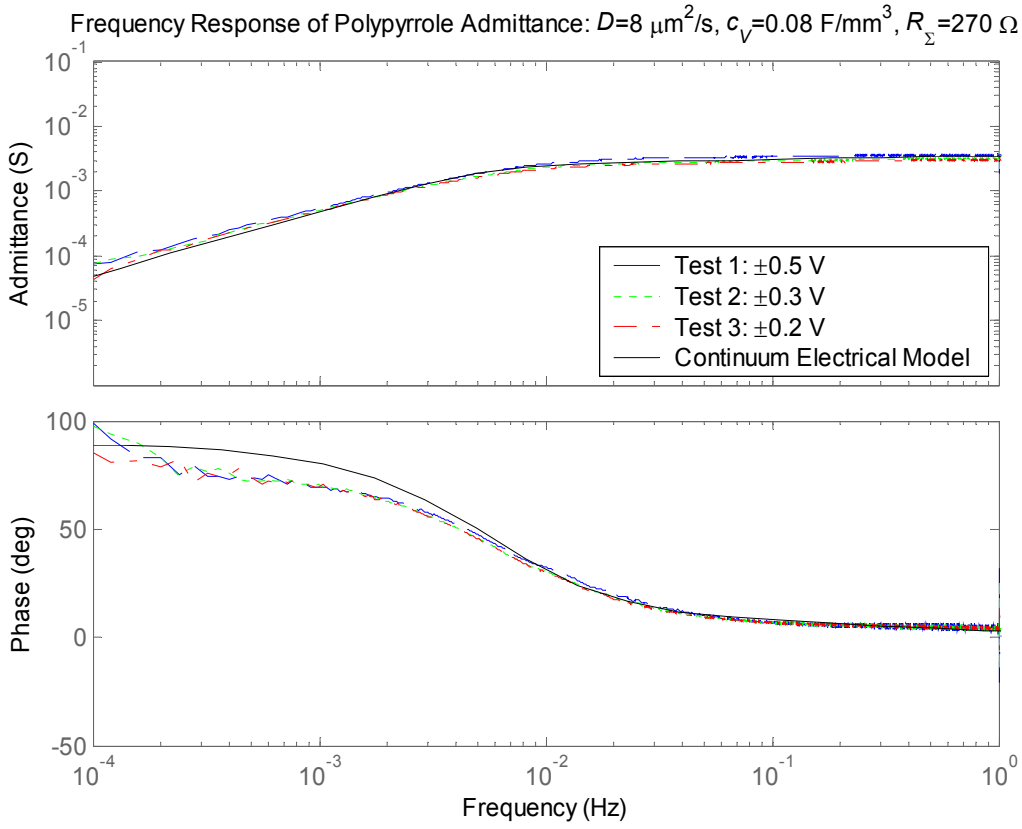

Figure 4-13 Simulated Fit of Polypyrrole Admittance Using Continuum Electrical Model

The magnitude of the high frequency response is used to determine the effective polymer and contact resistances. If the polymer is highly conductive, it is expected that this value will be identical to the measured circuit resistance. However, if the polymer film has low conductivity the effective resistance may be less than the measured circuit resistance. This is due to the continuum nature of conductivity, which can again be modeled as a reticulated transmission line. A good examination of the reticulated electrical domain is given by P. Madden [5].

4.4.2 Isotonic Testing with Voltage Input

This set of tests was used to observe the time response of the polymer electrical domain. Because there is an observable coupling from the electrical to mechanical domain it also gave some indication of the form of this coupling. The polymer was loaded isotonically while potential steps were applied.

The voltage was increased in steps of 0.1 V starting from about -0.5 V vs. $Ag/AgClO_4$. This was the initial estimate for the potential of zero charge, though later tests (as well as the results from these tests) indicate that the PZC is closer to -0.6 V vs. $Ag/AgClO_4$. After each potential step the current was allowed to drop to 30 μA before the next step was applied. This value was found to be sufficient to capture the majority of the time response of the polymer electrical domain. Figure 4-14 through Figure 4-17 show the potential input and current output for these tests. The polymer sample used in these tests was PPy6.

There are some unanticipated fluctuations in the potential data at the onset of testing. These occur because the potentiostat is initially disconnected which allows minor drift in potential as the polymer settles to equilibrium. Other noise in the potential data is the result of application of potential relative to the reference electrode through use of the potentiostat. This can cause quick transients as the input voltage is adjusted in order to maintain the desired potential at the reference electrode. Despite these minor errors in the data, the figures indicate that the electrical response of the polymer is primarily linear. The time constant of the current decay after each potential step appears to be approximately the same for all electrical and mechanical loading conditions.

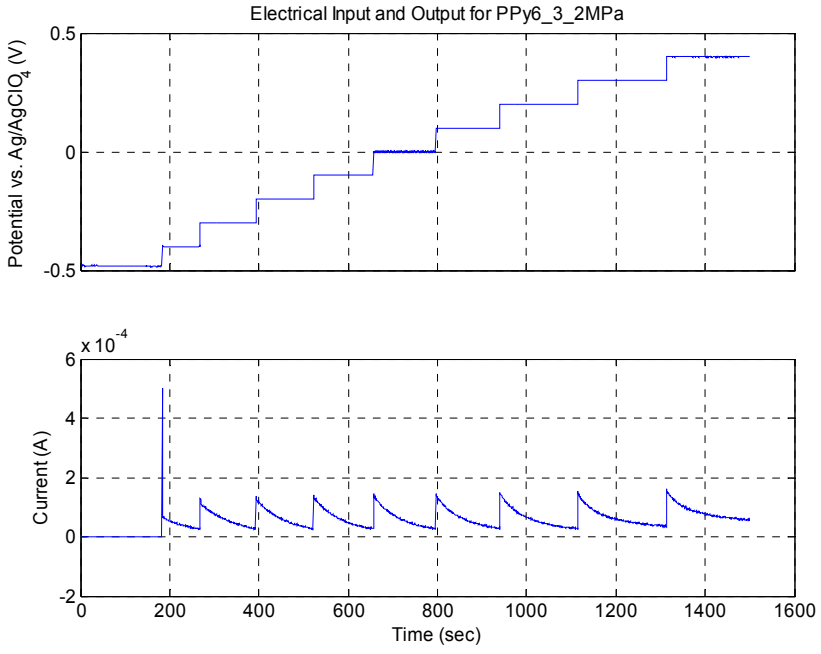

Figure 4-14: Electrical Potential Applied and Resulting Current vs. Time for 2 MPa Load

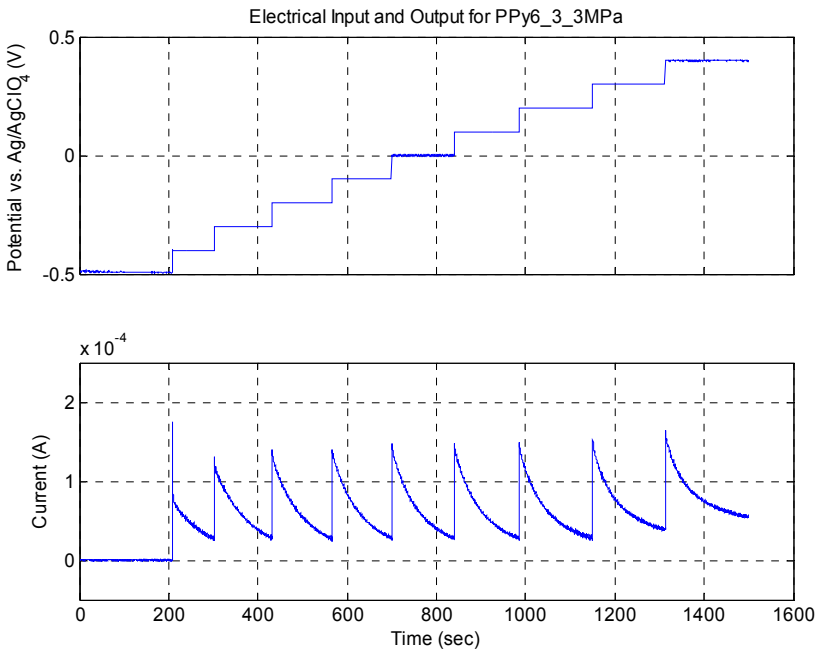

Figure 4-15: Electrical Potential Applied and Resulting Current vs. Time for 3 MPa Load

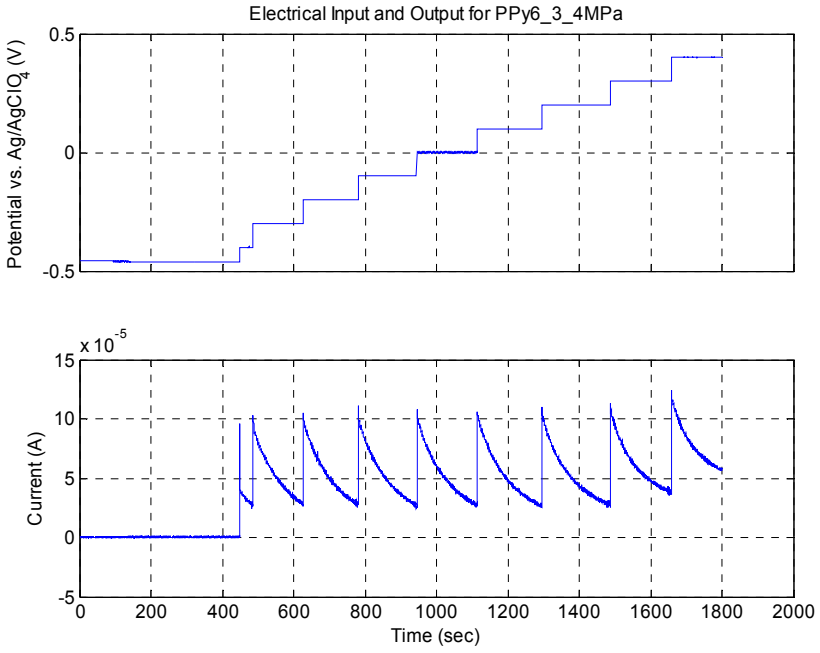

Figure 4-16: Electrical Potential Applied and Resulting Current vs. Time for 4 MPa Load

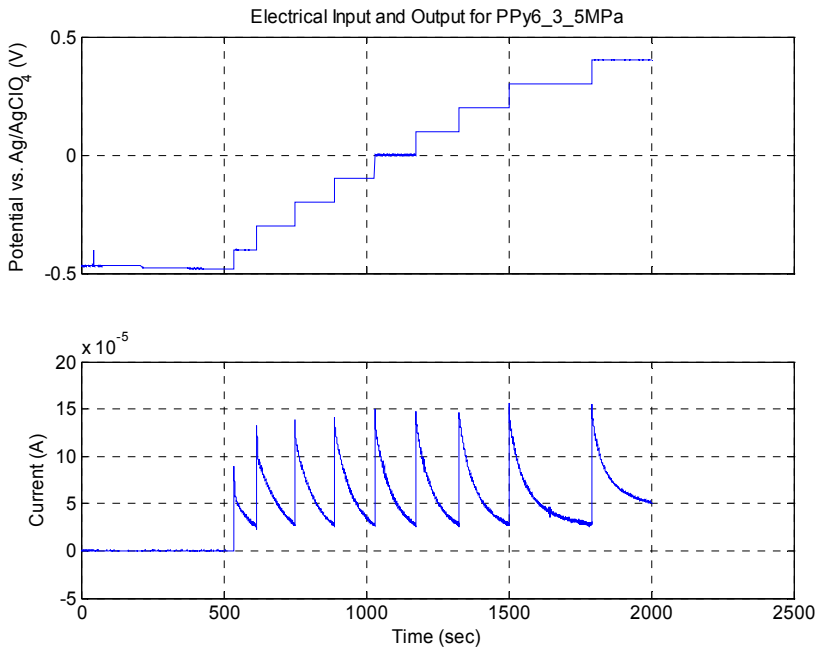

Figure 4-17: Electrical Potential Applied and Resulting Current vs. Time for 5 MPa Load

While these experiments provide validation of the linear electrical model, they also provide significant insight into the coupling between domains due to the large observable strains during testing. Figure 4-18 through Figure 4-21 show strain versus charge for the preceding tests.

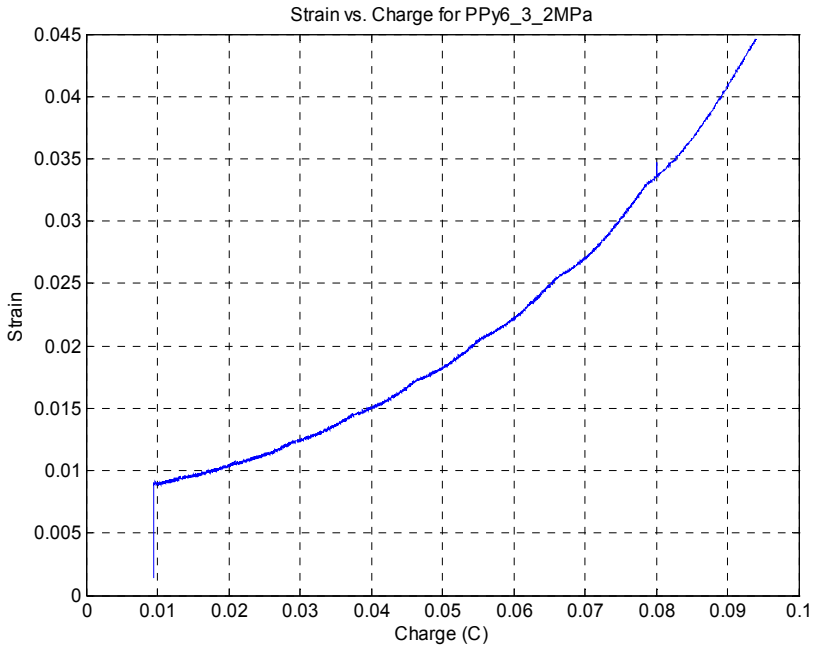

Figure 4-18: Strain versus Charge for Electrically Loaded Polymer with 2 MPa Mechanical Load

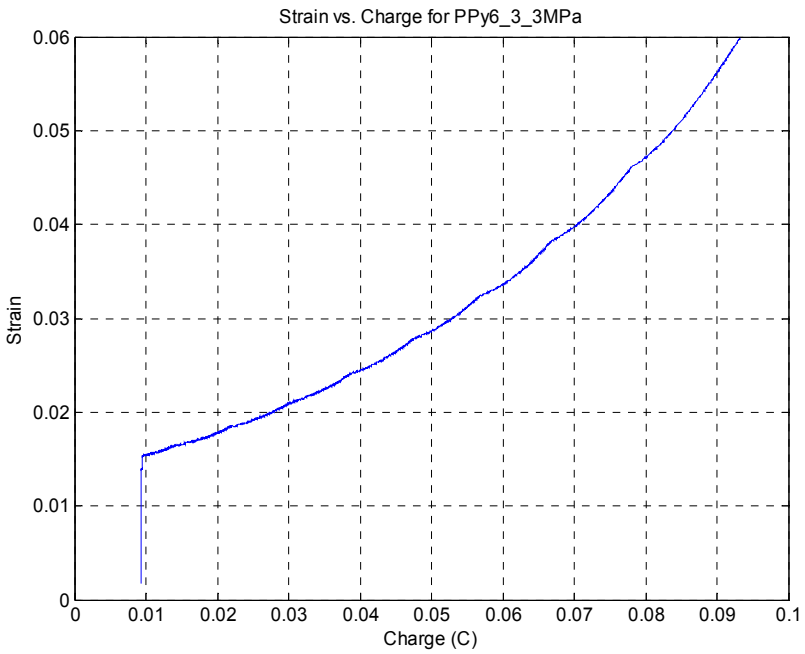

Figure 4-19: Strain versus Charge for Electrically Loaded Polymer with 3 MPa Mechanical Load

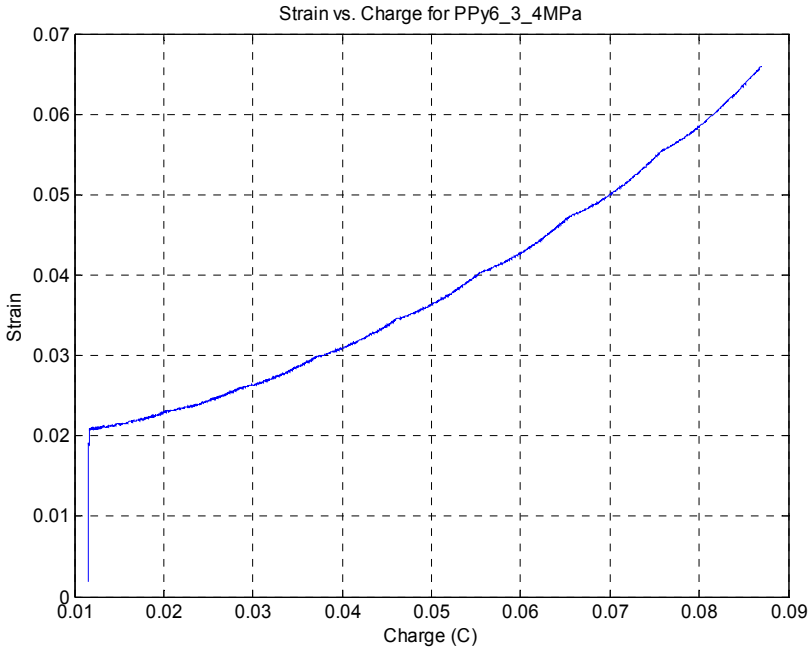

Figure 4-20: Strain versus Charge for Electrically Loaded Polymer with 4 MPa Mechanical Load

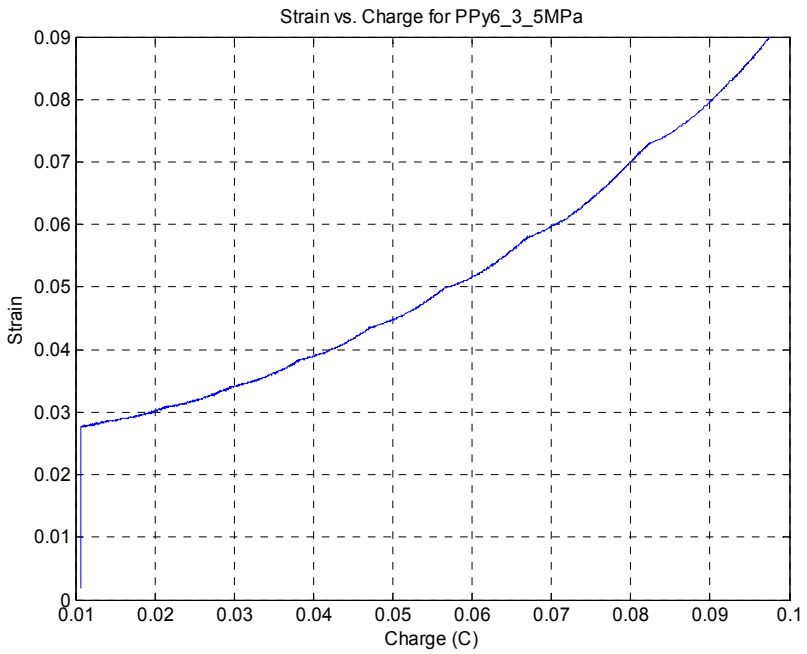

Figure 4-21: Strain versus Charge for Electrically Loaded Polymer with 5 MPa Mechanical Load

The results from these tests suggest that the coupling between domains is quadratic as expected based on the analysis of electromechanical coupling in Section 3.3. Further validation of this result is provided in the next section. The strain-charge curves exhibit a slight ripple that coincides with the application of potential steps. It will be demonstrated in Chapter 5 that the EAP dynamic model can reproduce this ripple, which results primarily from the effect of non-uniform charge distribution as discussed in Section 3.6.

After examining the previous data an additional test was performed on a different polymer sample in an attempt to reach mechanical equilibrium after applying electrical step inputs. The duration of the test was considerably longer with the application of each potential step lasting for 1 hour. The initial polymer potential was -0.7 V vs. $Ag/AgClO_4$. From Figure 4-22 it is seen that this potential is slightly below the PZC, with the application of -0.6V resulting in an initial negative strain. The results from this experiment again suggest that the coupling between domains exhibits a quadratic dependence on charge as seen in Figure 4-23.

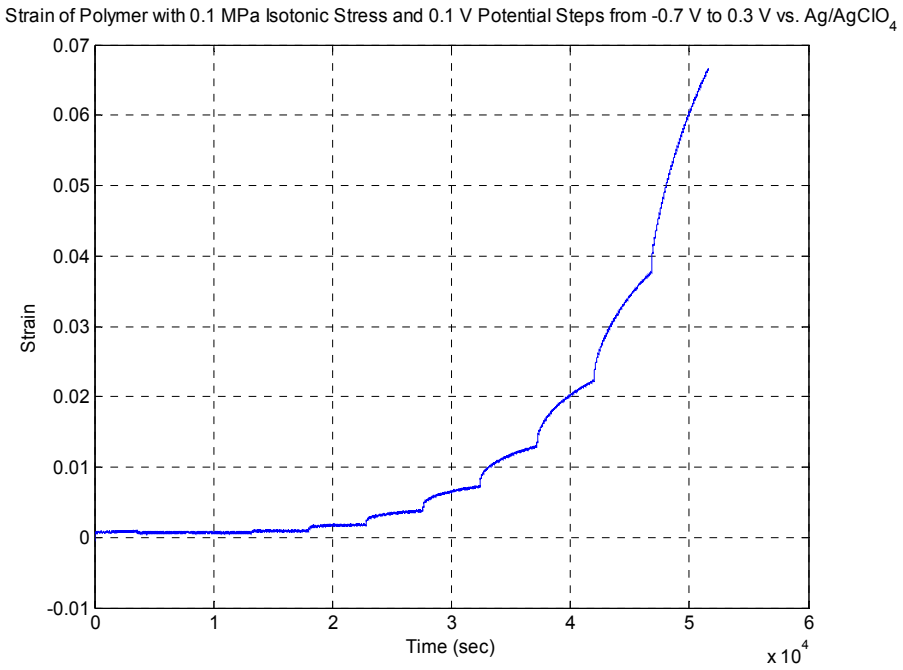

Figure 4-22: Strain of Polypyrrole vs. Time for 0.1 MPa Isotonic Loading with 0.1 V Potential Steps Applied Every Hour

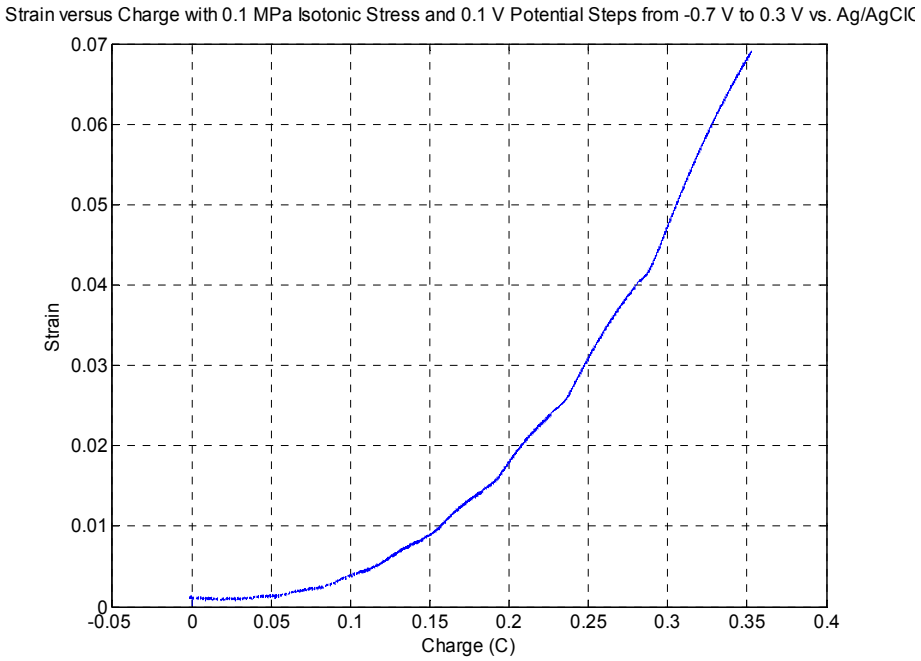

Figure 4-23: Strain of Polypyrrole vs. Charge for 0.1 MPa Isotonic Loading with 0.1 V Potential Steps Applied Every Hour

It is worth noting that the electrochemical strain achieved in this experiment was almost 7%. However, much of this strain is the result of electrochemically induced polymer viscoelasticity. The tests on the first polymer sample were performed over a much smaller time interval and exhibit only about 3% electrochemical strain for a potential of about 1 V relative to the PZC.

4.5 Electromechanical Testing

4.5.1 Isotonic Testing with Current Input

Using current input it is possible to directly determine the relationship between strain and charge. For these tests the polymer was first allowed to reach electrical equilibrium at a specified potential. Early tests used the open cell potential (OCP) as the initial potential and later tests started at -0.6V relative to the $Ag/AgClO_4$ reference electrode. This value was found to correspond to the minimum strain of the polymer suggesting that few electrolyte ions are diffused within the polymer at this potential, which suggests that it is the potential of zero charge. After the polymer reached electrical equilibrium the potentiostat was adjusted to its galvanostat mode to allow for input of constant current. The initial current was set to zero. The polymer was then loaded mechanically and allowed to creep for 1800 seconds. At this point a current of 120μA was applied to the polymer using galvanostatic input. Based on the volume of the polymer sample (0.966 mm^3) this represents a current density of 125 $\mu A/mm^3$. This is much lower than the current densities used in previously published experiments [6], which should allow for a better examination of quasi steady-state behavior including coupling between domains. The polymer sample used for this set of tests was PPy7.

The first test presented here shows the response of an 18μm sample of polypyrrole that was initially in electrochemical equilibrium at -0.7 V vs. $Ag/AgClO_4$. The electrical input and resulting strain is presented in Figure 4-24. The polymer clearly exhibits an initial decrease in strain upon application of current at 1800 seconds. This is caused by the removal of cations from the polymer. The strain bottoms out at around 1900 seconds before increasing again due to the insertion of anions into the polymer. This result indicates that the PZC of the polymer is above -0.7 V vs. $Ag/AgClO_4$. The tests in the previous section showed that the PZC is below -0.5 V vs. $Ag/AgClO_4$. From these two results the PZC is assumed to reside near -0.6 V vs. $Ag/AgClO_4$. Therefore, the remainder of the galvanostatic tests were started at -0.6V in order to avoid insertion of cations into the system, which complicates analysis of the actuator coupling dynamics.

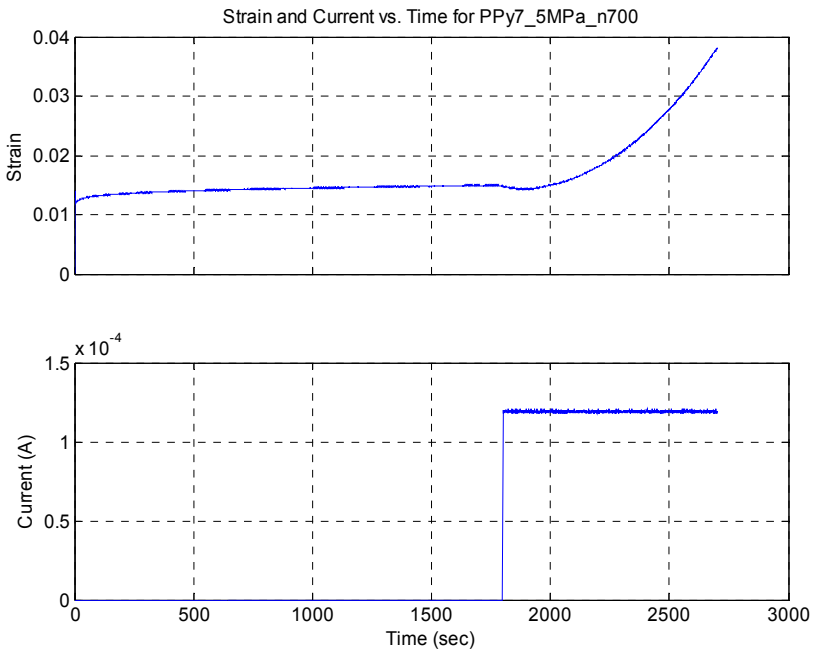

Figure 4-24: Electrical Current Input and Polymer Strain vs. Time for Isotonic Testing with Polymer Initially in Equilibrium at -0.7 V vs. $Ag/AgClO_4$

The ability of the polymer to exhibit positive strain with the application of a positive or negative current indicates that the system has non-minimum phase characteristics due to the quadratic nonlinearity at the PZC. This has major implications for control of EAP actuators, demonstrating that classical control methods can result in instability depending on the operating point of the system and allowable range of control inputs.

The relationship between charge and strain for the preceding test is shown in Figure 4-25. The data is fit with a quadratic curve to emphasis the quadratic nature of the coupling. The correlation between the data and the quadratic fit is extremely good with a maximum residual strain of just 2.14×10^{-4}. This provides strong validation of the analysis in Section 3.3. Using the equation of the curve that is shown in the figure, it is also possible to compare the quadratic coupling model from Section 3.3 to the linear coupling models published previously [4, 6]. The slope of the curve at 0.05 Coulombs is 24.8 (%/C). To convert this to the linear coupling coefficient, α, this value is multiplied by the volume of the polymer:

$$\alpha = 0.248 \cdot 9.66\times10^{-10} = 2.40\times10^{-10}\,\mathrm{m^3/C} \tag{4.6}$$

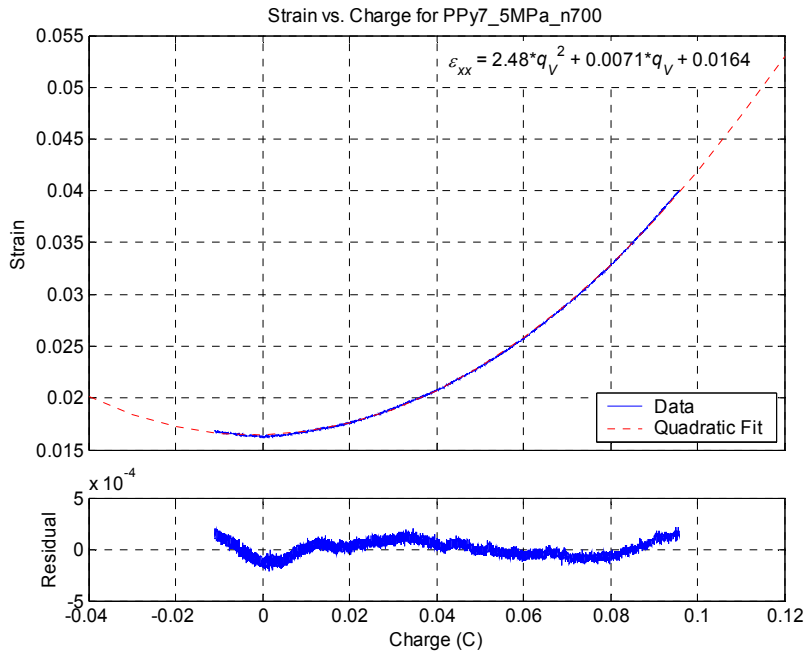

Figure 4-25: Quadratic Curve Fit of Strain vs. Charge for 5 MPa Isotonic, Galvanostatic Test with Polymer Initially at -0.7 V vs. $Ag/AgClO_4$

For comparison, published values of coupling coefficient are 1.2×10^{-10} [4] and 3×10^{-11} (m^3/C) [6]. The linearized coupling coefficient from this data is very close to the previously published strain-to-charge ratios. Possible sources of the discrepancy can also be accounted for. The values published by the other authors were obtained during relatively high-frequency periodic actuation (a period of about 60 seconds for Mazzoldi *et al* and a period of about 100 seconds for Madden), which may indicate why less strain was observed. Additionally, the material stiffness reported by both Mazzoldi *et al* and Madden was about 800 MPa. It was found during viscoelastic testing that the initial stiffness of this polymer sample was about 330 MPa and the relaxed stiffness at 2700 seconds could be as low as 200 MPa. Because the strain to charge coefficient is inversely proportional to stiffness, as shown in Section 3.5, this lower stiffness would result in a higher coefficient than reported for stiffer samples.

Additional tests were performed with the polymer initially in equilibrium at the PZC (-0.6 V vs. $Ag/AgClO_4$). The electrical inputs and resulting strains are shown below in Figure 4-27, which includes results from three isotonic experiments. The relationship between charge and strain for these three experiments is presented in Figure 4-27.

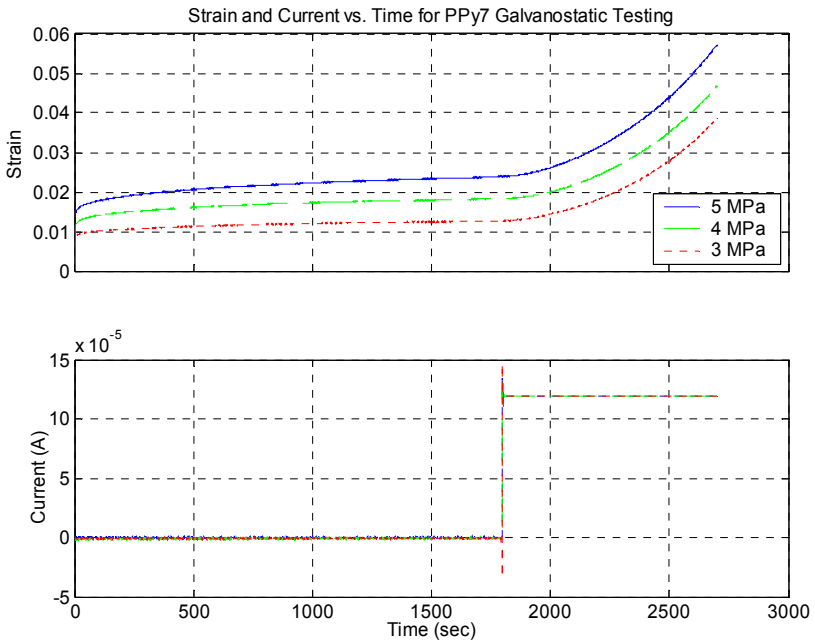

Figure 4-26: Electrical Current Input and Polymer Strain vs. Time for Isotonic Testing with Polymer Initially in Equilibrium at -0.6 V vs. $Ag/AgClO_4$

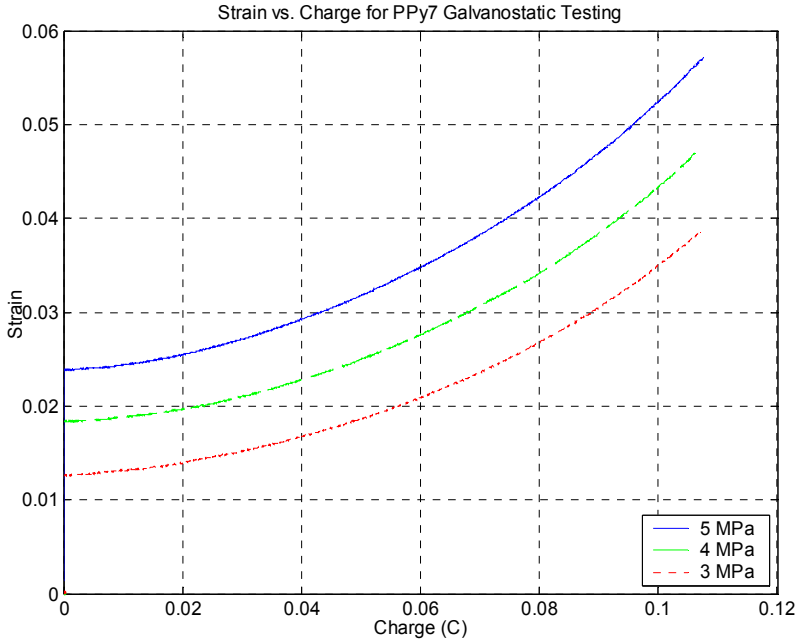

Figure 4-27: Strain versus Charge for 18µm Polypyrrole Sample with Constant Current Applied

The data again suggest a quadratic relationship between strain and charge. To validate the quadratic dependence, Figure 4-28 through Figure 4-30 present the curves from Figure 4-27 along with quadratic fits obtained using MATLAB function 'polyfit'.

The quadratic coefficients obtained from the quadratic fits range from 2.15 to 2.59 and seem to have some dependence on the mechanical load applied. This makes sense intuitively because the polymer would exhibit more creep under higher load than it would under lower load. Since the curve fit of the data does not discriminate between electrochemical stain and viscoelastic strain any mechanical creep that occurs during the application of electrical input affects the calculated charge-to-strain coupling equation.

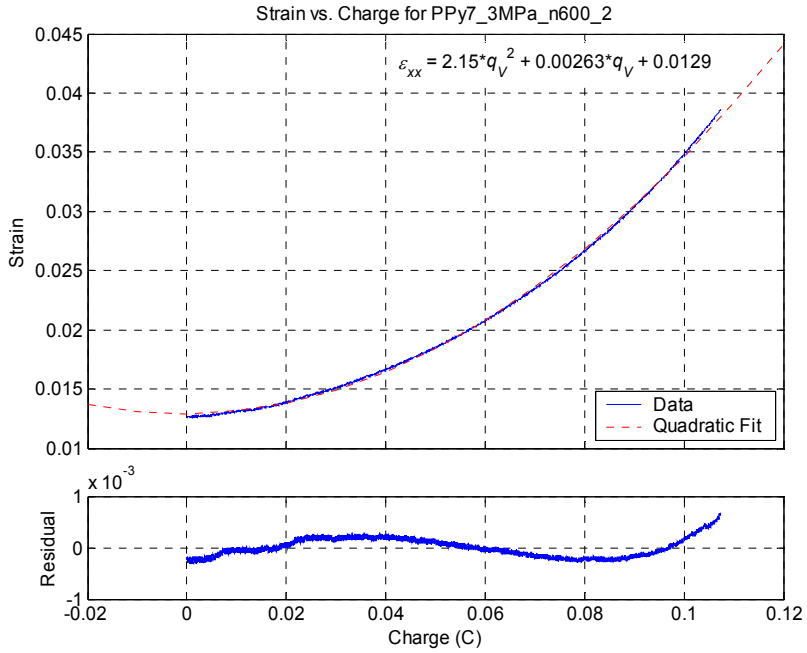

Figure 4-28: Quadratic Curve Fit of Strain vs. Charge for 3 MPa Isotonic, Galvanostatic Test with Polymer Initially at -0.6 V vs. $Ag/AgClO_4$

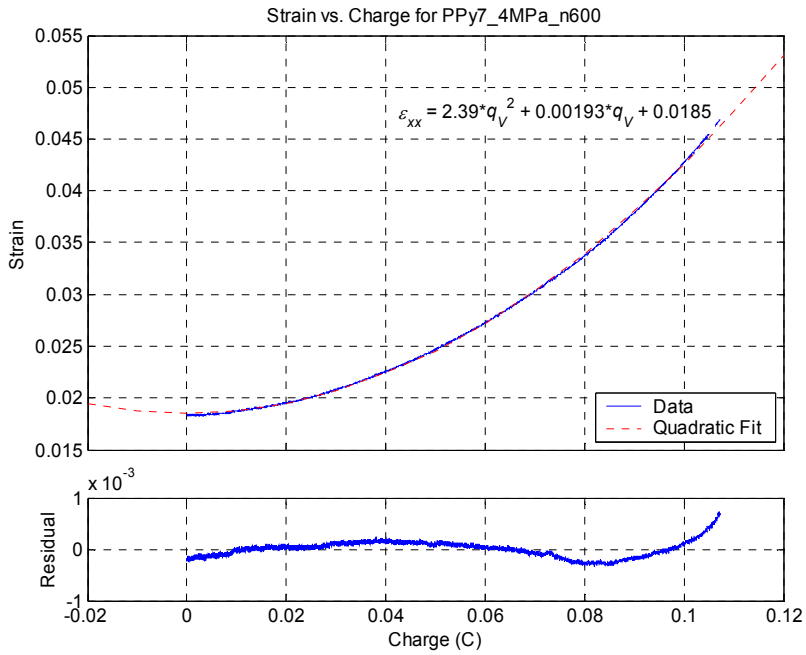

Figure 4-29: Quadratic Curve Fit of Strain vs. Charge for 4 MPa Isotonic, Galvanostatic Test with Polymer Initially at -0.6 V vs. $Ag/AgClO_4$

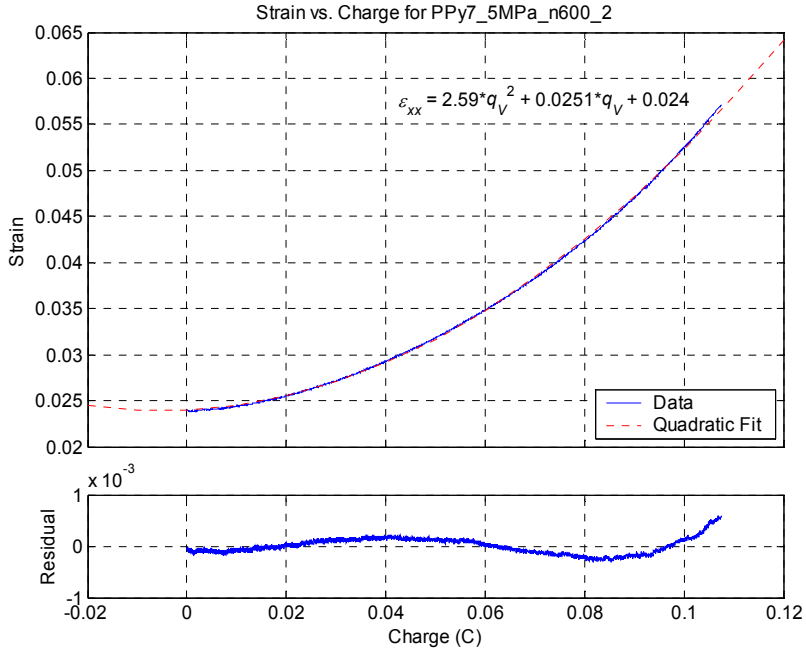

Figure 4-30: Quadratic Curve Fit of Strain vs. Charge for 5 MPa Isotonic, Galvanostatic Test with Polymer Initially at -0.6 V vs. $Ag/AgClO_4$

The analysis in Section 3.3 also indicated that the relationship between electrical potential and strain is quadratic. While that analysis pertains to steady-state conditions, Figure 4-31 demonstrates that the quadratic relationship is evident during slow dynamic response.

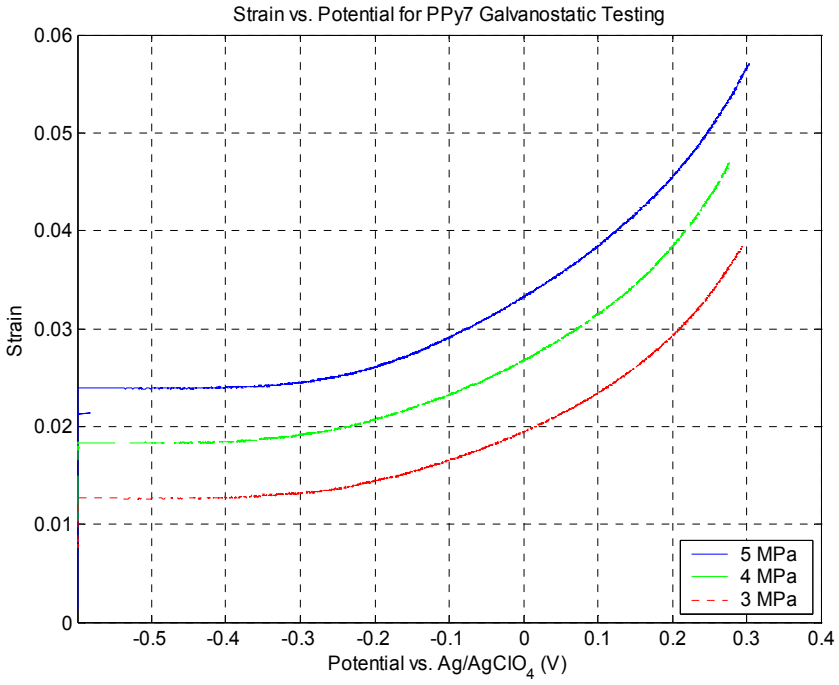

Figure 4-31: Strain versus Potential for 18μm Polypyrrole Sample with Constant Current Applied

Overall, the tests with electrical input support the hypothesis that strain is quadratically dependent on charge.

4.5.2 Equipotential Testing with Force Input

While the preceding tests demonstrate the coupling from the electrical domain to the mechanical domain, it is also possible to observe the induced electrical effects caused by mechanical loading. It was mentioned previously that electrical effects caused by mechanical inputs are negligible, indicating that EAP have high values of Poisson's ratio. In fact the model predicts that the observed electrical effects should completely disappear if the polymer is in equilibrium at the potential of zero charge. For this set of tests the polymer was given a fixed potential input using the potentiostat. After 900 seconds, mechanical step inputs were applied in order to observe induced currents in the electrical domain. Tests were performed at a range of potentials from -0.8 to 0.2 Volts vs.

$Ag/AgClO_4$. Mechanical loading during the tests followed the pyramidal shape depicted in Figure 4-32, which allowed the volume of the polymer to increase and decrease during the test.

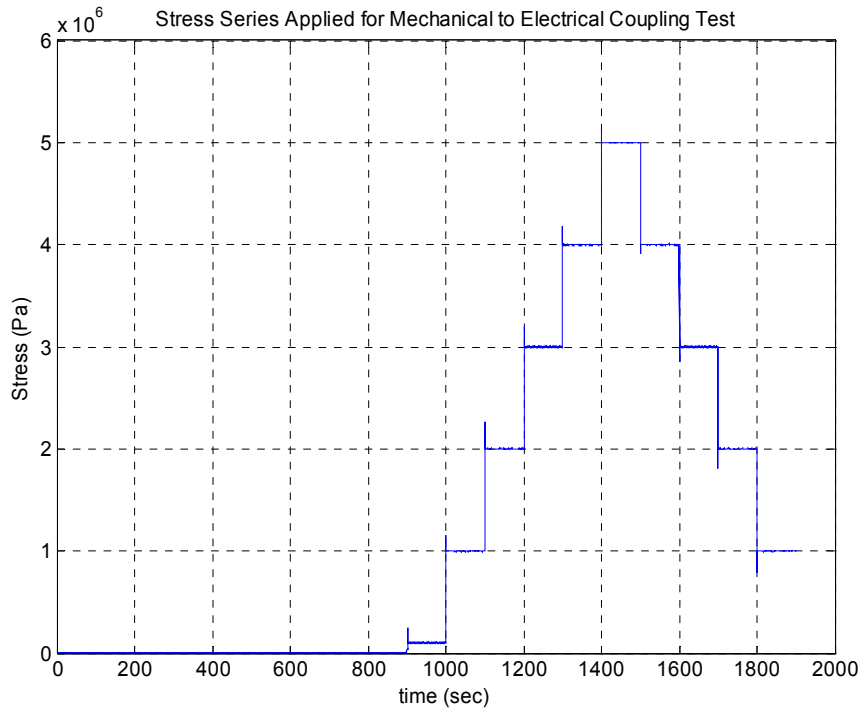

Figure 4-32: Stress Series Applied During Equipotential Testing with Mechanical Input

The first experiment started from 0.2V vs. $Ag/AgClO_4$ and the potential was lowered in steps of 0.1V for each successive test. The desired potential was applied at the beginning of each test so that large current transients could be observed as the polymer reached equilibrium. Figure 4-33 presents the current response of the polymer for the equipotential test at 0.1V vs. $Ag/AgClO_4$.

The current response of the polymer appears to be first-order as expected based on the results of Section 4.4. The induced current resulting from mechanical loading cannot be seen at this scale. To see the induced electrical effects it is necessary to examine a much smaller window of data. In addition, the data needs to be filtered because the signal to noise ratio is too small to observe the minimal currents that result from mechanical loading. After applying a twenty-second moving average filter to the data it is possible to observe induced electrical effects as shown in Figure 4-32, which presents results for six applied potentials.

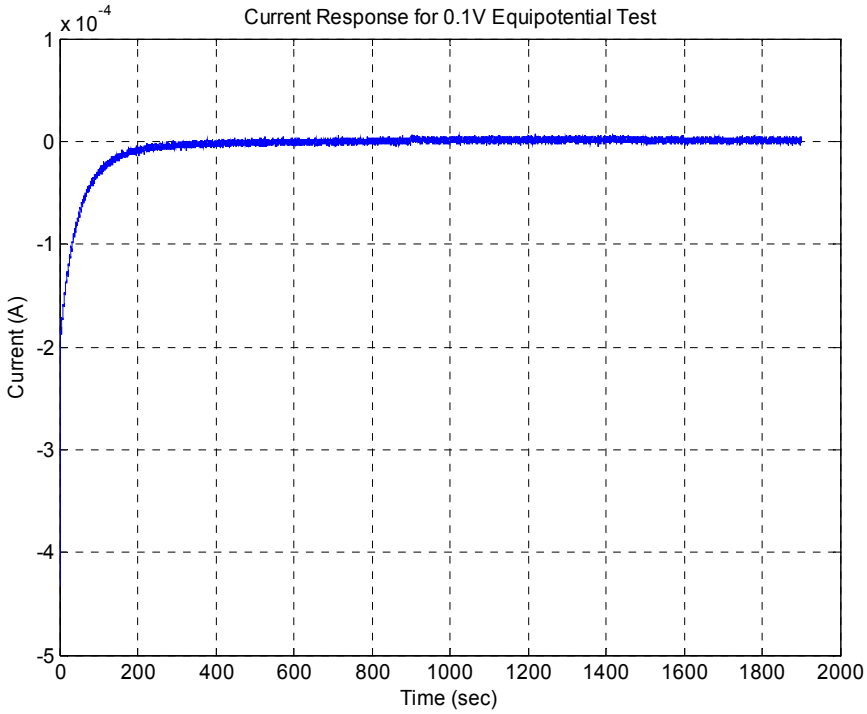

Figure 4-33: Current Response to Equipotential Input at t=0 and Mechanical Loading at t=900

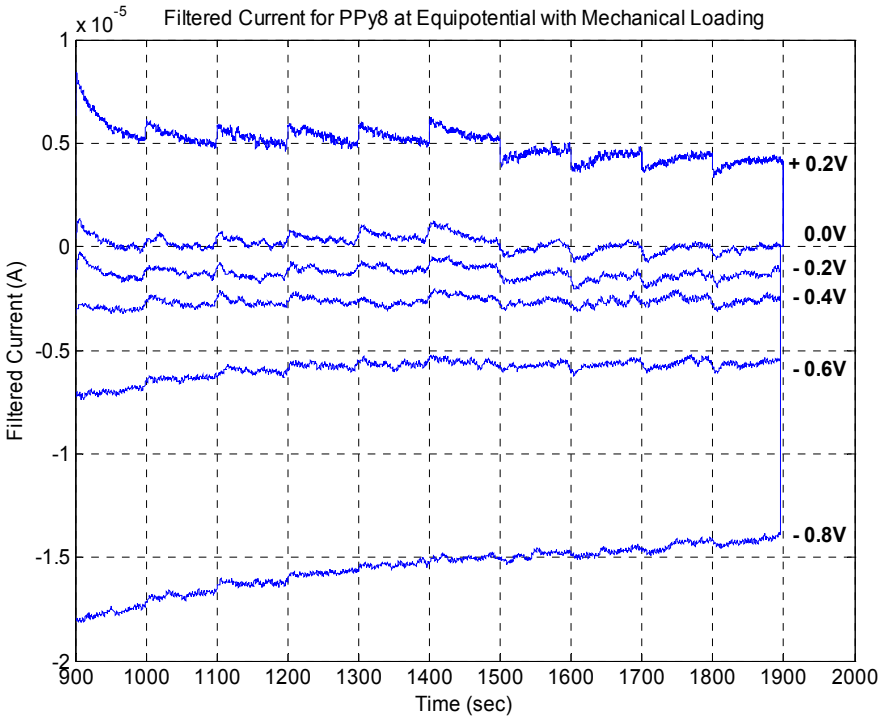

Figure 4-34: Induced Currents in Polymer from Mechanical Step Inputs

The offsets in the current seem to be related to the decay of input current as the polymer approaches equilibrium. For the first test, which examined an equipotential of 0.2V vs. $Ag/AgClO_4$, the offset current indicates that the polymer may have been charging still at the onset of mechanical loading. There is a large peak in the current with the application of the 0.1MPa load. This is because there was considerable slack in the polymer that was taken up during this first step input, which may have significantly changed its volume. The successive peaks all correspond to 1MPa increases or reductions in loading. The amplitudes of the associated current peaks are about 1μA relative to the offset current. Integrating the area under each of these current steps gives input or output charge of between 40 and 50 μC. Comparing Figure 4-33 and Figure 4-34, it is clear that the mechanically-induced current is more than two orders of magnitude less than the current needed to equilibrate a 0.1V step in potential. The charge transferred with the application of the step potential is about 0.01C, which is 200 times larger than the charge required to balance the 1MPa stress input.

For the 0.0V, -0.2V and -0.4V experiments there is minimal current offset at the initiation of mechanical input, which indicates that the distribution of anions in the polymer may have been close to equilibrium. The current spikes are still apparent in these tests; however, it is clear that their amplitudes are smaller than the 0.2V experiment. For the -0.6V test the offset current is much larger, which may be a cumulative effect as the distribution of ions in the polymer becomes less uniform due to the diffusion dynamics of the electrical domain. If the ion distribution in the polymer is not in equilibrium at -0.6V it would be expected that currents could still result despite earlier observations that this potential may correspond to the PZC of the polymer. Similarly, the experiment at -0.8V vs. $Ag/AgClO_4$ may still indicate leakage of anions from the polymer rather than input of cations. These explanations for the offset currents are certainly probable because the polymer was only allowed 900 seconds from the application of a potential to onset of mechanical loading. Additionally, the time allowed between tests ranged from only 140 to 1000 seconds. Despite these possible sources of error in the “equipotential” data, it is clear that the coupling from the mechanical domain to the electrical domain is significantly less as the polymer potential nears the PZC. It is almost impossible to distinguish peaks in current in the -0.8V test from measurement noise. This gives more credence to the coupling model by demonstrating that coupling from mechanical input to electrical output indeed diminishes as the polymer approaches the PZC.

4.6 Summary

Several experiments were performed on linear actuators composed of polypyrrole in order to validate the dynamic models developed in Chapter 3. The mechanical domain was analyzed using both step

inputs and frequency sweeps, and both verify that the polymer can be modeled as a reticulated structure of linear elements. Similarly, experiments on the electrical domain demonstrated that the reticulated electrical model can describe the dynamics of the electrical domain with a combination of linear elements. The result of the frequency sweep tests raises some questions about the validity of the electrical model at low frequencies; however, the model exhibits very little disparity in the magnitude of frequency response. The results of the electrical experiments all support the nonlinear constitutive equation that was formulated in Section 3.3. Additionally, the electrical experiments indicate that the potential of zero charge for the polypyrrole-TEAPF$_6$ actuator is near -0.6V vs. an Ag/AgClO$_4$ counter electrode. This is the point at which the polymer contains the fewest number of anions and cations, and coincides with the least amount of polymer strain. The less-observable coupling from mechanical inputs to electrical outputs was demonstrated with equipotential testing. The results of these tests also agree with the response predicted by the nonlinear coupling equation. The ability of the complete dynamic model to reproduce these experimental results will be demonstrated in the next chapter.

4.7 Chapter References

[1] Rinderknecht, Derek, "Design of a Dynamic Mechanical Analyzer for the Active Characterization of Conducting Polymer Actuators," B.S. Thesis, MIT, Cambridge, MA, 2002.

[2] Lennart Ljung, *System Identification, Theory for the User; Second Edition*. Upper Saddle River: Prentice Hall, 1999.

[3] Åström, Karl J. and Björn Wittenmark, *Computer-Controlled Systems, Theory and Design; Third Edition*, Upper Saddle River: Prentice Hall, 1997.

[4] Madden, John D. W., *Conducting Polymer Actuators*, Ph.D. Thesis, MIT, Cambridge, MA, 2000.

[5] Peter Madden. *Development and Modeling of Conducting Polymer Actuators and the Fabrication of a Conducting Polymer Based Feedback Loop*, Ph.D. Thesis, MIT, Cambridge, MA, 2003.

[6] Mazzoldi, A., A. Della Santa, and D. De Rossi, "Conducting Polymer Actuators: Properties and Modeling," in *Polymer Sensors and Actuators*, Y. Osada, and D. E. De Rossi, Eds., pp. 207-244, Springer Verlag, Heidelberg, 2000.

Chapter 5

Simulation of Experimental Results

Using the constitutive equations formulated in Chapter 3 it is possible to simulate the dynamic response of an EAP actuator. MATLAB ordinary differential equation solvers were used to simulate the coupled electrical and mechanical dynamics of an EAP actuator. Simulated responses were found for many of the electrical and mechanical loading conditions used during dynamic testing. The results of the simulations are compared to the test results and unknown parameters are tuned to approximate the actual response.

5.1 Required Model Complexity

The complexity of the EAP dynamic model depends on the desired frequency range of inputs and the parameters and dimensions of the polymer actuator system. For simulated polymers with a thickness at least one order of magnitude larger than the double layer thickness it is not necessary to include the double layer in the simulation. This is because the amount of charge stored in the double layer is an order of magnitude less than the charge stored in the polymer and does not contribute to actuator dynamics or electrical input. In addition, the number of reticulated diffusion elements needed in the model depends largely on the thickness of the polymer, a, the diffusion coefficient of the system, D, and the resistance of the electrochemical circuit, R_C. For a thin actuator or polymer with a fast diffusion coefficient fewer elements are needed to capture the diffusion dynamics. The varying amount of complexity needed in the polymer model is apparent in looking at Bode diagrams of the polymer admittance for a variety of parameters and polymer dimensions. The frequency response of polypyrrole admittance is simulated using several combinations of parameters. The response is found for reticulated models with 1, 4, and 8 elements and compared to the continuum model developed by Madden. The frequency responses depicted in Figure 5-1 to Figure 5-4 demonstrate the ability of the reticulated models to match the dynamics predicted by the continuum diffusion model. The responses shown in Figure 5-5 through Figure 5-8 demonstrate the effect of polymer thickness on the dynamics of the polymer electrical domain. The file used to produce these plots is provided in Appendix A.

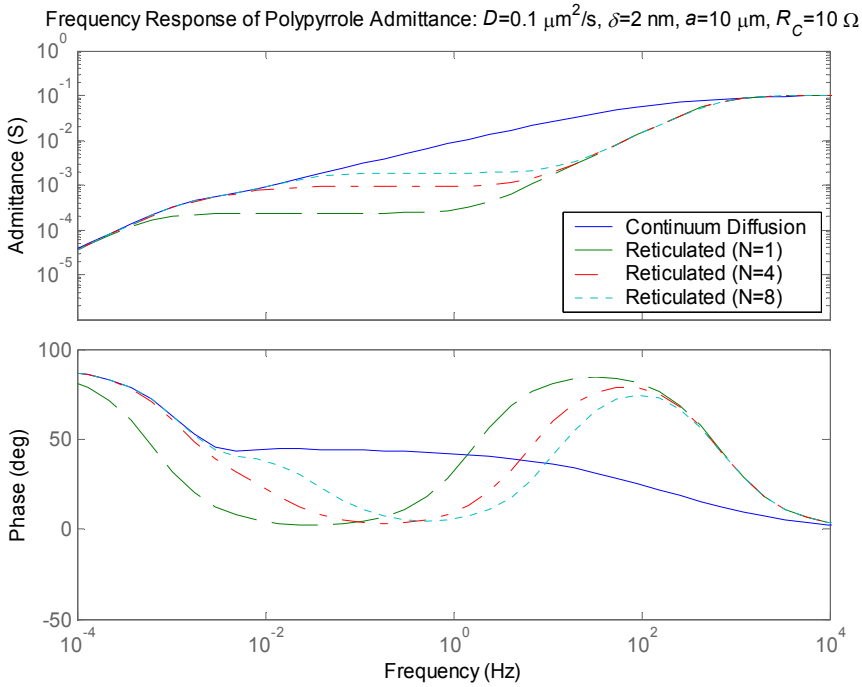

Figure 5-1: Polypyrrole Admittance with D=0.1 μm²/s, δ=2nm, a=10μm, and R_C=10Ω

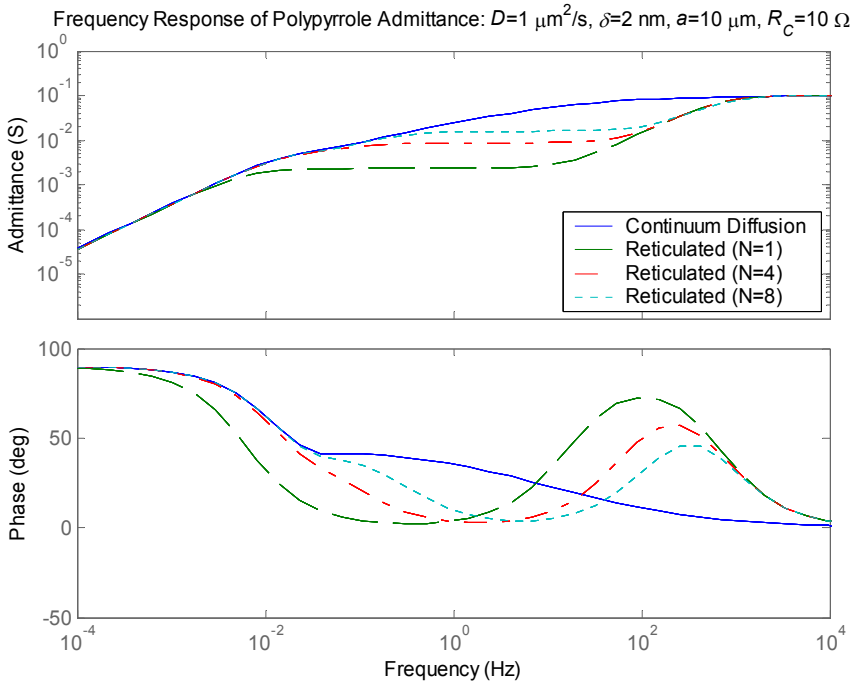

Figure 5-2: Polypyrrole Admittance with D=1 μm²/s, δ=2nm, a=10μm, and R_C=10Ω

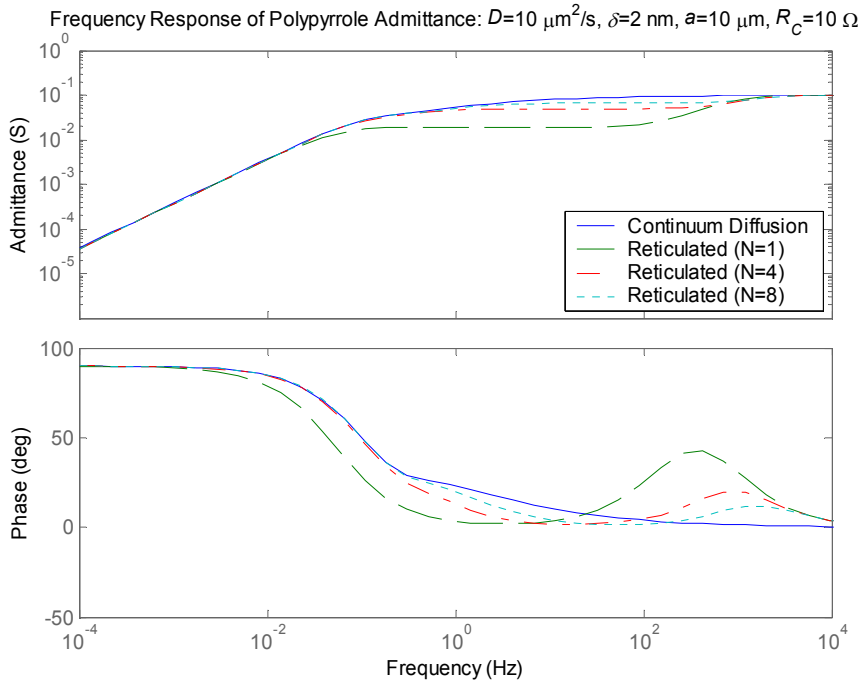

Figure 5-3: Polypyrrole Admittance with D=10 μm²/s, δ=2nm, a=10μm, and R_C=10Ω

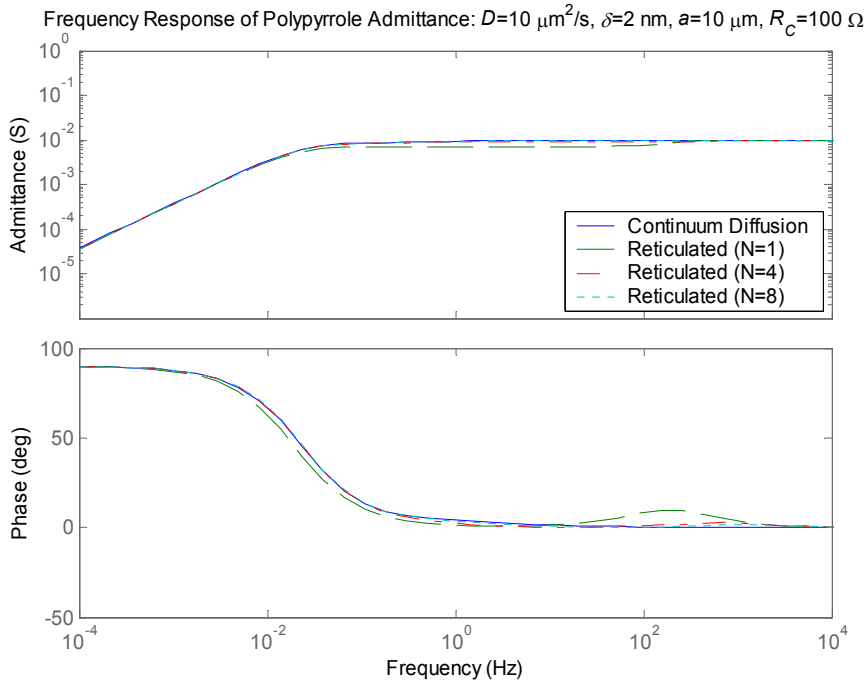

Figure 5-4: Polypyrrole Admittance with D=1 μm²/s, δ=2nm, a=10μm, and R_C=100Ω

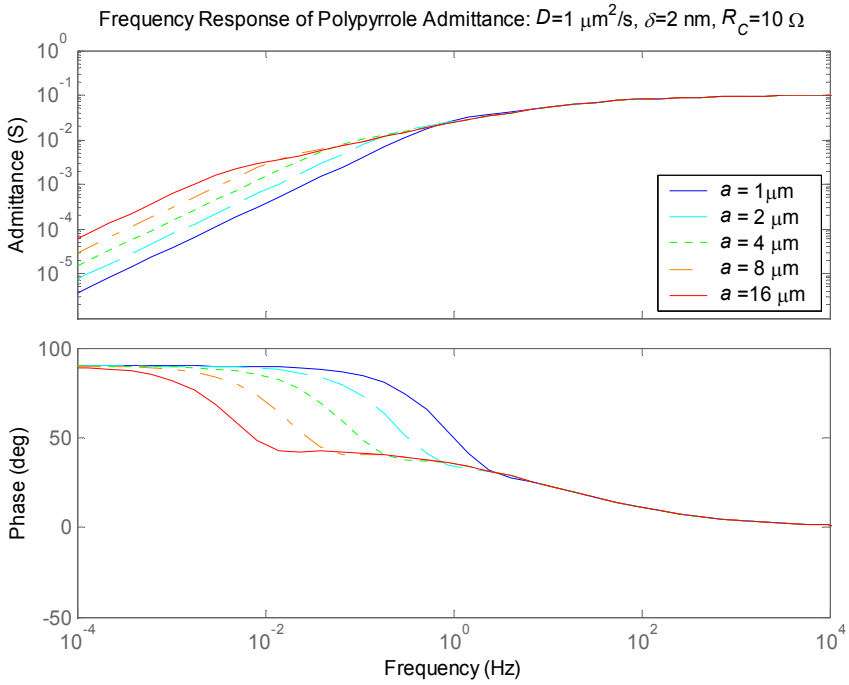

Figure 5-5: Polypyrrole Admittance with D=1 μm²/s, δ=2nm, and R_C=10Ω

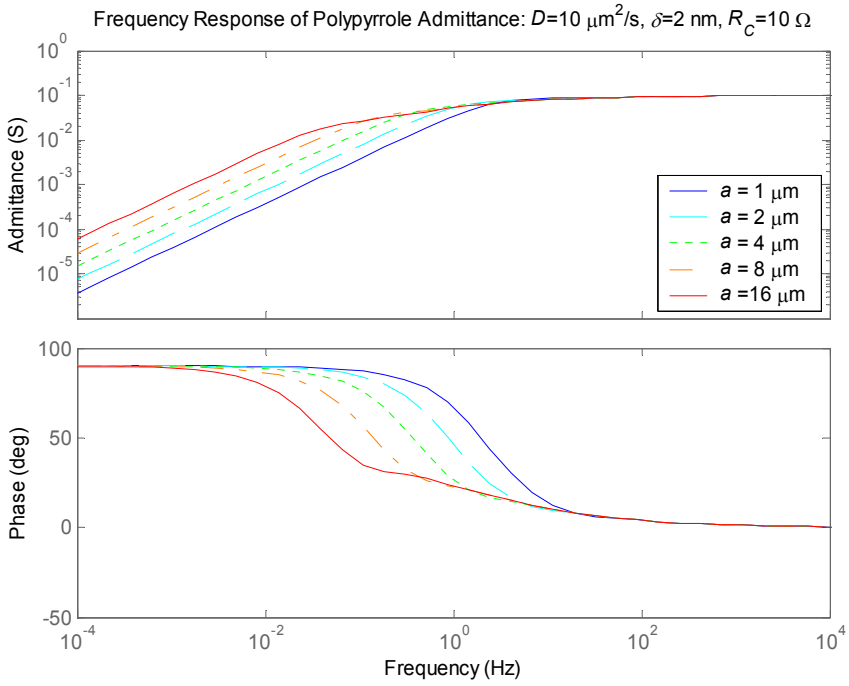

Figure 5-6: Polypyrrole Admittance with D=10 μm²/s, δ=2nm, and R_C=10Ω

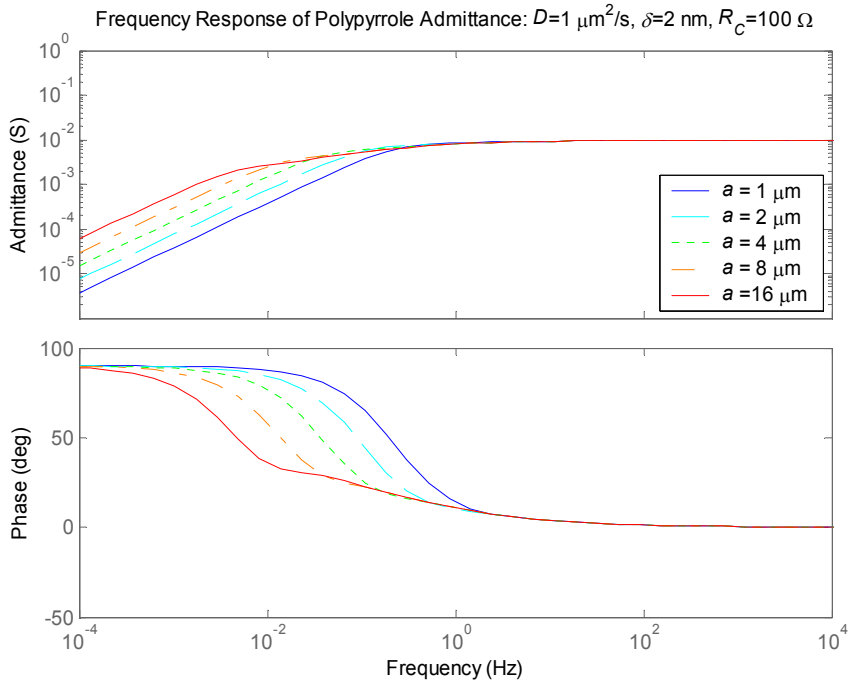

Figure 5-7: Polypyrrole Admittance with D=1 μm²/s, δ=2nm, and R_C=100Ω

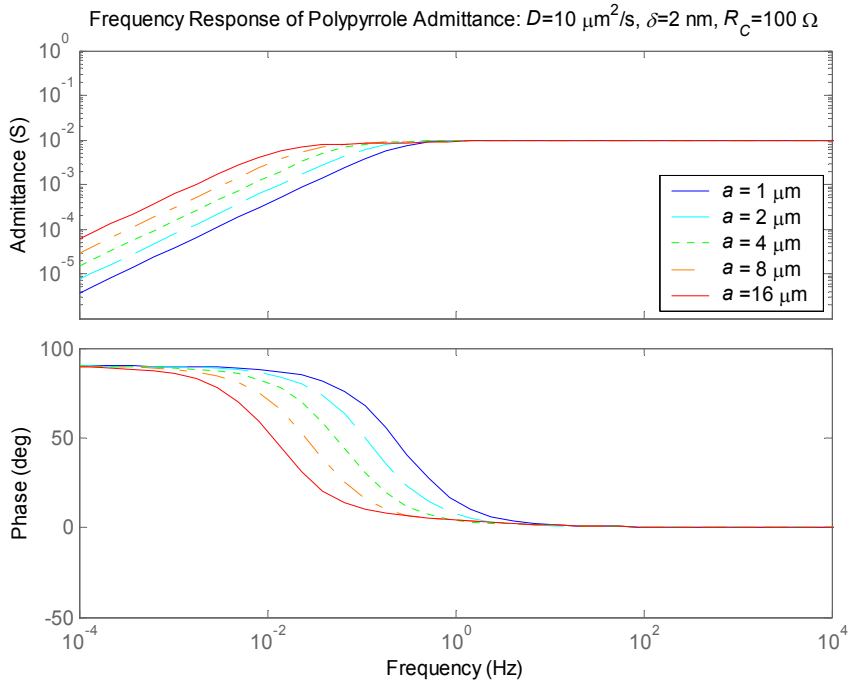

Figure 5-8: Polypyrrole Admittance with D=10 μm²/s, δ=2nm, and R_C=100Ω

It is evident in all of these plots that the frequency response of the polymer electrical domain exhibits mostly first-order behavior. The polymer is essentially an *RC* circuit with time constant determined by the total volumetric capacitance and series resistance. In Figure 5-1 to Figure 5-4 it is apparent that the reticulated model requires many elements if the diffusion dynamics contribute significantly to the actuator electrical response. As the diffusion dynamics diminish, the reticulated model requires fewer elements to reconstruct the dynamics predicted by the continuum model.

Figure 5-5 through Figure 5-8 demonstrate the effect that polymer thickness has on the actuator frequency response. Thinner samples have faster charging times and are impacted less by diffusion dynamics. In all of these figures it is apparent that a 1μm sample can be represented very well by a first order circuit. Only Figure 5-5 demonstrates some deviation from a first order response at frequencies above 1 Hz for a 1μm sample. For thicker samples the impact of diffusion is felt at lower frequencies. It is obvious in examining these figures that thinner samples are desirable if the actuator is to be operated at high frequencies. Additionally, it is beneficial to find combinations of polymer materials and electrolytes that have high diffusion coefficients. While large circuit resistances allow for use of first order models they increase the time constants of the system, limiting the applications for the actuator.

The complexity of the mechanical model depends on the duration of the actuator operation. It was demonstrated in Chapter 4 that polymer viscoelasticity impacts the mechanical response at every decade of the frequency domain. This is true whether the actuator is loaded mechanically or electrically, as electrical loads act on the polymer as hydrostatic pressures.

5.2 Model Comparison to Experimental Data

The reticulated electrical and mechanical models were combined in MATLAB using the constitutive relations from Chapter 3. The MATLAB ODE file used to simulate the response of the virtual actuator is provided in Appendix B. Solutions to the ODE file were determined using MATLAB command ‘ode23s,’ which allows poorly scaled state-space matrices to be solved quickly. The following subsections present the simulated response of the actuator compared with the experimental data when identical electrical and mechanical inputs were used. The initial conditions (charge and displacement) for all simulations were determined using the steady-state constitutive relations from Chapter 3. These relations are valid because all experiments were performed after the polymer had reached steady-state conditions.

5.2.1 Simulation of Isotonic Mechanical Testing

Parameters for the isotonic simulation were determined by examining the normalized data from the isotonic tests, which are shown below in Figure 5-9.

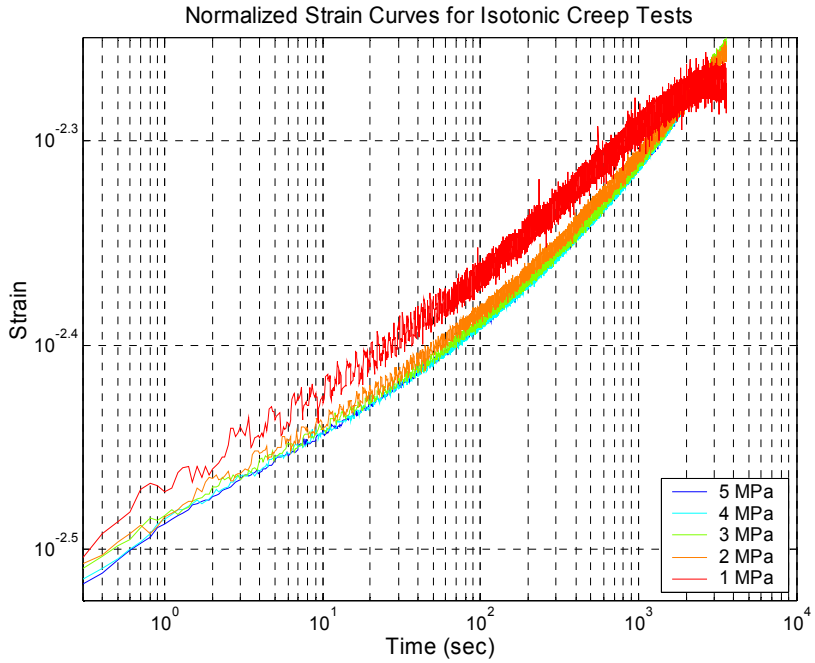

Figure 5-9: Logarithmic Plot of Isotonic Tests 1-5 MPa, Normalized by Load, 24 μm Polypyrrole Sample

The instantaneous strain at the initiation of loading is due to the combined stiffness of all the elastic elements in the viscoelastic model. This initial stiffness is easy to determine based on the intersection of the normalized curves with the y-axis. To determine the stiffness contributed by each of the elastic elements in the viscoelastic model it is necessary to break the step response down by decade. If it is assumed that the first viscoelastic element has a time constant of 1 second, the stiffness contributed by its elastic component, k_1, is found by comparing the strain at 1 second to the initial strain. The corresponding damping coefficient, b_1, is then determined from the 1 second time constant. The stiffness contribution from the second viscoelastic element, k_2, is found by comparing the strain at 10 seconds to the strain at 1 second. Because the associated time constant is assumed to be 10 seconds, the damping coefficient, b_2, can be determined. This process is repeated until the model contains the number of elements needed to recreate the observed mechanical response. Finally, the mechanical elasticity variables (with units of N/m^2) are determined based on the cross-sectional area of the polymer.

The parameters used to match the viscoelastic response are as follows: E_1 through E_7 are 60, 31.3, 33, 35.2, 46.2, 56.8, and 66 MPa, respectively; b_1 through b_7 are 10, 130, 1600, 1.71×10^4, 2.23×10^5, 2.76×10^6, and 3×10^7 kg/s, respectively. Simulating the mechanical response from the isotonic test presented in Section 4.3.1 gives the result shown below in Figure 5-10.

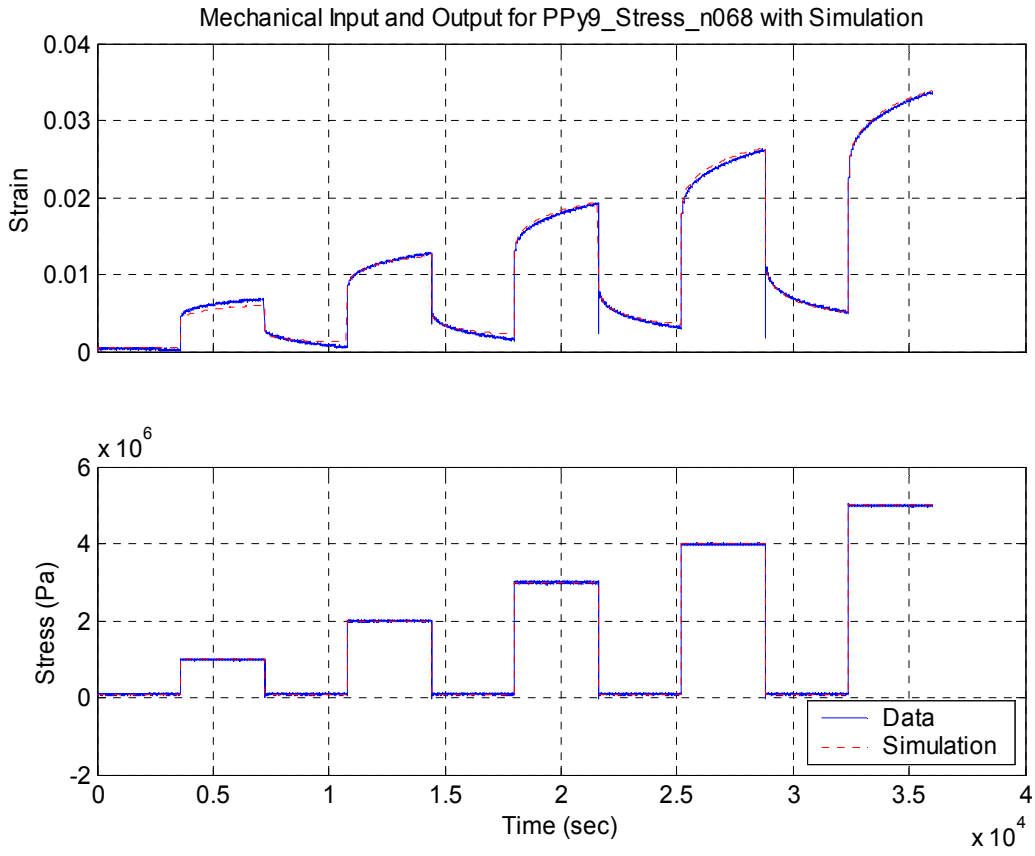

Figure 5-10: Simulated Response of Isotonically Loaded Polymer using 7-Element Viscoelastic Model

The simulated mechanical response of the polymer is almost identical to the observed response. This confirms that the standard linear model can reproduce the viscoelastic behavior of the polymer including relaxation after it is unloaded.

5.2.2 Simulation of Isotonic Testing with Voltage and Current Input

This set of simulations includes all aspects of the polymer dynamic model. The electrical domain is modeled by the linear reticulated diffusion model and the mechanical domain is modeled by the viscoelastic model. The electrical response of the polymer is dictated by the specific capacitance, c_V, diffusion coefficient, D, and series circuit resistance, R_Σ. The coupling between domains depends on

the elasticity of the material and Poisson's ratio, ν. The only other model parameters are the dimensions of the polymer, which were measured prior to testing. The free parameters were adjusted in order to get the best fit of the simulated response for each of the experiments. The free parameter values used in each of the simulations are tabulated in Table 5-1.

Table 5-1: Parameter Values Used in Simulations

Data File	c_V (F/m^3)	D (m^2/s)	R_Σ (Ohms)	ν
PPy6_3_2MPa	1.00e8	1e-12	800	0.44
PPy6_3_3MPa	1.05e8	1e-12	800	0.435
PPy6_3_4MPa	1.00e8	0.8e-12	1000	0.42
PPy6_3_5MPa	1.00e8	1e-12	800	0.41
PPy7_3MPa_n600_2	1.53e8	0.14e-12	270	0.41
PPy7_4MPa_n600	1.53e8	0.15e-12	270	0.40
PPy7_5MPa_n600_2	1.53e8	0.14e-12	270	0.39

The first four entries in this table are for sample PPy6 and the final three entries are for PPy7. The first sample, PPy6, was subjected to 0.1V potential steps from -0.5V vs. Ag/AgClO$_4$. The second sample, PPy7, had a constant current of 120μA applied. It is apparent from the values in the table that the properties of each sample were uniform for all tests. The only major discrepancy is for the electrical properties determined for the experiment labeled PPy6_3_4MPa, which was the 4MPa isotonic test with application of potential steps. Another apparent trend for all experiments is the dependence of Poisson's ratio on applied load, with higher loads having lower values of Poisson's ratio. While the exact source of this trend is not known, it may result from inaccuracies in the mechanical model, which would manifest as larger errors in strain at higher loads than at lower loads.

Because the polymer thickness is measured with a micrometer, the accuracy of the diffusion constant, D, and specific capacitance, c_V, are questionable. This is because the diffusion rate depends inversely on the square of the thickness and volumetric capacitance is proportional to thickness. This may explain the large disparity in the values obtained for the two samples, though the morphology of the samples may also affect this.

Simulated responses for the experiments on PPy6 are shown in Figure 5-11 through Figure 5-18. The responses for the three tests on PPy7 are shown in Figure 5-19 and Figure 5-20.

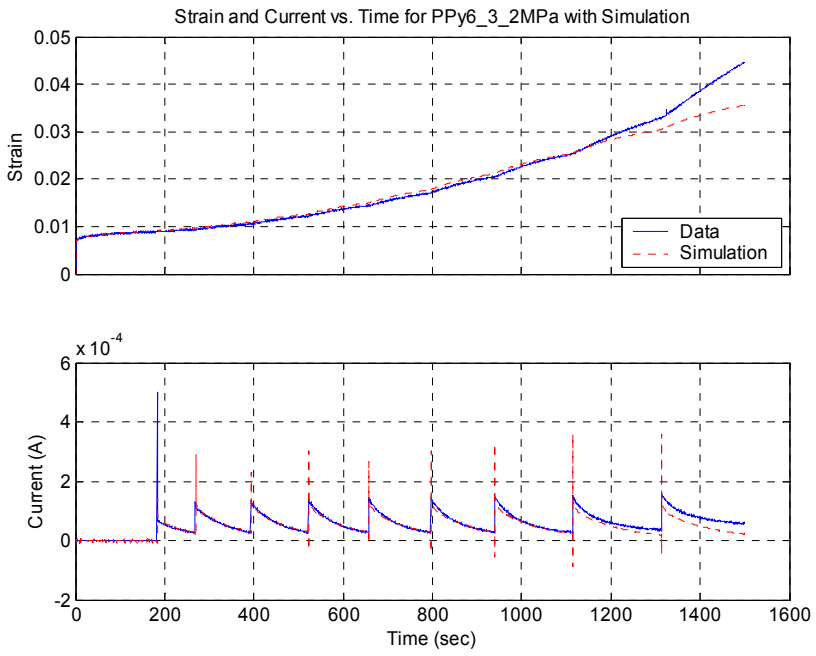

Figure 5-11: Simulated Electrical and Mechanical Response of Polymer with 2 MPa Isotonic Load and 0.1V Potential Steps from -0.5 V vs. Ag/AgClO$_4$

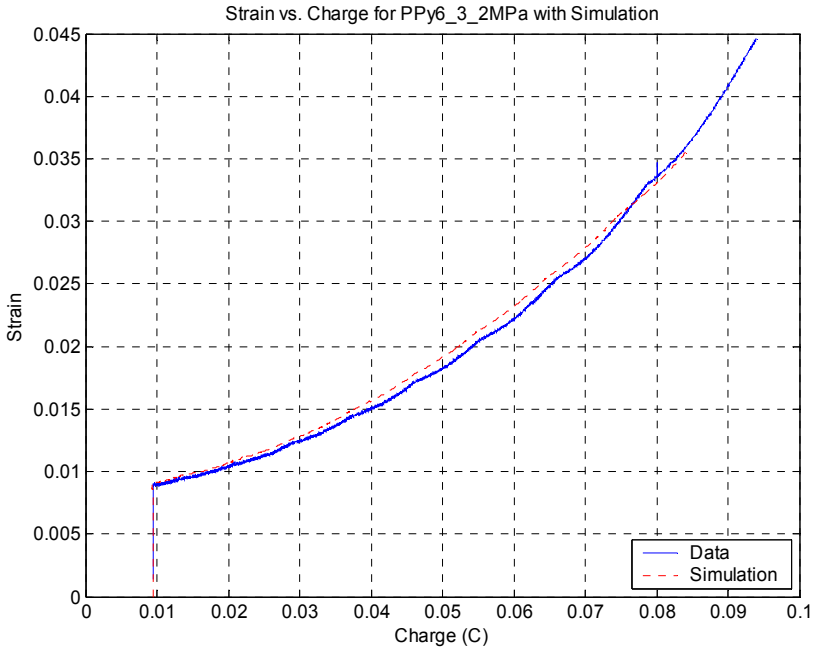

Figure 5-12: Simulated Strain vs. Charge for 2 MPa Isotonic Load with Potential Steps

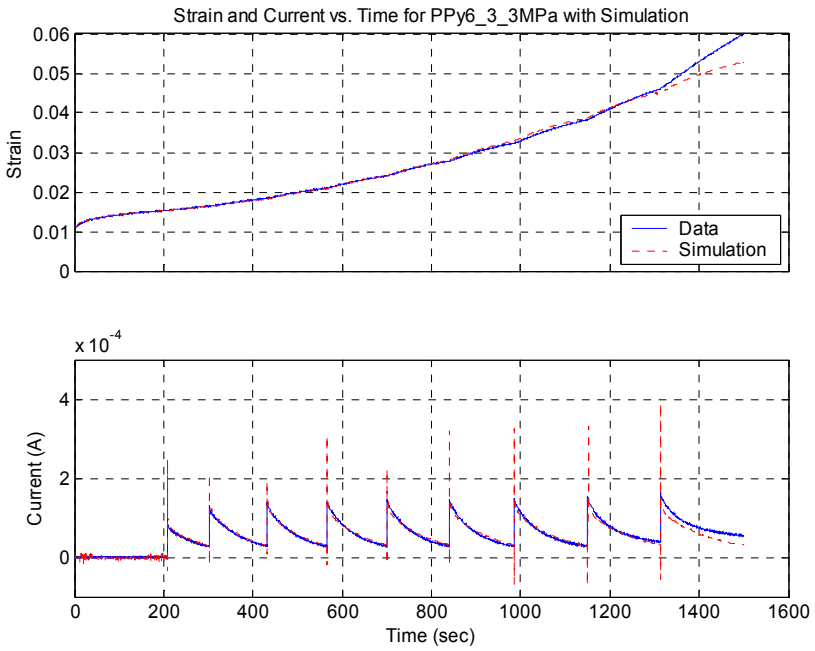

Figure 5-13: Simulated Electrical and Mechanical Response of Polymer with 3 MPa Isotonic Load and 0.1V Potential Steps from -0.5 V vs. $Ag/AgClO_4$

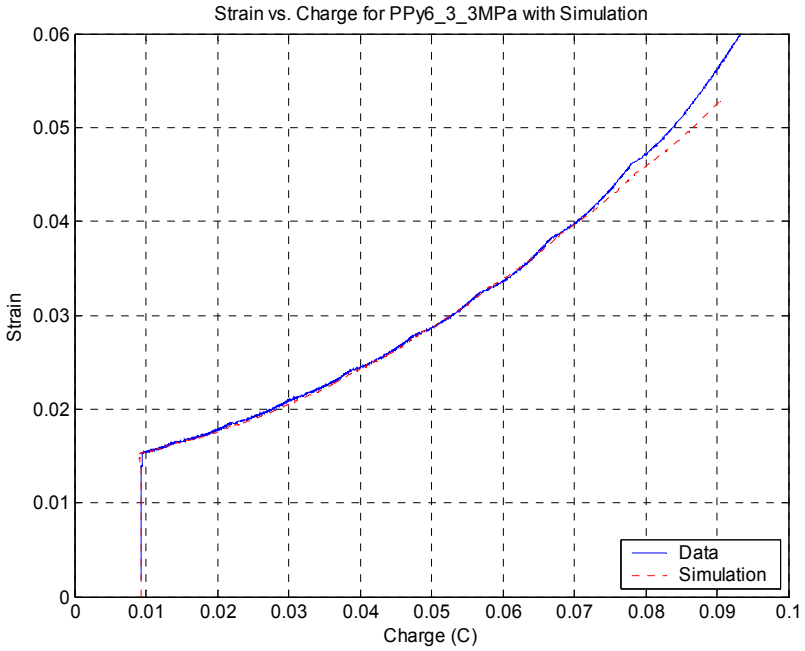

Figure 5-14: Simulated Strain vs. Charge for 3 MPa Isotonic Load with Potential Steps

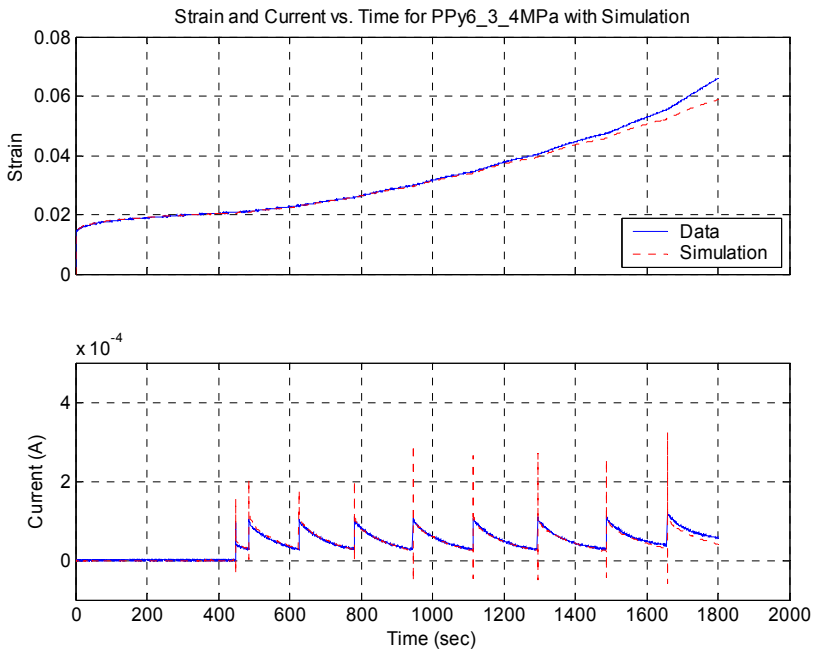

Figure 5-15: Simulated Electrical and Mechanical Response of Polymer with 4 MPa Isotonic Load and 0.1V Potential Steps from -0.5 V vs. Ag/AgClO$_4$

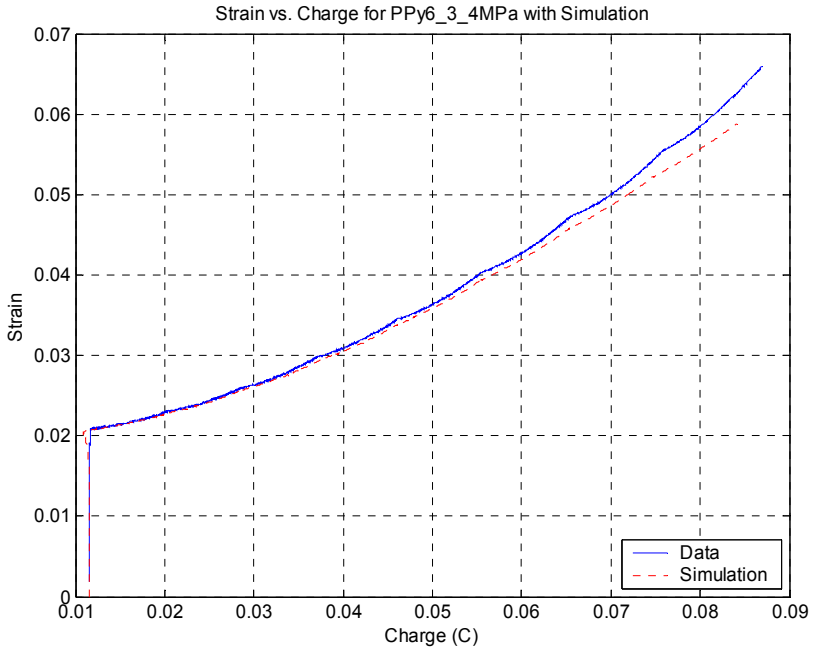

Figure 5-16: Simulated Strain vs. Charge for 4 MPa Isotonic Load with Potential Steps

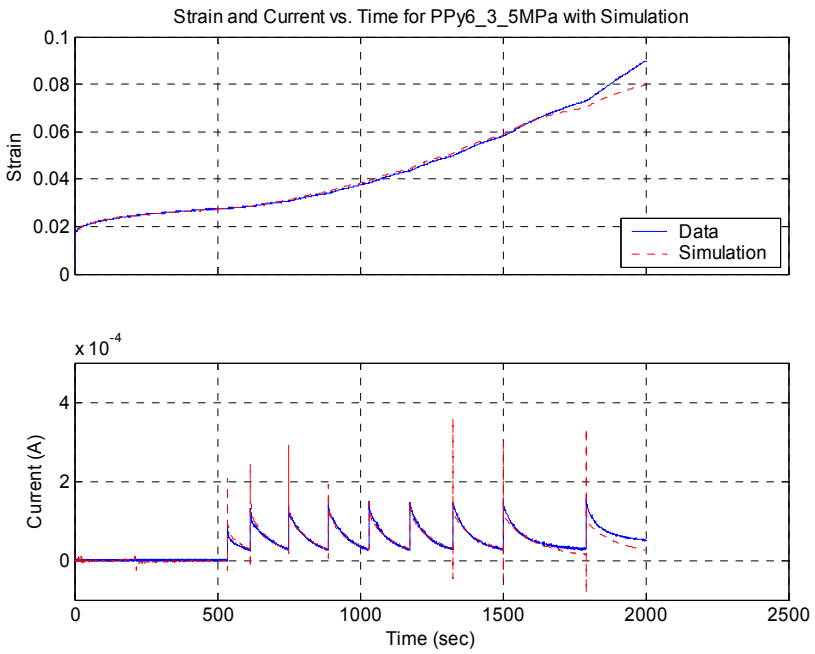

Figure 5-17: Simulated Electrical and Mechanical Response of Polymer with 5 MPa Isotonic Load and 0.1V Potential Steps from -0.5 V vs. $Ag/AgClO_4$

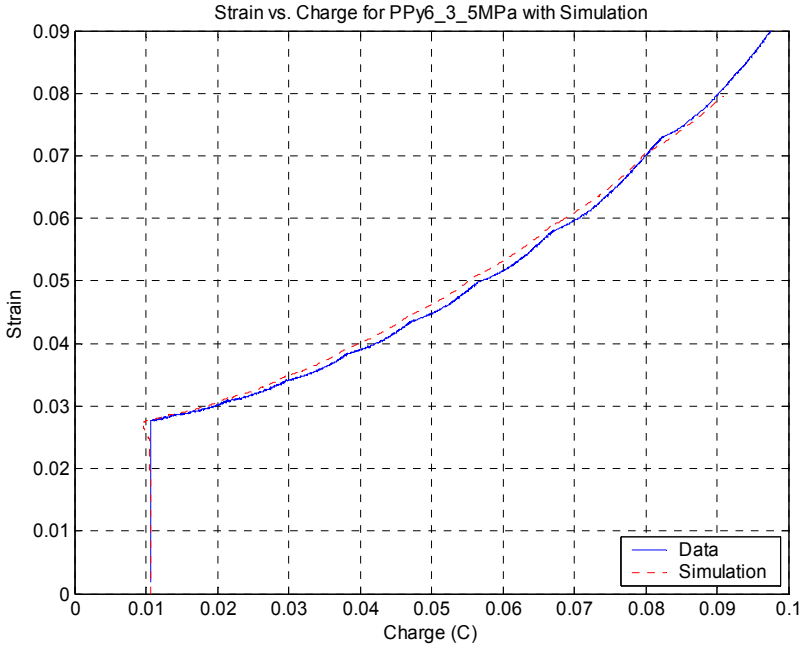

Figure 5-18: Simulated Strain vs. Charge for 5 MPa Isotonic Load with Potential Steps

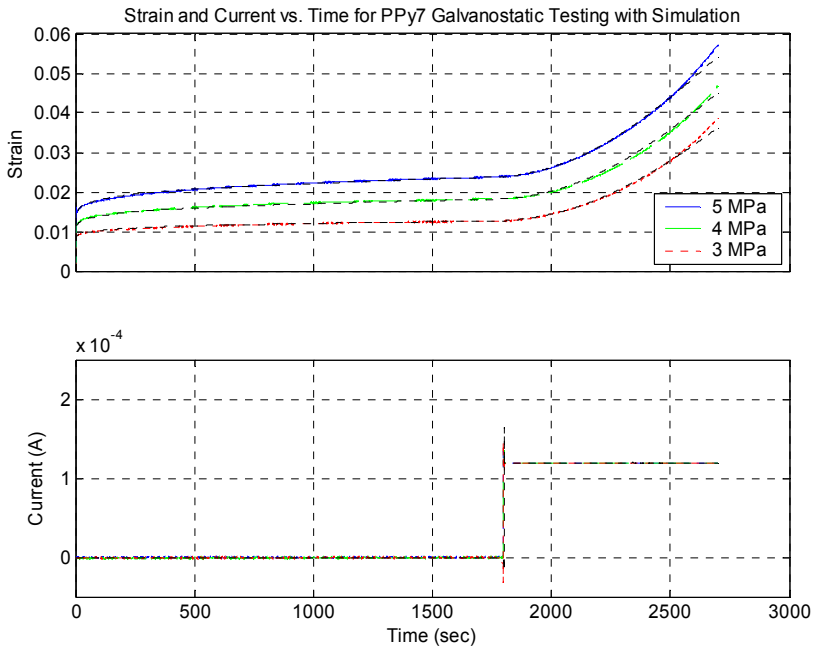

Figure 5-19: Simulated Response with Isotonic Loading and 120μA Current Input with Polymer Initially in Equilibrium at -0.6 V vs. Ag/$AgClO_4$

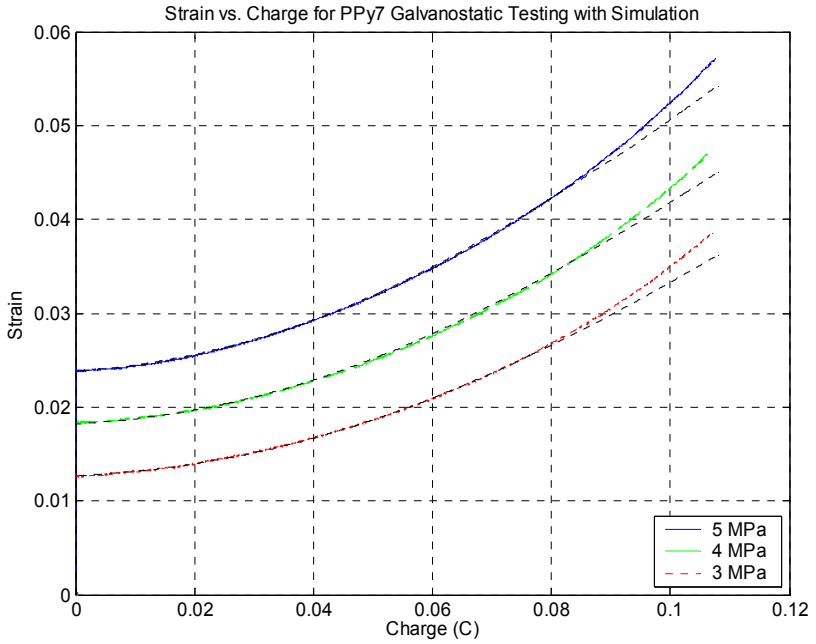

Figure 5-20: Simulated Strain vs. Charge for Isotonic Loading with 120μA Current Input

The agreement between the experimental data and the simulated responses is extremely good for all of these experiments. Simulated results match the observed responses almost perfectly up to applied potentials of about 0.2V vs. $Ag/AgClO_4$, which is 0.8V above the predicted PZC. This suggests that the assumptions of linear behavior begin to break down near this potential or that there is an unmodeled dependence on applied potential. If there is nonlinearity in the mechanical domain it may be the result of the elastic limits of the polymer, which may be reached at high electrochemical pressures. The relationship between volumetric strain and pressure is determined by the bulk modulus of the polymer:

$$K = \frac{E}{3(1-2\nu)} \tag{5.1}$$

If the applied pressure exceeds the elastic limits of the polymer the bulk modulus will decrease at the same rate as Young's modulus, *E*. Although the observed electrochemical strain is only a few percent, the hydrostatic stress required to induce this strain is extremely high. To determine this, the anticipated electrochemical pressure was calculated using the constitutive model developed in Section 3.3:

$$P = \frac{c_V e_V^2}{2} \tag{5.2}$$

This is the steady-state electrochemical pressure, which assumes uniform charge distribution. The dynamic pressure, which includes diffusion effects, is given by:

$$P = \frac{N}{4}\frac{\boldsymbol{q}_V^T \boldsymbol{q}_V}{c_V V^2} \tag{5.3}$$

Using this result, the electrochemical pressure was calculated for the simulation of the 2MPa isotonic test with voltage input, as shown in Figure 5-21.

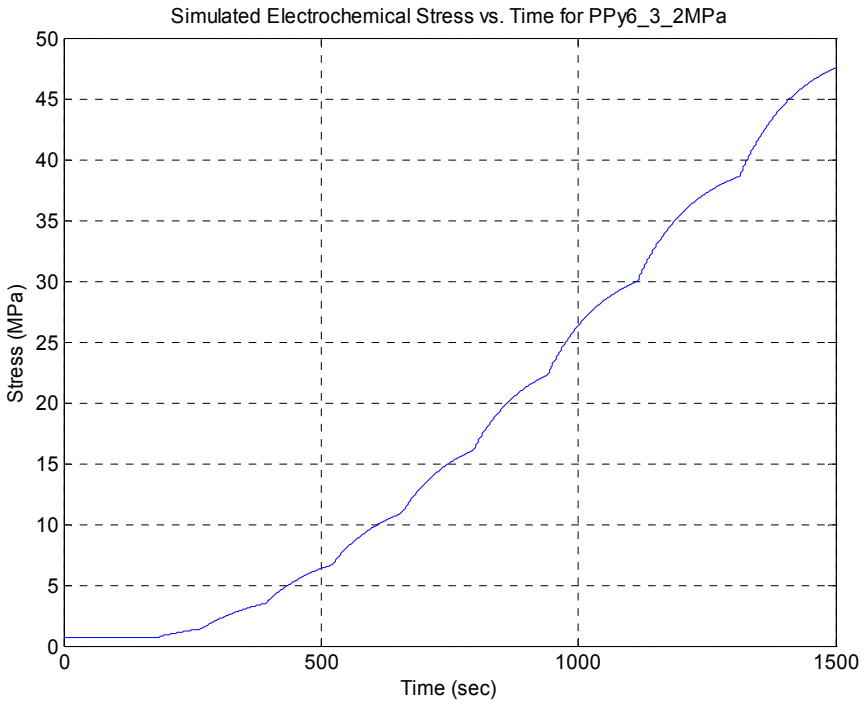

Figure 5-21: Calculated Electrochemical Stress from Simulation

The calculated electrochemical pressure reaches 50 MPa which is considerably higher than the mechanically applied load and may exceed the elastic limit of the material. Discrepancies between the data and model begin to occur around 1000 seconds for this test, which corresponds to a calculated electrochemical pressure of about 25. This suggests that the elasticity of the polymer becomes nonlinear in this region. This is consistent with the results of destructive testing on this polymer sample as presented previously in Section 4.3.3; these results are shown again in Figure 5-22. The reduction in elasticity at around 25 MPa suggests that the polymer becomes more compliant at higher load, which could cause the larger strains observed. Examining the steady-state electrochemical pressure, which is determined by applied potential and specific volumetric capacitance, it is plausible that breakdown of the polymer may occur if the applied potential causes an electrochemical pressure that exceeds the ultimate strength of the material. Using the ultimate strength of the polymer from Figure 5-22 and the specific capacitance determined for this sample the critical potential can be calculated as follows:

$$e_V = \sqrt{\frac{2\sigma_{ult}}{c_V}} = \sqrt{\frac{2 \cdot 31 \times 10^6}{1 \times 10^8}} = 0.79\text{V} \tag{5.4}$$

This potential seems low based on the actual potentials applied to the system, which were as high as 0.4V vs. $Ag/AgClO_4$ (1V vs. PZC). However, the ultimate stress of the polymer is highly dependent on the measured thickness, which could give as much as 10% error. It is certainly possible that the highest input potentials used were near the destructive limits of the polymer.

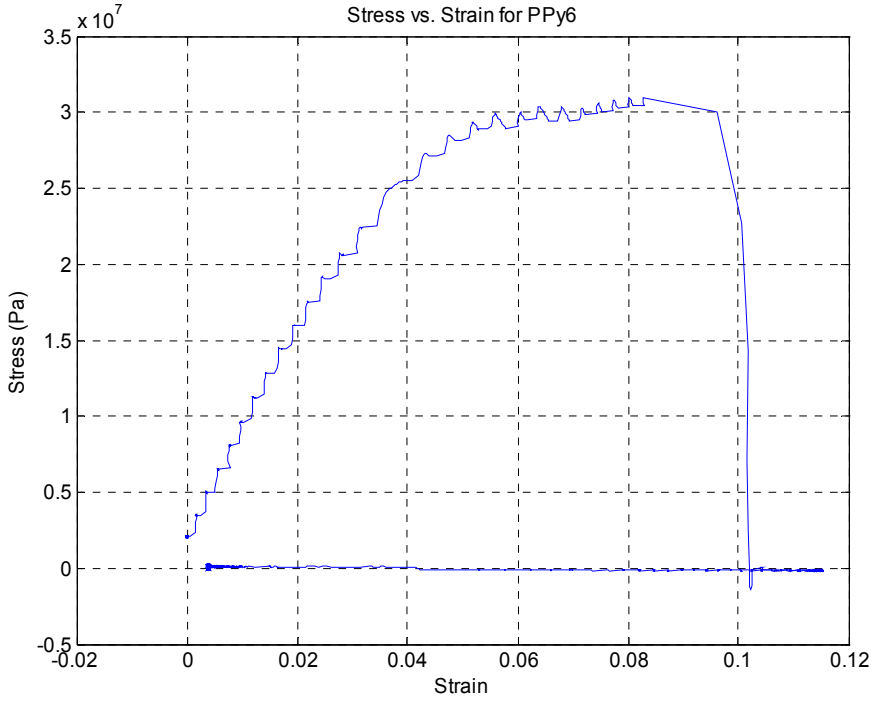

Figure 5-22: Nonlinear Elasticity of Sample PPy6 Determined Under Uniaxial Loading

While this result presents a convincing argument for nonlinearity in the mechanical domain, an alternative explanation for the discrepancy between the data and simulation is that the specific volumetric capacitance, c_V, is dependent on potential. It is known that at potentials less than about 100mV there is dependence on potential due to the contribution of the diffuse layer in the polymer double layer. It is certainly plausible that at higher potentials there are other dependencies. In particular, specific adsorption of ions may occur more readily at high potentials, which would reduce the double layer thickness and cause an increase in the specific volumetric capacitance. A larger volumetric capacitance requires more charge in order to balance the applied potential. All of the data from the potential step testing indicates that there is more current measured at higher potentials than predicted by simulation, and thus more charge inserted into the polymer to balance the applied potential. The linear model does not account for this additional charge insertion as demonstrated in Figure 5-23 through Figure 5-26.

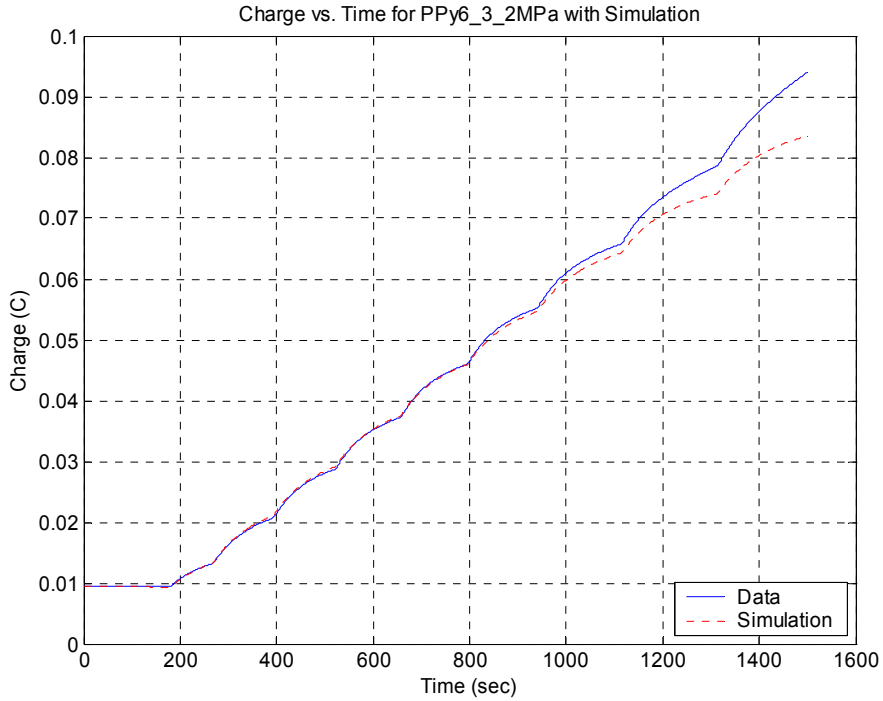

Figure 5-23: Measured Charge and Simulated Charge for 2 MPa Isotonic Load with Potential Steps

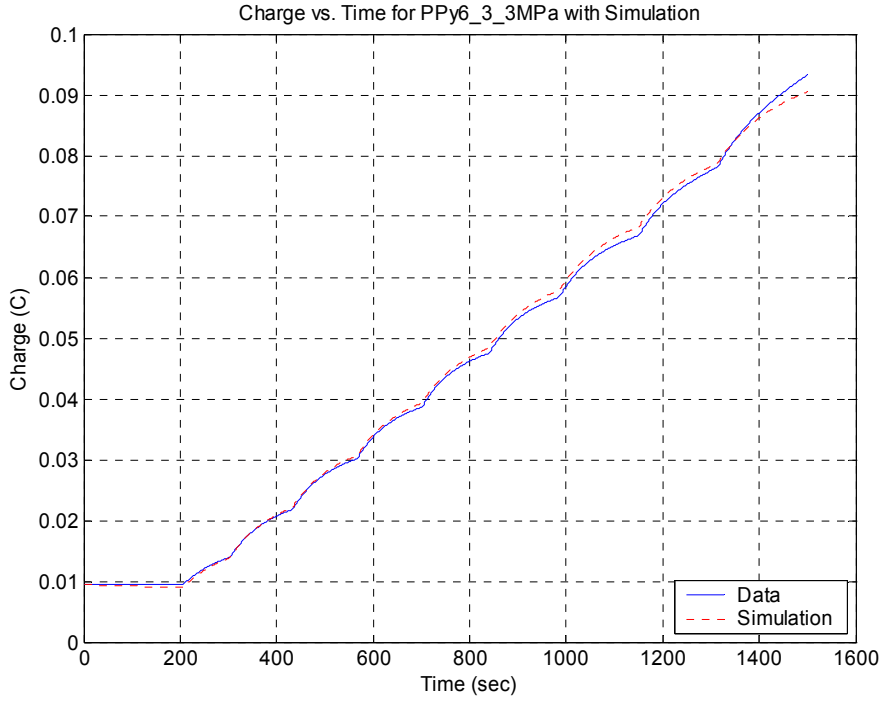

Figure 5-24: Measured Charge and Simulated Charge for 3 MPa Isotonic Load with Potential Steps

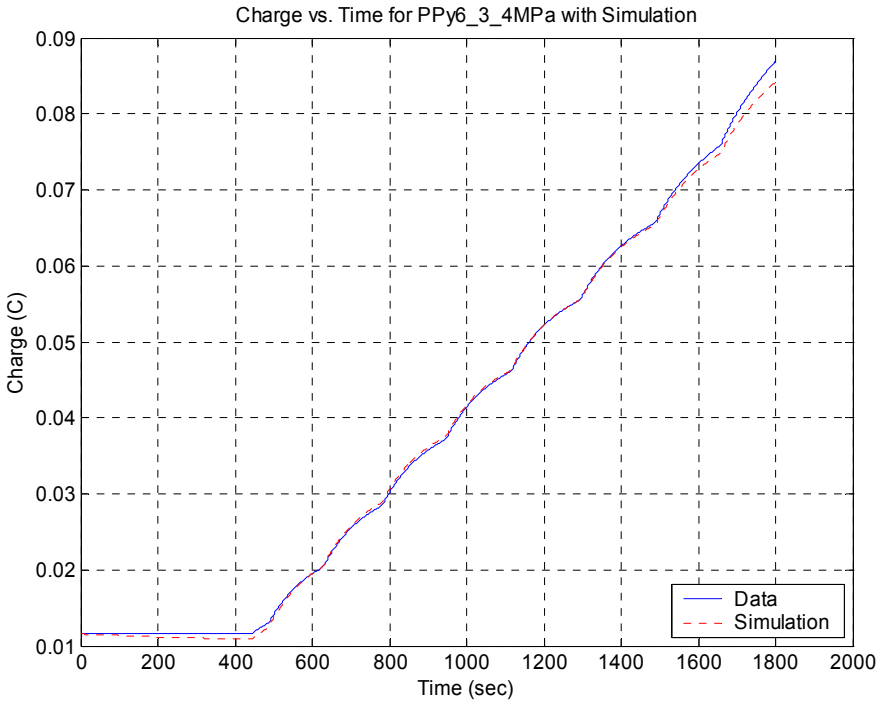

Figure 5-25: Measured Charge and Simulated Charge for 4 MPa Isotonic Load with Potential Steps

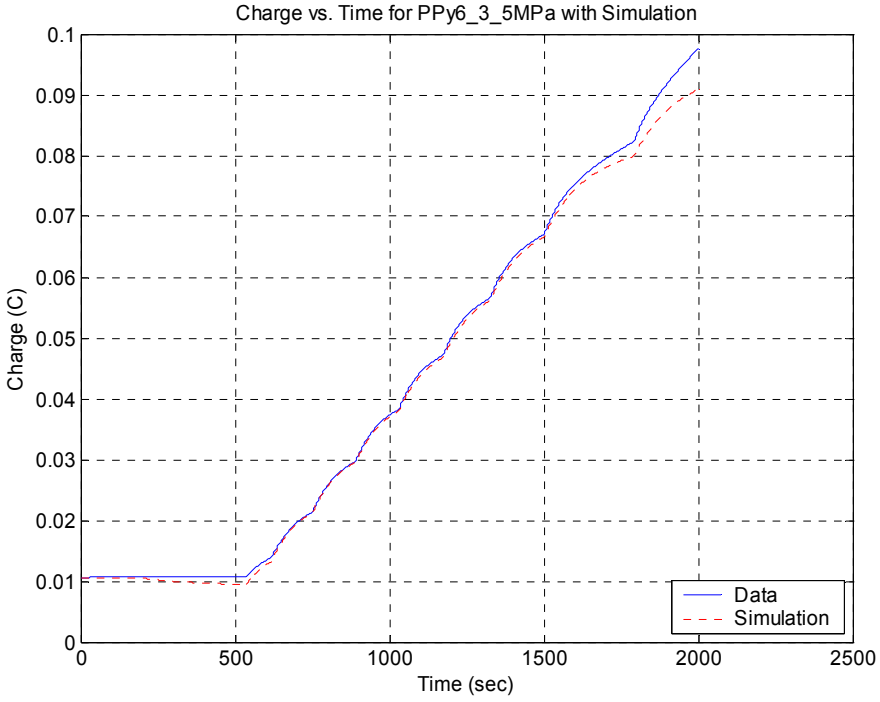

Figure 5-26: Measured Charge and Simulated Charge for 5 MPa Isotonic Load with Potential Steps

Unfortunately, it is difficult to determine if the discrepancy in the model is an electrical, mechanical, or combined effect. Increased strain that results from mechanical nonlinearities would also increase polymer capacitance. Alternatively, an increase in specific volumetric capacitance would result in larger coupling between potential and strain as well as potential and charge. This would account for the underestimation of both strain and charge in the simulated responses. While nonlinearities in the actual system may limit the range of the linear model, it is evident that the model can describe the response of the system very well within a normal operating range.

5.3 Summary

A dynamic model of an EAP linear actuator was implemented in MATLAB using the nonlinear constitutive equations formulated in Chapter 3. The low-order reticulated model is able to accurately describe the electrical, mechanical, and coupled behavior of a polymer actuator. Additionally, the uniformity of the best-fit parameters for each polymer sample demonstrates the robustness of the model over a range of different inputs. Although there is some discrepancy with the observed data, the simulated response of the polymer model is very good for applied potentials up to 0.8V above the potential of zero charge, exhibiting less than 5% error. Up to 1V above the PZC the model demonstrates less than 10% error. Clearly this model provides a competent description of the dynamics of a conducting polymer actuator.

Chapter 6

Control

With a model that is capable of reproducing the dynamic response of EAP to control inputs, it is possible to design a model-based compensator to optimize the performance of an EAP actuator. In particular, it is desirable to achieve fast response, command following, and disturbance attenuation. There are several methods that can be used to design a controller for the EAP actuator. Using classical control methods it is possible to design a feedback controller with proportional, integral, or derivative gains. If the system has full state feedback it is possible to place the poles of the system anywhere assuming that there is sufficient bandwidth in the controller. If all of the system states are not available it is possible to reconstruct the states with a state estimator if the states are observable. While all of these methods work with linear systems, it is also possible design a controller based on the non-linear model of the system. Each of these controller design techniques are discussed and evaluated to determine the best controller to use with EAP actuators. In addition, the controller design provides some information about the achievable system response and therefore, gives some insight about the limiting factors in the bandwidth of the actuator. This allows for optimization of the actuator.

6.1 Classical Control

Classical control methods involve simple feedback control of desired system states as shown in Figure 6-1.

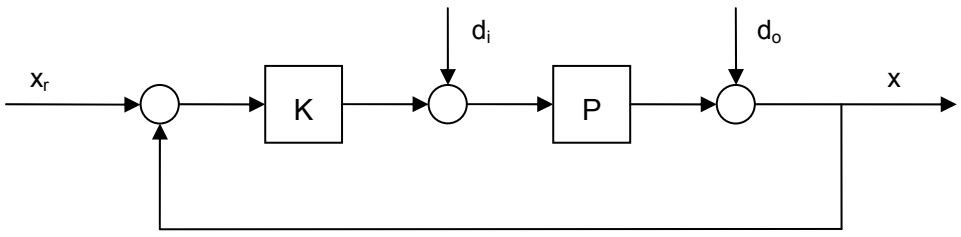

Figure 6-1: Simple Feedback Control Diagram

As an actuator, desired responses of the system may be displacement, force, or impedance. The most basic controllers combine proportional, integral, and derivative feedback of a measured output to augment the inputs to the actuator. Basic feedback control requires very little information about the system. There are really only two critical pieces of information that are required for stable PID control of EAP. The first is that the applied potential cannot be less than the potential of zero charge unless the polymer accepts only one ion species. This is due to the quadratic nonlinearity at the PZC, where insertion of cations or anions will result in positive displacements. Because the PZC also corresponds to the minimum coupling between domains, it may be advantageous to operate at potentials far from this point in order to maximize actuator speed and stroke. However, the maximum potential that can be applied is the second critical control limitation; the potential at the polymer double layer cannot exceed the breakdown potential of the polymer. Both of these constraints will have some effect on the control authority allowed to the system, which may limit the speed of actuator response and its ability to follow some desired trajectories. Researchers have presented proportional controllers with applied potential limits [1] as well as impedance controllers utilizing PID control loops [2].

While PID control offers a simple method for controlling EAP actuators, the ability of the actuator to perform precise command following is limited by the control authority allowed and by the size of feedback gains that can be used without instability. If large feedback gains cannot be used due to noisy sensor information or unmodeled system dynamics, then poor command following can result. Large tracking errors require significant control input to correct, which can lead to saturation of the controller and an inability to follow desired trajectories.

With a good model of the system dynamics, several model based methods might be used to control the system with improved accuracy. Unfortunately, one of the major limitations to the control of EAP actuators using model-based controllers is that full state feedback is not available due to the continuum nature of the system. The only available measurements in an EAP device are generally force, displacement, electrical potential, and current. This problem can be overcome with a state estimator based on the polymer model. However, uncertainty in the model can result in poor estimation and control.

The difficulties in implementing a model-based controller suggest that it may be more useful to design an adaptive controller. This approach allows one controller to be used with many different systems without the need to tune gains offline. In addition, adaptive controllers are generally able to

provide better command following than PID control once the adaptation parameters converge to the optimal values. An adaptive controller can also account for nonlinearities in the system.

6.2 System Control Properties

It was shown in Chapter 5 that the electrical response of EAP actuators is dominated by first-order dynamics. Therefore, the following transfer function from potential to charge can be used to approximate the electrical dynamics of an EAP actuator. This simple model allows for a very basic examination of control techniques.

$$H(s) = \frac{Q(s)}{V(s)} = \frac{1}{s+1} \tag{6.1}$$

To relate electrical inputs to mechanical outputs the relationship between strain and charge must be considered. This relationship is quadratic, as demonstrated in Chapter 3 through Chapter 5; however, for small changes in charge the relationship can be considered linear. If the ratio of strain to charge is assumed to be one-to-one at a particular operating point, then the transfer function from potential to strain is identical to the transfer function in (6.1).

Using this simple first-order approximation it is possible to design various proportional, integral, and derivative feedback controllers. The block diagrams and model structures associated with these controllers are presented in Appendix C. In an attempt to compare similar responses from each of the controllers, the undamped natural frequency of the closed-loop system was chosen to be 10 rad/s (this is not possible for the derivative controller). To minimize oscillation in the controllers containing integral feedback, the closed-loop poles were chosen to have equal real and imaginary parts, giving a damping coefficient of 0.71. The locations of the poles for each of the controllers are shown in Figure 6-2. The feedback gains used to place the desired closed-loop poles are presented in Table 6-1.

Table 6-1: Feedback Gains for Simple Proportional, Integral, and Derivative Control

	Proportional Gain, K_p	Integral Gain, K_i	Derivative Gain, K_d
Proportional	9	--	--
Integral	--	100	--
Derivative	--	--	1
PI	13	100	--
PD	19	--	1
PID	27	200	1

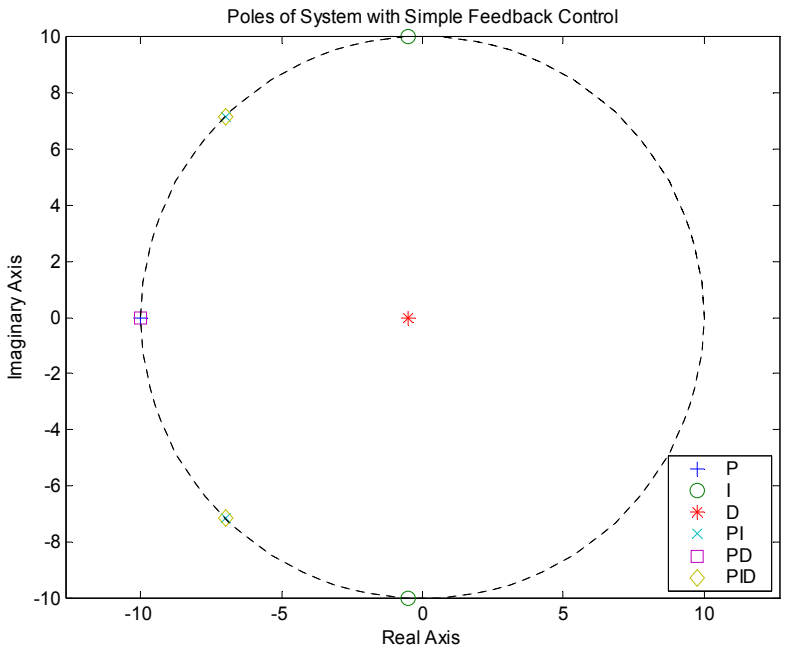

Figure 6-2: Poles of First-Order System with Various Combinations of Proportional, Integral, and Derivative Feedback

It is evident from this figure that the integral controller and derivative controller will both exhibit much slower settling times than the other controllers because the real parts of their poles are close to the origin. The feedback gain of the integral controller cannot augment the real part of the system poles so the settling time is the same as the open-loop system. The derivative gain can influence the real part of the system poles, but only in the direction that slows down the actuator settling time. The addition of a proportional feedback term to either of these controllers enables a much larger range of

responses. This term allows the settling time of the system to be adjusted arbitrarily, though the actual system may exhibit instability if the feedback gain is too large. In the case of the PI and PID controllers it is also possible to adjust the damping coefficient of the closed-loop system, which influences factors such as overshoot and rise time.

Simulations were run to determine the responses of the closed-loop system using the pole locations depicted in Figure 6-2. The impulse responses of the closed-loop systems are presented in Figure 6-3; the unit step responses are shown in Figure 6-4; Figure 6-5 demonstrates the ability of the closed-loop systems to follow a ramp function; the frequency responses of the closed-loop systems are depicted in Figure 6-6; and Figure 6-7 shows how well the systems track a 1 Hz sinusoidal trajectory.

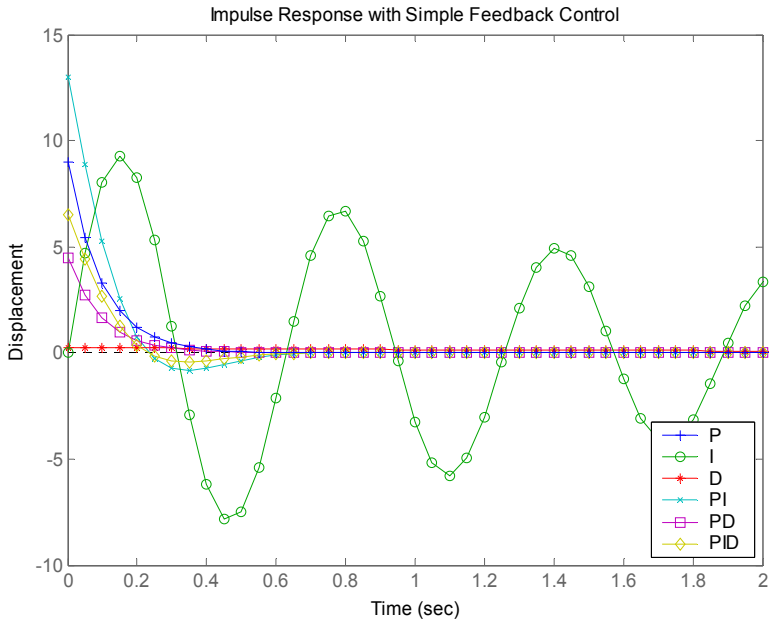

Figure 6-3: Impulse Responses for Closed-Loop System with Various Combinations of Proportional, Integral, and Derivative Feedback

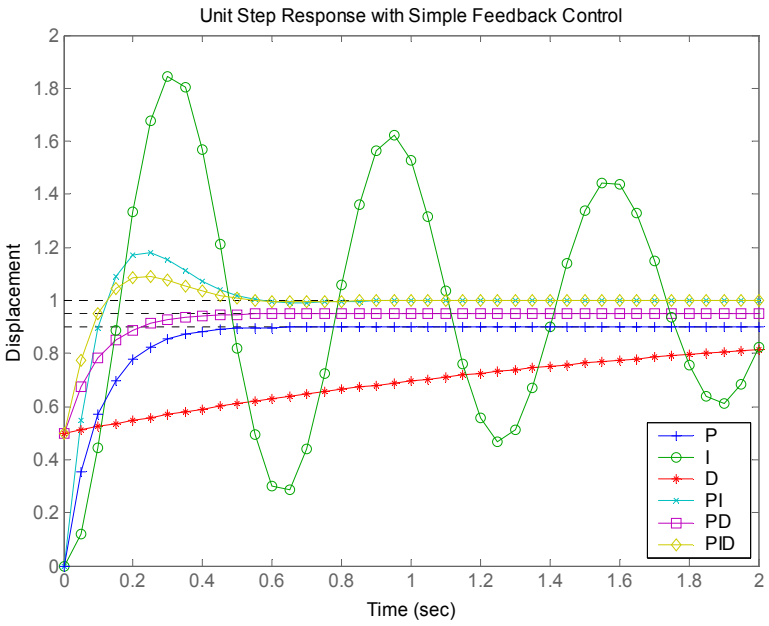

Figure 6-4: Unit Step Responses for Closed-Loop System with Various Combinations of Proportional, Integral, and Derivative Feedback

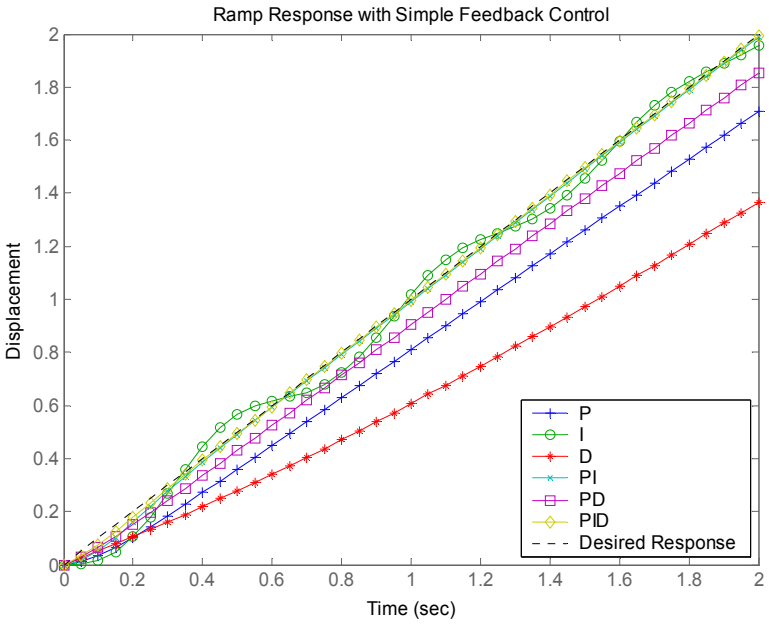

Figure 6-5: Ramp Responses for Closed-Loop System with Various Combinations of Proportional, Integral, and Derivative Feedback

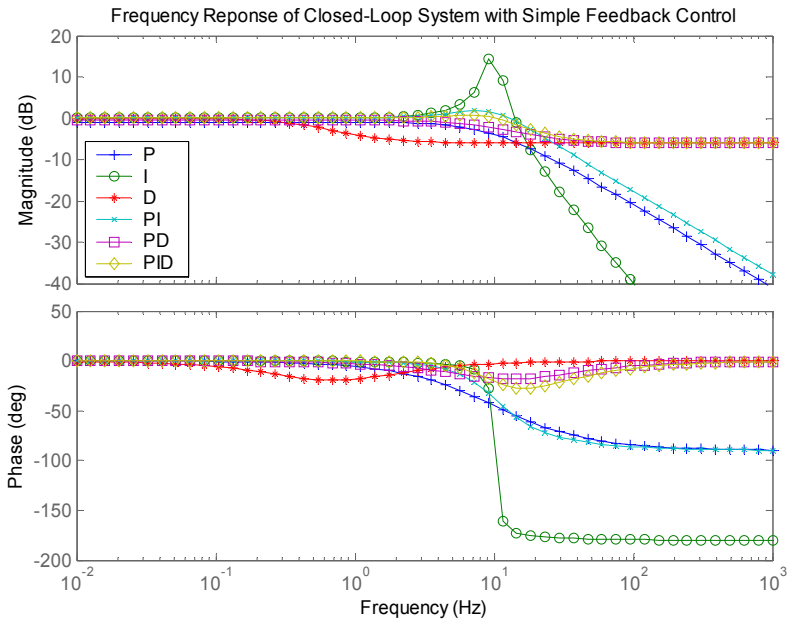

Figure 6-6: Frequency Responses for Closed-Loop System with Various Combinations of Proportional, Integral, and Derivative Feedback

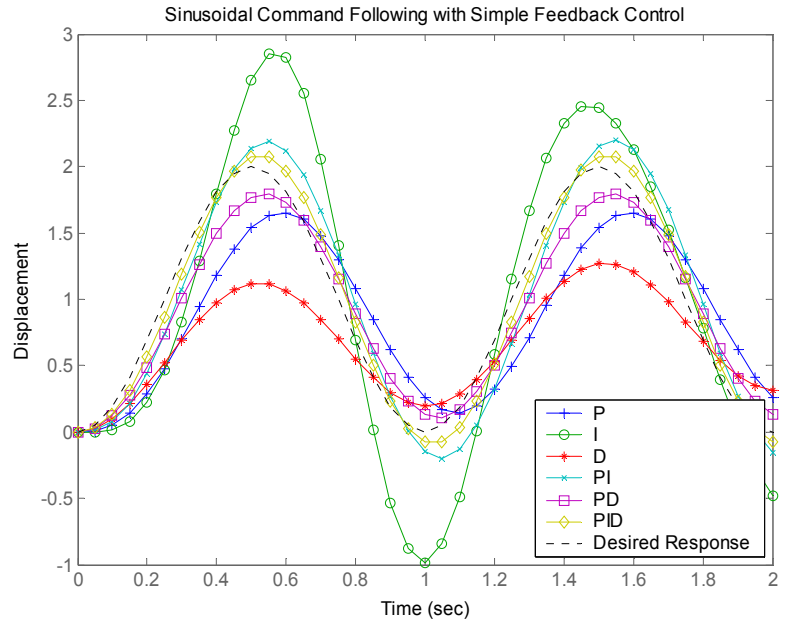

Figure 6-7: Tracking of 1 Hz Sinusoid for Closed-Loop System with Various Combinations of Proportional, Integral, and Derivative Feedback

The preceding feedback controllers demonstrate the closed-loop response of a simple first order system. A more appropriate first order approximation of the system includes more realistic high and low frequency gains:

$$H(s) = \frac{\frac{1}{R}}{s + \frac{1}{RC}} = \frac{0.01}{s + 0.01} \tag{6.2}$$

Although this system has the same capacitance as the previous system (1 Farad), the open-loop response is much slower due to increased circuit resistance. The magnitude of this transfer function drops off considerably at frequencies of only 0.01 rad/s because higher potentials are required to transfer the same amount of charge through a circuit with more resistance. While large feedback gains can improve the frequency response of the actuator, the closed-loop system may be limited by the amount of potential that can be applied.

The polymer material may also limit the closed-loop actuator response. The preceding model assumed that diffusion dynamics were faster than the time constant of the RC circuit, which basically means that the diffusion resistance is negligible compared to the electrical resistance of the circuit. However, even if the open-loop system does not exhibit limitations due to diffusion, the diffusion rate may be slower than the desired closed-loop response. This can result in potentials at the polymer double layer that may exceed the breakdown limits of the material.

From this analysis it is apparent that the limitations on the frequency response of an EAP actuator can be improved by lowering electrical resistance and series capacitance. Ding *et al* accomplished this by incorporating a helical wire within a conducting polymer [3]. Additional performance improvements can be gained by using combinations of polymer and electrolyte with low diffusion resistance.

6.3 Simulated PID Control

While the previous section provided some validation of classical feedback control on a simplified polymer model, it is necessary to examine how well the result will translate to the more complex reticulated model with non-linear coupling. The following simulations demonstrate the anticipated response of a polypyrrole actuator with PID feedback control. The modeled polymer has a circuit resistance of 100 Ω, specific volumetric capacitance of 1.5×10^{8} F/m^3, diffusion coefficient of 1×10^{-12} m^2/s, and thickness of 20μm. The length and width are 15 mm and 3 mm respectively. The

viscoelastic parameters are identical to those presented to match the isotonic loading data in Section 5.2.1. The selected value of Poisson's ratio was 0.42. The open-loop frequency response of the electrical domain is depicted in Figure 6-8. This figure shows the response predicted by the continuum model and a 16-element reticulated diffusion model, which should be sufficient for predicting the polymer response up to 1 Hz.

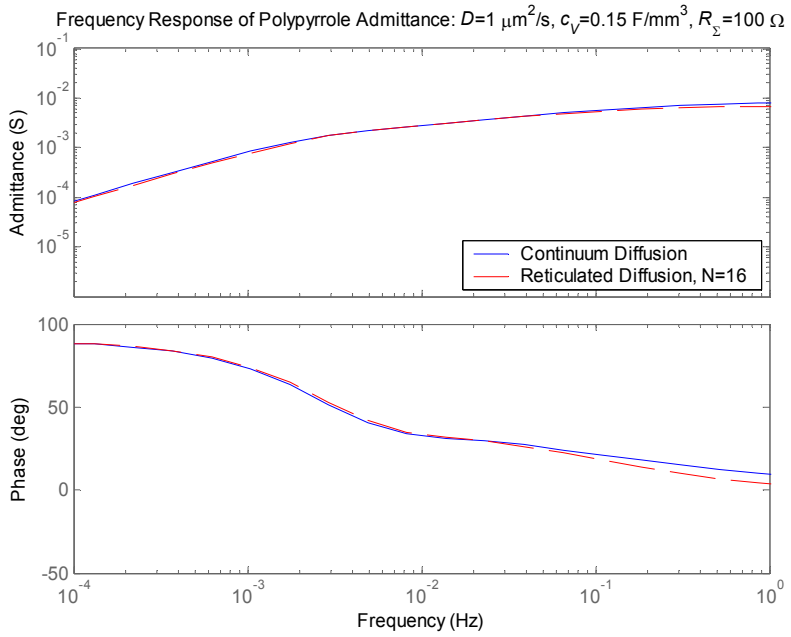

Figure 6-8: Open-Loop Frequency Response of Simulated Polymer

The system is dominated by first-order dynamics with a time constant of about 45 seconds as demonstrated by the electrical step response shown in Figure 6-9. Also included in the figure is the step response of a first-order approximation of the system, given by:

$$H(s) = \frac{0.0029}{s + 0.0215} \tag{6.3}$$

From the numerator of this model it is apparent that diffusion resistance contributes to the total circuit resistance giving an effective resistance of about 350 Ω. The correlation between the step responses of the first order model and reticulated model demonstrate that a PID controller designed for use on an approximate first order system may be valid for use on the polymer.

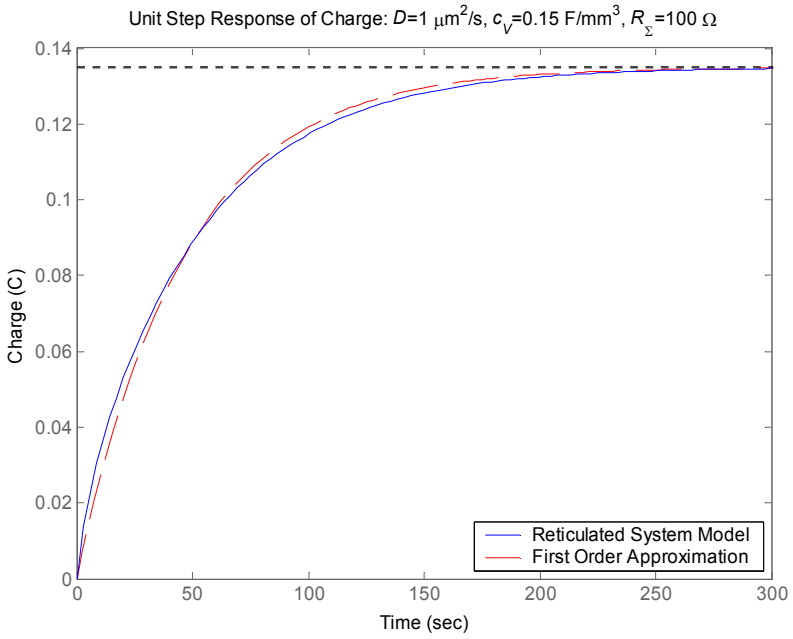

Figure 6-9: Step Response for Reticulated Polymer Model and Approximate First Order Model

In order to include the mechanical domain into this model the linearized coupling coefficient from charge to strain is used. In Section 4.5 it was shown that the linearized strain to charge ratio is about 25%/C at 0.05 C for the polypyrrole samples used during testing. Therefore, the approximate first-order open loop transfer function from potential to strain is given by:

$$H(s) = \frac{0.00072}{s + 0.0215} \tag{6.4}$$

The closed-loop transfer function of the system with PID control is then given by:

$$G(s) = \frac{0.00072\left(K_d s^2 + K_p s + K_i\right)}{\left(1 + 0.00072K_d\right)s^2 + \left(0.0215 + 0.00072K_p\right)s + 0.00072K_i} \tag{6.5}$$

The associated poles are located at:

$$\sigma_{PID} = \frac{-\left(0.0215 + 0.00072K_p\right) \pm \sqrt{\left(0.0215 + 0.00072K_p\right)^2 - 0.0029K_i\left(1 + 0.00072K_d\right)}}{2\left(1 + 0.00072K_d\right)} \tag{6.6}$$

The small coefficients on the feedback gains indicate that very large gains are required to move the closed-loop poles. To provide an undamped natural frequency of 0.0318 rad/s (0.005 Hz) and a damping coefficient, ξ, of 0.71, the following feedback gains were used: K_p=67, K_i=3, and K_d=140. This controller should give a rise time, $(\pi-\xi)/\omega_d$, of 76 seconds and a settling time, 5τ, of 220 seconds. To get an undamped natural frequency of 0.0636 rad/s (0.01 Hz) the required gains are: K_p=165, K_i=12.5, and K_d=140. This set of gains should give a rise time of 38 seconds and a settling time of 110 seconds. In theory, the feedback gains can be made arbitrarily large; however, unmodeled system dynamics and sensor noise can lead to instability if the feedback gains are too large.

The closed-loop response of the complete non-linear EAP model was simulated using both sets of gains. Figure 6-10 shows the simulated step response of the open loop system and closed loop PID controlled system with the first set of gains. The same response is shown in Figure 6-12 for the second set of PID gains. The control potentials required to achieve these step responses are presented in Figure 6-11 and Figure 6-13. The potentials at the polymer double layer are shown in Figure 6-14 and Figure 6-15. The MATLAB files used in this analysis are provided in Appendix C.

It is evident from the step responses of the closed-loop, PID-controlled systems that the predicted rise times and settling times are achieved. The first system was designed to have a rise time of 76 seconds and a settling time of 220 seconds. The simulated response shows a rise time of 48 seconds and a settling time of about 160 seconds. The improvement in the simulated response over the predicted response is likely due to the linearization of the model about an operating point that is below the desired step response; this results in more coupling from charge to strain than anticipated by the linear model, and thus, a larger contribution from the feedback gains. A similar result is seen with the faster system, which has a rise time of 22 seconds and a settling time of 90 seconds versus the predicted times of 38 and 110 seconds, respectively.

The control potentials required to achieve the closed-loop responses are certainly reasonable, particularly considering that the polymer is being commanded to a 2% strain, which is near the limit of typical polypyrrole actuation. The predicted polymer double layer potentials are a little high, though the polymer may be able to endure double layer potentials greater than 1.5V for short intervals. This makes either one of these PID controllers suitable for use on this actuator, assuming that large step inputs are not frequently required.

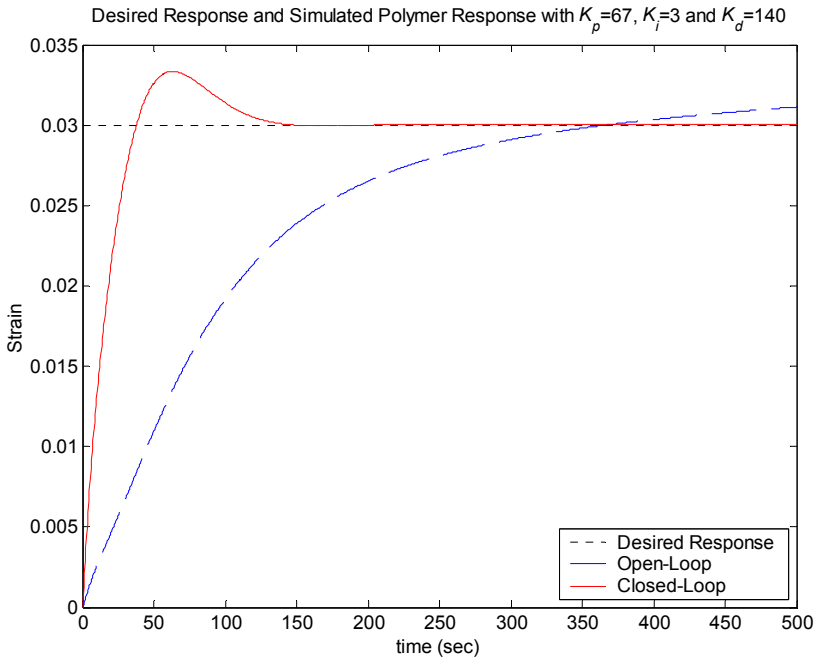

Figure 6-10: Open- and Closed-Loop Step Response of PID Controlled Polymer with Desired ω_n=0.005Hz

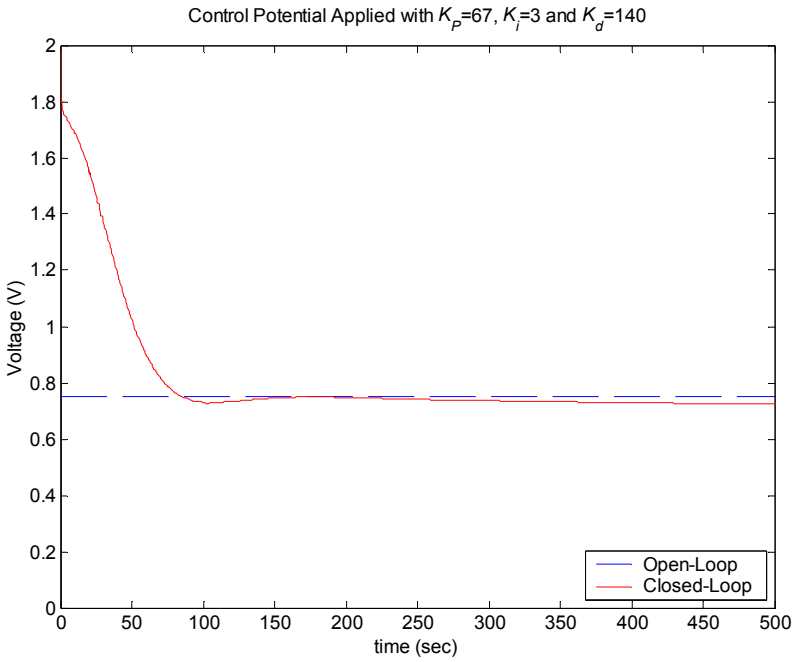

Figure 6-11: Control Potentials Required for Step Response of Polymer with Desired ω_n=0.005Hz

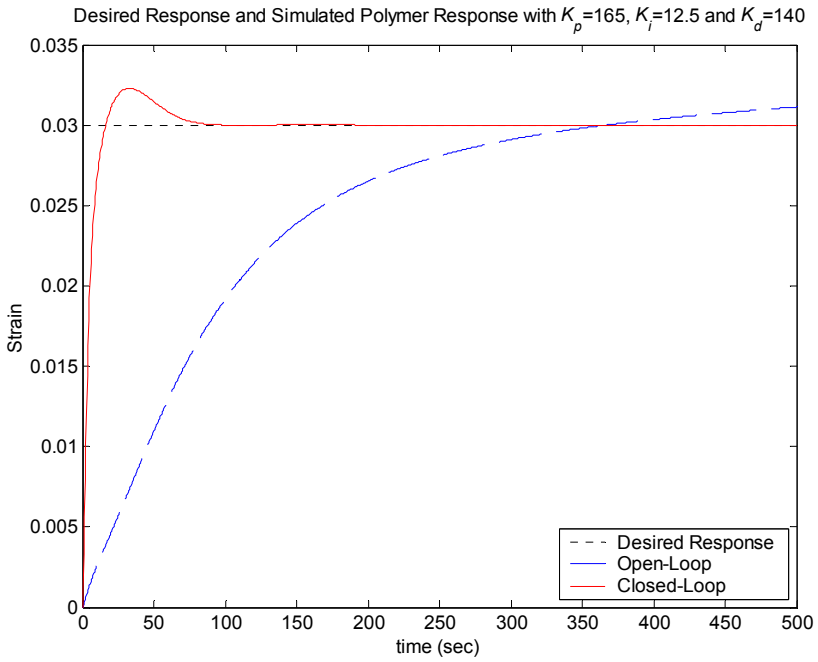

Figure 6-12: Open- and Closed-Loop Step Response of PID Controlled Polymer with Desired ω_n=0.01Hz

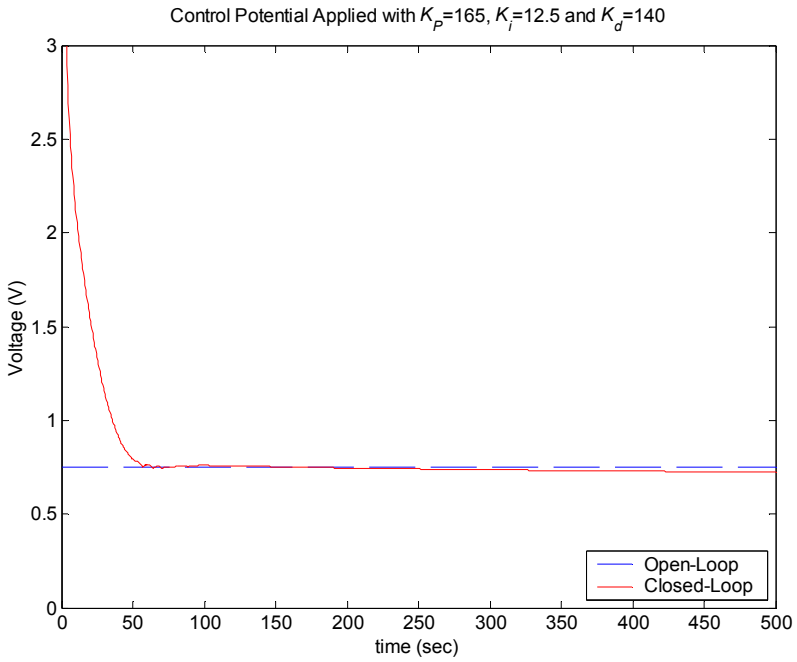

Figure 6-13: Control Potentials Required for Step Response of Polymer with Desired ω_n=0.01Hz

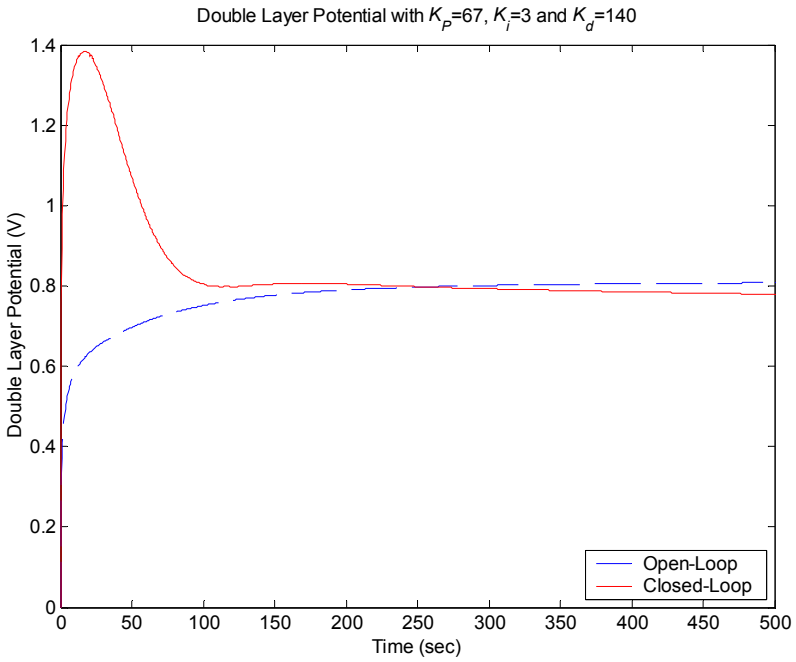

Figure 6-14: Double Layer Potential Resulting from Step Response of Polymer with Desired ω_n=0.005Hz

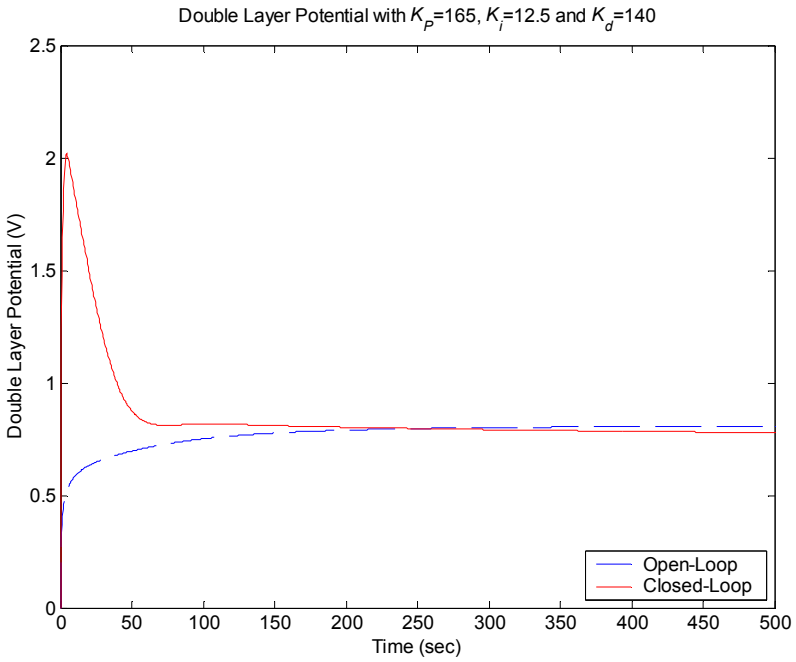

Figure 6-15: Double Layer Potential Resulting from Step Response of Polymer with Desired ω_n=0.01Hz

The ability of the actuator to follow a periodic desired trajectory was also simulated for both sets of PID gains. The frequency of the reference signal was 0.01 Hz, which matches the undamped natural frequency of the faster closed-loop system response.

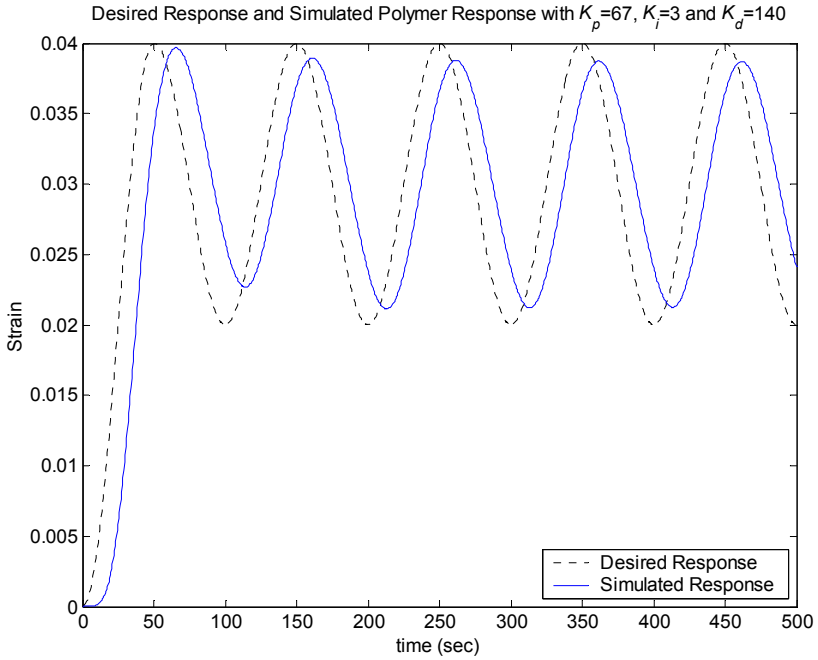

Figure 6-16: Closed-Loop Response of Polymer with ω_n=0.005Hz Following a 0.01Hz Desired Trajectory

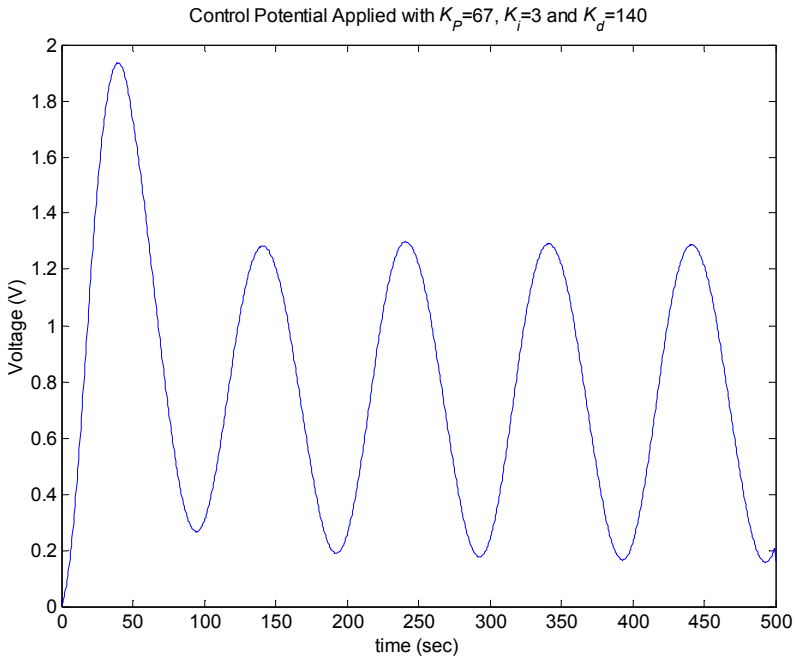

Figure 6-17: Control Potential Required for 0.01Hz Sinusoidal Command Following for ω_n=0.005Hz

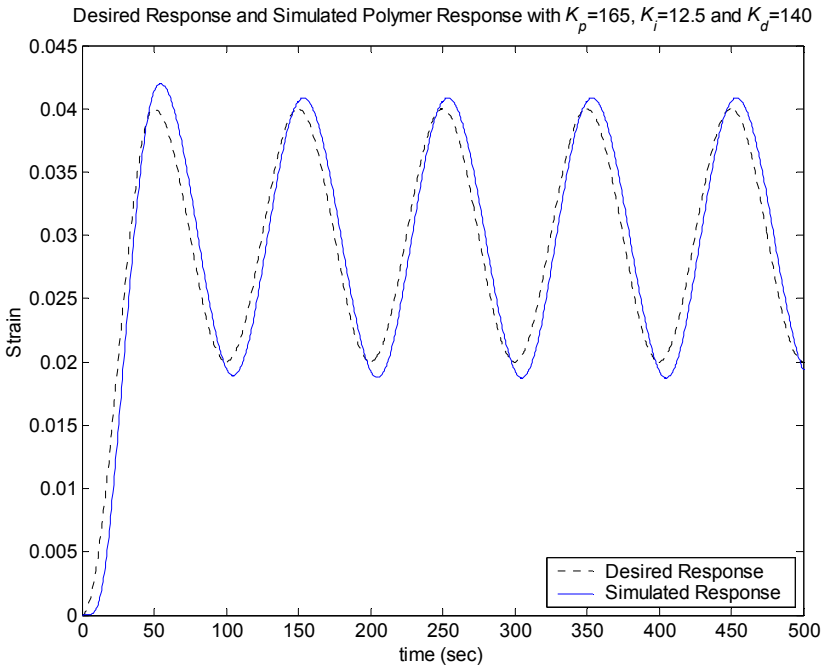

Figure 6-18: Closed-Loop Response of Polymer with ω_n=0.01Hz Following a 0.01Hz Desired Trajectory

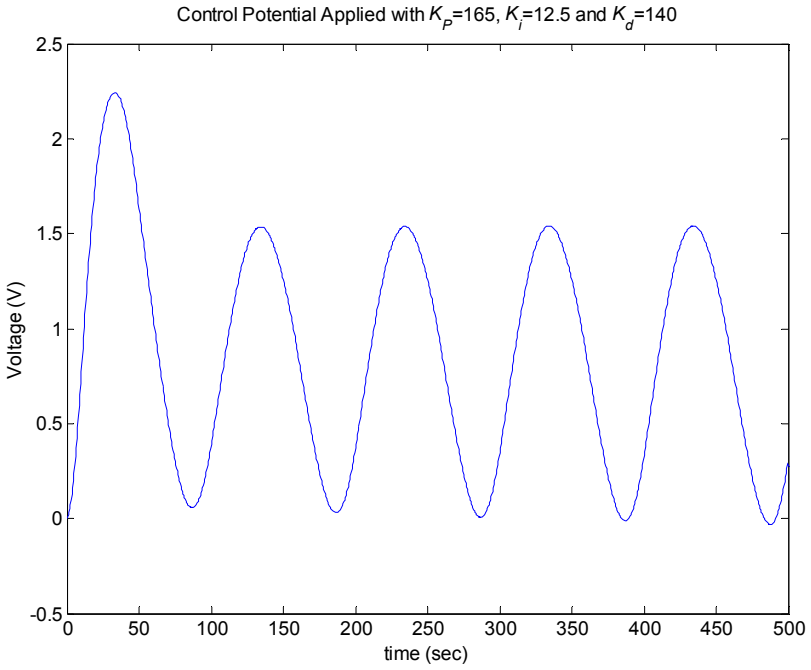

Figure 6-19: Control Potential Required for 0.01Hz Sinusoidal Command Following for ω_n=0.005Hz

It is clear from the PID controller analysis that PID control is a feasible control strategy in certain regions in the actuator performance space. For the sinusoidal trajectory that was simulated, the mean strain of the polymer was chosen as 3% in order to avoid the unstable nonlinearity at zero strain. It can be seen that both controllers provide reasonable tracking of the 0.01Hz desired trajectory. This suggests that if the open-loop actuator dynamics are improved it would also be possible to improve the tracking performance of the actuator on smaller time scales.

The desired closed-loop response of an EAP actuator can only be guaranteed when operating in a range of the design space that is adequately approximated by the linearized transfer function. Near the PZC, for instance, the reduction in coupling between domains requires significantly larger control inputs to achieve the same magnitude responses that are easily attainable at higher potentials. It would be ideal to have a controller that can account for the nonlinear dynamics of the system and operate equally well in all regions of the actuator performance space.

6.4 Adaptive Control

While the EAP dynamic model can competently describe the behavior of EAP, difficulty in control comes from nonlinearity in the constitutive equations. The model of the electrical domain can be treated as linear though the volumetric capacitance of the system depends on actuator strain. The mechanical domain, on the other hand, has a quadratic dependence on charge stored in the polymer making it highly nonlinear.

Additional complication arises because it is difficult to parameterize an EAP actuator. Part of the difficulty lies in the amount of testing needed to fully characterize the system (the time constants of the system can be very long depending on actuator geometry). In addition, every sample of the actuator material can have different properties depending on the procedure used to make it. Because of the uncertainty of parameters, it is desirable from a controls perspective to have a controller that does not require exact knowledge of system parameters. Use of an adaptive controller can allow for tracking of a desired trajectory despite nonlinearity and can also handle unknown or slowly varying system parameters.

The major difficulty in implementing a controller for an ionic EAP actuator is that full state feedback is not available. The only available measurements are input potential, force, displacement, and current, which can be integrated to give the total charge transferred in the system. The electrical domain is essentially linear with a dependence on the volume of the polymer causing some nonlinearity. Because of uncertainty in the model and lack of full-state feedback, it is necessary to use

an adaptive controller that can simultaneously provide state and parameter estimation. A controller structure that is capable of this is presented by Slotine and Li in Section 8.4.1 of *Applied Nonlinear Control* [4]. This controller is only guaranteed to exhibit stability for linear systems, so there may be some difficulty in implementing this controller with the EAP actuator. This is of particular concern in regions of the actuator performance space where the nonlinearity of the system is highly pronounced, such as at the potential of zero charge.

The adaptive controller presented in the text allows the response of a linear system to track the response of a desired system of the same order and relative degree. While the desired system response can be set arbitrarily within the allowed structure of the model, the performance of the actual system is limited by control authority, modeling inaccuracies, sensor bandwidth, and computing resources. Using this method it is not necessary to know the parameters of the actual plant. In addition, it may be possible to deal with some slowly time varying parameters as long as the convergence rate of parameter estimation is faster than parameter drift. The form of the adaptive controller for a system with a relative degree of 1 is shown below in Figure 6-20.

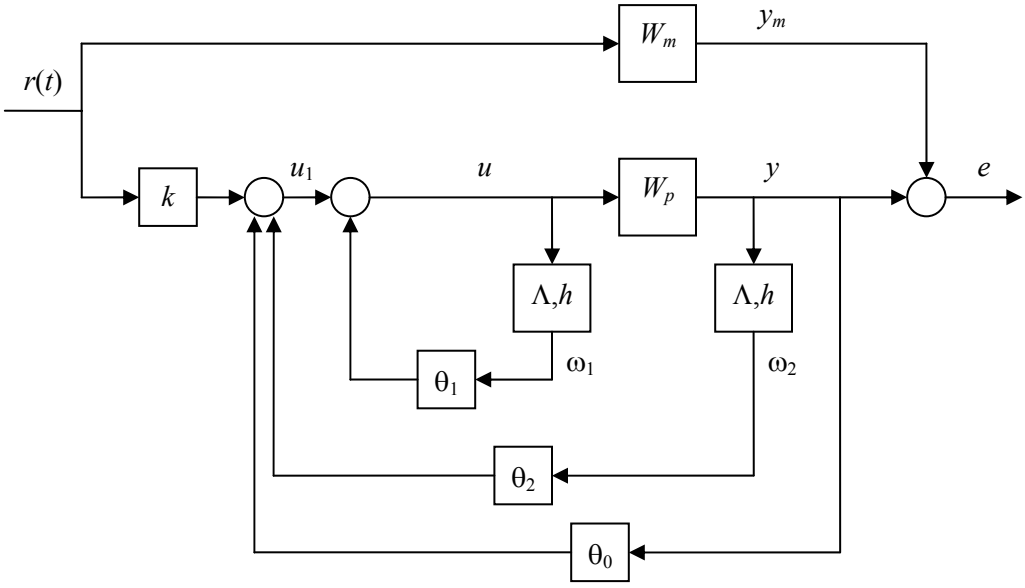

Figure 6-20: Block Diagram of Controller with State Estimation and Parameter Adaptation

In this figure $r(t)$ is the reference input, W_m is the desired input-output transfer function of the plant, and y_m is the desired system response. The adaptation loop uses the reference command and the measurement of the actual system response, y, along with the filtered response, ω_2, and filtered

control input, ω_1, to adjust the adaptation gains k, θ_0, θ_1, and θ_2. The filter associated with the adaptive feedback variables is determined by Λ and h, where Λ is the filter gain matrix with poles that are equal to the zeros of the desired plant, and h is any vector that provides controllability. Because the filter gain matrix contains the zeros of the desired plant, a particular choice of θ_1, which is found through adaptation, cancels the actual plant zeros and replaces them by the zeros of desired model. Similarly, θ_2 and θ_0 are used to place the poles of the actual plant at the poles of the desired model. The vector h affects the sensitivity of the feedback on individual states and was chosen to be a vector of ones for this analysis. The equations corresponding to the control and adaptation are as follows:

$$\begin{aligned}
&\dot{\boldsymbol{\omega}}_1 = \boldsymbol{\Lambda}\boldsymbol{\omega}_1 + \mathbf{h}u \\
&\dot{\boldsymbol{\omega}}_2 = \boldsymbol{\Lambda}\boldsymbol{\omega}_2 + \mathbf{h}y \\
&\boldsymbol{\theta}(t) = \begin{bmatrix} k(t) & \boldsymbol{\theta}_1(t) & \boldsymbol{\theta}_2(t) & \theta_0(t) \end{bmatrix}^T \\
&\boldsymbol{\omega}(t) = \begin{bmatrix} r(t) & \boldsymbol{\omega}_1(t) & \boldsymbol{\omega}_2(t) & y(t) \end{bmatrix}^T \\
&u(t) = \boldsymbol{\theta}^T(t)\boldsymbol{\omega}(t) \\
&\dot{\boldsymbol{\theta}} = -\gamma e(t)\boldsymbol{\omega}(t)
\end{aligned} \tag{6.7}$$

If the desired trajectory of the EAP system is a mechanical output such as displacement, the mechanical domain needs to be incorporated in the adaptive controller. However, the mechanical domain is coupled to the electrical domain through nonlinear constitutive relations. There are a few ways to incorporate the mechanical domain and each has its advantages and disadvantages. The first method assumes that the distribution of ions in the polymer is uniform and that viscoelastic effects are much slower than the electrochemically driven strain. Under these assumptions displacement is no longer dependent on $k\boldsymbol{q_V}^{\mathrm{T}}\boldsymbol{q_V}$ but on q_V^2, where q_V is the sum of the elements in the vector $\boldsymbol{q_V}$. From this relationship the desired volumetric charge can be determined from a desired strain using the following equation:

$$q_V = \sqrt{\frac{2C_V V E \varepsilon_x}{1-2\nu}} \tag{6.8}$$

Because input current is measured, q_V can be determined through integration. The desired plant transfer function, W_m, can then be inverted to determine the transfer function from desired charge to input potential. This allows the reference potential to be determined from the reference charge. The overall form of the system is depicted in Figure 6-21, where dashed lines represent hidden adaptation

structure from Figure 6-20 and solid lines demonstrate the path associated with estimation of input current using desired displacement and output strain using current measurement.

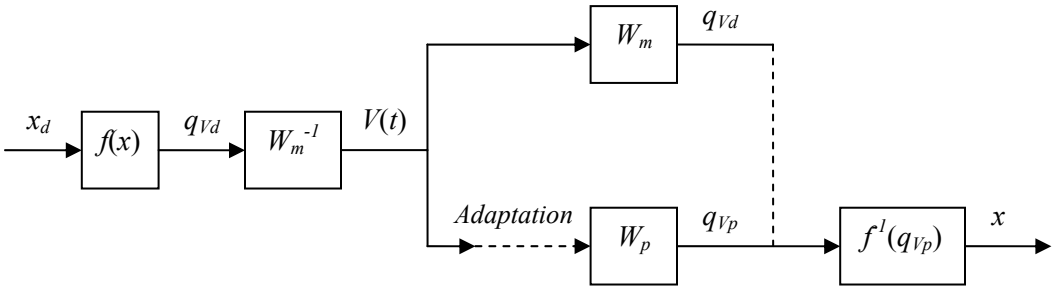

Figure 6-21: Adaptive Controller with Feedback of the Desired Electrical Response

To analyze this adaptive controller the desired plant model was given first-order open-loop dynamics that were twice as fast as the simulated "actual" plant. The step responses of the desired and actual plants are shown in Figure 6-22. The MATLAB code for the following adaptive controller simulations is given in Appendix E.

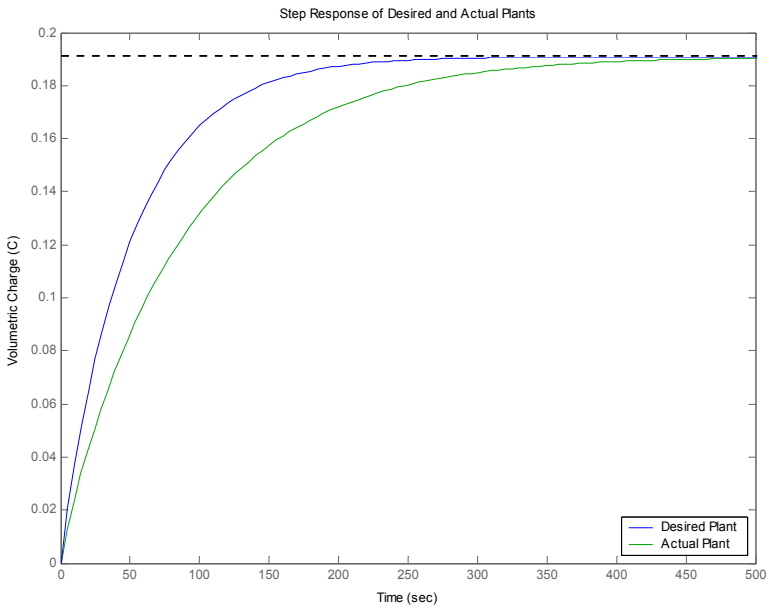

Figure 6-22: Step Response of Desired and Actual Plant Used in Simulation

The desired and actual electrical responses of the actuator are shown below in Figure 6-23 and Figure 6-24 with adaptation gains of 1 and 10, respectively.

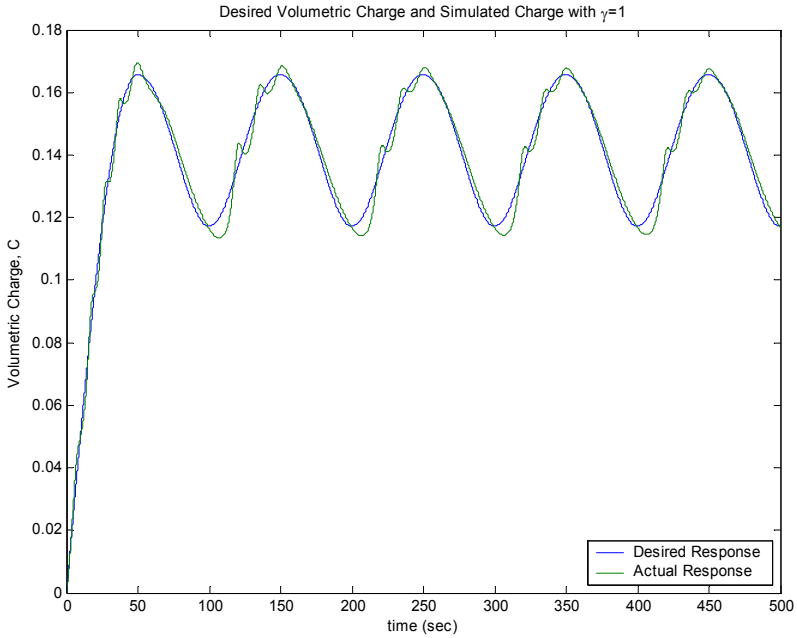

Figure 6-23: Electrical Response of Actuator with Feedback of Q_V and γ = 1

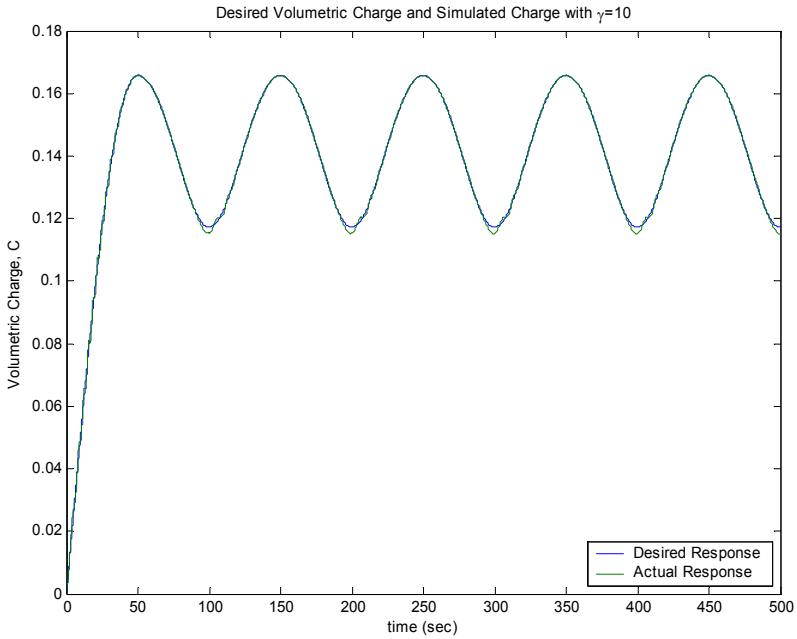

Figure 6-24: Electrical Response of Actuator with Feedback of Q_V and γ = 10

It is evident that this controller provides very good tracking of the desired electrical state. Performance improves with larger adaptation gain; however, the controller bandwidth required increases. This is apparent by comparison of Figure 6-25 and Figure 6-26 which depict the input potential required to achieve the electrical responses shown in Figure 6-23 and Figure 6-24, respectively.

Perfect tracking in the electrical domain should lead to perfect tracking in the mechanical domain; however, this controller is open loop in the mechanical domain. As the controller tracks the desired electrical response the mechanical response is not fed back. Therefore, any errors in the constitutive equation relating charge and displacement will result in errors in the desired trajectory. The response of the system is shown below in Figure 6-27 assuming that the relationship between charge and displacement is perfectly known. This is the case where $\gamma = 10$.

Alternatively, Figure 6-28 depicts the displacement of the polymer actuator if the actual constitutive equation relating charge and displacement is different than the equation used in the controller. In this case the assumed value of Poisson's ratio was 0.41 and the actual value simulated was 0.39.

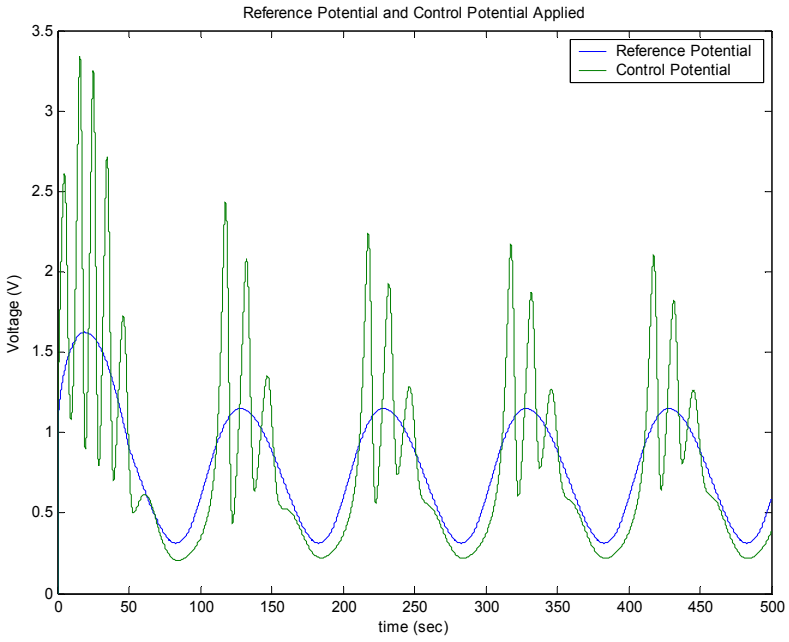

Figure 6-25: Input to Actuator with Feedback of Q_V and $\gamma = 1$

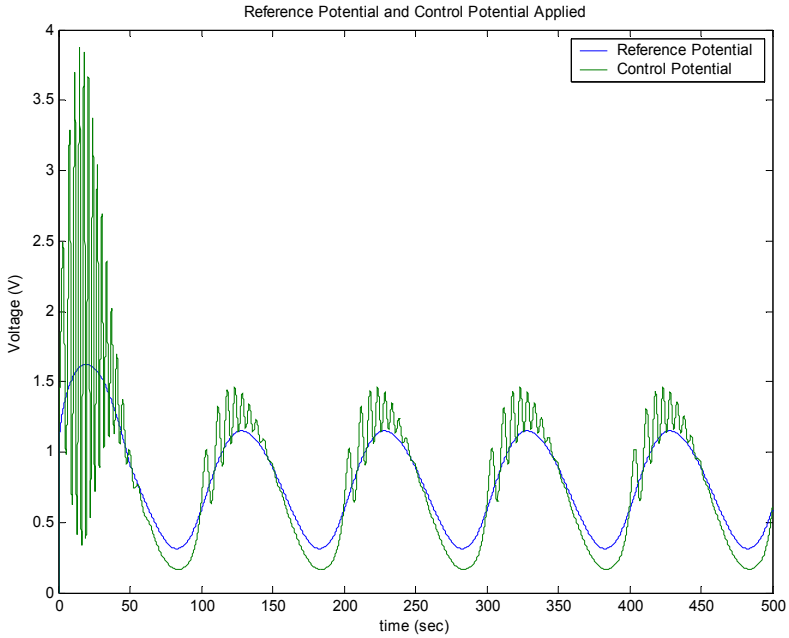

Figure 6-26: Input to Actuator with Feedback of Q_V and $\gamma = 10$

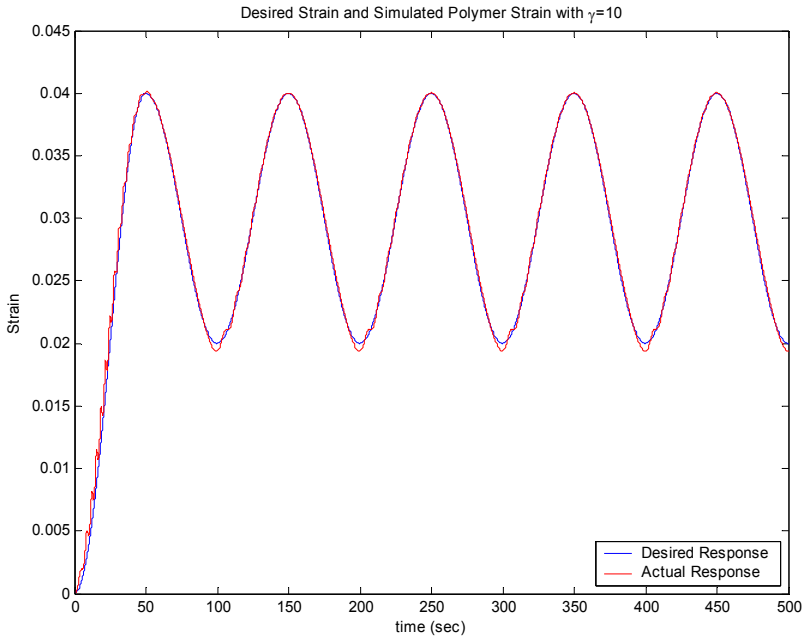

Figure 6-27: Displacement of Actuator with Feedback of Q_V

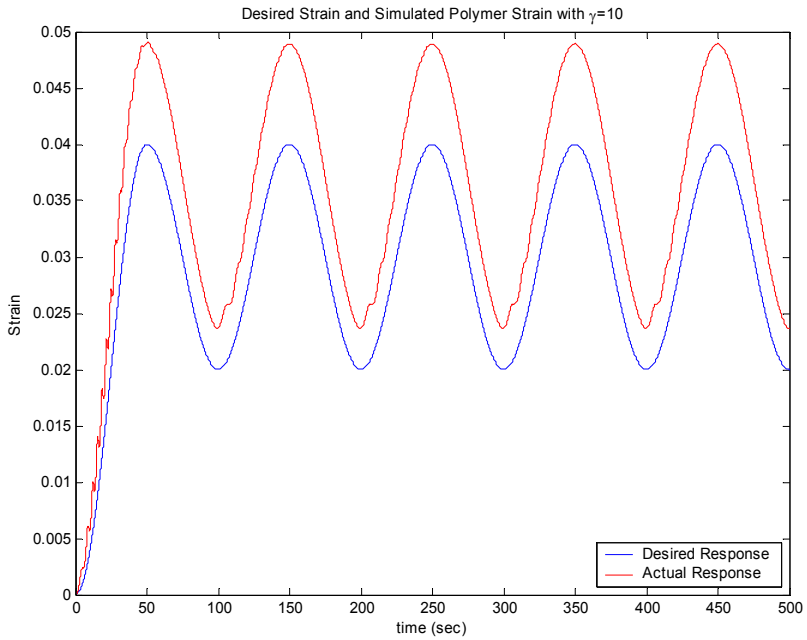

Figure 6-28: Displacement of Actuator with Feedback of Q_V and Imperfect Constitutive Equation

With only a minor difference in the polymer constitutive equation there is a 25% overshoot in the desired response of the actuator.

The equation that is used to determine the desired charge also assumes that the distribution of ions in the polymer is uniform, but this is not the case if the desired response is considerable faster than the diffusion process. Even with a perfect model of the constitutive relationship, if the desired trajectory is changing too quickly, the uniform charge assumption is invalid. This is demonstrated in Figure 6-29 which shows the displacement of the polymer if the desired trajectory is changing twice as fast as the time constant of ion diffusion into the polymer.

Additionally, any bias errors in current measurement would be integrated to give the desired state, q_V. This leads to large errors in actual charge versus desired charge, which results in even larger errors in displacement due to the quadratic dependence on charge. The outcome is shown below in Figure 6-30, which assumes a bias error of 0.5 mA on the current measurement.

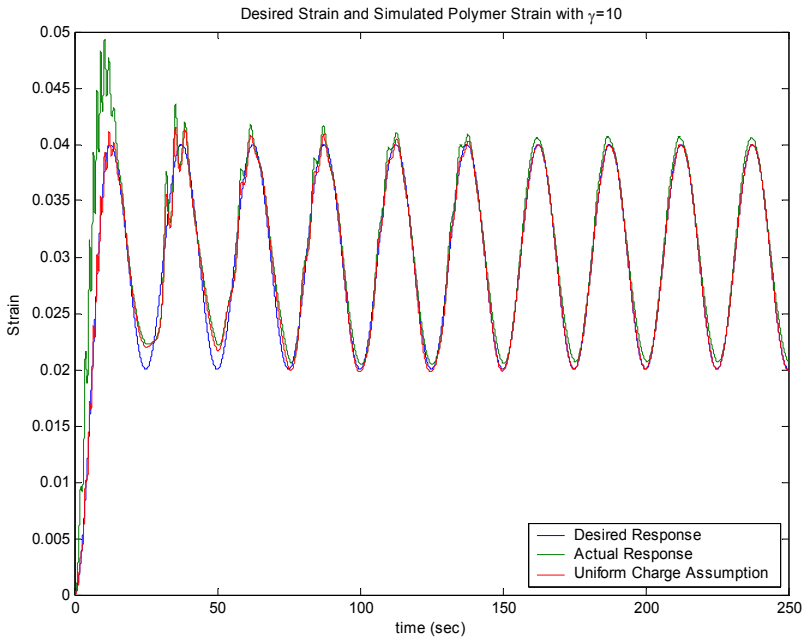

Figure 6-29: Displacement of Polymer Using Uniform Charge Assumption with Fast Desired Response

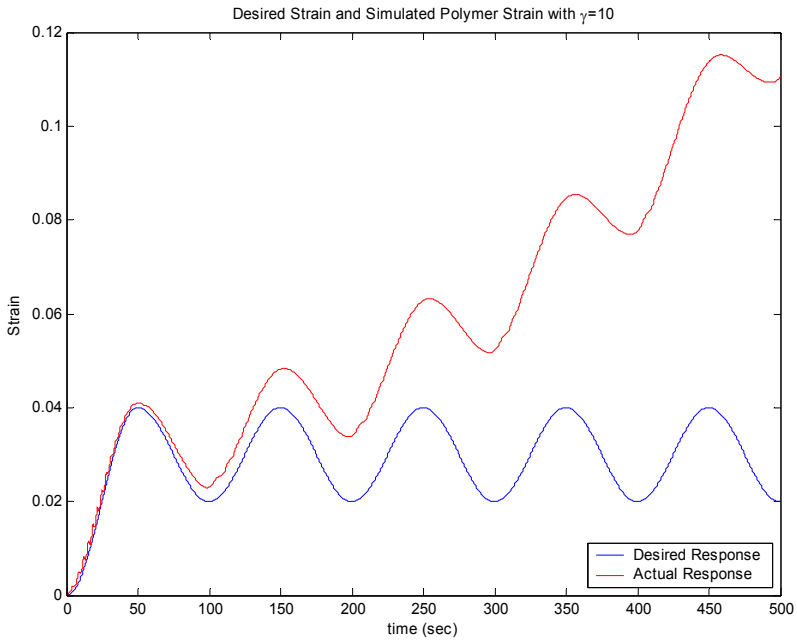

Figure 6-30: Displacement of Actuator with Bias Error in Current Measurement

Similar problems also arise due to uncertainty in the initial state of the system. It is clear from all of these shortcomings that feedback of displacement is needed to alleviate error in the desired actuator displacement.

If the range of desired trajectories is small enough, it is possible to linearize the mechanical constitutive equations within that range and include the mechanical domain in the adaptive controller. The linearization of the mechanical constitutive equation is given by the following:

$$\varepsilon_x = \frac{(1-2\nu)q_0}{EC_V V} q_V \tag{6.9}$$

where q_0 is the average charge expected during actuation for each diffusion capacitance element. From this equation the state space of the entire system can be written as:

$$\begin{bmatrix} \dot{\mathbf{q}}^{k+1\times 1} \\ \Delta\dot{\mathbf{x}}^{3\times 1} \end{bmatrix} = \begin{bmatrix} \mathbf{A}_{\text{electrical}}^{k+1\times k+1} & \mathbf{0}^{k+1\times k+1} \\ \mathbf{0}^{3\times 1} \quad (k\alpha)^{3\times k} & \mathbf{A}_{\text{mech}}^{3\times 3} \end{bmatrix} \begin{bmatrix} \mathbf{q} \\ \Delta\mathbf{x} \end{bmatrix} + \begin{bmatrix} \mathbf{b}_{\text{electrical}} \\ \mathbf{0} \end{bmatrix} \mathbf{V}_{\text{in}} \tag{6.10}$$

where, $\alpha = \frac{w_0 a_0}{b_1} \frac{(1-2\nu)q_0}{C_V V}$, $\mathbf{A}_{\text{electrical}}$ and $\mathbf{b}_{\text{electrical}}$ are the state-space model structures of the reticulated electrical model and $\mathbf{A}_{\text{mech}}$ is the state-space model of the viscoelastic mechanical model. With this linearized state equation it is possible to implement the adaptive controller using feedback of displacement. Once again it is necessary to invert the transfer function of the desired plant in order to determine the input that corresponds to the desired displacement. This leads to the model structure depicted below in Figure 6-31.

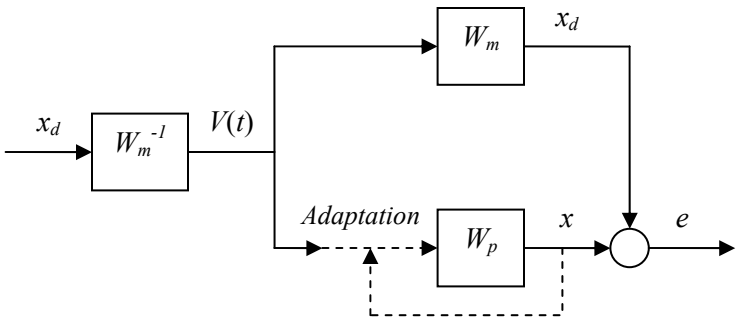

Figure 6-31: Adaptive Controller with Feedback of the Desired Mechanical Response

Figure 6-32 and Figure 6-33 show the electrical and mechanical response of the system to the desired trajectory used in the preceding simulations.

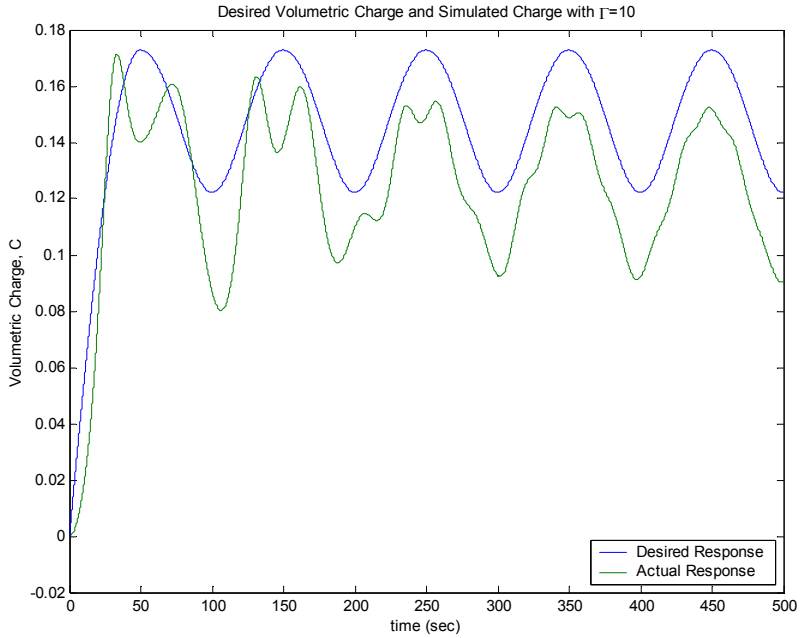

Figure 6-32: Electrical Response of Actuator with Feedback of Displacement and $\gamma = 10$

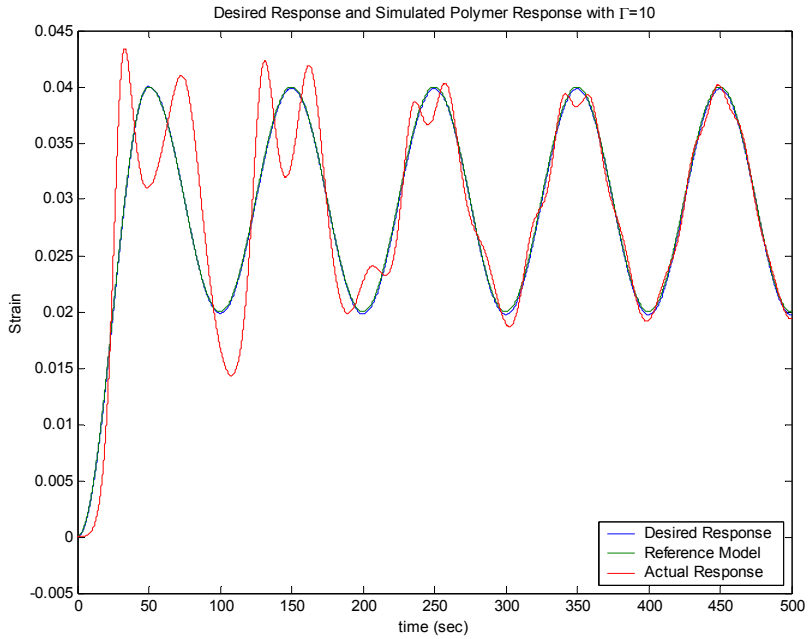

Figure 6-33: Displacement of Actuator with Feedback of Position and $\gamma = 10$

It is immediately evident from these figures that the controller with displacement feedback does not provide as smooth a response as the controller with electrical feedback. However, the inclusion of displacement in the model allows the system to reach the desired response even if there are errors in the constitutive equations or if there is a bias error in current measurement. Therefore, the linearized model of the system provides for more robust control. The control authority needed to achieve this response is shown below in Figure 6-34.

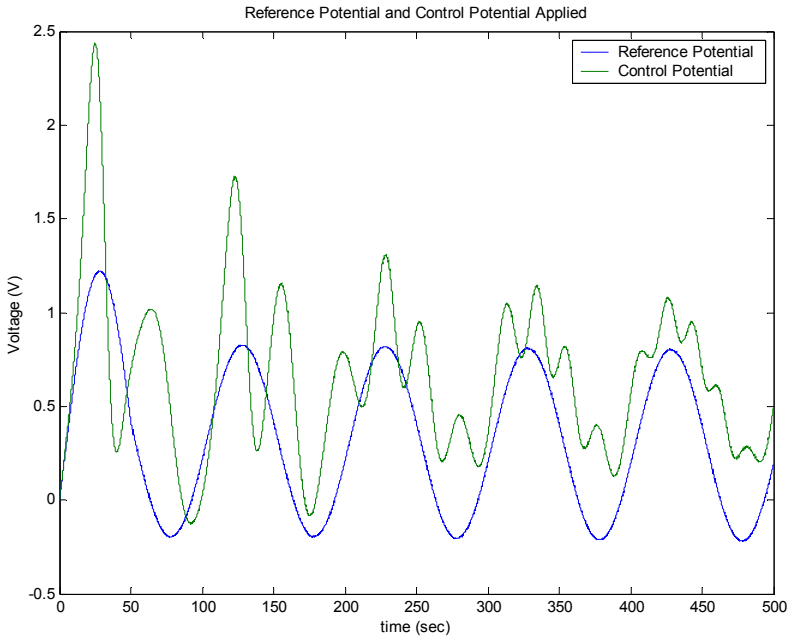

Figure 6-34: Input Potential with Feedback of Position and $\gamma = 10$

This controller requires much larger input potentials to track the desired trajectory. However, once the range of the actuator displacement is fixed to a small region, the nonlinearities in the constitutive equation are less problematic. This is seen very clearly in Figure 6-35, which shows the adaptation of several control parameters.

To demonstrate the effect that the linearization has on the plant response, an open loop response was simulated using the reference signal obtained by assuming that the plant was exactly known. The displacement of the actuator is depicted in Figure 6-36.

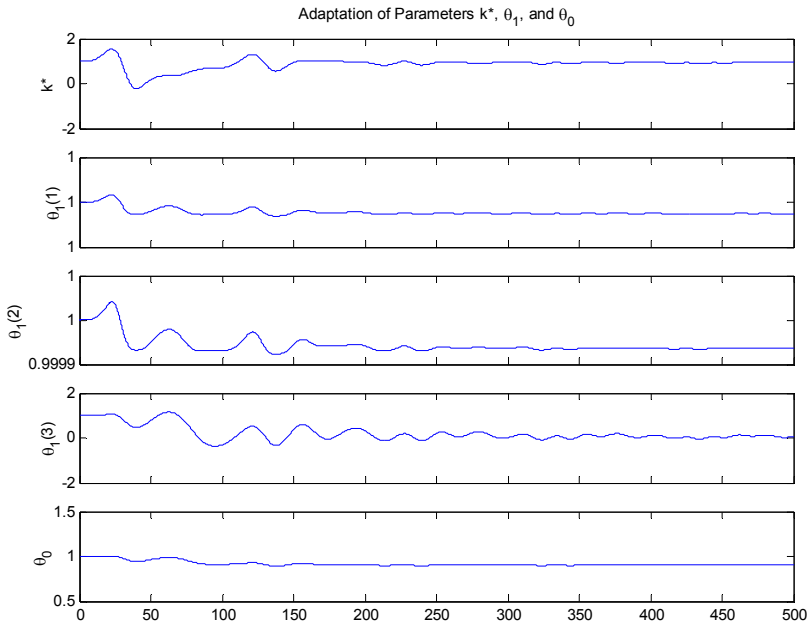

Figure 6-35: Adaptation of Control Parameters with $\gamma = 10$

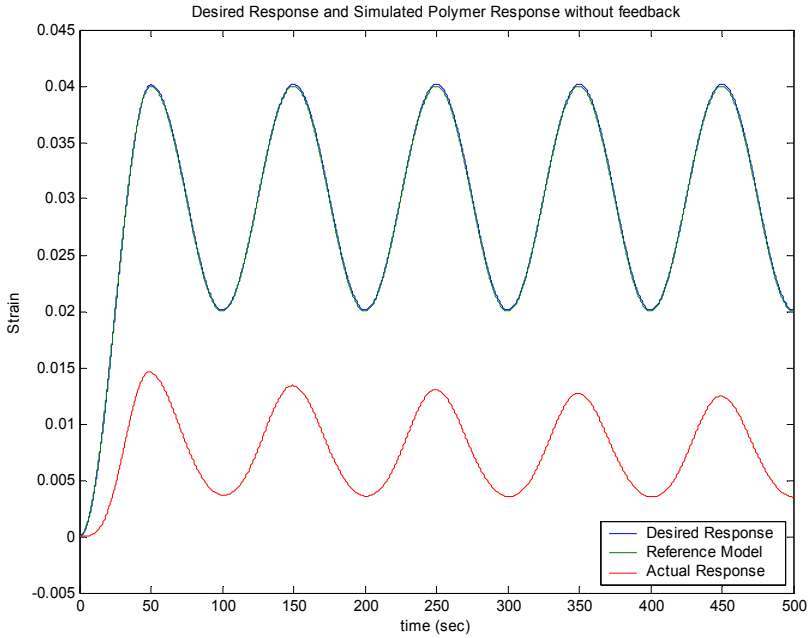

Figure 6-36: Open Loop Response of Actuator to Desired Command

Although the linearized model of the plant is able to track the desired trajectory, the actual plant, which is nonlinear, cannot track the desired response open-loop. Through feedback and adaptation, the nonlinearities in the plant are accounted for. However, because the plant parameters continue to vary due to the nonlinearity of the system, the controller over compensates part of the time and under compensates part of the time. Because of this continuous adaptation, the linearized model never reaches a true steady state tracking convergence. This is demonstrated by the following figure, which shows the response of the system with an adaptation gain of 100. The large gain amplifies the inconsistencies between the model and true system.

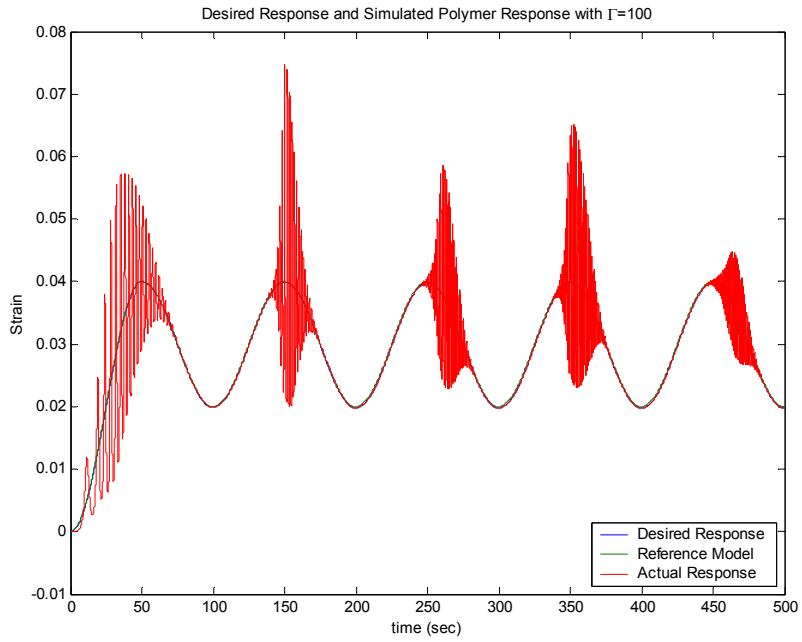

Figure 6-37: Displacement of Actuator using Position Feedback with γ = 100

Because this controller utilizes a linearized model, instability may be possible. This can occur if the adaptation gain is too large, if the vector *h* from the feedback filter is too large, or if the desired trajectory spans a region that is highly nonlinear, such as near the PZC. Instability can also result if the desired response is much faster than the open loop response of the system.

Although both of the adaptive controllers presented here has its drawbacks, they can both be used to control a system with uncertain parameters. The first controller presented requires better knowledge of the coupling from electrical to mechanical domain, but is able to provide a very smooth response due to the linearity of the electrical domain. If good sensors are used, this controller may be sufficient for following a simple actuator trajectory.

The second controller, which uses feedback of displacement, is more robust to modeling uncertainty. Although it may require more time to converge to the desired trajectory due to the linearization of the nonlinear coupling model, this controller can provide very good tracking of a desired response if the operating range remains fairly linear or if the speed of adaptation is faster than the effect of nonlinearities. It is likely that for most applications, EAP actuators will be used in a range that can be treated as linear. The second controller is an ideal controller for EAP actuators because it can account for all types of parameter uncertainty and requires very little knowledge of system parameters, which may change over time.

6.5 Summary

The controllers presented in this chapter demonstrate two very different approaches to EAP actuator control. Simple feedback controllers demonstrate the power of using low-order system models to describe EAP dynamics. With these simple models of the system it is possible to tune the closed-loop response of the actuator. There are some limitations to using linear control techniques on a nonlinear system, particularly in the region of the actuator performance space where the system exhibits non-minimum phase behavior due to the quadratic coupling between electrical and mechanical domains. At the other end of the controller design spectrum, very complicated adaptive controllers can utilize the complete dynamics of the EAP system to improve actuator response throughout its performance space. The adaptive controller presented here is able to handle the nonlinearities in the system better than a PID controller because it is always changing feedback gains in order to recreate the response of a desired plant. As with the PID controller, the adaptive controller cannot handle the nonlinear behavior of the system around zero potential. While neither of the proposed controllers offers a perfect solution to actuator control, each offers insight into what may be possible for EAP control. Certainly, control of EAP actuators requires a significant amount of additional research.

6.6 Chapter References

[1] Qi, Baohua, Wen Lu, and Benjamin R. Mattes, "Control System for Conducting Polymer Actuators," *Smart Structures and Materials 2002: Electroactive Polymer Actuators and Devices (EAPAD)*, Yoseph Bar-Cohen, Ed., *Proceedings of SPIE*, **4695** (2002): 359-366.

[2] Richardson, Robert C., Kevin Watterson, Mike D. Brown, Martin C. Levesley, Jamie A. Hawkes, and Peter G. Walker, "Biologically inspired control for artificial muscles," *Smart*

Structures and Materials 2002: Electroactive Polymer Actuators and Devices (EAPAD), Yoseph Bar-Cohen, Ed., *Proceedings of SPIE*, **4695** (2002): 315-322.

[3] Ding, Jie, Lu Liu, Geoffrey M. Spinks, Dehzi Zhou, Gordon G. Wallace, and John Gillespie, "High performance conducting polymer actuators utilizing a tubular geometry and helical wire interconnects," *Synthetic Metals*, **138** (2003): 391-398.

[4] Slotine, Jean-Jacques E., and Weiping Li, *Applied Nonlinear Control*, Upper Saddle River: Prentice Hall, 1991.

Chapter 7

Conclusions

This thesis describes the formulation of a low-order model to describe the dynamics of an electro-active polymer actuator. While several models of EAP actuators have been developed, these models are unable to describe some of the important dynamics of these materials. By examining electrical and mechanical energy storage in an EAP, an energy-conserving constitutive equation was formulated. This chapter discusses the major contributions from this research and proposes additional work that can be done towards creating viable EAP actuators.

7.1 Contributions to Knowledge

Perhaps the most important result from this thesis has been the development of a nonlinear constitutive equation to describe the energetic coupling between the electrical, chemical, and mechanical domains. By examining the EAP as a two-port energy storing transducer, it was possible to determine the energy contributed by electrical and mechanical inputs. Using the expression for the total stored energy, an energy-conserving constitutive equation was formulated. This equation provides insight into EAP behavior, in particular, the observation that uniaxially-applied mechanical inputs generate negligible electrical effects while electrical inputs produce considerable strains. The constitutive equation contains physically-relevant parameters such as specific volumetric capacitance and Poisson's ratio, making it possible to design an actuator material and electrochemical system to achieve a desired level of performance.

The EAP constitutive equation describes the coupling that results from a uniform distribution of ions. However, a non-uniform distribution of ions in the polymer can have a significant impact on the amount of predicted coupling from volumetric charge to strain. By itself, therefore, the constitutive equation cannot estimate the coupled dynamics resulting from a non-uniform volumetric charge. Fortunately, the development of a reticulated diffusion model allowed the constitutive equation to be applied to the dynamic response of an EAP actuator. The low-order reticulated model is very powerful, reproducing the response of a continuum diffusion model, and also providing information

about the ion distribution within the polymer. This distribution is a key element in determining the amount of coupling from charge to strain, and enabled the constitutive equation to be used for dynamic analysis of the actuator.

A reticulated model was also utilized to describe the continuum mechanics of the polymer. Requiring very few dynamic elements—only one per decade of anticipated loading—the low-order model of viscoelasticity greatly simplifies the description of the mechanical domain. By creating low-order models for the electrical and mechanical domain, it was possible to simulate the response of EAP to inputs. In addition, the low-order models allowed for design and analysis of potential controllers.

Experimental results on an actuator composed of polypyrrole were used to validate the electro-mechanical coupling model. The response of the low-order actuator model was simulated MATLAB for the input conditions used in experimentation. The results verify that the model accurately describes the experimentally-observed behavior of the system with very good correlation between the results for electrically-induced strains up to 3% and applied potentials up to 1 Volt above the potential of zero charge (PZC). The experimental data also demonstrated that the polymer exhibits non-minimum phase behavior at the PZC. This result has important implications for control of the actuator, indicating that instability may result if the polymer is operated near this region.

The dynamic model of EAP was also used to examine actuator control. A simple PID controller was designed to illustrate how the performance of the actuator can be improved with feedback control. This simple controller also demonstrated that the nonlinearity of the polymer behavior may not be critical as long as operating potentials are well above the PZC. A more complicated controller that utilizes the polymer model was also proposed. This alternative controller uses adaptation in order to replace the dynamics of the actuator with the dynamics of a desired plant model. The simulated results from both the PID and adaptive controller suggest that these may be feasible options for actuator control.

An ancillary contribution from this work has been the application of an analysis methodology that can be adapted to modeling of similar systems. Through use of the bond graph notation, and analysis of energy storage and dissipation, it is extremely easy to examine transmission of power in a system. Even for a medium such as a polymer, which is generally analyzed using partial differential equations and continuum analyses, it is possible to simplify the description of the system through use of low-order reticulated models. The physical insight that results from reducing the complexity of the model

enables optimization of the system through identification of critical parameters. Additionally, the low order model is ideal for application of highly-developed control techniques.

7.2 Future Work

With a better understanding of the parameters that influence and limit actuator performance, it should be possible to optimize EAP actuators. Specifically, it will be possible to design actuators with response speeds and power densities that are equivalent to or better than muscle. The constitutive relationships developed here should allow for selection of ideal electrolytes, solvents, and polymers. The design of an optimal actuator will also include geometric considerations and may incorporate parallel structures of actuator fibers that can support greater loads while maintaining quick response times. Ultimately, it is conceivable that EAP will replace traditional actuators in many common devices.

The constitutive model formulated here specifically applies to an isotropic material; however, anisotropy is frequently encountered in EAP. Based on the mechanism responsible for conversion of electrical to mechanical energy it is actually favorable to align polymer chains such that massive anisotropy results. The governing equations for these stretch-aligned polymers will be slightly different than the equations for an isotropic actuator material. The same energy conservation techniques can be employed in examining anisotropic materials with the only difference in the derivation resulting from the anisotropic three-dimensional stress-strain relation.

Another limitation on the proposed model is its simplistic treatment of ionic charge. The model treats ions like electrons, which does not allow for simultaneous inclusion of both anions and cations within the physical structure. In the actual EAP system, however, it is certainly possible for ions of more than one species to be within the polymer. These oppositely charged ions would be in a neutral state electrically; however, from the perspective of the coupling equations, the ions would each contribute to polymer strain. In the course of this research, this limitation of the model was avoided by operating within a range of potentials that only allowed for anion inclusion. This is certainly a reasonable approach as it has been shown throughout this thesis that instabilities can result when trying to operate at potentials where both anions and cations can diffuse into the polymer. If the dynamics related to a second ionic species are required for a particular application, a more sophisticated model may be needed.

While the nonlinear EAP constitutive equation utilizes physically-relevant parameters in describing coupling between domains, the relationships between these parameters have not yet been studied. In

particular, it would be worthwhile to evaluate how properties such as Young's modulus and Poisson's ratio relate in polymer materials. It is known that the level of cross-linking in the polymer affects the material stiffness, and it seems feasible that this would also increase the coupling between dimensional strains, thus lowering Poisson's ratio. When these two effects are applied to the EAP coupling equation it is difficult to determine what the net result would be on actuator performance. So, while the EAP constitutive equation gives some indication of the parameters that can be adjusted to improve performance, it is not yet known whether it is possible to independently adjust these parameters.

Although the PID and adaptive controllers developed here are first-pass examples of what may be possible, they should be implemented on the physical system in order to demonstrate that the anticipated performance is achievable. Once the performance of the controllers is verified it will be possible to design a more suitable controller for the actuator system. There are certainly many possible controller structures that can be used to augment the closed-loop dynamics of the actuator. The selection of particular controller will depend on the desired characteristics of the system and on the anticipated operating range of the actuator.

Ultimately, the work from this thesis will allow future researchers to improve upon all aspects of electro-active polymer actuators and devices.

Appendix A: Polypyrrole Admittance Frequency Response Models

```
%POLYPYRROLE ADMITTANCE MODELS

L0=13.9e-3;                         %Initial Polymer Length, m
W0=3.2e-3;                          %Initial Polymer Width, m
a0=8.5e-6;                          %Initial Polymer Thickness, m
V0=L0*W0*a0;                        %Initial Polymer Volume, m^3
k=66;                               %Electrolyte dielectric
e0=8.85e-12;                        %Permittivity of Free Space, F/m
d=2e-9;                             %Double Layer Gap, m
D=2.1e-12;                          %Diffusion Coefficient, m^2/s
Rc=31;                              %Electrode-Polymer Contact Resistance, Ohm
Cppy=1.3e8;                         %Polymer Capacitance, F/m^3


%POLYMER DOUBLE LAYER CAPACITANCE
Cp=2*(k*e0*L0*W0/d);                %Polymer Double-Layer Capacitance (two sides), F
Rs=Rc;%Rp+Rc+Re;                    %Total Circuit Resistance, Ohms
R_diff=2*a0*d/(D*Cp);               %T-net resistive element
C_diff=a0*Cp/(2*d);                 %T-net capacitive element


%SINGLE ELEMENT DIFFUSION MODEL
A1=[-1/(Cp*Rs)-1/(Cp*R_diff/4) 1/(C_diff*R_diff/4)
    1/(Cp*R_diff/4) -1/(C_diff*R_diff/4)]
B1=[1/Rs 0]';
C1=[1 1];


%N-ELEMENT RETICULATED DIFFUSION MODEL (USED WITH N=4 and 8)
N=8;
for i=1:N/2
    R_N(i+1)=R_diff/(2*N);
    C_N(i)=2*C_diff/N;
end
R_N(1)=R_diff/(4*N);
C_N(N/2)=2*C_diff/N;
A_N=zeros(N/2+1,N/2+1);
A_N(1,1)=-1/(Rs*Cp)-1/(R_N(1)*Cp)-1/(Rs*Ce);
A_N(1,2)=1/(R_N(1)*C_N(1))-1/(Rs*Ce);
A_N(2,1)=1/(R_N(1)*Cp);
for i=1:N/2-1
    A_N(1,i+2)=-1/(Rs*Ce);
    A_N(i+1,i+1)=-1/(R_N(i)*C_N(i))-1/(R_N(i+1)*C_N(i));
    A_N(i+1,i+2)=1/(R_N(i+1)*C_N(i+1));
    A_N(i+2,i+1)=1/(R_N(i+1)*C_N(i));
end
A_N(N/2+1,N/2+1)=-1/(R_N(N/2)*C_N(N/2));
B_N=zeros(N/2+1,1);
B_N(1)=1/Rs;
C_N=ones(1,N/2+1);


%JOHN MADDEN'S CONTINUUM MODEL

w=logspace(-6,5);
Hz=w/(2*pi);
clear j
for i=1:length(w)
       Y(i)=j*w(i)/Rs*(sqrt(D)/d*tanh(a0/2*sqrt(j*w(i)/D))+sqrt(j*w(i)))/(sqrt(j*w(i))/(Rs*Cp
       )+(j*w(i))^(3/2)+sqrt(D)/d*j*w(i)*tanh(a0/2*sqrt(j*w(i)/D)));

       %Y(i)=j*w(i)/Rs*(sqrt(C_diff/(R_diff*Cp^2))*tanh(sqrt(j*w(i)*R_diff*C_diff))+sqrt(j*w(
       i)))/(sqrt(j*w(i))/(Rs*Cp)+(j*w(i))^(3/2)+sqrt(C_diff/(R_diff*Cp^2))*j*w(i)*tanh(sqrt(
       j*w(i)*R_diff*C_diff)));

       Ymag(i)=abs(Y(i));
       Yphase(i)=180*angle(Y(i))/pi;
end
```

```
[num1,den1]=ss2tf(A1,B1,C1,0);
sys1=tf(num1,den1);
sys1a=tf(conv([1,0],num1a),den1);

[num4,den4]=ss2tf(A4,B4,C4,0);
sys4=tf(num4,den4);
sys4a=tf(conv([1,0],num4a),den4);

[num8,den8]=ss2tf(A8,B8,C8,0);
sys8=tf(num8,den8);
sys8a=tf(conv([1,0],num8a),den8);

[mag1,phase1]=bode(sys1a,w);
[mag4,phase4]=bode(sys4a,w);
[mag8,phase8]=bode(sys8a,w);
for i=1:length(mag1)
    Mag1(i)=mag1(:,:,i);
    Phase1(i)=phase1(:,:,i);
    Mag4(i)=mag4(:,:,i);
    Phase4(i)=phase4(:,:,i);
    Mag8(i)=mag8(:,:,i);
    Phase8(i)=phase8(:,:,i);
end

figure(1)
set(0,'FontSize',12)
subplot('position',[.15 .515 .755 .36])
loglog(Hz,Ymag,Hz,Mag1,'--',Hz,Mag4,'-.',Hz,Mag8,':')
axis([10^-4,10^4,10^-6,10^-1])
title(['Frequency Response of Polypyrrole Admittance: {\itD}=',num2str(D*1e12),' \mum^2/s,
{\it\delta}=',num2str(d*1e9),' nm, {\itR}=',num2str(Rc),' \Omega'])
set(gca,'ytick',[10^-5,10^-4,10^-3,10^-2,10^-1],'XColor',[.4     .4     .4],'YColor',[.4     .4
.4],'XTickLabel',[])
ylabel('Admittance (S)','Color','k')
legend('Continuum Diffusion','Reticulated (N=1)','Reticulated (N=4)','Reticulated (N=8)',4)
%legend('{\ita} = 1 \mum','{\ita} = 2 \mum','{\ita} = 4 \mum','{\ita} = 8 \mum','{\ita} =16
\mum',4)

subplot('position',[.15 .115 .755 .36])
semilogx(Hz,Yphase,Hz,Phase1,'--',Hz,Phase4,'-.',Hz,Phase8,':')
axis([10^-4,10^4,-50,100])
set(gca,'XColor',[.4 .4 .4],'YColor',[.4 .4 .4])
xlabel('Frequency (Hz)','Color','k')
ylabel('Phase (deg)','Color','k')
hold on
```

Appendix B: Polypyrrole Actuator Simulation

B.1 Polypyrrole Actuator Dynamic Model

```
%%%SIMULATION USING DMA DATA - DYNAMIC MODEL

function PPydot=f(t,x);

global T Tf current potential stress L0 W0 a0 V0 A_mech b1 nu ECpoly k e0 d D Rc N Vref POT

PPydot=zeros(N/2+15,1)';

%x(1:7);                %Viscoelastic Elements for Length Displacement, m
w(1:7)=x(8:14);         %Viscoelastic Elements for Width Displacement, m
Qp=x(15);               %Double-Layer Charge, C

L=L0+x(1);                          %Total Length, m
W=W0+w(1);                          %Total Width, m
a=a0*W/W0;                          %Total Polymer Thickness (strain is identical to width), m
V=L0*W0*a0*(1+x(1)/L0+2*w(1)/W0);  %Volume (Small Strain Assumption), m^3

%%%DATA INPUTS

Voltage=potential(floor(t*(length(T)-1)/T(end))+1)-Vref;  %Get Voltage Input from Data
%Current = current(floor(t*(length(T)-1)/T(end))+1);      %Get Current Input from Data
Stress = stress(floor(t*(length(T)-1)/T(end))+1);         %Get Stress Input from Data

%%%ELECTRICAL DOMAIN

%POLYMER LENGTH-DEPENDENT RESISTANCE - (More Important for Low-Conductivity Samples)
%Rp=1/(ECpoly*W*a/L);           %Total Polymer Resistance, Ohms

%POLYMER DOUBLE LAYER CAPACITANCE
Cp=2*(k*e0*L*W/d);              %// Plate Capacitor Model of Polymer Double-Layer Capacitance
(two sides), F
Rs=Rc;%Rp                       %Total Circuit Resistance, Ohms

%N-ELEMENT TRANSMISSION LINE DIFFUSION MODEL (STATE-SPACE FORM)
R_diff=2*a*d/(D*Cp);            %T-net resistive element
C_diff=a*Cp/(2*d);              %T-net capacitive element

C_N(1:N)=2*C_diff/N;
R_N(2:N)=R_diff/(2*N);
R_N(1)=R_diff/(4*N);

A_N=zeros(N/2+1,N/2+1);

if POT=='P'                     %Voltage Input
    A_N(1,1)=-1/(Rs*Cp)-1/(R_N(1)*Cp);
    A_N(1,2)=1/(R_N(1)*C_N(1));
    A_N(2,1)=1/(R_N(1)*Cp);
    for i=1:N/2-1
        A_N(i+1,i+1)=-1/(R_N(i)*C_N(i))-1/(R_N(i+1)*C_N(i));
        A_N(i+1,i+2)=1/(R_N(i+1)*C_N(i+1));
        A_N(i+2,i+1)=1/(R_N(i+1)*C_N(i));
    end
    A_N(end,end)=-1/(R_N(end)*C_N(end));
    B_N=zeros(N/2+1,1);
    B_N(1)=1/Rs;

    Qdot=A_N*x(15:15+N/2)+B_N*Voltage;

elseif POT=='C'                 %Current Input
    A_N(1,1)=-1/(R_N(1)*Cp);
    A_N(2,1)=1/(R_N(1)*Cp);
    for i=1:N/2-1
        A_N(i,i+1)=1/(R_N(i)*C_N(i));
        A_N(i+1,i+1)=-1/(R_N(i)*C_N(i))-1/(R_N(i+1)*C_N(i));
```

```
        A_N(i+2,i+1)=1/(R_N(i+1)*C_N(i));
    end
    A_N(end-1,end)=1/(R_N(end)*C_N(end));
    A_N(end,end)=-1/(R_N(end)*C_N(end));
    B_N=zeros(N/2+1,1);
    B_N(1)=1;

    Qdot=A_N*x(15:end)+B_N*Current;

else
    POT=input('Error, Please specify P for (P)otential Input or C for (C)urrent Input\n>>
','s')
end

Qv=x(16:end);

%%%MECHANICAL (VISCOELASTIC & ELECTROMECHANICAL) DYNAMICS

Ldot=A_mech*W0*a0/L0*x(1:7)'+W0*a0*(Stress+(1-2*nu)*((Qv'*Qv*N/2)/(2*C_diff*L*W*a)))/b1;
Wdot=A_mech*L0*a0/W0*w'+L0*a0*(-nu*Stress+(1-2*nu)*(Qv'*Qv*N/2)/(2*C_diff*L*W*a))/b1;

PPydot=[Ldot',Wdot',Qdot']';
```

B.2 Polypyrrole Actuator Parameter and Output File

```
%%%SIMULATION USING DMA DATA - PARAMETER FILE

global T dt current potential stress L0 W0 a0 V0 A_mech b1 nu ECpoly k e0 d D Ce Rc Re N Vref
POT q0

POT='P';%input('Was (P)otential or (C)urrent used as input?\n>> ','s');

Rc=300;                         %Measured Polymer and Contact Resistance, Ohms
N=20;                           %Number of Elements in Diffusion Model

L0=height/1e3;                  %Initial Polymer Length (from data), m
W0=width/1e3;                   %Initial Polymer Width (from data), m
a0=thickness/1e3;               %Initial Polymer Thickness (from data), m
V0=L0*W0*a0;                    %Initial Polymer Volume, m^3

%Free Mechanical Variables
E1=60e6;                        %Polymer Elasticity (Relaxed), N/m^2
E2=31.3e6;                      %First Viscoelastic Stiffness, N/m^2
E3=33e6;                        %Second Viscoelastic Stiffness, N/m^2
E4=35.2e6;
E5=46.2e6;
E6=56.8e6;
E7=77e6;
b1=30;                          %Virtual Damper
b2=130;                         %First Viscoelastic Dissipator, kg/s
b3=1600;                        %Second Viscoelastic Dissipator, kg/s
b4=17113;
b5=223344;
b6=2.76e6;
b7=3e7;
nu=0.43;                        %Poisson's Ratio

A_mech=[-E1/b1 -E2/b1 -E3/b1 -E4/b1 -E5/b1 -E6/b1 -E7/b1
    -E1/b1 -(E2/b1+E2/b2) -E3/b1 -E4/b1 -E5/b1 -E6/b1 -E7/b1
    -E1/b1 -E2/b1 -(E3/b1+E3/b3) -E4/b1 -E5/b1 -E6/b1 -E7/b1
    -E1/b1 -E2/b1 -E3/b1 -(E4/b1+E4/b4) -E5/b1 -E6/b1 -E7/b1
    -E1/b1 -E2/b1 -E3/b1 -E4/b1 -(E5/b1+E5/b5) -E6/b1 -E7/b1
    -E1/b1 -E2/b1 -E3/b1 -E4/b1 -E5/b1 -(E6/b1+E6/b6) -E7/b1
    -E1/b1 -E2/b1 -E3/b1 -E4/b1 -E5/b1 -E6/b1 -(E7/b1+E7/b7)];

%Free Electrical Variables
d=2.1e-9;                       %Double Layer Gap, m
D=1e-12;                        %Diffusion Coefficient, m^2/s
```

```
%ECpoly=.35;%4.3e5;               %Electrical Conductivity, S/m
%%%Rc and ECpoly have been lumped into Rc, which is a measureable quantity.
%%%Although total resistance depends on the strain of the polymer, the
%%%polymer resistance is small making its fluctuations negligible in the analysis.

%Constants
PZC=-.6;                    %Voltage at which Polymer is Free of Ions (PZC)
k=66;                       %Electrolyte Dielectric, F/m
e0=8.85e-12;                %Permittivity of Free Space, F/m

plotdata                    %Plot Raw Data using 'plotdata'

%%%Initial conditions are determined based on equilibrium of polymer. The
%%%uncharged potential of the polymer is -0.6V (from experiment) resulting
%%%in some initial charge at any other initial potential. It is *very*
%%%important that equilibrium is reached before collecting data for this
%%%model to work properly (if not, initial conditions, x0, must be
%%%specified based on some observation of transients at beginning of data
%%%collection). Initial conditions are determined using constitutive model.

x0=zeros(N/2+15,1);
x0(1)=L0*((1-2*nu)*(potential(1)-PZC)^2*k*e0/(2*E1*d^2)); %Equil. Displacement, length
x0(8)=W0*((1-2*nu)*(potential(1)-PZC)^2*k*e0/(2*E1*d^2)); %Equil. Displacement, width
x0(16:end)=2*q0/N;

Tf=T(end);                  %Final time (some versions of MATLAB require different variable)
dT=.05;
t=0:dT:Tf;

[T,Q]=ode23s('PPysimdot',t,x0);

strain=Q(:,1)/L0;%-.015;    %Strain of Polymer, may need to include offset from data
Strain=fft(strain);

charge=zeros(length(Q),1);
for i=1:length(Q)
    charge(i)=sum(Q(i,15:end));
end
Charge=fft(charge);

current=zeros(length(Q),1);
for i=2:length(Q)
    current(i)=(charge(i)-charge(i-1))/dT;
end
Current=fft(current);

Admit=Current./Potential;
AdmitMag=abs(Admit);                        %Magnitude of admittance transfer function
AdmitPhase=angle(Admit)*180/pi;             %Phase of admittance transfer function, degrees
W=1/(dT*length(Admit)):1/(dT*length(Admit)):1/dT;  %Frequency Range of FFT in Hz

Pot2Charge=Charge./Potential;
P2CMag=abs(Pot2Charge);
P2CPhase=angle(Pot2Charge)*180/pi;

Charge2Strain=Strain./Charge;
C2SMag=abs(Charge2Strain);
C2SPhase=angle(Charge2Strain)*180/pi;

Pot2Strain=Strain./Potential;
P2SMag=abs(Pot2Strain);
P2SPhase=angle(Pot2Strain)*180/pi;

Compliance=Strain./Stress;
CompMag=abs(Compliance);
CompPhase=angle(Compliance)*180/pi;

%%%Creates 1-D time history of charge profile across polymer thickness.
%%%This is important for observing how inputs translate through the bulk of
%%%the polymer.
```

```
%Diffusion=zeros(length(Q),N/2);
%for i=1:(length(Q)-1)/1000
%    for j=1:N/2
%        Diffusion(i,j)=Q((i-1)*1000+1,7+j)/2;
%        Diffusion(i,N+1-j)=Q((i-1)*1000+1,7+j)/2;
%    end
%end
%M=avifile('diffusion2.avi');
%for i=1:(length(T)-1)/1000
%    figure(15)
%    plot(Diffusion(i,:))
%    grid
%    axis([0,N+1,min(min(Diffusion)),max(max(Diffusion))])
%    F=getframe(gcf);
%    M=addframe(M,F);
%end
%M=close(M);
%movie(M)

color=[1,0,0];                          %Set color of output data in figures

figure(1)
subplot(411);
plot(T,potential,'color',color)
set(gca,'FontSize',12,'XTickLabel',[])
title(['Electrical       and       Mechanical       Inputs       and       Outputs       for
',datafile],'FontSize',12,'Interpreter','none')
ylabel('Potential vs. Ag/AgClO_4 (V)','FontSize',12)
grid on;
hold on

subplot(412);
plot(T,current,'color',color)
set(gca,'FontSize',12,'XTickLabel',[])
ylabel('Current (A)','FontSize',12)
grid on;
hold on

subplot(413)
plot(T,stress,'color',color)
set(gca,'FontSize',12,'XTickLabel',[])
ylabel('Stress (Pa)','FontSize',12)
grid on;
hold on

subplot(414);
plot(T,strain,'color',color)
set(gca,'FontSize',12)
xlabel('Time (sec)','FontSize',12)
ylabel('Strain','FontSize',12)
grid on;
hold on;

figure(2)
plot(T,potential,'color',color)
set(gca,'FontSize',12)
title(['Potential vs. Time for ',datafile],'FontSize',12,'Interpreter','none')
xlabel('Time (sec)','FontSize',12)
ylabel('Potential vs. Ag/AgClO_4 (V)','FontSize',12)
grid on
hold on

figure(3)
plot(T,current,'color',color)
set(gca,'FontSize',12)
title(['Current vs. Time for ',datafile],'FontSize',12,'Interpreter','none')
xlabel('Time (sec)','FontSize',12)
ylabel('Current (A)','FontSize',12)
grid on
hold on
```

```
figure(4)
subplot(211)
plot(T,potential,'color',color)
set(gca,'FontSize',12,'XTickLabel',[])
title(['Electrical Input and Output for ',datafile],'FontSize',12,'Interpreter','none')
ylabel('Potential vs. Ag/AgClO_4 (V)','FontSize',12)
grid on
hold on

subplot(212);
plot(T,current,'color',color)
set(gca,'FontSize',12)
xlabel('Time (sec)','FontSize',12)
ylabel('Current (A)','FontSize',12);
grid on
hold on

figure(5)
plot(potential,current,'color',color)
set(gca,'FontSize',12)
title(['Current vs. Potential for ',datafile],'FontSize',12,'Interpreter','none')
xlabel('Potential vs. Ag/AgClO_4 (V)','FontSize',12)
ylabel('Current (A)','FontSize',12)
grid on
hold on

figure(6)
subplot(211)
plot(T,strain,'color',color)
set(gca,'FontSize',12,'XTickLabel',[])
title(['Mechanical Input and Output for ',datafile],'FontSize',12,'Interpreter','none')
ylabel('Strain','FontSize',12)
grid on
hold on

subplot(212)
plot(T,stress,'color',color)
set(gca,'FontSize',12)
xlabel('Time (sec)','FontSize',12)
ylabel('Stress (Pa)','FontSize',12)
grid on
hold on

figure(7)
plot(strain,stress,'color',color)
set(gca,'FontSize',12)
title(['Stress vs. Strain for ',datafile],'FontSize',12,'Interpreter','none')
xlabel('Strain','FontSize',12)
ylabel('Stress (Pa)','FontSize',12)
grid on
hold on

figure(8)
loglog(T,strain,'color',color)
set(gca,'FontSize',12)
title(['Strain vs. Time for ',datafile],'FontSize',12,'Interpreter','none')
xlabel('Time (sec)')
ylabel('Strain','FontSize',12)
grid on
hold on

figure(9)
plot(charge,strain,'color',color)
set(gca,'FontSize',12)
title(['Strain vs. Charge for ',datafile],'FontSize',12,'Interpreter','none')
xlabel('Charge (C)','FontSize',12)
ylabel('Strain','FontSize',12)
grid on
hold on

figure(10)
```

```
plot(potential,strain,'color',color)
set(gca,'FontSize',12)
title(['Strain vs. Potential for ',datafile],'FontSize',12,'Interpreter','none')
xlabel('Potential vs. Ag/AgClO_4 (V)','FontSize',12)
ylabel('Strain','FontSize',12)
grid on
hold on

figure(11)
subplot(211)
plot(T,strain,'color',color)
set(gca,'FontSize',12,'XTickLabel',[])
title(['Strain and Current vs. Time for ',datafile],'FontSize',12,'Interpreter','none')
ylabel('Strain','FontSize',12)
grid on
hold on

subplot(212)
plot(T,current,'color',color)
set(gca,'FontSize',12)
xlabel('Time (sec)','FontSize',12)
ylabel('Low Pass Filtered Current (A)','FontSize',12)
grid on
hold on

figure(12)
plot(T,charge,'color',color)
set(gca,'FontSize',12)
xlabel('Time (sec)','FontSize',12)
ylabel('Charge (C)','FontSize',12)
grid on
hold on

figure(13)
PPybode(W,AdmitMag,AdmitPhase,['Polypyrrole Admittance Frequency Response for
',datafile],'Admittance (S)',color)
%PPybode(Omega,GMag,GPhase,'Polypyrrole Admittance Frequency Response','Admittance
(S)',color)

figure(14)
PPybode(W,CompMag,CompPhase,['Polypyrrole Compliance Frequency Response for
',datafile],'Compliance (1/MPa)',color)

figure(15)
PPybode(W,P2SMag,P2SPhase,['Potential to Strain Frequency Response for ',datafile],'Magnitude
(1/V)',color)

figure(16)
PPybode(W,C2SMag,C2SPhase,['Charge to Strain Frequency Response for ',datafile],'Magnitude
(1/C)',color)

figure(17)
PPybode(W,P2CMag,P2CPhase,['Capacitance Frequency Response for ',datafile],'Magnitude
(F)',color)
```

Appendix C: Simple Feedback Control of a First-Order System

The block diagrams presented in Figure C-1 through Figure C-6 depict various combinations of proportional, integral, and derivative control along with their associated closed loop transfer functions.

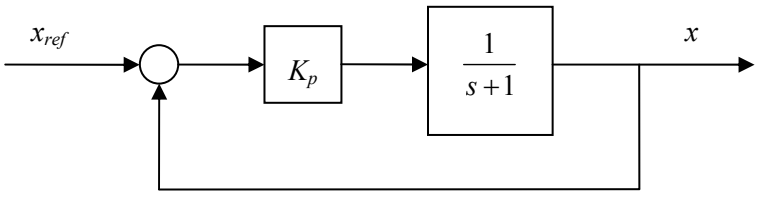

$$G(s) = \frac{K_p}{s+1+K_p}$$

Figure C-1: Proportional Controller Feedback Loop

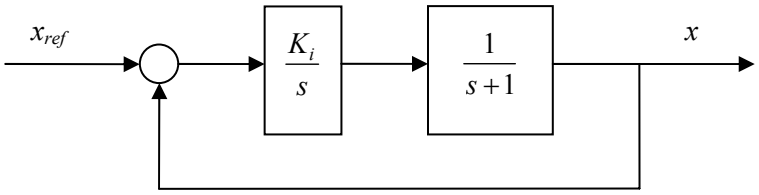

$$G(s) = \frac{K_i}{s^2+s+K_i}$$

Figure C-2: Integral Controller Feedback Loop

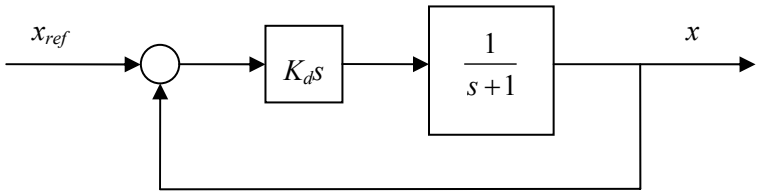

$$G(s) = \frac{K_d s}{(1+K_d)s+1}$$

Figure C-3: Derivative Controller Feedback Loop

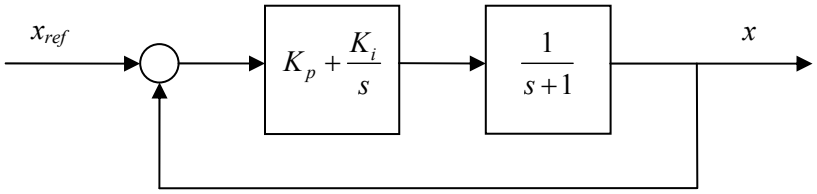

$$G(s) = \frac{K_p s + K_i}{s^2 + (1+K_p)s + K_i}$$

Figure C-4: Proportional-plus-Integral Controller Feedback Loop

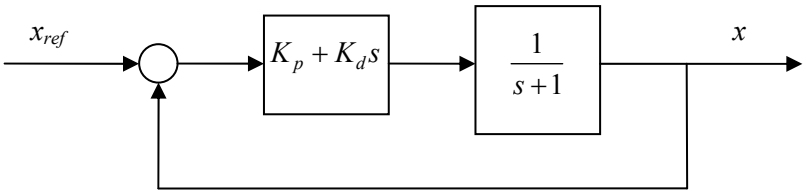

$$G(s) = \frac{K_d s + K_p}{(1+K_d)s+1+K_P}$$

Figure C-5: Proportional-plus-Derivative Controller Feedback Loop

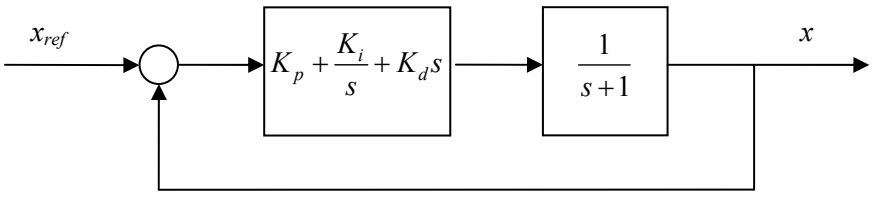

$$G(s) = \frac{K_d s^2 + K_p s + K_i}{(1+K_d)s^2 + (1+K_p)s + K_i}$$

Figure C-6: Proportional-plus-Integral-plus-Derivative Controller Feedback Loop

From the feedback transfer functions the poles of the closed-loop system can be determined. The poles are given by the following equations:

$$\begin{aligned}
\sigma_P &= -(1+K_p) \\
\sigma_I &= \frac{-1 \pm \sqrt{1-4K_i}}{2} \\
\sigma_D &= -\frac{1}{1+K_d} \\
\sigma_{PI} &= \frac{-(1+K_p) \pm \sqrt{(1+K_p)^2 - 4K_i}}{2} \\
\sigma_{PD} &= -\frac{1+K_p}{1+K_d} \\
\sigma_{PID} &= \frac{-(1+K_p) \pm \sqrt{(1+K_p)^2 - 4K_i(1+K_d)}}{2(1+K_d)}
\end{aligned} \tag{6.11}$$

From these equations it is evident that P, D, and PD controllers have one real pole while I, PI, and PID controllers can have two real or complex conjugate poles depending on the feedback gains used.

Appendix D: PID Controller Simulation

D.1 PID Controller ODE File

```
function dot=Adaptdot(t,x);

global N n T Kp Ki Kd k e0 d Rs D L0 W0 a0 V0 nu b1 A_pid B_pid C_pid D_pid A_mech strain_ref

dot=zeros(n+16,1);

q(1:n)=x(1:n);
dx(1:7)=x(n+1:n+7);
dw(1:7)=x(n+8:n+14);
pid=x(n+15:end);

Yd=strain_ref(floor(t*(length(strain_ref)-1)/T(end))+1);
error=Yd-dx(1)/L0;

%%%Control Law
Stress=0e6;

pid_dot=A_pid*pid+B_pid*error;
u=C_pid*pid+D_pid*error;

if u>3
    u=3;                          %Saturation on Control Potential
elseif u<0
    u=0;
end

L=L0+dx(1);                         %Total Length, m
W=W0+dw(1);                         %Total Width, m
a=a0*W/W0;                          %Total Thickness (strain in y and z are identical), m
V=L0*W0*a0*(1+dx(1)/L0+2*dw(1)/W0); %Volume (Small Strain Assumption), m^3

%%%ELECTRICAL DOMAIN
%POLYMER DOUBLE LAYER CAPACITANCE
Cp=2*(k*e0*L*W/d);             %// Plate Capacitor Model of Polymer Double-Layer, F

%N-ELEMENT TRANSMISSION LINE DIFFUSION MODEL (STATE-SPACE FORM)
R_diff=2*a*d/(D*Cp);            %T-net resistive element
C_diff=a*Cp/(2*d);              %T-net capacitive element

C_N(1:n)=2*C_diff/N;
R_N(2:n)=R_diff/(2*N);
R_N(1)=R_diff/(4*N);

A_N=zeros(N/2+1,N/2+1);
A_N(1,1)=-1/(Rs*Cp)-1/(R_N(1)*Cp);
A_N(1,2)=1/(R_N(1)*C_N(1));
A_N(2,1)=1/(R_N(1)*Cp);
    for i=1:N/2-1
        A_N(i+1,i+1)=-1/(R_N(i)*C_N(i))-1/(R_N(i+1)*C_N(i));
        A_N(i+1,i+2)=1/(R_N(i+1)*C_N(i+1));
        A_N(i+2,i+1)=1/(R_N(i+1)*C_N(i));
    end
A_N(end,end)=-1/(R_N(end)*C_N(end));
B_N=zeros(N/2+1,1);
B_N(1)=1/Rs;

Qdot=A_N*q'+B_N*u;
Qv=q(2:end)';

%%%MECHANICAL (VISCOELASTIC & ELECTROMECHANICAL) DYNAMICS
Ldot=A_mech*W0*a0/L0*dx'+W0*a0*(Stress+(1-2*nu)*((Qv'*Qv*N/2)/(2*C_diff*V)))/b1;
Wdot=A_mech*L0*a0/W0*dw'+L0*a0*(-nu*Stress+(1-2*nu)*(Qv'*Qv*N/2)/(2*C_diff*V))/b1;

dot=[Qdot',Ldot',Wdot',pid_dot']';
```

D.2 PID Controller Parameter and Output File

```
%%%PID Controller Simulation Parameter File

global N n T Kp Ki Kd k e0 d Rs D L0 W0 a0 V0 nu b1 A_pid B_pid C_pid D_pid A_mech strain_ref

L0=15/1000;                 %Initial Polymer Length, m
W0=3/1000;                %Initial Polymer Width, m
a0=.020/1000;               %Initial Polymer Thickness, m
V0=L0*W0*a0;                %Initial Polymer Volume, m^3

%Free Mechanical Variables
E1=60e6;                    %Polymer Spring Constant, N/m^2
E2=31.3e6;                  %First Relaxation Spring Constant, N/m^2
E3=33e6;                    %Second Relaxation Spring Constant, N/m^2
E4=35.2e6;
E5=46.2e6;
E6=56.8e6;
E7=66e6;
b1=40;                      %Virtual Damper
b2=130;                     %First Relaxation Dissipator, kg/s
b3=1600;                    %Second Relaxation Dissipator, kg/s
b4=17113;
b5=223344;
b6=2.76e6;
b7=3e7;
nu=0.42;                    %Poisson's Ratio

A_mech=[-E1/b1 -E2/b1 -E3/b1 -E4/b1 -E5/b1 -E6/b1 -E7/b1
    -E1/b1 -(E2/b1+E2/b2) -E3/b1 -E4/b1 -E5/b1 -E6/b1 -E7/b1
    -E1/b1 -E2/b1 -(E3/b1+E3/b3) -E4/b1 -E5/b1 -E6/b1 -E7/b1
    -E1/b1 -E2/b1 -E3/b1 -(E4/b1+E4/b4) -E5/b1 -E6/b1 -E7/b1
    -E1/b1 -E2/b1 -E3/b1 -E4/b1 -(E5/b1+E5/b5) -E6/b1 -E7/b1
    -E1/b1 -E2/b1 -E3/b1 -E4/b1 -E5/b1 -(E6/b1+E6/b6) -E7/b1
    -E1/b1 -E2/b1 -E3/b1 -E4/b1 -E5/b1 -E6/b1 -(E7/b1+E7/b7)];

%Electrical Constants
PZC=-.6;                          %Voltage at which Polymer is Free of Ions (From Bottom of
Parabola on Strain vs. Charge)
k=66;                       %Electrolyte Dielectric, F/m
e0=8.85e-12;                %Permittivity of Free Space, F/m

%%%SIMULATED PLANT PARAMETERS
Rs=100;
d=1.9733e-9;
D=1e-12;

%N-ELEMENT TRANSMISSION LINE DIFFUSION MODEL (STATE-SPACE FORM)
N=20;
n=N/2+1;

Tf=500;                     %Final Time
dt=.5;
T=0:dt:Tf;

%strain_ref=.03*ones(length(T),1);
strain_ref=zeros(length(T),1);
freq=0.01;
for i=1:length(T)
    if i<=1/(2*freq*dt)
        strain_ref(i)=.02-.02*cos(2*pi*freq*T(i));
    else
        strain_ref(i)=.03+.01*cos(2*pi*T(i-50/dt)*freq);
   end
end

Kp=67;%165;
Ki=3;%12.5;
Kd=140;
num=1e3*[Kd Kp Ki];
```

```
den=[1 1e3 0];
[A_pid,B_pid,C_pid,D_pid]=tf2ss(num,den);

initial=zeros(n+16,1);

[T,Q]=ode23s('Adaptdot1',T,initial);

StrainActual=zeros(length(Q),1);
ChargeV=zeros(length(Q),1);
for i=1:length(Q)
    StrainActual(i)=Q(i,n+1)/L0;
    ChargeV(i)=sum(initial(2:n))+sum(Q(i,2:n));
end
current=zeros(length(Q),1);
for i=2:length(Q)
    current(i)=(ChargeV(i)-ChargeV(i-1))/dt;
end

set(0,'defaultlinelinewidth',1)

figure(1)
plot(T,strain_ref,T,StrainActual)
set(gca,'FontSize',12)
title(['Desired Response and Simulated Polymer Response with {\itK_p}=' num2str(Kp),',
{\itK_i}=' num2str(Ki),' and {\itK_d}=' num2str(Kd)])
xlabel('time (sec)')
ylabel('Strain')
legend('Desired Response','Actual Response',4)
legend('Desired Response','Open-Loop','Closed-Loop',4)
hold on

figure(2)
plot(T,ChargeV)
set(gca,'FontSize',12)
title(['Simulated Volumetric Charge with {\itK_P}=' num2str(Kp),', {\itK_i}=' num2str(Ki),'
and {\itK_d}=' num2str(Kd)])
xlabel('time (sec)')
ylabel('Volumetric Charge, C')
legend('Open-Loop','Closed-Loop',4)
hold on

%Potential=.75*ones(length(Q),1);
Potential=zeros(length(Q),1);
strain_ref_dot=zeros(length(Q),1);
StrainActual_dot=zeros(length(Q),1);
Error=zeros(length(Q),1);
ErrorInt=zeros(length(Q),1);
Error(1)=strain_ref(1)-StrainActual(1);
for i=1:length(Q)-1
    strain_ref_dot(i)=(strain_ref(i+1)-strain_ref(i))/dt;
    StrainActual_dot(i)=(StrainActual(i+1)-StrainActual(i))/dt;
    Error(i+1)=strain_ref(i+1)-StrainActual(i+1);
    ErrorInt(i+1)=ErrorInt(i)+Error(i+1)*dt;
end
for i=1:length(Q)
    Potential(i)=Ki*ErrorInt(i)+Kp*Error(i)+Kd*(strain_ref_dot(i)-StrainActual_dot(i));
end

figure(3)
plot(T,Potential)
set(gca,'FontSize',12)
title(['Control Potential Applied with {\itK_P}=' num2str(Kp),', {\itK_i}=' num2str(Ki),' and
{\itK_d}=' num2str(Kd)])
xlabel('time (sec)')
ylabel('Voltage (V)')
legend('Open-Loop','Closed-Loop',4)
hold on

figure(4)
plot(T,Q(:,1)/(2*k*e0*L0*W0/d))
set(gca,'FontSize',12)
```

```
title(['Double Layer Potential with {\itK_P}=' num2str(Kp),', {\itK_i}=' num2str(Ki),' and
{\itK_d}=' num2str(Kd)])
xlabel('Time (sec)')
ylabel('Double Layer Potential (V)')
legend('Open-Loop','Closed-Loop',4)
hold on

figure(6)
plot(T,current)
set(gca,'FontSize',12)
title(['Current with {\itK_P}=' num2str(Kp),', {\itK_i}=' num2str(Ki),' and {\itK_d}='
num2str(Kd)])
xlabel('Time (sec)')
ylabel('Double Layer Potential (V)')
legend('Open-Loop','Closed-Loop',4)
hold on

potential=current*Rs;
plot(T,current)
```

Appendix E: Adaptive Controller Simulation

E.1 Adaptive Controller ODE File

```
function dot=Adaptdot(t,x);

global N n Lambda h T Voltage yd gamma Cv_p L0 W0 a0 V0 nu A_elect_p B_elect_p A_mech b1

dot=zeros(5*(n+7)-2,1);

q(1:n)=x(1:n);
dx(1:7)=x(n+1:n+7);
omega1(1:n+6)=x(n+8:2*(n+7)-1);
omega2(1:n+6)=x(2*(n+7):3*(n+7)-2);
k=x(3*(n+7)-1);
theta1(1:n+6)=x(3*(n+7):4*(n+7)-2);
theta2(1:n+6)=x(4*(n+7)-1:5*(n+7)-3);
theta0=x(5*(n+7)-2);

y=dx(1)/L0;
r=Voltage(floor(t*(length(Voltage)-1)/T(end))+1);
Yd=yd(floor(t*(length(yd)-1)/T(end))+1);

theta=[k theta1 theta2 theta0]';
omega=[r omega1 omega2 y]';

%%%Control Law
u=theta'*omega;

%%%Simulated Plant Response
Qdot=A_elect_p*q'+B_elect_p*u;
xdot=W0*a0*A_mech/L0*dx'+W0*a0*(1-2*nu)*(q(1:n)*q(1:n)'*N/2)/(2*Cv_p*V0)/b1;

%%%System Dynamics
omega1dot=Lambda*omega1'+h*u;
omega2dot=Lambda*omega2'+h*y;
thetadot=-gamma*(y-Yd)*omega;

dot=[Qdot',xdot',omega1dot',omega2dot',thetadot']';
```

E.2 Adaptive Controller Parameter and Output File

```
%%%Adaptive Controller Parameters

global N n Lambda h T Voltage yd gamma Cv_p L0 W0 a0 V0 nu A_elect_p B_elect_p A_mech b1

L0=15e-3;                   %Initial Polymer Length, m
W0=3e-3;                    %Initial Polymer Width, m
a0=20e-6;                   %Initial Polymer Thickness, m
V0=L0*W0*a0;                %Initial Polymer Volume, m^3

%Free Mechanical Variables
E1=60e6;                    %Polymer Elasticity, N/m^2
E2=31.3e6;                  %First Relaxation Elasticity, N/m^2
E3=33e6;                    %Second Relaxation Elasticity, N/m^2
E4=35.2e6;
E5=46.2e6;
E6=56.8e6;
E7=66e6;
b1=40;                      %Virtual Damper
b2=130;                     %First Relaxation Dissipator, kg/s
b3=1600;                    %Second Relaxation Dissipator, kg/s
b4=17113;
b5=223344;
b6=2.76e6;
```

```
b7=3e7;
nu=0.42;                    %Poisson's Ratio

%Constants
PZC=-.6;                    %Voltage at which Polymer is Free of Ions
k=66;                       %Electrolyte Dielectric, F/m
e0=8.85e-12;                %Permittivity of Free Space, F/m

%%%DESIRED PLANT and SIMULATED PLANT PARAMETERS
Rs_d=50;                    %Electrode-Polymer Contact Resistance, Ohm
d_d=2e-9;                   %Double Layer Gap, m (1e-9 to 3.5e-9)
D_d=1e-12;                  %Diffusion Coefficient, m^2/s (0.3e-12 to 2.1e-12)
Cp_d=2*(k*e0*L0*W0/d_d);    %Helmholz Model of Polymer Double-Layer (two faces), F
Rv_d=2*a0*d_d/(D_d*Cp_d);   %T-net resistive element
Cv_d=a0*Cp_d/(2*d_d);       %T-net capacitive element

Rs_p=100;
d_p=2e-9;
D_p=1e-12;
Cp_p=2*(k*e0*L0*W0/d_p);    %Helmholz Model of Polymer Double-Layer (two faces), F
Rv_p=2*a0*d_p/(D_p*Cp_p);   %T-net resistive element
Cv_p=a0*Cp_p/(2*d_p);       %T-net capacitive element

%N-ELEMENT TRANSMISSION LINE DIFFUSION MODEL (STATE-SPACE FORM)
N=10;
n=N/2;

Tf=500;                     %Final Time
dt=.1;
T=0:dt:Tf;

strain0=0.03;
charge0=sqrt(strain0*2*Cv_d*V0*E1/(1-2*nu));
strain_ref=zeros(length(T),1);
charge_ref=zeros(length(T),1);
freq=0.01;
for i=1:length(T)
    if i<=1/(2*freq*dt)
        strain_ref(i)=.02-.02*cos(2*pi*freq*T(i));
    else
        strain_ref(i)=.03+.01*cos(2*pi*T(i-50/dt)*freq);
   end
    charge_ref(i)=sqrt(strain_ref(i)*2*Cv_d*V0*(E1+E2+E3+E4+E5+E6+E7)/(1-2*nu));
end

%%%Desired Plant Response
Rn_d(1)=Rv_d/(4*N);
Rn_d(2:N/2)=Rv_d/(2*N);
Cn_d(1:N/2)=2*Cv_d/N;

A_elect_d=zeros(n,n);
A_elect_d(1,1)=-1/((Rs_d+Rn_d(1))*Cn_d(1))-1/(Rn_d(2)*Cn_d(2));
for i=2:n
    A_elect_d(i,i)=-1/(Rn_d(i)*Cn_d(i))-1/(Rn_d(i)*Cn_d(i));
    A_elect_d(i-1,i)=1/(Rn_d(i)*Cn_d(i));
    A_elect_d(i,i-1)=1/(Rn_d(i)*Cn_d(i-1));
end
A_elect_d(n,n)=-1/(Rn_d(end)*Cn_d(end));
B_elect_d=zeros(n,1);
B_elect_d(1,1)=1/Rs_d;
C_elect_d=ones(1,n);

%%%Actual Plant Response
Rn_p(1)=Rv_p/(4*N);
Rn_p(2:N/2)=Rv_p/(2*N);
Cn_p(1:N/2)=2*Cv_p/N;

A_elect_p=zeros(n,n);
A_elect_p(1,1)=-1/((Rs_p+Rn_p(1))*Cn_p(1))-1/(Rn_p(2)*Cn_p(2));
for i=2:n
    A_elect_p(i,i)=-1/(Rn_p(i)*Cn_p(i))-1/(Rn_p(i)*Cn_p(i));
```

```
    A_elect_p(i-1,i)=1/(Rn_p(i)*Cn_p(i));
    A_elect_p(i,i-1)=1/(Rn_p(i)*Cn_p(i-1));
end
A_elect_p(n,n)=-1/(Rn_p(end)*Cn_p(end));
B_elect_p=zeros(n,1);
B_elect_p(1,1)=1/Rs_p;
C_elect_p=ones(1,n);

[Z_d,P_d,K_d]=ss2zp(A_elect_d,B_elect_d,C_elect_d,0)
Admit_d=zpk([Z_d',0],P_d,K_d)
[Z_p,P_p,K_p]=ss2zp(A_elect_p,B_elect_p,C_elect_p,0)
Admit_p=zpk([Z_p',0],P_p,K_p)

figure(1)
bode(Admit_d,Admit_p)

A_mech=[-E1/b1 -E2/b1 -E3/b1 -E4/b1 -E5/b1 -E6/b1 -E7/b1
    -E1/b1 -(E2/b1+E2/b2) -E3/b1 -E4/b1 -E5/b1 -E6/b1 -E7/b1
    -E1/b1 -E2/b1 -(E3/b1+E3/b3) -E4/b1 -E5/b1 -E6/b1 -E7/b1
    -E1/b1 -E2/b1 -E3/b1 -(E4/b1+E4/b4) -E5/b1 -E6/b1 -E7/b1
    -E1/b1 -E2/b1 -E3/b1 -E4/b1 -(E5/b1+E5/b5) -E6/b1 -E7/b1
    -E1/b1 -E2/b1 -E3/b1 -E4/b1 -E5/b1 -(E6/b1+E6/b6) -E7/b1
    -E1/b1 -E2/b1 -E3/b1 -E4/b1 -E5/b1 -E6/b1 -(E7/b1+E7/b7)];

A_d=zeros(n+7,n+7);
A_d(1:n,1:n)=A_elect_d;
A_d(n+1:end,1:n)=W0*a0*(1-2*nu)*charge0*(N/2)/(Cv_d*V0*b1);
A_d(n+1:end,n+1:end)=W0*a0*A_mech/L0;
B_d=zeros(n+7,1);
B_d(1,1)=1/(Rs_d+Rv_d(1));
C_d=[zeros(1,n),1/L0,0,0,0,0,0,0];

[Z,P,K]=ss2zp(A_d,B_d,C_d,0)
Wd_V2X=zpk(Z,P,K)
INVzeros=[-1e3*ones(1,3),Z'];
Wd_V2Xinv=zpk(P,INVzeros,1e3^3/K);
Voltage=lsim(Wd_V2Xinv,strain_ref,T);
yd=lsim(Wd_V2X,Voltage,T);

V2Q=zpk(Z_d,P_d,K_d);
Qd=lsim(V2Q,Voltage,T);

figure(2)
plot(T,strain_ref,T,yd)
hold on

figure(3)
plot(T,charge_ref,T,Qd)
pause

A_p=zeros(n+7,n+7);
A_p(1:n,1:n)=A_elect_p;
A_p(n+1:end,1:n)=W0*a0*(1-2*nu)*charge0*(N/2)/(Cv_p*V0*b1);
A_p(n+1:end,n+1:end)=W0*a0*A_mech/L0;
B_p=zeros(n+7,1);
B_p(1,1)=1/(Rs_p+Rv_p(1));

Lambda=diag([-1e3*ones(1,1),Z']);
h=ones(length(Lambda),1);
gamma=10;

initial=zeros(5*(n+7)-2,1);
initial(3*(n+7)-1)=1;
initial(3*(n+7):end)=1;

[T,Q]=ode23s('Adaptdot3',[0:dt:Tf],initial);

StrainActual=zeros(length(Q),1);
ChargeV=zeros(length(Q),1);
for i=1:length(Q)
    StrainActual(i)=Q(i,n+1)/L0;
```

```
    ChargeV(i)=sum(Q(i,1:n));
end
figure(18)
plot(T,yd,T,strain_ref,T,StrainActual)
title(['Desired Response and Simulated Polymer Response with \Gamma=' num2str(gamma)])
xlabel('time (sec)')
ylabel('Strain')
legend('Desired Response','Reference Model','Actual Response',4)

figure(19)
plot(T,charge_ref,T,ChargeV)
title(['Desired Volumetric Charge and Simulated Charge with \Gamma=' num2str(gamma)])
xlabel('time (sec)')
ylabel('Volumetric Charge, C')
legend('Desired Response','Actual Response',4)

OMEGA1=zeros(length(T),n+6);
OMEGA2=zeros(length(T),n+6);
K=zeros(length(T),1);
THETA1=zeros(length(T),n+6);
THETA2=zeros(length(T),n+6);
THETA0=zeros(length(T),1);
THETA=zeros(length(T),2*(n+7));
OMEGA=zeros(length(T),2*(n+7));
VOLTAGE=zeros(length(T),1);

for i=1:length(T)
    OMEGA1(i,1:n+6)=Q(i,n+8:2*(n+7)-1);
    OMEGA2(i,1:n+6)=Q(i,2*(n+7):3*(n+7)-2);
    K(i)=Q(i,3*(n+7)-1);
    THETA1(i,1:n+6)=Q(i,3*(n+7):4*(n+7)-2);
    THETA2(i,1:n+6)=Q(i,4*(n+7)-1:5*(n+7)-3);
    THETA0(i)=Q(i,5*(n+7)-2);
    THETA(i,:)=[K(i) THETA1(i,:) THETA2(i,:) THETA0(i)];
    OMEGA(i,:)=[Voltage(i) OMEGA1(i,:) OMEGA2(i,:) StrainActual(i)];
    VOLTAGE(i)=THETA(i,:)*OMEGA(i,:)';
end
figure(17)
plot(T,Voltage,T,VOLTAGE)
title('Reference Potential and Control Potential Applied')
xlabel('time (sec)')
ylabel('Voltage (V)')
legend('Reference Potential','Control Potential')

figure(22)
subplot(511)
plot(T,K)
set(gca,'XTickLabel',[])
ylabel('k*')
title('Adaptation of Parameters k*, \theta_1, and \theta_0')

subplot(512)
plot(T,THETA1(:,1))
set(gca,'XTickLabel',[])
ylabel('\theta_1(1)')

subplot(513)
plot(T,THETA1(:,2))
set(gca,'XTickLabel',[])
ylabel('\theta_1(2)')

subplot(514)
plot(T,THETA1(:,3))
set(gca,'XTickLabel',[])
ylabel('\theta_1(3)')

subplot(515)
plot(T,THETA0)
ylabel('\theta_0')

figure(23)
```

```
plot(T,Q(:,1)/Cv_p(1))
title('Double Layer Potential')
xlabel('Time (sec)')
ylabel('Double Layer Potential (V)')
```